

3-D Cubic Slot Antennas with Application in Wireless Sensor Networks

by

Souren Shamsinejad

A thesis submitted in partial fulfillment of the requirements for the degree of

Doctor of Philosophy

in

Electromagnetics and microwaves

Department of Electrical and Computer Engineering
University of Alberta

© Souren Shamsinejad, 2017

Abstract

Designing cost-effective, easy-to-implement hermetic antenna-package is a big challenge. These devices are particularly advantageous in portable scenarios with size and power restrictions. Their applications include but not limited to military, medical, space, and environmental monitoring where reliable communication among numerous monitoring nodes is crucial for the Wireless Sensor Networks (WSN) to fulfill requirements of simultaneous data transfer and massive connectivity.

In this dissertation, we focused on design, simulation and fabrication of several types of hermetic antenna packages which are especially suitable for low cost mass production due to their compatibility with 3D printing manufacturing. Additionally, by employing conformal slot configuration on cubic structures, we managed to implement a structure with hollow interior space for electronic circuit placement to achieve low-profile design and keep the outer surface purely conductive to guarantee EMI protection to handle harsh environmental conditions.

Proposed configurations are prototyped on cubic structures as their symmetric shapes provide eminent suitability to offer horizontally polarized omnidirectional radiation pattern in the azimuth plane. This enhances the performance of terrestrial communication in wireless sensor networks where distribution of angle of arrivals is more concentrated around horizon which is an improvement upon current designs as it has the capability to reduce interference usually experienced by vertically-polarized counterparts.

Special wireless sensor network applications covet antennas capable of switching beams between directive and omnidirectional states to handle both terrestrial and sky communications where the former is used in adhoc network among sensory nodes and the latter is used between a hub installed on a drone or a satellite and sensory nodes. To address this need, we also developed a *reconfigurable* antenna-package which offers both broadside radiation patterns toward top and bottom faces of the cube as well as omnidirectional radiation pattern in the azimuth plane to cover all 3D space around the antenna.

In addition, to serve applications where beam forming or MIMO is required for high speed communication or communication in the areas where multipath propagation is dominant, a *multiport* cubic structure is proposed which can switch between omnidirectional and directional radiation patterns in the azimuth plane.

Proposed antennas are the best compromise between solution to ISM-band bandwidth scarcity and adaptability with WSN technologies (Heart and ZigBee).

PREFACE

This thesis is an original work by Souren Shamsinejad. Chapter 4-2 of this thesis has been published as S. Shamsinejad, F. De Flaviis, and P. Mousavi, “Microstrip-Fed 3-D Folded Slot Antenna on Cubic Structure,” *IEEE Antennas Wireless and Propagation Letter.*, vol. 15, pp. 1081–1084, 2016 [1]. Chapter 4-3 of this thesis has been published as S. Shamsinejad, F. M. Monavar, F. De Flaviis, G. Moradi, and P. Mousavi, “Three-dimensional-folded annular slot antenna-package,” *Microwave and Optical Technology Letter*, vol. 59, no. 8, pp. 1871–1876, Aug. 2017 [2]. Chapters 4-4 is suitable for IEEE letter and will be published as S. Shamsinejad, F. M. Monavar, F. De Flaviis, G. Moradi, and P. Mousavi, “Single feed 3D folded slot antenna array”. Chapter 5-2 is suitable for IEEE transaction and will be published as S. Shamsinejad, S. Shamsadini, F. M. Monavar, G. Moradi, and P. Mousavi, “Reconfigurable Cubic Slot Antenna”. Chapter 5-3 is suitable for PIER journal and will be published as S. Shamsinejad, S. Shamsadini, F. M. Monavar, and P. Mousavi, “Multi feed conformal 3D slot antenna”.

ACKNOWLEDGEMENT

I am grateful for working with great professors and smart students at University of Alberta during the past few years. First, I would like to take this opportunity to express my sincere gratitude to my supervisor, professor Pedram Mousavi who supported me during my program in university of Alberta. Additionally, I would like to thank Dr. Gholamreza Moradi for his great advices and useful discussions.

I am also thankful of my qualification and thesis committee members professors Ashwin Iyer, Vien Van, Masoud Ardakani, and Neda Nazemifard. It was an honor to have them on my committees and learnt from their valuable feedbacks. I would like to acknowledge Natural Science and Engineering Research Council (NSERC), Alberta Innovates Technology Features (AITF), TR-Tech for their generous funding of my PhD research and M2M, IWT, the microwave laboratory at University of California Irvine, and Calit2 for their support. I would like to thank ECE professors and staffs in university of Alberta who taught me how to approach a problem helped me to think beyond the box and broaden my knowledge. Additionally, my acknowledgement goes to Ms. Pinder Bains, our graduate student advisor for her kind support. I am also grateful to my colleagues Ali Kiaee, Hamid Moghadas, Mahmoud Mazrouei Sebdani and Farhad Khosravi who shared their thoughts with me during my program. My special thank goes to Fatemeh Mohamadi Monavar who has been my great research partner and helped me in preparing this dissertation as well. I would like to thank my co-workers in Qualcomm and SpaceX who taught me critical thinking in industry's perspective especially my managers Drs. Ali Tassoudji and Nima Mahanfar who patiently sat with me, monitored my thoughts and helped me to develop my career.

Most importantly, my sincere thanks go to my dear parents and loving family who have tough me to achieve my goals, without them this work would not be done. Their unconditional love has been the greatest source of strength to me.

Last, not least, my greatest thanks are due to my best friend, my colleague, and my love Shila Shamsadini, whose understanding, caring and positive attitude have always encouraged me to go forward during difficult times. Her never-ending love has been an inspiration, made the completion of this work possible. Thank you for every day.

Table of contents

Contents

1	INTRODUCTION.....	1
1.1	Why WSN.....	2
1.2	Why metallic package and conformal slot.....	3
1.3	Why conformal slot antenna on cubic structures.....	3
1.4	Why 3-D structures.....	3
1.5	3-D printing.....	5
1.6	Conclusion	6
2	REVIEW OF LITERATURE.....	7
2.1	Introduction.....	7
2.2	3-D Antennas	7
2.3	Slot antennas	14
2.4	Pattern and Polarization Reconfigurable antenna	15
2.5	3-D Printing and Printing Electronics.....	19
2.5.1	<i>2D inkjet conductive printing on flexible sheets [10], [56].....</i>	<i>20</i>
2.5.2	<i>3-D Conformal printing by deposition of conductive inks on 3-D [57]</i>	<i>20</i>
2.5.3	<i>Ink deposition in trenches on 3-D object [4], [19].....</i>	<i>20</i>
2.5.4	<i>Multi-material 3-D Micro-dispensing by nScrypt printers [58].....</i>	<i>21</i>
2.5.5	<i>Laser Direct Structuring (LPKF co.) [59]–[61]</i>	<i>22</i>
2.5.6	<i>Pad Printing [62], [63].....</i>	<i>22</i>
2.6	Antenna for sensor	23
2.7	Conclusion	24
3	CONFORMAL CUBIC ANTENNA MODELING AND ANALYSIS... 25	
3.1	Introduction.....	25
3.2	Slot Antenna.....	25
3.2.1	<i>Planar slot antenna on infinite ground plane.....</i>	<i>26</i>
3.2.2	<i>Planar slot antenna with finite ground plane.....</i>	<i>27</i>
3.2.3	<i>Planar slot antenna with folded finite ground plane.....</i>	<i>29</i>
3.2.4	<i>Folded Slot Antenna</i>	<i>40</i>
3.3	Cubic slot antenna array.....	52
3.3.1	<i>Circular array theory.....</i>	<i>53</i>

Table of contents

3.3.2	<i>Circular array with slot antenna elements</i>	56
3.3.3	<i>Circular array with folded slot antenna element</i>	63
3.4	Mutual coupling in circular slot array.....	68
3.5	Single feed cubic slot antenna.....	72
3.5.1	<i>Planar folded single feed slot antenna</i>	73
3.5.2	<i>3-D folded single feed slot antenna</i>	76
3.6	Conclusion	79
4	CUBIC ARCHITECTURES WITH OMNIDIRECTIONAL RADIATION PATTERN	80
4.1	Introduction.....	80
4.2	Microstrip Fed 3-D Folded Cubic Slot Antenna.....	82
4.2.1	<i>Analysis and design</i>	83
4.2.2	<i>Simulation and Parametric Study</i>	85
4.2.3	<i>Fabrication and Measurement</i>	88
4.3	3-D Folded Annular Slot Antenna-Package	90
4.3.1	<i>Design Considerations</i>	91
4.3.2	<i>Simulations and Critical Parameters</i>	93
4.3.3	<i>Fabrication and Measurement</i>	97
4.4	3-D Folded Cubic Slot Antenna Array	99
4.4.1	<i>Design consideration</i>	99
4.4.2	<i>Feeding structure</i>	101
4.4.3	<i>Current Distribution</i>	102
4.4.4	<i>Antenna Fabrication</i>	103
4.4.5	<i>Measurement and Simulation Results</i>	103
4.5	Conclusion	105
5	CUBIC ARCHITECTURES WITH RECONFIGURABLE RADIATION PATTERN	107
5.1	Introduction.....	107
5.2	Cubic conformal slot antenna array	109
5.2.1	<i>Antenna Geometry and Prototype Design Consideration</i>	110
5.2.2	<i>Design considerations</i>	111
5.2.3	<i>Parameter study and coupling</i>	117
5.3	Reconfigurable Cubic Slot Antenna	131

Table of contents

5.3.1	<i>Antenna Geometry</i>	131
5.3.2	<i>Design Considerations</i>	134
5.4	Conclusion	161
6	CONCLUSION AND FUTURE RESEARCH	163
6.1	Conclusion	163
6.2	Future research.....	166
	REFERENCES	168
	APPENDIX I: 3-D PRINTING	174
I-1.	FDM (Fused Deposition Modeling).....	174
I-2.	FTI (Film Transfer Imaging)	174
I-3.	Inkjet3-DPrinting.....	174
I-4.	Micro dispensing for conformal printing of conductive layout	174
I-5.	Poly Jetting_ Photo polymer based.....	175
I-6.	Selective Heat Sintering (SHS).....	175
I-7.	Stereo Lithography Apparatus (SLA) PhotoPolymerBased	175
I-8.	Selective Laser Melting (SLM) and Selective Laser Sintering (SLS)....	175
I-9.	Robotic dispensing on 3-D objects	176

List of Tables

Table 4-1. Dimensions of our proposed microstrip fed 3-D folded cubic slot antenna	86
Table 4-2. Dimension of proposed antenna for 2.4GHz	94
Table 4-3. Dimension of Antenna Structure reported in Fig. 4-18 (a).....	101
Table 5-1. Definition of Design Parameters in Antenna Structure	111
Table 5-2. Dimension of proposed antenna for 2.44GHz	112
Table 5-3. Definition of Design Parameters in Antenna Structure.	133
Table 5-4. description for Different deviation from baseline cubic antenna Fig. 5-28	140
Table 5-5. Dimensions of Antenna Structure.....	146

List of Figures

Fig. 2-1 a) Geometry of cubic antenna reported by Nassar et al. In [14], b) Geometry of complete FDR design reported in [15] (Top left: 3-D view. Top right: top view. Bottom: fabricated 2.4-/4.8-GHz FDR) 9

Fig. 2-2 Geometry of Cubic antennas proposed by Kruesi et al [20]., a) Evenly symmetric Cube, b) oddly symmetric Cub, and c) manufactured through inkjet printing on paper..... 10

Fig. 2-3 Geometry of cubic antenna reported in [13]..... 11

Fig. 2-4 Geometry of cubic antenna designed and manufactured in [22] from cardboard..... 11

Fig. 2-5 Geometry of the antenna designed and manufactured in [23]..... 11

Fig. 2-6 Geometry of the antenna reported in [24] 12

Fig. 2-7 Invented ultra-small folded cubic strip antenna [25]..... 12

Fig. 2-8 Realized 6-sector antenna, without (a) and with (b) the upper substrate, c) Folded Vivaldi antenna[26] 12

Fig. 2-9 Characteristic modes of TM_{10} antenna with and without offset pitches. Circles represent current nulls 13

Fig. 2-10 a) A 4-arms TM_{10} monopole [27], and b) Hybrid architecture (H8) [28]. 13

Fig. 2-11 a) outer-wall loop antenna, and b) measurement setup proposed in [30]. 13

Fig. 2-12 Three-dimensional current distribution of a slot antenna (Right figure) and loop antenna(Left figure) presented in [36], (a) and (d) Longitudinal-directed equivalent magnetic current distribution, (b) and (e) Transversal -directed equivalent magnetic current distribution, c) and (f) Configuration of the antenna with a CPW feed [36] 14

Fig. 2-13 a) Illustration of the impedance scaling with the number of the slots presented in [38], and b) Quasi-Optical Amplifier 4×4 Array proposed in [39]. 15

Fig. 2-14 Polarization reconfigurable antenna reported by Yue Li et al. in [47]. 16

Fig. 2-15 a) Schematics of the pattern reconfigurable U-slot antenna, b) Photograph of the pattern reconfigurable U-slot antenna [48]..... 16

Fig. 2-16 Antenna reported in [49]	17
Fig. 2-17 Photographs of the antenna proposed in [50]. (a) Top view. (b) Bottom view.....	17
Fig. 2-18 Simulation of proposed antenna, a) Four active pairs: uniform current distribution and omnidirectional beam, and b) Single active pair: one active element and directional beam, c) Layout of proposed antenna [44]	17
Fig. 2-19 Antenna presented in [43], a) Top view, b) Bottom view, c) Side view, d) Antenna dimension	18
Fig. 2-20 Reconfigurable Cubic Antenna reported in [46]	19
Fig. 2-21 Constructed antenna: (a) rear view and (b) side view, c) Bias Network [52].....	19
Fig. 2-22 Conformal 3-D printing of Antennas on hemisphere by J. T. Bernhard [57].....	20
Fig. 2-23 3-D printed electronic circuit by Macdonald et al. in [4]	21
Fig. 2-24 3-D printing electronics offered by Nscrypt [58].....	21
Fig. 2-25 3-D printed Antenna by Nasser et al. reported in a) [19], and b) [18] .	22
Fig. 2-26 LDS process introduced by LPKF for mass production of 3-D printing electronics [59]–[61].....	22
Fig. 2-27 cellphone antenna fabricated by pad printing [62], [63]	22
Fig. 2-28 Multi- SIR based N bit chipless RFID integrating humidity sensing proposed in [64].....	23
Fig. 2-29 Configuration of antenna and sensor, a) Triangular microstrip patch antenna with sensor, b) Capacitive ethylene sensor [65].....	23
Fig. 2-30 (a) Second configuration of RFID sensor with 3- bit code of (110), (b) (Sensor) capacitor integrated at the end of the transmission line, and c) Schematic illustration of code generation using reflected pulses, in PPM representation [66]	24
Fig. 3-1 Structure of slot antenna with infinite ground plane (CST open Boundaries touched ground plane).....	26
Fig. 3-2 Slot with infinite ground plane, a) Input matching, b) ϕ polarized directivity at 2.45GHz in the azimuth plane, and c) ϕ polarized directivity of antenna at 2.45GHz in 3-D space	27

Fig. 3-3 Slot antenna with finite ground plane, a) structure, and b) Input matching	28
Fig. 3-4 Total directivity of slot antenna at 2.45GHz on finite ground plane, a) GW=50mm, and b) GW=100mm	28
Fig. 3-5 Total directivity of slot antenna at 2.45GHz on finite ground plane, a) GW=150mm, and b) GW=200mm	29
Fig. 3-6 Slot folded in X direction	30
Fig. 3-7 Input reflection coefficient of slot antenna on folded finite ground plane for various GW	31
Fig. 3-8 Total directivity of slot antenna at 2.45GHz on folded finite ground plane, a) GW=50, b) GW=100mm, and c) GW=150mm	32
Fig. 3-9 Bending slot in the direction perpendicular to slot axis and studying GW variation for GWZ=120mm, a) ϕ polarized directivity at 2.44GHz in $\phi=90^\circ$ plane, b) ϕ polarized directivity at 2.44GHz in $\theta=90^\circ$ plane, and c) Input reflection coefficient.....	34
Fig. 3-10 Slot folded in both X and Z direction.....	35
Fig. 3-11 Bending slot in the direction perpendicular to slot axis and studying GW variation for GWZ=80mm, a) ϕ polarized directivity at 2.44GHz in $\phi=90^\circ$, b) ϕ polarized directivity at 2.44GHz in $\theta=90^\circ$, and c) Input reflection coefficient	36
Fig. 3-12 Folding ground plane in slot's axial direction and studying GWZ variation for GW=120mm, a) ϕ polarized directivity at 2.44GHz in $\phi=90^\circ$ plane, b) ϕ polarized directivity at 2.44GHz in $\theta=90^\circ$ plane, and c) Input reflection coefficient.....	38
Fig. 3-13 Folding ground plane in slot's axial direction and studying GWZ variation for GW=80mm, a) ϕ polarized directivity at 2.44GHz in $\phi=90^\circ$ plane, b) ϕ polarized directivity at 2.44GHz in $\theta=90^\circ$ plane, and c) Input reflection coefficient.....	39
Fig. 3-14 Folded slot antenna.....	40
Fig. 3-15 Folding slot in slot's axial directions and studying GWZ variation for GW=120mm, a) ϕ polarized directivity at 2.44GHz in $\phi=90^\circ$ plane, b) ϕ polarized directivity at 2.44GHz in $\theta=90^\circ$ plane, and c) Input reflection coefficient.....	42
Fig. 3-16 Folding slot in slot's axial directions and studying GWZ variation for GW=80mm, a) ϕ polarized directivity at 2.44GHz in $\phi=90^\circ$ plane, b) ϕ polarized directivity at 2.44GHz in $\theta=90^\circ$ plane, and c) Input reflection coefficient	43

Fig. 3-17 Folded slot antenna on a cubic structure	45
Fig. 3-18 Analyticaly calculated normalized directivity at 2.45GHz of a folded slot antenna for SL=61.25mm, GWZ=60mm, SW=1mm, GW=39.5mm and $a=GW/2$, (3dB Beam width for E_ϕ at elevation plane=78°)	50
Fig. 3-19 Analyticaly calculated normalized directivity at 2.45GHz of a folded slot antenna for SL=61.25mm, GWZ=30mm, SW=1mm, GW=39.5mm and $a=GW/2$, (3dB Beam width for E_ϕ at elevation plane=84°)	50
Fig. 3-20 Folded slot antenna on a cubic structure, a) folded slot antenna, ad b) Straight slot antenna.....	51
Fig. 3-21 Normalized directivity at 2.45GHz obtained through EM simulation for a folded slot antenna shown in with SL=73.5mm, GWZ=40mm, SW=1mm, GW=125mm and $a=GW/2$, a) elevation plane, and b_) Azimuth plane (3dB Beam width for E_ϕ at elevation plane=112.5°)	51
Fig. 3-22 Normalized directivity at 2.45GHz obtained through EM simulation for a folded slot antenna shown in with SL=73.5mm, GWZ=100mm, SW=1mm, GW=125mm and $a=GW/2$, a) elevation plane, and b_) Azimuth plane (3dB Beam width for E_ϕ at elevation plane=75.5°)	52
Fig. 3-23 Figure from a book which shows circular array configuration, a) source local coordinate, and b) far field coordinate at observation point (courtesy of [67])	53
Fig. 3-24 Theoretical Array Factor of a basic 2.445GHz circular uniform array for a) $a = \lambda 4$, and b) $a = \lambda 8$	54
Fig. 3-25 Configuration of circular array with directive antenna elements (Courtesy of [69])	55
Fig. 3-26 Top view of our proposed array analyzed as a circular array.....	57
Fig. 3-27 Contribution of neighboring elements in array factor over the entire observation angles in the azimuth plane.	58
Fig. 3-28 Circular array made of four slot antenna elements.....	60
Fig. 3-29 Input reflection coefficient of slot antenna circular array for radius of 50, 55, 75mm	60

Fig. 3-30 Circular antenna array for $a=75\text{mm}$, a) Total directivity at 2.45GHz in 3-D space, b) Total directivity at 2.45GHz in $\theta=90^\circ$ plane, and c) Total directivity at 2.45GHz in $\phi=0$ plane 61

Fig. 3-31 Circular antenna array for $a=55\text{mm}$, a) Total directivity at 2.45GHz in 3-D space, b) Total directivity at 2.45GHz in $\theta=90^\circ$ plane, and c) Total directivity at 2.45GHz in $\phi=0$ plane 62

Fig. 3-32 Circular antenna array for $a=50\text{mm}$, a) Total directivity at 2.45GHz in 3-D space, b) Total directivity at 2.45GHz in $\theta=90^\circ$ plane, and c) Total directivity at 2.45GHz in $\phi=0$ plane 63

Fig. 3-33 Multi-feed cubic slot circular array excited through lamped ports 64

Fig. 3-34 Analytically calculated normalized directivity of a circular folded slot antenna array at 2.45GHz for $SL=73.5\text{mm}$, $GWZ=70\text{mm}$, $SW=1\text{mm}$, $GW=39.5\text{mm}$ and $a=GW/2$, (3dB Beam width for E_ϕ at elevation plane= 84°)..... 66

Fig. 3-35 Analytically calculated normalized directivity of a circular folded slot antenna array for $SL=73.5\text{mm}$, $GWZ=40\text{mm}$, $SW=1\text{mm}$, $GW=39.5\text{mm}$ and $a=GW/2$, (3dB Beam width for E_ϕ at elevation plane= 92°) 66

Fig. 3-36 Normalized directivity obtained through EM simulation for a circular folded slot antenna array shown in Fig. 3-33 at 2.45GHz for $SL=73.5\text{mm}$, $GWZ=40\text{mm}$, $SW=1\text{mm}$, $GW=39.5\text{mm}$ and $a=GW/2$, a) Elevation plane when all elements are excited in phase , and b) Azimuth plane when all elements are excited in phase (3dB Beam width for E_ϕ at elevation plane= 82.5°)..... 67

Fig. 3-37 Normalized directivity obtained through EM simulation for a circular folded slot antenna array shown in Fig. 3-33 at 2.45GHz for $SL=73.5\text{mm}$, $GWZ=100\text{mm}$, $SW=1\text{mm}$, $GW=39.5\text{mm}$ and $a=GW/2$, a) Elevation plane when all elements are excited in phase , and b) Azimuth plane when all elements are excited in phase (3dB Beam width for E_ϕ at elevation plane= 91.5°)..... 68

Fig. 3-38 Circular array geometry used for coupling simulation, $GW=100\text{mm}$, $GWZ=300\text{mm}$, $SlotL=73.5\text{mm}$, and $SlotW=1\text{mm}$, a) slot antenna element, and b) circular array 69

Fig. 3-39 Magnitude of coupling between, a) slot 1 and 2 (neighbors), and b) slot 1 and 3 (facing each other)..... 71

Fig. 3-40 Phase of coupling between, a) slot 1 and 2 (neighbors), and b) slot 1 and 3 (facing each other)	72
Fig. 3-41 folded slot antenna, structure 1 CPW feed	73
Fig. 3-42 CPW fed planar annular slot antenna	74
Fig. 3-43 CPW fed planar annular slot antenna	74
Fig. 3-44 CPW fed planar annular slot antenna	75
Fig. 3-45 Microstrip fed planar folded slot antenna.....	75
Fig. 3-46 Magnetic current and electric field on Microstrip fed planar folded slot antenna	76
Fig. 3-47 3-D folded slot antenna array structure, a) singlemode structure on FR4 substrates, and b) Reconfigurable structures on Rogers	77
Fig. 3-48 Nominal magnetic current and electric field on 3-D folded slot antenna array	77
Fig. 3-49 3-D annular ring slot antenna with single feed, a) nominal magnetic currents and electric fields, and b) cubic structure	78
Fig. 3-50 3-D folded microstrip fed slot antenna, a) nominal magnetic currents and electric fields, and b) cubic structure	78
Fig. 4-1 Folded Slot Antenna (a) Planar 2D , (b)3-D Cubic.....	84
Fig. 4-2 (a) Geometry of antenna, and (b)Microstrip feeding.....	85
Fig. 4-3 , Parameter study (a) Input reflection coefficient Vs. Width of slot, (b) Radiation Pattern vs. Width of slot, and (c) Radiation Pattern Vs. Extended length of slot on top face of cube	87
Fig. 4-4 Effect of potential electronic circuit modeled by a PEC box in pink on antenna performance (a) Intensity of Electric field in logarithmic scale, and (b) Far field radiation pattern.	88
Fig. 4-5 (a) PCB fabrication, and (b) 3-D printing.	88
Fig. 4-6 Input reflection coefficient	89
Fig. 4-7 Gain of proposed microstrip fed 3-D folded cubic slot antenna at 2.44GHz through far field Measurement Vs. Simulation results.	90
Fig. 4-8 Notional tangential electric field and magnetic current distribution of a) planar annular slot antenna, b) proposed 3-D folded annular ring slot antenna	92

Fig. 4-9 a) Antenna geometry, b) CPW feeding configuration.....	93
Fig. 4-10 Input reflection coefficient acquired through measurement vs. simulation results	94
Fig. 4-11 Antenna gain patterns acquired through measurement at 2.44GHz vs. simulation results	95
Fig. 4-12 Input reflection coefficient of antenna versus width of slot.....	96
Fig. 4-13 Co and cross polarization directivity for different slot widths at 2.44GHz	96
Fig. 4-14 Intensity of E-field at 2.44GHz in presence of circuits modeled by a PEC plate.....	98
Fig. 4-15 Fabricated antenna.....	99
Fig. 4-16 Measurement set-up.....	99
Fig. 4-17 Designing antenna based on nominal magnetic current and electric field distribution.	100
Fig. 4-18 3-D antenna geometry and its feeding architecture. a) Proposed 3-D folded slot antenna array, b) Differential and common electric field on CPW line and radiator slots.....	101
Fig. 4-19 Current distribution of 3-D structure, a) Vertical sides, and b) Top/Bottom side	103
Fig. 4-20 Prototype manufacturing, a) Flattened open cube view, and b) 3-D fabricated cube	103
Fig. 4-21 Radiation Pattern Measurement Setup at three orthogonal planes in Far field Antenna Measurement Chamber, a) XZ, b) XY, and c) YZ	104
Fig. 4-22 Input reflection coefficient of the proposed antenna.....	104
Fig. 4-23 Antenna gain in Elevation and Azimuth cuts at 2.45GHz.....	105
Fig. 5-1 a) Antenna Geometry, b) Current distribution when one antenna is excited	110
Fig. 5-2 Input reflection coefficient of a single folded slot obtained from full wave simulation.....	113
Fig. 5-3 Magnitude of coupling between slot antennas on cube faces obtained from full wave simulation.....	113

Fig. 5-4 Phase of coupling between slot antennas on cube faces obtained from full wave simulation	113
Fig. 5-5 Total realized gain of antenna at 2.44GHz in case only slot 1 is excited, a) Realized Gain, b) Directivity	114
Fig. 5-6 Total realized gain of antenna at 2.44GHz in case two slots are excited slot1 and slot 2, a) Realized Gain, b) Directivity.....	114
Fig. 5-7 Total realized gain of antenna at 2.44GHz in case three slots are excited slot4, slot1 and slot 2, a) Realized Gain, b) Directivity.....	115
Fig. 5-8 Total realized gain of antenna at 2.44GHz in case all slots are excited for an omnidirectional radiation pattern, a) Realized Gain, b) Directivity.....	115
Fig. 5-9 Pattern Flatness at Azimuth plane	116
Fig. 5-10 Correlation Coefficient in dB scale for two ports excitation obtained from full wave simulation.....	116
Fig. 5-11 Diversity Gain in dB scale for two ports excitation obtained from full wave simulation	117
Fig. 5-12 Input matching vs width of slot.....	118
Fig. 5-13 Coupling versus width of slot, a) Magnitude, and b) Phase.....	119
Fig. 5-14 Co pol directivity vs width of slot, a) Azimuth plane, and b) Elevation plane.....	120
Fig. 5-15 Input matching versus cube size (GW)	121
Fig. 5-16 Coupling versus cube size (GW) at 2.44GHz, a) Magnitude, and b) Phase	122
Fig. 5-17 Co pol directivity vs size of cube (GW) at 2.44GHz, a) Azimuth plane, and b) Elevation plane	123
Fig. 5-18 Input matching vs total length of slot antenna, a) S11, and b) smith chart	125
Fig. 5-19 Coupling between antennas vs total length of slot antenna at 2.44GHz, a) Magnitude, and b) phase.....	126
Fig. 5-20 Co pol directivity vs total length of slot antenna (SlotL) at 2.44GHz, a) Azimuth plane, and b) Elevation plane.....	127
Fig. 5-21 Input matching versus length of open circuit stub.....	128

Fig. 5-22 Coupling between antennas vs length of stub at 2.44GHz, a) Magnitude, and b) phase 129

Fig. 5-23 Co pol directivity vs total length of stub (StubL) at 2.44GHz, a) Azimuth plane, and b) Elevation plane..... 130

Fig. 5-24 Antenna structure including switches, a) Perspective view, and b) Top view..... 132

Fig. 5-25 T-shaped flattened view of cubic antenna in slot array mode. Top and bottom faces are designated with T and B respectively. Arrows are for the purpose of illustrating how different faces are folded against the edges to make the final cube antenna. Also, the middle part of the figure is enclosed by a dashed red rectangle to highlight the top and bottom faces connection to the $-Y$ face of the cube where the CPW feeding is accommodated. 134

Fig. 5-26 Designing antenna based on nominal magnetic current and electric field distribution. 136

Fig. 5-27 Electric field intensity over 2D folded slots 137

Fig. 5-28 Different deviation from baseline cubic antenna..... 139

Fig. 5-29 Total normalized electric field at 2.44GHz at different Z planes inside cube 142

Fig. 5-30 Total normalized electric field at 2.44GHz at different XY locations inside cube 143

Fig. 5-31 Antenna excitation modes using CPW transmission line, (a) common mode slot pair, and (b) differential mode slot pair..... 145

Fig. 5-32 Fabrication process 146

Fig. 5-33 Fabricated antenna (a) mode 1, (b) mode 2 147

Fig. 5-34 Input reflection coefficient, (a) mode1, (b) mode 2 148

Fig. 5-35. Realized gain from Simulation vs measurement at 2.44GHz, a) mode 1, and b) mode2..... 149

Fig. 5-36. Current distribution on the excited face of the cube..... 150

Fig. 5-37. Surface current distribution over conductive parts of the cube at 2.44GHz 150

Fig. 5-38. Magnetic current distribution over slots at 2.44GHz 151

Fig. 5-39. Current distribution on -Y face in patch mode at 2.44GHz 151

Fig. 5-40. Current distribution on cube antenna in patch at 2.44GHz 152

Fig. 5-41 Characteristic impedance and guided wavelength in a microstrip slot vs. slot width for relative permittivity of 3 and substrate thickness of 1.55mm 153

Fig. 5-42 Mode1 parameter study for width of slot, (a) Co pol directivity at 2.44GHz in the azimuth plane $\theta = 90$, and (b) S11 154

Fig. 5-43 Mode 1 Parameter study on cube size (GW), (a) Co-pol directivity at 2.44GHz in the azimuth plane $\theta=90$, and (b) S11..... 156

Fig. 5-44 Input reflection coefficient variation versus cube height in mode 1 ... 157

Fig. 5-45 Antenna parameter variation at 2.44GHz versus cube height in mode 1 157

Fig. 5-46 Mode 2: SlotWZ parameter study, (a)Co-pol directivity at 2.44GHz in $\varphi=0$ plane, (b)Co-pol directivity at 2.44GHz in $\varphi=90$ plane, (c) S11..... 158

Fig. 5-47 Input reflection coefficient variation versus cube height in mode2 160

Fig. 5-48 Antenna parameter variation at 2.44GHz versus cube height in mode 2 160

Fig. 5-49 Input reflection coefficient variation versus stub length SCZ, (a) mode 1, (b) mode 2 161

Chapter 1

1 Introduction

Wireless communication, originally introduced for professional and expensive communication between organizations, recently found its application almost in all aspects of life as an undeniable replacement for wired connection even in low cost and trivial matters. Changing the application of wireless communication affects the market demand and subsequently alters the objective of designers and manufacturers from high efficiency, expensive and complicated devices to low cost, simple architectures. Simultaneously, manufacturing processes are getting evolved to lower the fabrication cost by introducing advanced methods. The trend of future electronics will be all in one step implementation and fabrication of devices, in which electronics, antennas, sensors and packages are built together.

Following this technology trend, novel architectures are designed and proposed especially in the field of electronic and microwave whose implementation might not be feasible with traditional fabrication devices, but with emerging manufacturing process, it

will be feasible. Among these advancements are new nano-technology fabrication and 3-D printing.

1.1 Why WSN

Sensor Network, a network of sensory nodes connected to a gateway to monitor specific parameters in the environment, has been introduced as a substantial change in human life and recently it is evolving to find even more applications in nature, bio, vehicular, and industrial areas. Establishing conventional wire connections between nodes and hub can be highly costly and very time consuming. Following the world trend toward wireless communication, in Wireless Sensor Network (WSN), wired telecommunication links have been replaced with wireless links to lower the installation and maintenance costs and improve the efficiency and capability of debugging. Generally, a WSN is a monitoring network consists of several nodes sensing the environment and communicating with a base station or a hub through a wireless link directly or through adjacent nodes to optimize the data communication routings [3]. Recently, WSN has found applications in almost every environment where there is high demand for low cost, durable and high performance sensory nodes. In order to offer WSN as a promising solution almost in all environments, massive research is conducted in the field. Due to the enormous number of sensory nodes in a wireless sensor network, any simplification in their architectures, manufacturing or installation dramatically alleviates the total cost and time of network implementation. In order to potentially improve the radiation performance and simplify the manufacturing process using low cost technologies such as 3-D printing [4], the antenna should be integrated into a package of a wireless device. On the other hand, employing antenna-packages with direction-insensitive radiation patterns facilitates installation and maintenance of the network leading to cost-efficient solutions. WSN can be setup in urban areas where multipath propagation is dominant as well as rural areas where nodes and hub are installed almost at the same height. As distribution of angle of arrivals is more concentrated around horizon in both environments, an omnidirectional radiation pattern in the azimuth plane would be preferred for terrestrial communications. However, in some specific application, there is a need to be able to switch between omnidirectional and directional patterns.

1.2 Why metallic package and conformal slot

In a variety of cases, WSN Wireless sensor nodes are among the devices which are exposed to harsh environmental conditions, such as strong electromagnetic interference or space application where dielectric surface charging is a concern. This accentuates the benefit of wireless hermetic and conductive packaging of telecommunication devices due to the protection it provides to the electronic circuits installed inside the cubic package against any outside interference. Additionally, not only the conductive surface of the cube acts as a protective shell against external electromagnetic interference (EMI) which guarantees the isolation of the device, but also the antenna could be mapped on the package to simplify production process and improve device performance. Furthermore, communicating in horizontal polarization through slot antennas carved in a package can lower the interference as most of the wireless devices use vertical polarization.

1.3 Why conformal slot antenna on cubic structures

Capability to be embedded in conductive plates and offering wide bandwidth comparing to conventional patch antennas make slot antennas the best choice for conformal antenna packages particularly for military applications where simple and low cost fabrication is a major concern [5].

Here, we map our proposed slot antenna on a cubic structure. The reason for this choice is because cubes are categorized as the most appropriate 3-D shapes for WSN node packages as they can meet all the following requirements at the same time; stability, symmetric structure and simple fabrication. Furthermore, the hollow interior cube volume can be reserved for future placement of transceivers and sensors.

1.4 Why 3-D structures

Although there is a vast history behind planar structures both in electronic circuits and antennas where they find their applications as the most convenient and traditional geometries, they do not necessarily use the available space efficiently and are not the best solutions. Planar antenna has limitation in fulfilling the requirements of wireless sensor

network as they can only offer a satisfactory performance if installed accurately. In WSN applications where often, antennas are tossed in a random direction, a planar antenna due to lack of compatibility is not capable of produce satisfactory results. Furthermore, in a dense urban environment full of obstacles where multipath fading is dominant, having a fixed directional beam is not beneficial, but an omnidirectional, isotropic or a reconfigurable radiation pattern proves to be more advantageous.

Recently, introducing low cost and reliable fabrication technologies in the market accelerated the trend toward designing 3-D architectures. Not even 3-D antennas, but also designing 3-D ICs by stacking up more layers of circuits to miniaturize the chips, are being considered as a serious alternative solution for advanced small and high-performance devices. Conventionally, considering the limitation of planar devices, antennas were designed and fabricated as a separate part of any telecommunication device unless in expensive military applications where conformal aperture antennas were curved on the body of missiles or aircrafts.

Here, we are proposing design and implementation of novel 3-D cubic antennas with interesting features and applications in the industry such as direction-insensitive radiation patterns and smart reconfigurable architectures to facilitate installation and maintenance of wireless sensor networks. Since antenna-packages are mainly intended for WSN applications, they are designed to cover the unlicensed 2.45GHz ISM frequency band to be compatible with most of WSN technologies such as Heart and ZigBee. We have reported microstrip 3-D folded slot antenna which has been used in most of our designs. In order to simplify the manufacturing procedure while improving the performance, folded slot antenna is patterned on a cube to offer a package for low cost wireless devices, like a WSN node, as well. Consequently, considering less labor-intensive installation and maintenance processes along with simpler fabrication procedure especially in advanced prototyping, the overall cost of the WSN made of 3-D cubic antennas is lower than the traditional networks. In another word for the same cost, a denser network can be implemented to acquire more accurate and reliable data from environment.

Furthermore, WSN nodes need to have an omnidirectional radiation pattern in the azimuth plane. The omnidirectional pattern is not only advantageous for rural service areas

where the possibility of line of sight is the highest, but also proves to be an ideal solution for urban environments due to its efficacy in multipath-fading reduction by maintaining a reasonably high gain around the azimuth plane, where more signal is arrived. Also, using horizontally polarized signal can lower the interference with frequently-used vertically polarized devices which leads to enhancement of the network performance. To facilitate the realization of omnidirectional radiation pattern, a 3-D symmetrical package such as sphere or cube must be used. However, a cubical configuration has better mechanical stability and therefore is the favorable choice.

1.5 3-D printing

Recently, 3-D printing electronic have been introduced as a good candidate for rapid prototyping of high frequency devices with industrial and space applications [6]–[9]. Proposed antenna-packages have potential for 3-D prototyping by 3-D printers and mass production from plastic cubes patterned by conductive layouts. In this research, to explore and verify using 3-D printing compatible materials, one cubic antenna prototype has been fabricated by the aid of Objet EDEN 3-D printer where its internal space has been reserved for placement of sensor and electronic circuits.

Employing printing technology in fabrication of planar electronic circuits has been started in the past decade and its application is extended recently by introducing inkjet conductive printing technology [10] and even semiconductor components together with the conductive layouts could be printed on flexible sheets [11]. Emerging of high resolution printers along with the availability of low loss materials like nanoparticle conductive inks, has made 3-D printing a promising and cost-efficient solution for the fabrication of high-frequency devices specially antennas on flexible sheets of environment-friendly materials. Low cost home fabrication of durable structures plays the key role in worldwide approval and applause of this new technology.

Moreover, in WSN applications where portable antenna packages are used in excessive numbers to improve the sensing accuracy, providing easy and low-cost table-top fabrication to reduce the required marketing time becomes extremely important. In view of the above concerns, we suggest 3-D printable antenna package, as the most effective

solution for applications in wireless sensor networks (WSN) since a metal package improves interference resistance and 3-D printing offers possibility of low-cost mass production.

1.6 Conclusion

My PhD project is focused on design, implementation and measurement of novel 3-D cubic antenna architectures compatible with 3-D printing electronics. The outline of this dissertation is as follows. In chapter 2, literature review is presented. Chapter 3 is dedicated to design, modeling and simulation of cubic antennas, folded slot and circular arrays. In chapter 4, design and fabrication of three configurations of 3-D printable cubic slot antenna with omnidirectional radiation pattern are presented. These structures offer omnidirectional horizontally polarized radiation pattern with which is a very significant feature in comparison to common vertically polarized antennas in advanced communication. The material presented in this chapter are either published [1], [2]. or submitted for publication. In chapter 5 we elaborate on design and implementation of two printable cubic structures with reconfigurable radiation patterns. These structures are also fully analyzed, fabricated and measured. The outcome of this chapter resulted in two publications on reconfigurable antennas where one is already submitted and the other one will be submitted in near future. Finally, in chapter 6 we have summarized our conclusion and provided some ideas which would hopefully open new research fronts for the interested reader to follow up this work in the future.

Chapter 2

2 Review of Literature

2.1 Introduction

In my PhD thesis, design, fabrication and measurement of a variety of 3-D cubic antennas mostly designed based on 3-D folded microstrip slot antenna have been investigated. Hence, in this chapter we review most of 3-D antennas published till now, as well as planar slot antennas and pattern reconfigurable antennas as two major fundamentals in our works. Additionally, we review 3-D printing electronics to cover our implementation. Antenna sensors are reviewed here as well because they can be a good extension of our current work in the future.

2.2 3-D Antennas

Prior to introducing printed circuit boards which integrate all electronic circuits and components as well as planar antennas, 3-D bulky antennas were prominent technologies both in military radars or Radio/TV broadcasting. These high power antennas were used in conjunction with waveguide structures and usually offer high gain and performance [12].

So, even concept of 3-D antennas made of conductive metals is not something new at all, extending 2D planar antenna designs to 3-D ones is a novel field of research recently highlighted because of state of the art fabrication methods offered by 3-D multi material printers. In some cases the 3-D structure can even be used as package to simplify the device implementation as well [13]. In this section, most recent 3-D cubic or spherical architecture reported by researchers have been reviewed. They are mostly based on folded dipoles.

In Fig. 2-1(a), the 3-D antenna reported by Nassar et al. in [14] has been illustrated. Their proposed antenna operates at 2.4GHz with application in narrow band wireless sensor network. The authors attempted to approach the Chu limit by lowering Ka^1 through using high dielectric material at the expense of lowering gain and efficiency. They have patterned a meandered dipole antenna on a semi-cube structure and reserved the interior for placement of sensor and electronic circuits. The antenna is excited through a balanced-to-imbalance line transition on the third side of the structure. Efficiency and gain measurement were done using Wheeler Cap, and 3-antennas method, respectively. Furthermore, they have suggested Direct-write printing techniques to deposit conductor on flexible and non-planar surfaces in mass production [14]. In cubic antennas, due to unequal or out of phase radiation from antenna elements on vertical faces of cube, obtaining a ripple free and pure omnidirectional radiation pattern from 3-D folded antenna is challenging. 3-D folded meander dipole antenna published in [14] has a semi omnidirectional pattern, but it is orientation sensitive because of 5dB ripple in its radiation pattern in azimuth plane [14].

Adding a 4.8GHz dipole antenna passing through a diode doubler as a passive second harmonic generator to the architecture, they have reported a compact 3-D Harmonic repeater with application in passive wireless sensing as shown in Fig. 2-1(b) [15]. Their reported repeater operates by receiving a 2.4GHz signal with power of -30 to -20dBm and re-radiating a 4.8GHz signal with conversion gain of -13.3 dB. Additionally, they have proposed a new approach for remote calibration of passive sensors using orthogonal polarization of the interrogation signal in their paper for determination of path loss between

¹ Ka used in defining Chu limit, is wave number times the radius of the spherical volume circumscribes the antenna

the interrogator and the remote node [15]. Their design can be fabricated by the aid of modern 3-D printing technologies as well [16]–[19].

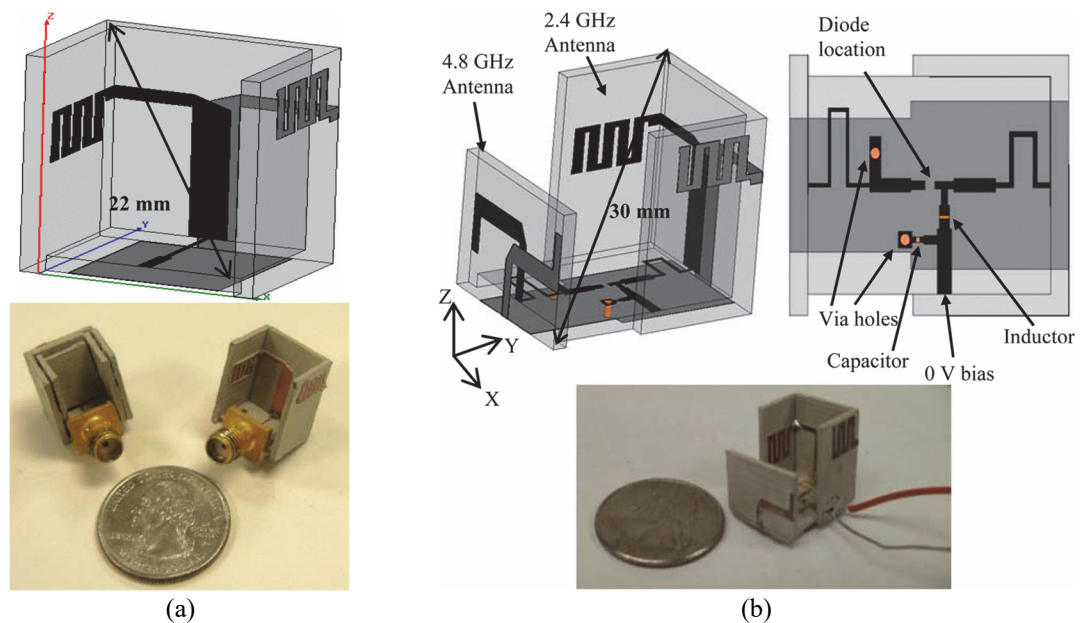


Fig. 2-1 a) Geometry of cubic antenna reported by Nassar et al. in [14], b) Geometry of complete FDR design reported in [15] (Top left: 3-D view. Top right: top view. Bottom: fabricated 2.4-/4.8-GHz FDR)

In [20] and [21], Tentzeris et al. reported a novel 3-D cubic antenna with omnidirectional radiation pattern employing two dipole antennas folded over the surface of a cube, one as a driver and the other one as a director excited through parasitic coupling. The antenna was designed at 902 MHz-928 MHz (centered at 915 MHz) to be compatible with UHF RFID application. Edge length of their reported cubic antenna is 3 cm or $\lambda/11$. Sensor equipment and related electronic circuits can be placed inside the cube and they have named this feature as smart packaging. Their proposed architecture has been prototyped on six planar sides of a liquid crystal polymer (LCP) substrate, and then folded into a cube. As shown in Fig. 2-2, they have designed two structures, based on even and odd symmetry between two poles of the driver or parasitic dipoles and manufactured them by the aid of conductive inkjet printing of paper folded into a cube. Low-cost weather tracking especially in turbulent scenarios, such as tornadoes has been suggested as a main application of this architecture if it will be designed at WSN operating frequency. The folded dipole antenna with semi isotropic radiation pattern reported in [20], [21] is still suffering from lack of symmetry in azimuth plane at $\theta = 90$ because driver and parasitic

dipoles do not radiate exactly in-phase and equal. However, they could achieve pure direction insensitive pattern in elevation planes.

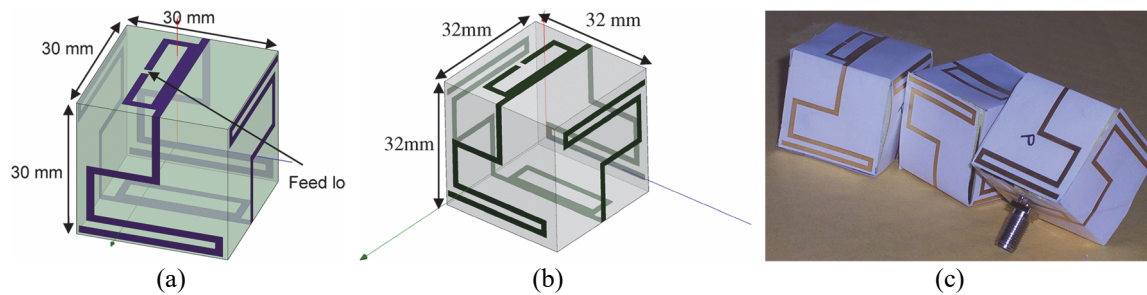


Fig. 2-2 Geometry of Cubic antennas proposed by Kruesi et al [20]., a) Evenly symmetric Cube, b) oddly symmetric Cub, and c) manufactured through inkjet printing on paper

In [13], Enayati et al. reported their architecture named as e-CUBE as a packaging solution for wireless sensor network nodes working at 17.2GHz K band frequency. As shown in Fig. 2-3, eight dipole antennas have been placed on vertical faces of a cube as a circular array with uniform excitation through power dividers to achieve a dipole like radiation pattern with vertical polarization. The package made by bonding PCBs together can contains all the electronics inside, without interfering with the radiated power. Employing required phase shifters and switches, their architecture can be extended to an antenna with steerable radiation pattern.

In [22], Monti et al. presented a novel Radio Frequency Identification (RFID) reader antenna with omnidirectional radiation pattern and a circular polarization. This antenna consists of four patch antennas placed on the lateral faces of a cardboard cube. The antenna has been designed to operate at frequency range of European UHF RFID systems [860 MHz, 870 MHz] [22].

In [23], Shamim et al. reported a 3-D cubic antenna with near isotropic radiation pattern at 2.4GHz with application in wireless sensor networks shown in Fig. 2-5. Their proposed antenna has been designed by folding a 1.5λ dipole antenna around a cube with edge length of 13mm which is 0.1λ . They have printed the antenna on a paper substrate from conductive ink and embedded the electronic circuits inside the cube to prove that antenna performance is not affected by the presence of embedded circuits [23].

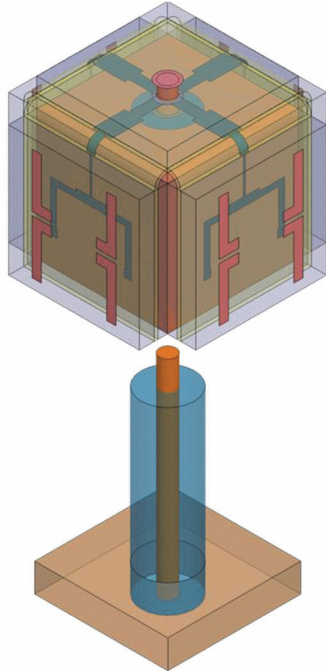
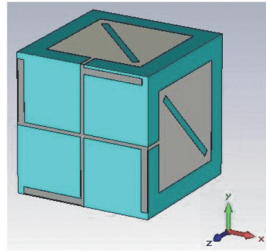
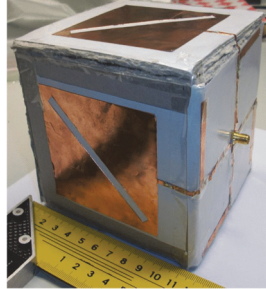


Fig. 2-3 Geometry of cubic antenna reported in [13]

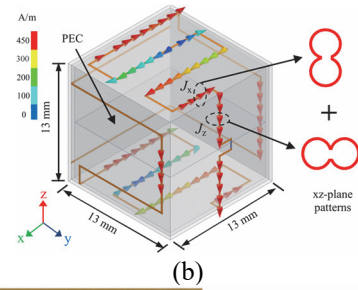


(a)

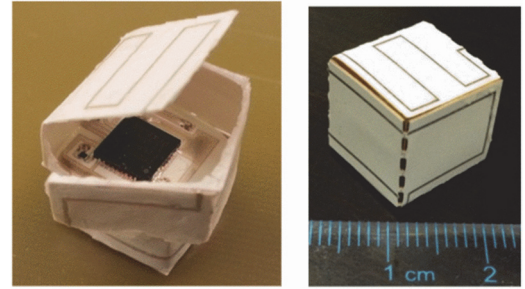


(b)

Fig. 2-4 Geometry of cubic antenna designed and manufactured in [22] from cardboard



(b)



(b)

Fig. 2-5 Geometry of the antenna designed and manufactured in [23]

As shown in Fig. 2-6 S. Nikolaou et al. [24], reported a folded dual monopole antenna patterned on two faces of a 1cm^3 box, one “fat” wideband monopole operating at 6.5GHz uplink band and one folded monopole operating at 2.4 GHz ISM band for downlink, both use common feed. The sensor IC is embedded inside the cube. Despite their claim of achieving near isotropic radiation pattern, the measured radiation pattern is distorted due to non-planar shape of the antenna [24].

In [25], Q. Rao et al. reported an ultra-small cubic folded antenna with application in handset devices shown in Fig. 2-7. This antenna was designed by wrapping a wire or strip around a cube in order to achieve desired radiation pattern and bandwidth. Additionally, they claimed that volume of their proposed antenna is very small compared to traditional PIFA design and its performance is higher [25].

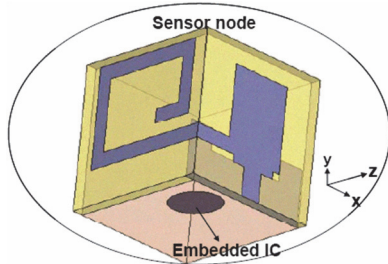


Fig. 2-6 Geometry of the antenna reported in [24]

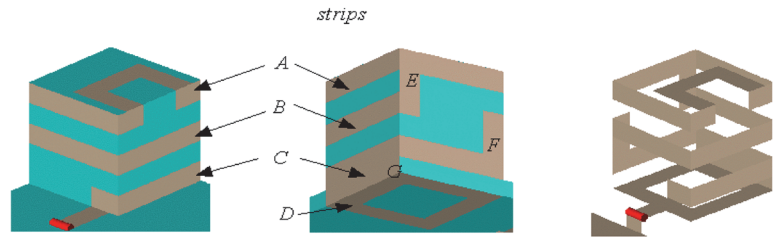


Fig. 2-7 Invented ultra-small folded cubic strip antenna [25].

In [26], Tong et al. reported a novel folded Vivaldi antenna and employed it in a 3-D low-profile 6-sectors MIMO antenna system with application in home networking at 5 GHz WLAN band made of FR4 as shown in Fig. 2-8. In order to improve the isolation between contiguous sectors, they put orthogonal polarized sectors in contiguous sections [26].

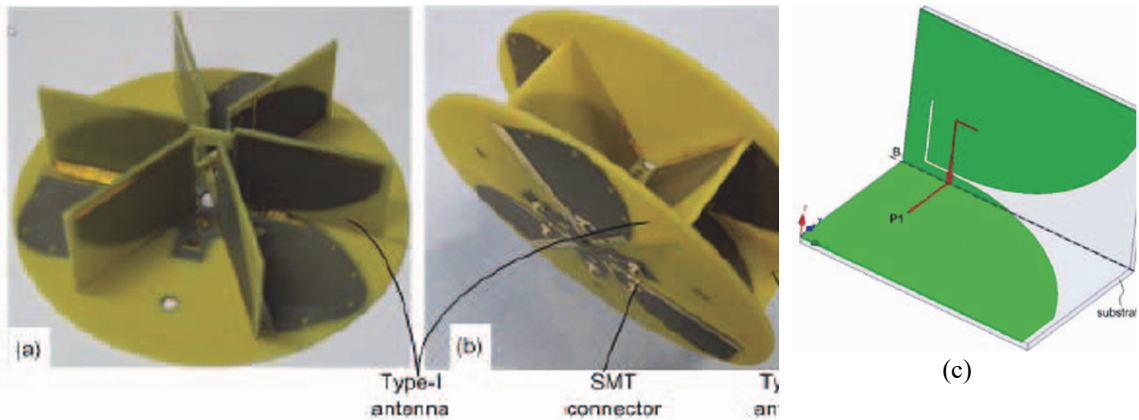


Fig. 2-8 Realized 6-sector antenna, without (a) and with (b) the upper substrate, (c) Folded Vivaldi antenna [26]

In [27], Bernhard et al. used characteristic mode theory to analyze and design a multi-resonance mode TM_{10} antenna to double its bandwidth. Using different pitches at antenna adjacent arms as shown in Fig. 2-9, they matched multiple non radiating anti-resonance modes rather than resonance modes to keep the radiation pattern unaffected while achieving higher bandwidth [27]. In [28], they have proposed a hybrid geometry shown in Fig. 2-10-b which has an efficiency similar or better than the spherical helix, first reported by Steven R. Best in [29], and impedance matching as easy as spherical meander antenna proposed in [27]. All three architectures were fabricated via conformal printing on hemispherical substrates by conductive inks [28] and their efficiency, Q, and matching were compared.

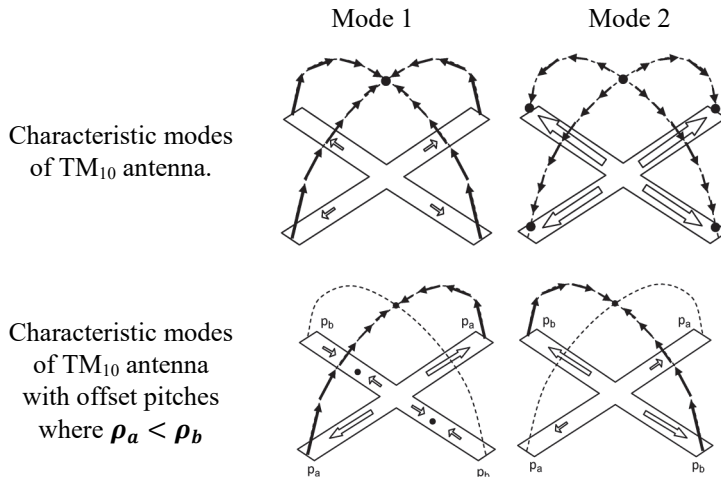


Fig. 2-9 Characteristic modes of TM_{10} antenna with and without offset pitches. Circles represent current nulls

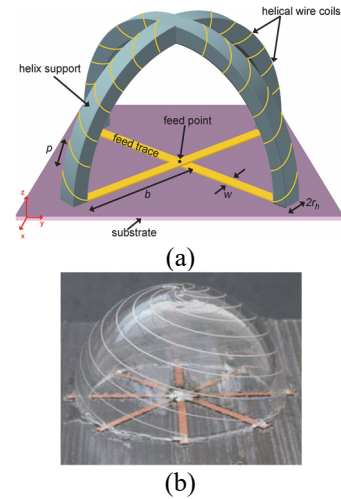


Fig. 2-10 a) A 4-arms TM_{10} monopole [27], and b) Hybrid architecture (H8) [28].

In [30], Yun et al. reported a conformal meander line loop antenna shown in Fig. 2-11 printed on outer body of a capsule with application in capsule endoscopy to efficiently use the capsule's outer surface and achieve higher gain and higher bandwidth of 260MHz (from 370 to 630 MHz) respect to inner antennas. They have reported antenna efficiency of 43.7% (-3.6 dB) when identical antenna pairs in the equivalent body phantom fluid are used in the measurement [30].

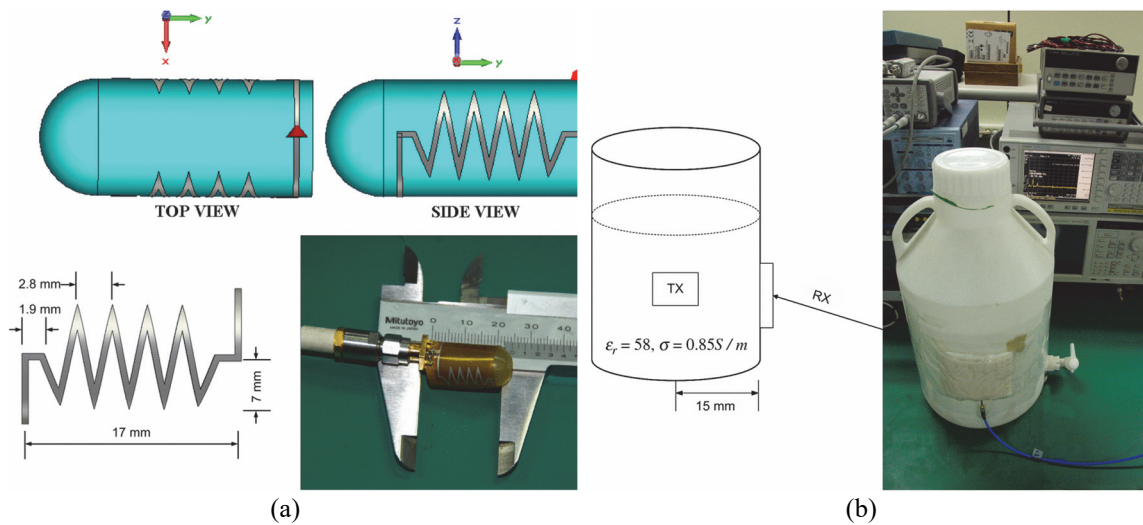


Fig. 2-11 a) outer-wall loop antenna, and b) measurement setup proposed in [30].

2.3 Slot antennas

Slot line on dielectric substrate is a popular transmission line for many microwave and mm-wave applications [31]–[33]. Slot antennas is a dual for dipole antennas on planar substrate with some advantages to the dipole like broader bandwidth and orthogonal polarization. The antenna can be excited through a microstrip line beneath the slot or a differential or coaxial line connected to the edges of slot. The feeding point can have an offset from center for proper impedance matching [5]. Appropriate model in obtaining the input impedance of the microstrip fed slot antenna has been developed and reported by researchers such as Mirshekar et al. [34]. Hermans et al. proposed an equivalent circuit for slot antenna by application of the Lorentz reciprocity theorem and its parameters are determined with the aperture theory [35]. Alternatively, slot antennas can be excited through a coplanar waveguide line at the same layer which need a configuration simpler than microstrip feeding [36]. The slot antenna can be a ring annular slot or a simple half wavelength antenna if proper matching has been fulfilled as investigated by Alexopoulos et al. and shown in Fig. 2-12 [36]. Zhu et al. in [37] developed a complete circuit model for microstrip-fed slot radiator. They introduced “short and open calibration” (SOC) method which let us calibrate (or de-embed) results of a full-wave MoM. Their network modeled the slot as a series complex impedance standing for the radiating slot and a pair of shunt capacitances. Their proposed model can be applied to both narrow and wide slots.

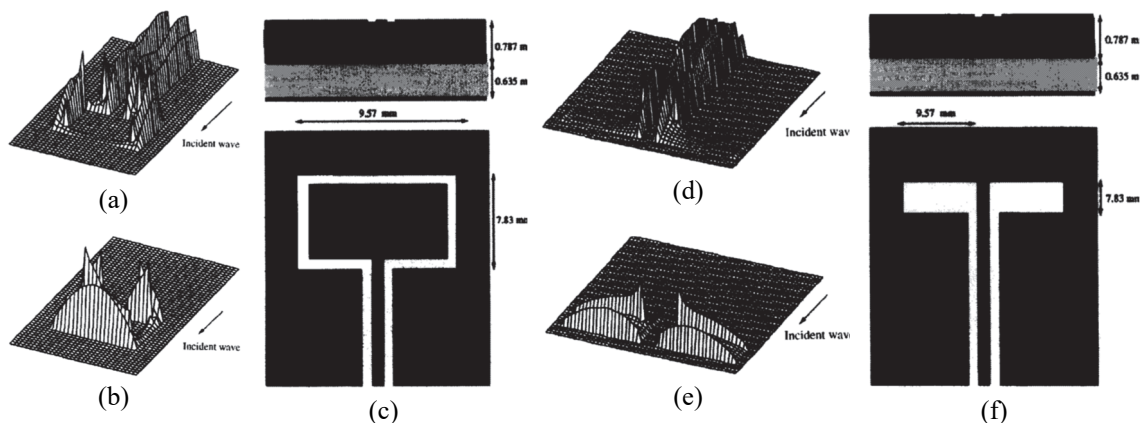


Fig. 2-12 Three-dimensional current distribution of a slot antenna (Right figure) and loop antenna (Left figure) presented in [36], (a) and (d) Longitudinal-directed equivalent magnetic current distribution, (b) and (e) Transversal-directed equivalent magnetic current distribution, (c) and (f) Configuration of the antenna with a CPW feed [36]

Similar to folded dipole antennas, slot antenna can be folded as well, but its input impedance decreases $Z_{in} = \frac{Z_{slot}}{N^2}$ while in folded dipole it increases $Z_{in} = N^2 Z_{Dipole}$. A Folded slot antenna has large bandwidth and its fabrication is easy. In [38], useful design information for a CPW-fed folded slot antenna has been proposed by Tsai and York as shown in Fig. 2-13.. They used folded slot architecture in designing a Quasi-Optical Amplifier 4 x 4 Array without matching network at 11GHz with gain of 10dB and bandwidth of 4% which has been shown Fig. 2-13 [39]. Rebeiz et al. presented guidelines for single and double folded slot (DFS) as well [40].

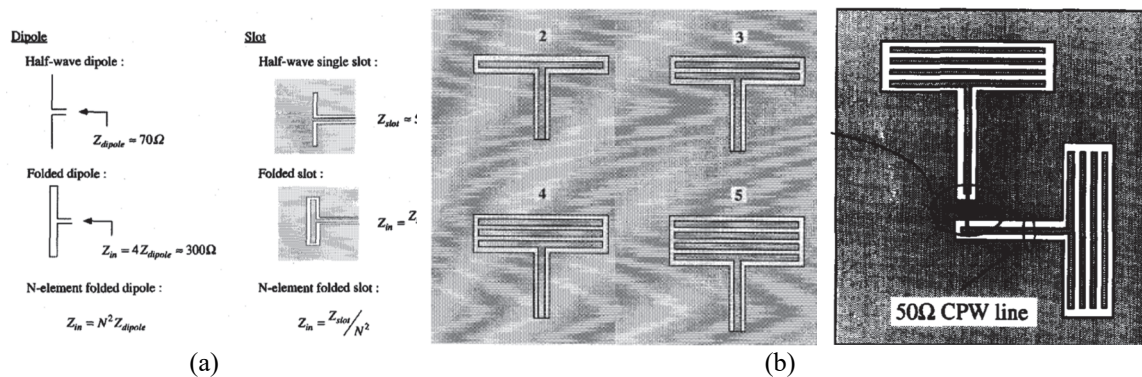


Fig. 2-13 a) Illustration of the impedance scaling with the number of the slots presented in [38], and b) Quasi-Optical Amplifier 4x4 Array proposed in [39].

2.4 Pattern and Polarization Reconfigurable antenna

There are many type of reconfigurabilities in antennas parameters such as reconfigurability in frequency, polarization or pattern. Pattern reconfigurability has been already investigated by researchers who were challenging to cover the whole frequency band as well as switching between omnidirectional and directional reconfigurable radiation patterns [41]–[44]. A general overview about antenna reconfigurability has been published by Bernard as well [45]. Substantial body of research can be found in literatures for planar antenna structures, but a few reconfigurable 3-D antennas [46] are available. Li et al. in [47], reported a wideband reconfigurable square slot antenna operating at 2.4GHz shown in Fig. 2-14 excited through a CPW line. Turning on/off two PIN diode can turn the CPW line to a slot line to change its polarization [47].

Qin et al. in [48], reported a pattern reconfigurable patch antenna connected through PIN diodes to eight shorting posts surrounding it as shown in Fig. 2-15. A U-slot is carved

in the patch to increase the bandwidth. Conducting ring pads on top layer have been added to the posts to facilitate mounting small diodes in wide gaps between patch and posts. The operating mode of the antenna changes from monopolar patch mode to normal patch mode while the two modes are designed to cover similar frequency bandwidth of 6% at 5.32 GHz. As a result, the radiation pattern of the antenna can switch between conical and boresight, respectively. In conical mode the plane with maximum power level can switch between Z-Y and Z-X orthogonal planes, hence the antenna has three states in pattern reconfigurability. Using their proposed antenna in MIMO systems increases the channel capacity and they have reported its correlation coefficient and diversity gain in the paper [48].

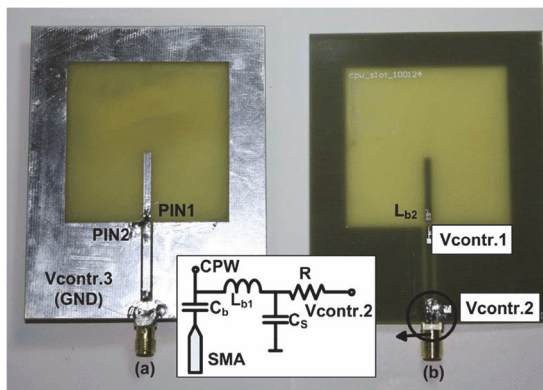


Fig. 2-14 Polarization reconfigurable antenna reported by Yue Li et al. in [47].

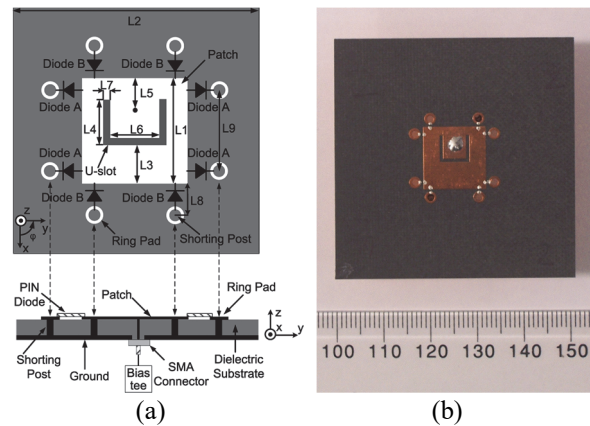


Fig. 2-15 a) Schematics of the pattern reconfigurable U-slot antenna, b) Photograph of the pattern reconfigurable U-slot antenna [48].

Lei et al. in [49], proposed a pattern and pattern/frequency reconfigurable antennas shown in Fig. 2-16. Their structure consists of an L-shaped slot, PIN diodes, lumped capacitors and bias networks which used to create short circuits across the slot, changing the current distribution around slot and reconfiguring the radiation pattern of the antenna. They have extended their structure to frequency/pattern reconfigurable antennas by using Varactor diodes. This structure could achieve maximum gain of 0.72dBi at operating frequency of 2.4GHz [49].

Fakharian et al. in [50], proposed a reconfigurable antenna shown in Fig. 2-17. The polarization of the antenna can be switched among linear, circular left hand and right hand at 2.4GHz and 5.8GHz. This antenna consists of an extended U-slot patch antenna on a modified ground plane which slot can be turn ON/OFF using the switches. So, the switches can change the length of the slot arms in four states to alter the polarization.

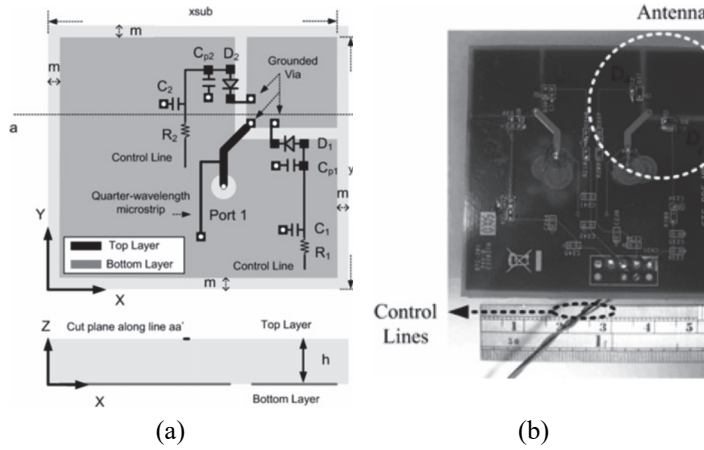


Fig. 2-16 Antenna reported in [49]

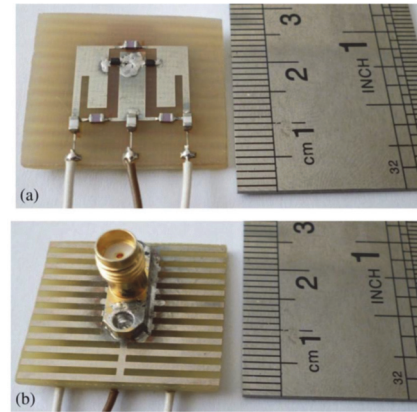


Fig. 2-17 Photographs of the antenna proposed in [50]. (a) Top view. (b) Bottom view.

Patron et al. in [44], designed a pattern reconfigurable antenna at 3.8GHz shown in Fig. 2-18 employing a circular array where its elements are rotating as well. They have switched among four dipole antennas to get four directional and one omnidirectional radiation pattern by changing the architecture between the Alford loop antenna and dipole with three reflectors, respectively[44].

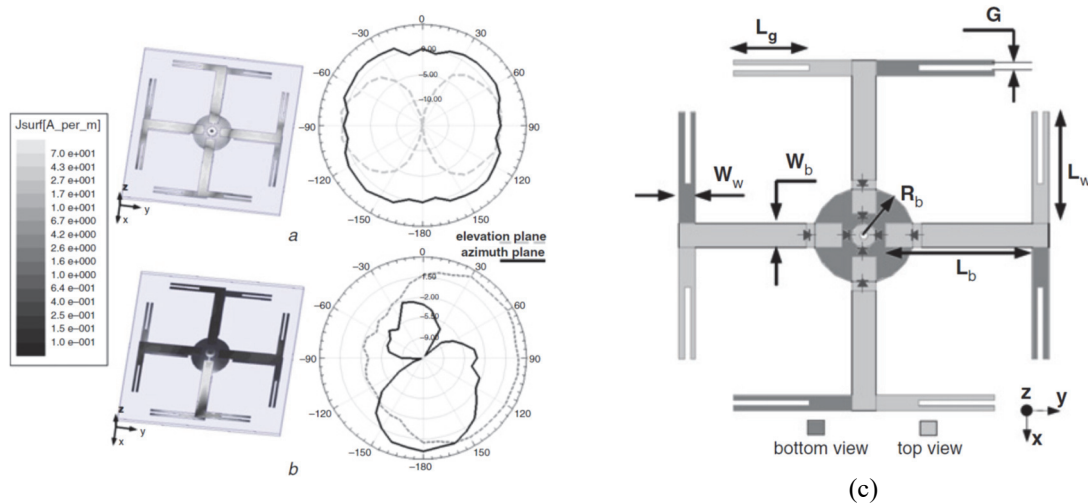


Fig. 2-18 Simulation of proposed antenna, a) Four active pairs: uniform current distribution and omnidirectional beam, and b) Single active pair: one active element and directional beam, c) Layout of proposed antenna [44]

Muhamud-Kayat et al. in [42], presented an antenna consisting of two truncated rhombus-like slotted patch antennas in back-to-back configuration which is reconfigurable both in frequency and radiation pattern using its slotted patch and parasitic elements, respectively[42].

Nguyen et al. in [43], designed a four port antenna at 2.7GHz consisting of eight L-shaped quarter-wavelength slot antenna element embedded at edge of a square substrate covering 360° by turning switches on and off and supplying desired ports as shown in Fig. 2-19. They could achieve maximum gain of 4dB in horizontal plane and as their architecture has four ports, it has proper application in MIMO systems [43].

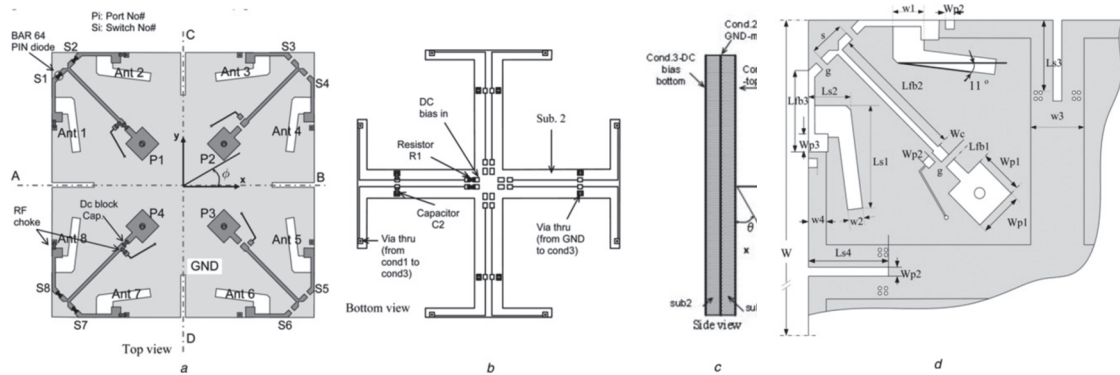


Fig. 2-19 Antenna presented in [43], a) Top view, b) Bottom view, c) Side view, d) Antenna dimension

Jamlos et al. in [51], reported a Beam Steering Radial Line Slot Array (RLSA) Antenna with Reconfigurable Operating Frequency.

Sarrazin et al in [46] used a metallic box as a cavity to design and report a pattern reconfigurable cubic antenna operating at 5GHz shown in Fig. 2-20. The disadvantage of this structure is using the internal space of the antenna as a resonant cavity which makes it impossible to put electronic circuits inside the cube. The antenna has great application in pattern and space diversity which can improve the telecommunication performance. Their proposed structure is actually a metallic cubic cavity with rectangular slot radiators. PIN diode switches mounted on the slots can short circuit the slot and take care of pattern reconfiguration. Their proposed structure switches among three uncorrelated different radiation patterns in a 4π steradian range, each one can receive all polarizations. They have evaluated the diversity performances of their architecture through calculation of the envelope correlation coefficient.

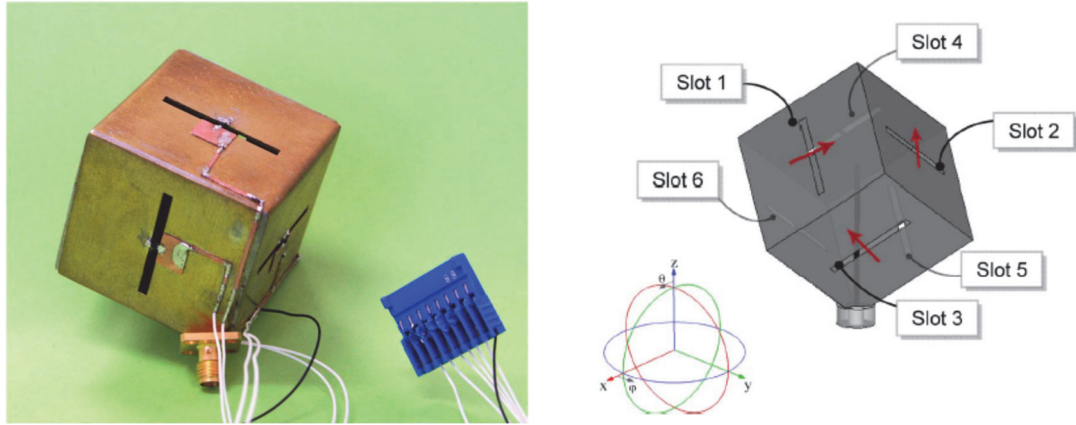


Fig. 2-20 Reconfigurable Cubic Antenna reported in [46]

In [52], Bernhard et al. proposed a frequency reconfigurable small antenna with simple bias network through RF feed and a wide tuning range from (410-990 MHz, 2.1-3.5 GHz; VSWR = 2:1) [52]. Hence, they could suppress the negative effect of coupling to bias lines which distort the pattern. Their design highlights the radiation efficiency limitations associated with the desirable planar topology for electrically small antennas with very wide tuning range requirements[52].

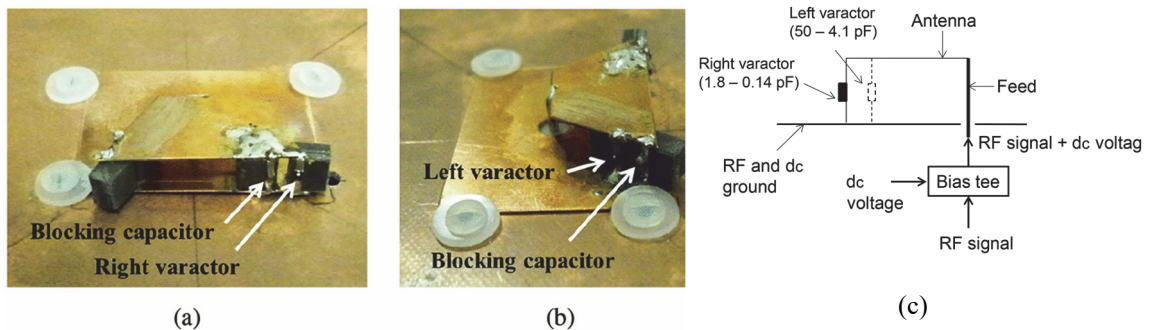


Fig. 2-21 Constructed antenna: (a) rear view and (b) side view, (c) Bias Network [52]

Recently, MIMO cube has been introduced as a new concept and architecture which can improve performance of MIMO systems even more than planar structures [53]–[55].

2.5 3-D Printing and Printing Electronics

As a revolution in the fabrication of electronic devices, printing electronic has been introduced recently. Patterning electronic circuits on standard or nonstandard substrates guarantees the fabrication flexibility of electronic circuits. In contrast with traditional industrial PCBs, electronic circuits up to mm wave frequencies can be printed even on

papers using conductive inks. Combining the printing electronics and 3-D printing, reviewed at Appendix 0 of this document, 3-D printing electronics was born. To put it into a nutshell we can categorize different printing technologies into the following list each one has been developed by a company or an academic research group.

2.5.1 2D inkjet conductive printing on flexible sheets [10], [56]

Tentzeris et al. conducted substantial research on printing electronics especially inkjet printing. They have printed UWB antennas on paper sheets through conductive inks and reported the characteristic of paper and ink for applications up to 10GHz. They have introduced it as a big step in low cost implementation of flexible electronic circuits with especial application in wireless sensor networks [10], [56].

2.5.2 3-D Conformal printing by deposition of conductive inks on 3-D [57]

Printing electronic has been extended to 3-Ds recently. Few research groups including our group patterned 3-D printed structures with conductive inks to proof the concept[8], [9]. Bernhard by the aid of a Nordson 3-D dispensing robot, , patterned their proposed antennas onto the convex and concave surfaces of hemisphere glass substrates [57] which can be seen in Fig. 2-22.

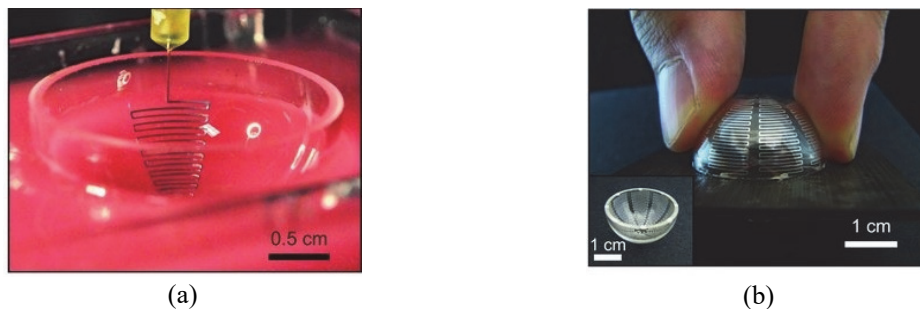


Fig. 2-22 Conformal 3-D printing of Antennas on hemisphere by J. T. Bernhard [57]

2.5.3 Ink deposition in trenches on 3-D object [4], [19]

MacDonald et al. made trenches on 3-D printed structures filled by conductive ink or electronic components to introduce a rapid 3-D prototyping for electronic circuits on the packages shown in Fig. 2-23 [4].



Fig. 2-23 3-D printed electronic circuit by Macdonald et al. in [4]

2.5.4 Multi-material 3-D Micro-dispensing by nScript printers [58]

Recently, nScript released a commercially available printer to the market which uses micro dispensing technology which can take care of 3-D printing electronic all in one step [58]. It means the device can print the 3-D object and conductive layouts simultaneously. Fig. 2-24 illustrates some samples of 3-D printing electronic fabricated by nScript 3-D printer.

Nasser et al. fabricated body of their antennas shown in Fig. 2-25 from Acrylonitrile Butadiene Styrene plus (ABS) using Dimension SST 768 3-D Printer and its conductive pattern from Dupont CB-028 silver ink deposited by nScript 3-D-450 [19]. They have printed body of almost the same antenna using stereo lithography and painted by nScript machine [18].



Fig. 2-24 3-D printing electronics offered by Nscript [58]

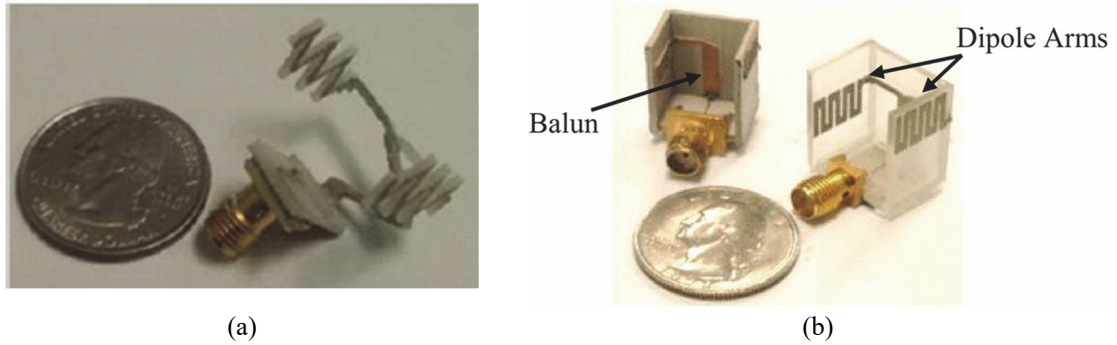


Fig. 2-25 3-D printed Antenna by Nasser et al. reported in a) [19], and b) [18]

2.5.5 Laser Direct Structuring (LPKF co.) [59]–[61]

LPKF Co. offered 3-D Laser Direct Structuring (LDS) as solution to pattern conductive layout on 3-D conformal objects. It is too time consuming and not at all perfect for rapid prototyping. After printing the 3-D object with a 3-D printer, it needs to be covered with a material (like photoresist). Then the layout will be patterned using a laser on the body of structure and copper will be deposited using electrolyte. LDS found its application in mass production of printing mobile antennas inside the mobile case and electronic circuits in wheel of a car which means it can be a good candidate for industrial mass fabrication of our work as well [59]–[61].

2.5.6 Pad Printing [62], [63]

Application of Pad printing, briefly overviewed in [63], investigated by some researchers in 3-D antenna manufacturing specially in mass fabrication. Cellphone antenna shown in Fig. 2-27 was prototyped by Xiong et al. by the aid of this method [62].

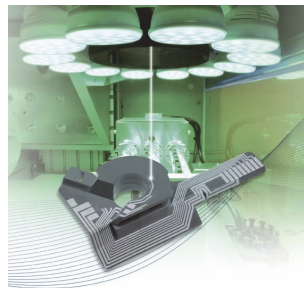


Fig. 2-26 LDS process introduced by LPKF for mass production of 3-D printing electronics [59]–[61].

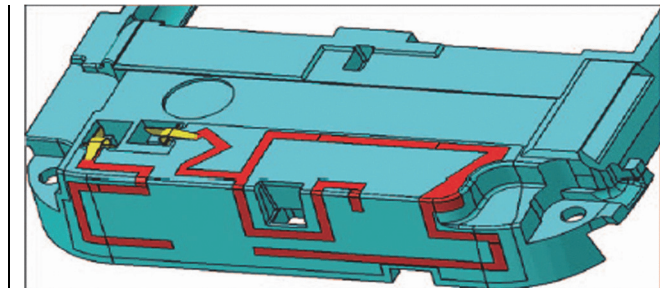


Fig. 2-27 cellphone antenna fabricated by pad printing [62], [63]

2.6 Antenna for sensor

As already mentioned in the previous sections, the main application of our architecture could be found in nodes of wireless sensor networks. A sensor connected to a transceiver electronic circuit measures a specific parameter of the environment surrounding the node and transmit the data to the main hub or base station. Some researchers used the body of the antenna as a sensor as well. Amin et al. [64] developed a low cost printable humidity sensor which can be used in chipless RFID technology. Their proposed RFID sensor has been designed based on planar Stepped Impedance Resonator (SIR) structure shown at Fig. 2-28. They sense the humidity level by tracking the variation of dielectric constant of the substrate which is Kapton HN polyamide in their design. Balachandran et al. [65] designed a capacitive tin oxide (SnO_2) sensor integrated with a microstrip patch antenna (Fig. 2-29) with application in passive detection of ethylene gas. Ethylene (0-100 ppm) decrease the capacitance which resulted in reduction of the antenna resonant frequency and return loss (by 7 MHz and 9.5 dB). So, it can be sensed wirelessly. This antenna acts an RFID passive sensor.

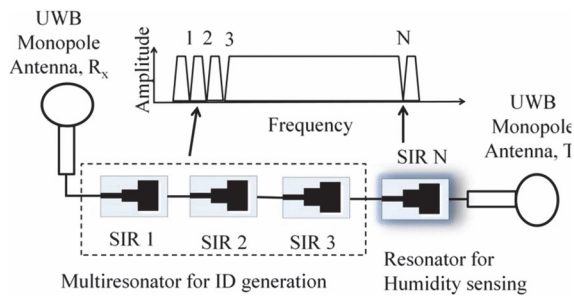


Fig. 2-28 Multi- SIR based N bit chipless RFID integrating humidity sensing proposed in [64].

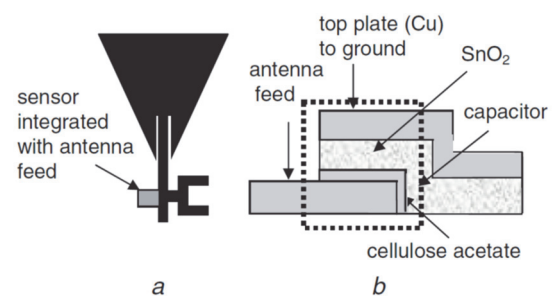


Fig. 2-29 Configuration of antenna and sensor, a) Triangular microstrip patch antenna with sensor, b) Capacitive ethylene sensor [65]

Shrestha et al. [66] designed a chip-less RFID sensor system for cyber centric monitoring applications. They have proposed two configurations, one consists of RFID antenna connected to the integrated sensor, and the other one where the RFID antenna connected to the sensor through a meander transmission delay line as ID generation which in their prototype allow 8 different ID codes. Their reader communicates to the sensory tag at 915-MHz carrier signal through load modulated backscattered techniques. They have tested the system for detecting presence of ethylene gas[66].

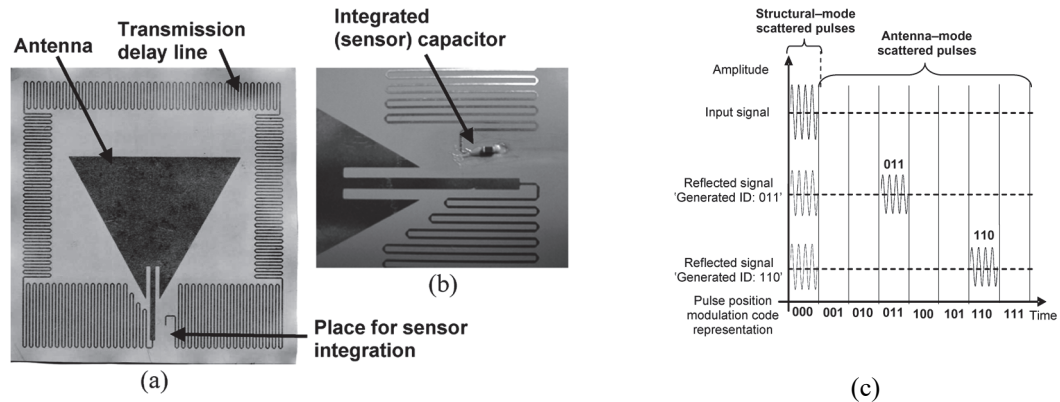


Fig. 2-30 (a) Second configuration of RFID sensor with 3-bit code of (110), (b) (Sensor) capacitor integrated at the end of the transmission line, and (c) Schematic illustration of code generation using reflected pulses, in PPM representation [66]

2.7 Conclusion

In this chapter, most recent 3-D printable antennas were reviewed and their pros and cons and innovative architectures were discussed. As they have different architectures, and designed for different purposes, one cannot compare them considering only one figure of merit. Additionally, slot antennas and pattern reconfigurable antennas, two major fundamental concept behind our designs were reviewed here. Antenna sensor which can be an extension for my project to find more application in WSN networks was reviewed at the end.

Chapter 3

3 Conformal cubic antenna modeling and analysis

3.1 Introduction

Considering cubic antennas, as special kind of conformal antennas, in this chapter we talk about analysis and design of a general conformal antenna array. Once we establish basic notations and concepts, we then adopt the procedure to analyze the particular case of cubic antennas. A conformal antenna can be modeled as an array if the whole structure can be divided into a set of antenna elements. As almost all our structures have been designed using slot antenna as an antenna element, here we will study slot antenna in general in section 3.2 and elaborate on their characteristic differences when the ground planes are finite or folded. In section 3.3, we will describe circular array theory and develop an analytical solution using folded slot as antenna element. The study of mutual coupling between elements of such array is presented in section 3.4. In section 3.5, we propose three novel techniques that can be employed in designing *single feed* cubic slot antennas.

3.2 Slot Antenna

Slot antennas are dual of dipole antennas and have found broad applications in waveguide-based structures due to the fact that their metallic structure is capable of

handling high power signals and their compliance with conformal antennas. Here we first study slot antennas on infinite ground plane and then investigate how a finite ground plane can affect the antenna performance especially its radiation pattern and input impedance.

3.2.1 Planar slot antenna on infinite ground plane

To verify the theory behind slot antennas, we have started our investigation with a slot antenna cut in an infinitely large perfect electric conductor as a ground plane shown in Fig. 3-1. In this case slot antenna can be modeled using its dual which is a dipole for a half wavelength long narrow slot antenna. This means its radiation pattern will be omnidirectional in the plane perpendicular to the slot axis like dipole however in contrast to dipole, it will be ϕ polarized. For our studies in the following, we have used a slot antenna which is 73.5mm long and 1mm wide excited with a lumped port with a 15mm offset from the center of the slot for proper matching and power delivery at 2.44GHz as shown in Fig. 3-2.

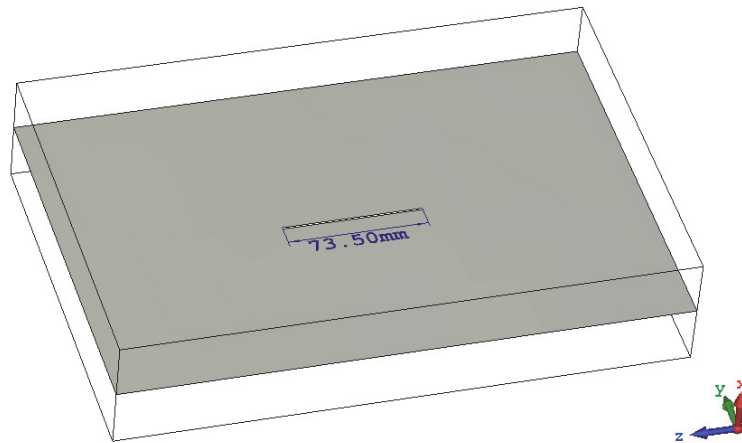


Fig. 3-1 Structure of slot antenna with infinite ground plane (CST open Boundaries touched ground plane)

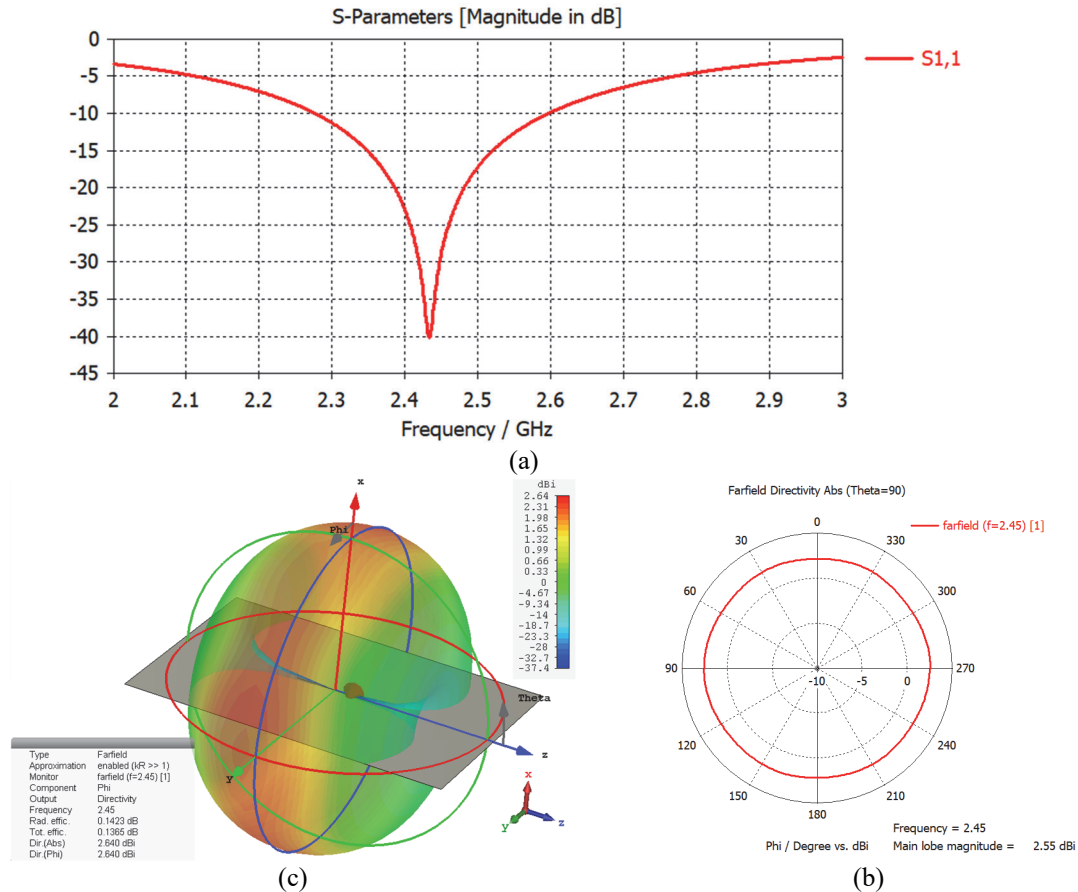


Fig. 3-2 Slot with infinite ground plane, a) Input matching, b) ϕ polarized directivity at 2.45GHz in the azimuth plane, and c) ϕ polarized directivity of antenna at 2.45GHz in 3-D space

3.2.2 Planar slot antenna with finite ground plane

In this sub section, we have truncated the antenna ground plane to study how size of finite ground plane affects antenna radiation pattern. As shown in Fig. 3-3, having a finite ground plane mismatches the antenna input to some extent due to the ground plane edge effect. Because of the limited aperture size in this case and edge effect, the antenna pattern changed to a directional pattern with high directivity in broadside direction instead of omnidirectional pattern in infinite ground plane case. The directivity of the radiation pattern is increasing by enlarging the aperture, here ground plane. However, when the aperture length happened to be bigger than a wavelength, 122mm in our case for 2.45GHz, ripples begin to appear in the radiation pattern due to diffraction from the edges of ground plane. Here, we have investigated the antenna when width of ground plane (represented by GW in this text) is increasing from 50mm to 200mm in 50mm steps.

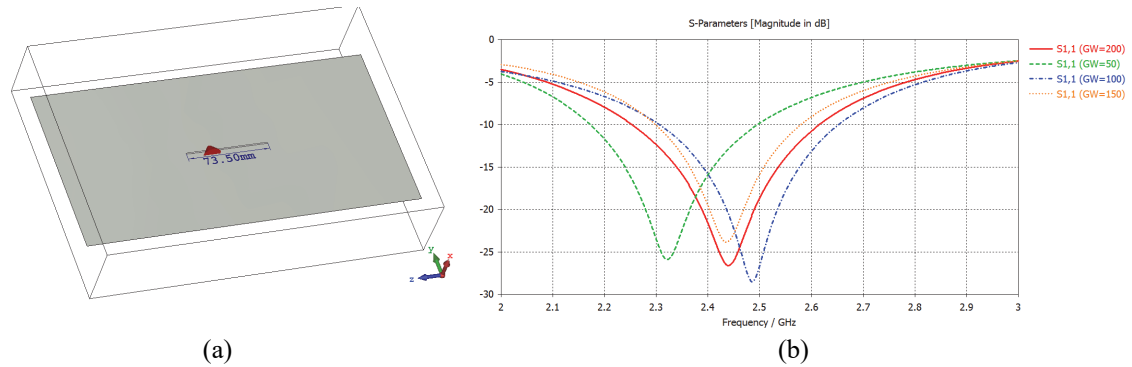


Fig. 3-3 Slot antenna with finite ground plane, a) structure, and b) Input matching

As shown in Fig. 3-4, we see highest directivity achieved when $GW=100$ but the pattern is not distorted because ground plane is smaller than wavelength which guarantees distance between antenna and edges of ground plane is smaller than half a wavelength.

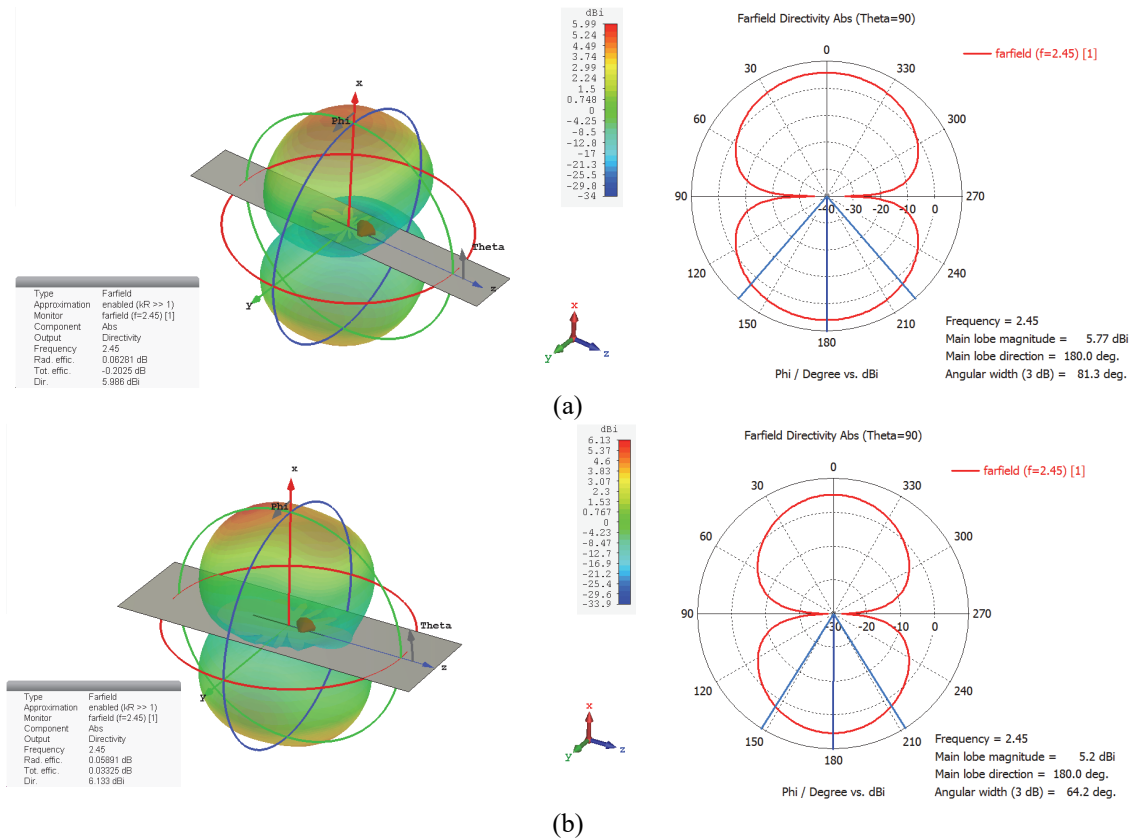


Fig. 3-4 Total directivity of slot antenna at 2.45GHz on finite ground plane, a) $GW=50$ mm, and b) $GW=100$ mm

In this case, surface currents flowing on the ground plane and their reflection from edges of a finite ground plane create standing waves responsible for more directive broadside radiation pattern through enlarging the radiation aperture. Hence, there is no local maximum on the plane other than the main maximum in the location of slot antenna

and surface current distribution tapered out moving to the edge. Fig. 3-5 (a) shows how ripple appears and pattern is disturbed when $GW=150\text{mm}$, which is equal to 1.22λ at 2.45GHz . As shown in Fig. 3-5 (b), two main lobes appear in the pattern with a very large ground plane for $GW=200\text{mm}$ as opposed to the single main lobe in the case of small ground planes. In this case, when the ground plane is too big, out of phase radiation from some part of ground plane which are further away from our antenna even divides the main lobe to two lobes by adding a null at broadside.

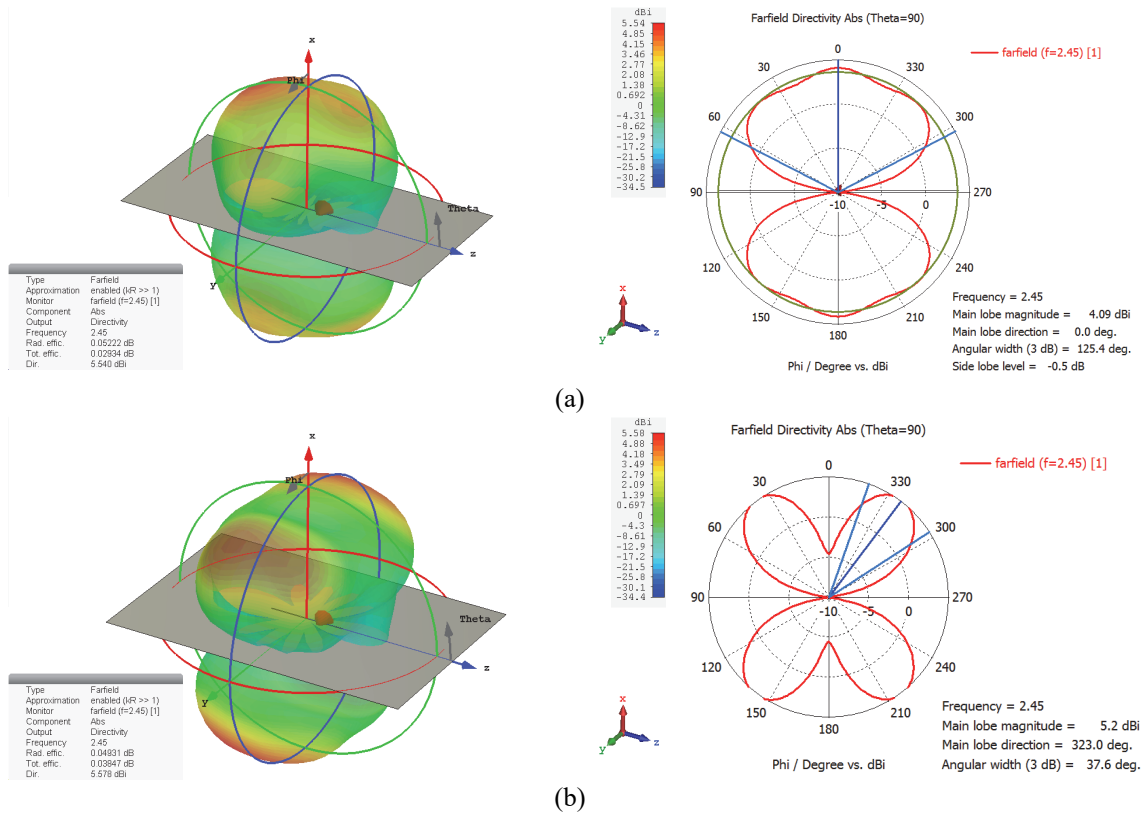


Fig. 3-5 Total directivity of slot antenna at 2.45GHz on finite ground plane, a) $GW=150\text{mm}$, and b) $GW=200\text{mm}$

3.2.3 Planar slot antenna with folded finite ground plane

Here we investigated the effect of folding the antenna ground plane and compared it to the previous case where the ground plane was truncated and finite. Similar to the finite ground plane case, here we expect surface currents flowing on the ground plane to interfere with the antenna radiation, leading to a more directive pattern respect to the antenna in infinite ground plane. However, surface currents running on the folded parts of the ground plane radiate in the $\phi=0^\circ$, 90° , 180° and $\phi=270^\circ$ directions, broaden the antenna radiation pattern and as a result decrease the directivity and gain of the antenna respecting to the

antenna with finite and truncated ground plane. To put it into a nutshell, directivity of antenna with folded ground plane should be higher than infinite ground plane and lower than finite and truncated ground plane due to having a conformal aperture. At following we have studied folding at direction parallel and perpendicular to the slot axis in separate sections in order to separate their effect on antenna performance. At the end, we even move further with the latter case and studied the case when slot antenna is folded as well.

3.2.3.1 *Folded ground plane in the direction in parallel with the slot axis*

As depicted in Fig. 3-6, in this section we have folded the ground plane along Z axis which is in parallel with slot axis. GW, and GWZ represent width of ground plane in X, and Z directions, respectively and FLX is the length of the part of ground plane which is bent down in Y direction.

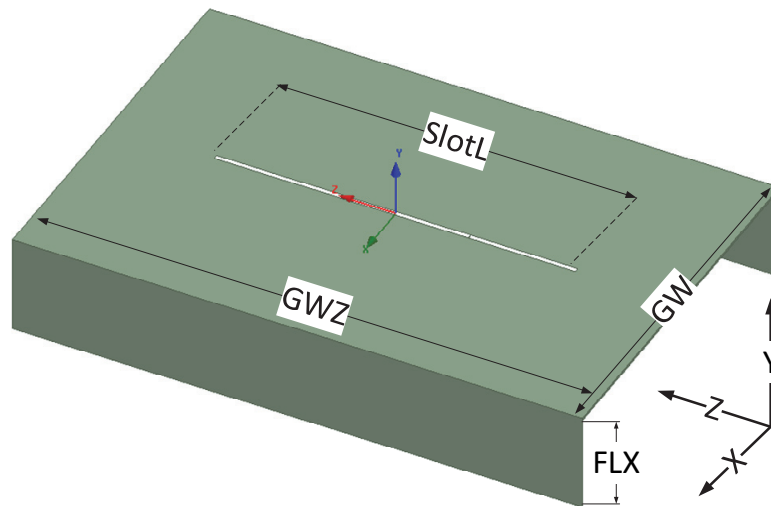


Fig. 3-6 Slot folded in X direction

a. *Parameter study on GW where GWZ=120mm and FLX=20mm*

In Fig. 3-7, we have compared radiation pattern and input matching of the antenna for different ground plane sizes (GW) while size of the folded section of the ground plane (FLX) is constant. In contrast to the previous section, impact of decreasing the size of finite ground plane on resonance frequency of the antenna is different. For instance, here for

GW=50mm case, we observe that the resonance frequency shifts up while it shifted down in the previous case.

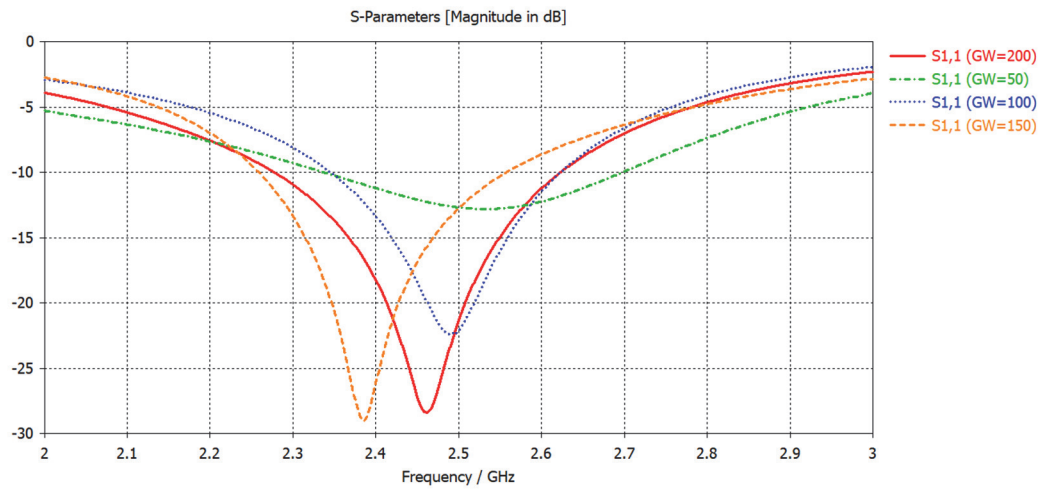
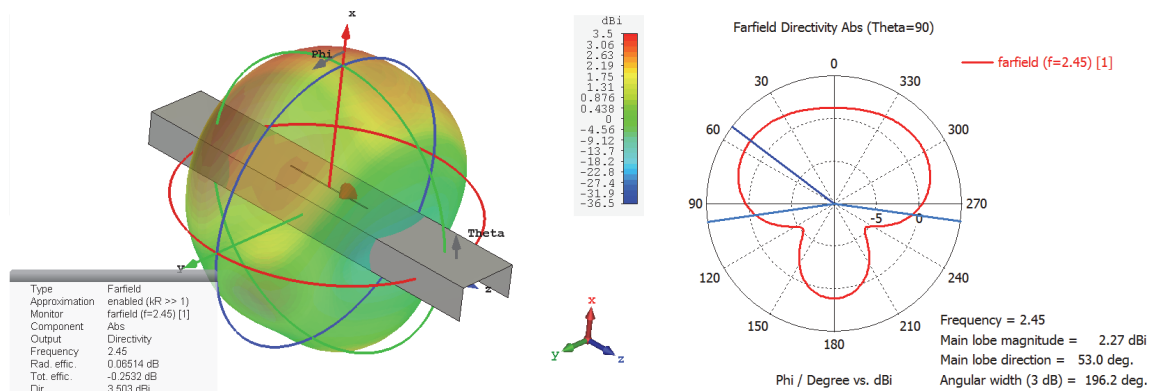


Fig. 3-7 Input reflection coefficient of slot antenna on folded finite ground plane for various GW

As shown in Fig. 3-8, folding the ground plane affects the back-lobe radiation. It has narrowed the beam width and focused the radiation much like a horn antenna. Similar to the previous section, having a very large ground plane with GW=150mm or larger distorts the pattern, but in this case, it causes grating lobes to appear at $\phi=\pm 90^\circ$ instead of adding a null at broadside. Holding on the same assumption made in the previous section, standing wave on ground plane add two peaks on folded section of the antenna in this case which are responsible for two lobes at $\phi=\pm 90^\circ$ due to their long distance from main radiator.



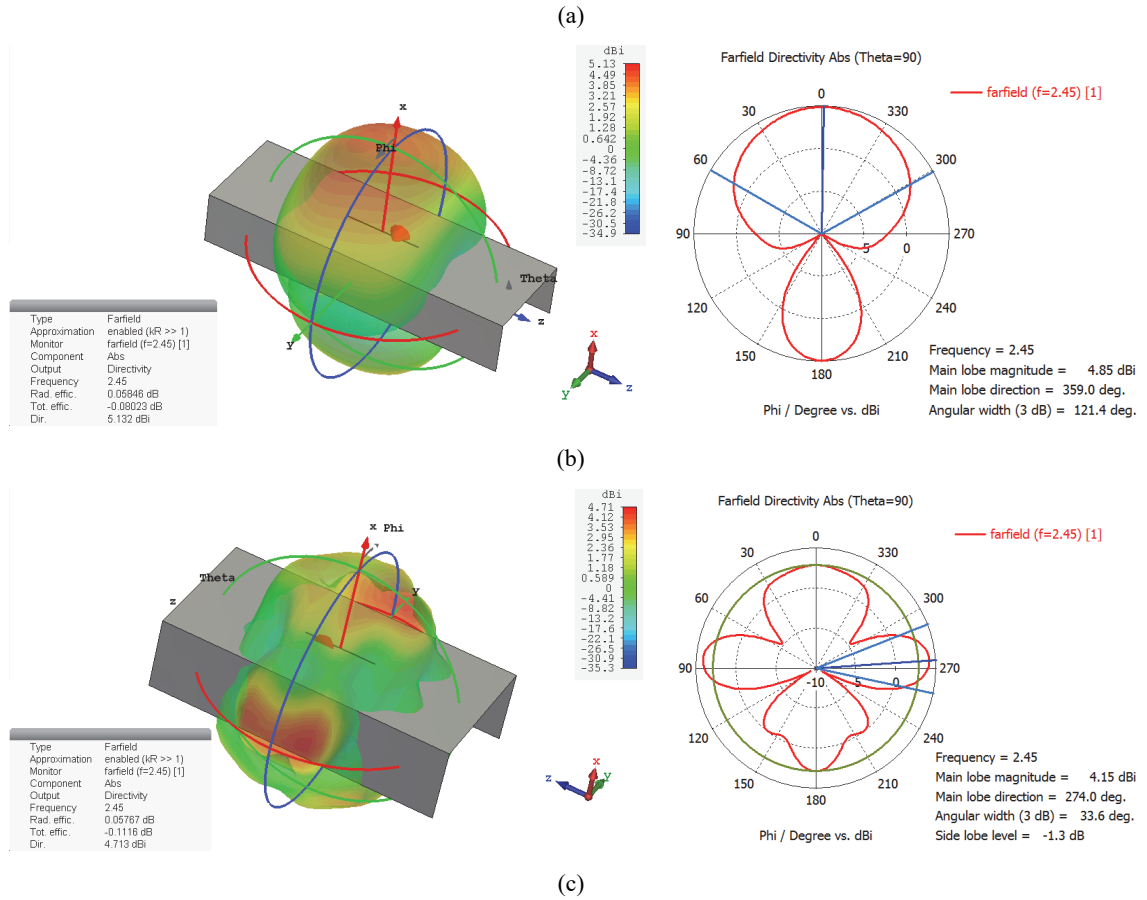


Fig. 3-8 Total directivity of slot antenna at 2.45GHz on folded finite ground plane, a) GW=50, b) GW=100mm, and c) GW=150mm

b. Parameter study on GW and FLX where GWZ=120mm and FLY=0

In Fig. 3-9, we repeat the same parameter study, while we have bended a 120mm long ground plane at various locations where $2 \times \text{FLX} + \text{GW} = 120\text{mm}$ and $\text{GWZ} = 120\text{mm}$ for all variations of GW. It means the parameter FLX is changing to maintain $2 \times \text{FLX} + \text{GW}$ at a constant value of 120mm.

As we can see in Fig. 3-9 (b) for $\text{GW} = 120\text{mm}$ where $\text{FLX} = 0$, the pattern in the azimuth plane is similar to the pattern of an antenna with finite ground already illustrated in Fig. 3-2. It is a distortion free pattern with two nulls appearing at the $\phi = 0^\circ$ and $\phi = 180^\circ$ directions due to infinitesimal aperture at these directions. In this case, shrinking the ground plane will reduce the aperture size at broadside in one hand (GW) and enlarge the aperture at $\phi = 0^\circ$ and $\phi = 180^\circ$ in another hand (FLX) both responsible in broadening the radiation pattern in the plane of folding (here XY) which lowers the total directivity in both planes (here XY and YZ) as verified in Fig. 3-9 (a) and (b). Back radiation of slot is decreased significantly as well because larger FLX is constraining the slot aperture with two PEC walls. Also, Fig. 3-9 (c) shows the resonance frequency of the antenna is slightly changing which means the antenna is detuned slightly.

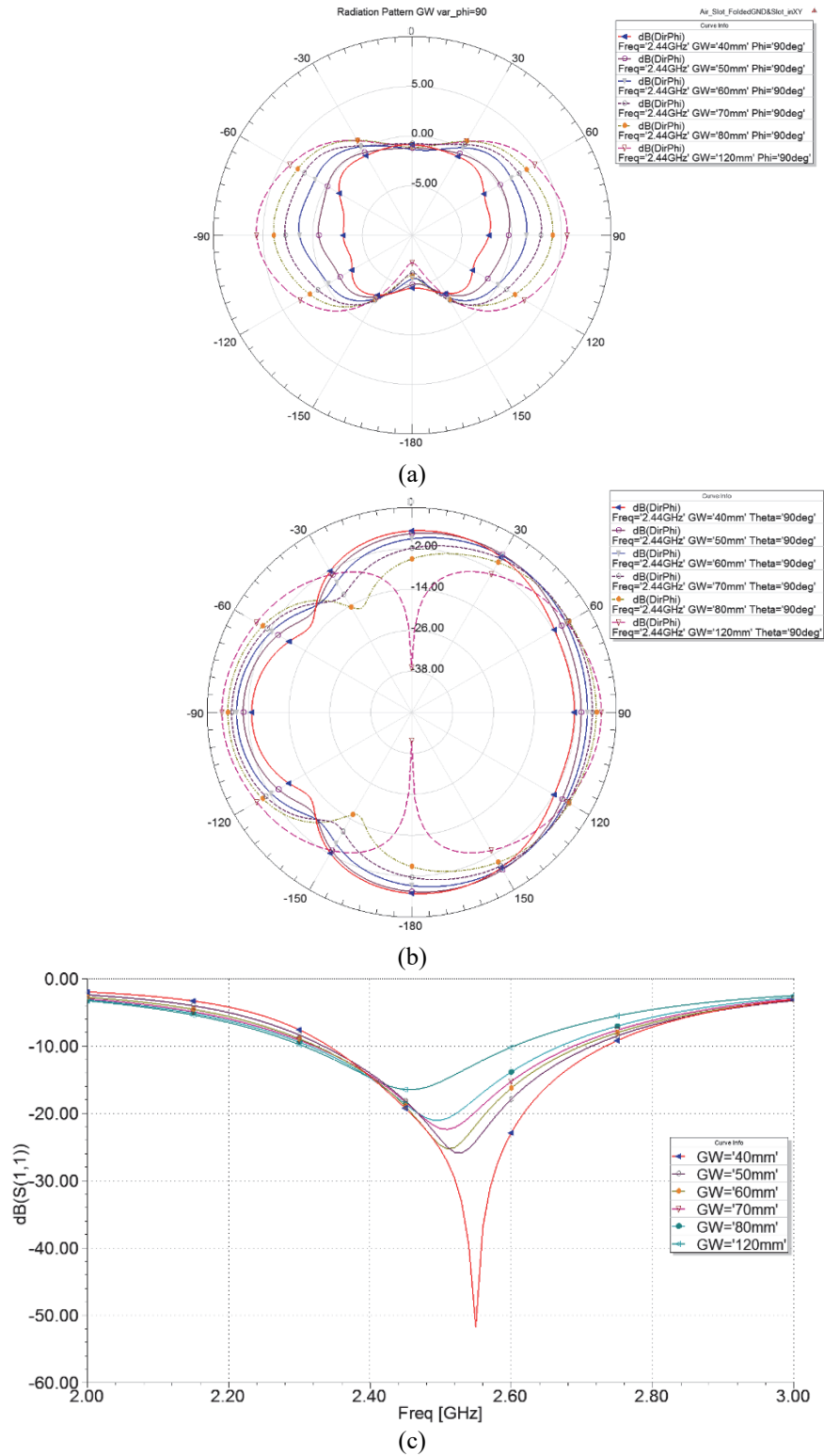


Fig. 3-9 Bending slot in the direction perpendicular to slot axis and studying GW variation for GWZ=120mm, a) ϕ polarized directivity at 2.44GHz in $\phi=90^\circ$ plane, b) ϕ polarized directivity at 2.44GHz in $\theta=90^\circ$ plane, and c) Input reflection coefficient

c. *Parameter study on GW where GWZ=80mm and FLY=20mm*

In the previous parameter study, we have GWZ=120mm while sweeping the GW parameter. As shown in Fig. 3-10, here we are reverifying the results with GWZ=80mm and FLY=20mm while sweeping GW and FLX simultaneously to maintain $2 \times \text{FLX} + \text{GW} = 120\text{mm}$ condition. Radiation pattern follows the same trend except for some minor differences in the $\theta=90^\circ$ plane specially for GW=120mm where the nulls are completely disappeared as shown in Fig. 3-11 (b). Fig. 3-11 (a) illustrated the pattern in YZ plane ($\phi=90$) which is quite similar to the previous case. Fig. 3-11 (c) shows that resonant frequency of antenna shifted up by shrinking ground plane and enlarging FLX which is similar to the previous case again.

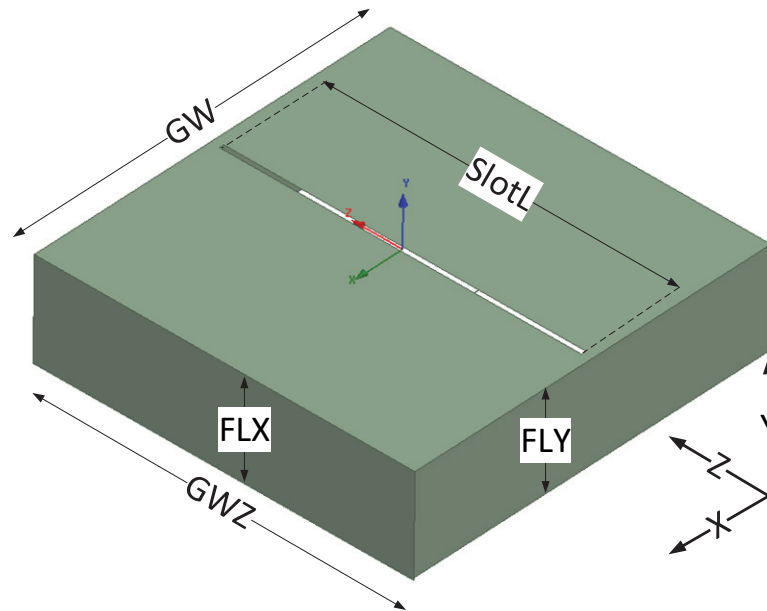


Fig. 3-10 Slot folded in both X and Z direction

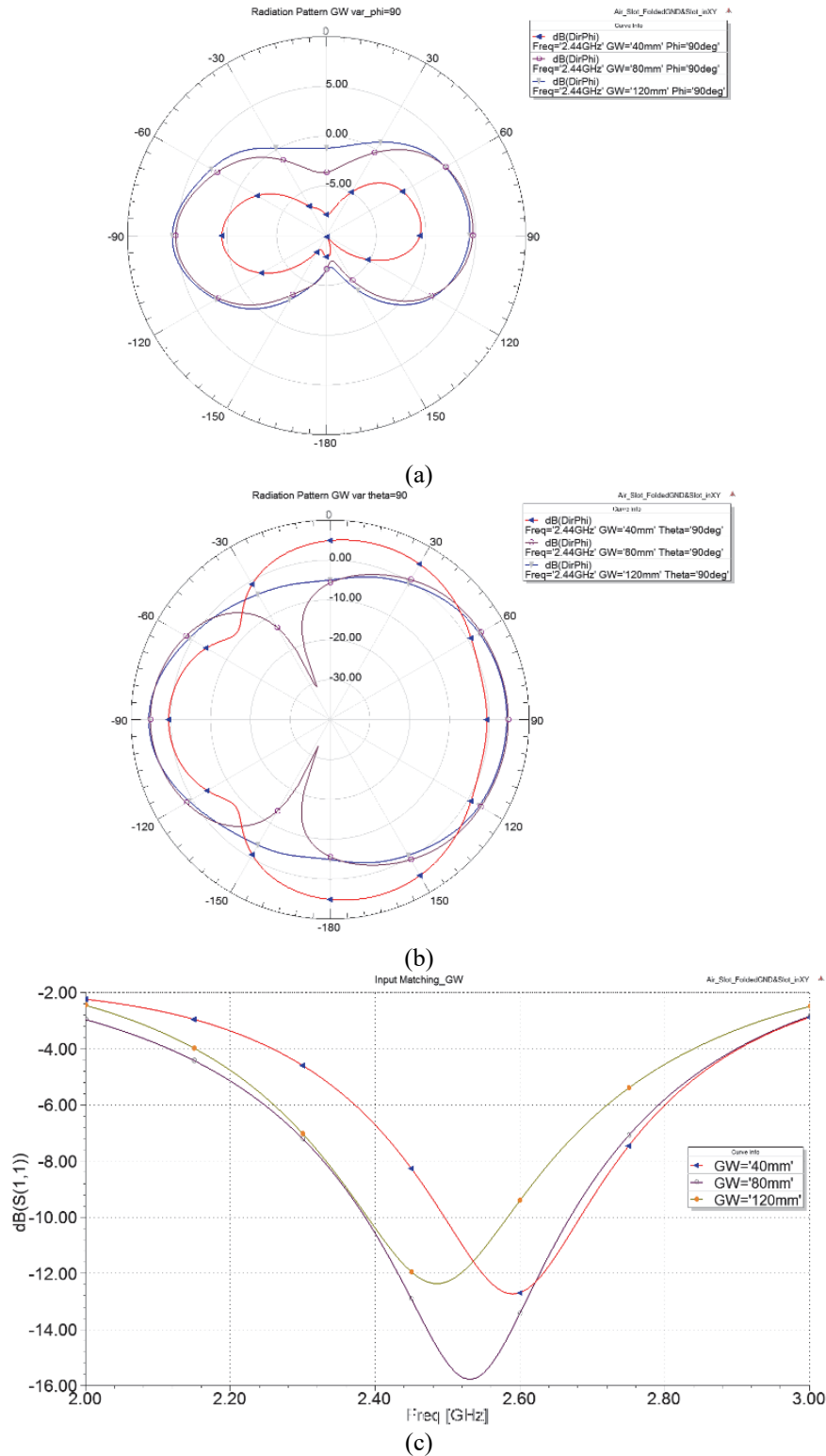


Fig. 3-11 Bending slot in the direction perpendicular to slot axis and studying GW variation for GW=80mm, a) ϕ polarized directivity at 2.44GHz in $\phi=90^\circ$, b) ϕ polarized directivity at 2.44GHz in $\theta=90^\circ$, and c) Input reflection coefficient

3.2.3.2 *Folded ground plane in the direction perpendicular to the slot axis*

a. *GWZ parameter study where $GW=120\text{mm}$ and $FLX=0$*

Folding the ground plane of the antenna in the direction perpendicular to the slot axis (along X axis) slightly affects the antenna radiation pattern in both $\phi=90^\circ$ (ZY plane) and $\theta=90^\circ$ plane (XY plane) where GWZ is much larger than SlotL which means end of slots have enough distance to the line where ground plane is folded and length of folded section (FLY) is small. Here, we set $GW=120\text{mm}$ and swept GWZ while maintaining $2 \times \text{FLY} + \text{GWZ} = 120\text{mm}$ condition by varying FLY synchronously. As shown in Fig. 3-12 (a) and (b), it slightly changes the maximum directivity for $\text{GWZ}=100\text{mm}$ and 120mm while drastically suppressing $\phi=0^\circ$ and $\phi=180^\circ$ nulls in XY plane ($\theta=90^\circ$ plane) for $\text{GWZ}=80\text{mm}$ due to radiation from surface currents running on big folded area facing Z axis with length of FLY which is contributing through U shaped section facing X axis.

As expected this affects the antenna input matching and detunes S_{11} to higher values as GWZ is becoming smaller.

b. *GWZ parameter study where $GW=80\text{mm}$ and $FLX=20\text{mm}$*

Fig. 3-13 reverify the same experiment with $GW=80\text{mm}$ which means the ground plane is now folded in the X direction. Here the null for $\text{GWZ}=80\text{mm}$ is appeared again as FLX blocked contribution of slot back radiation in null cancelation.

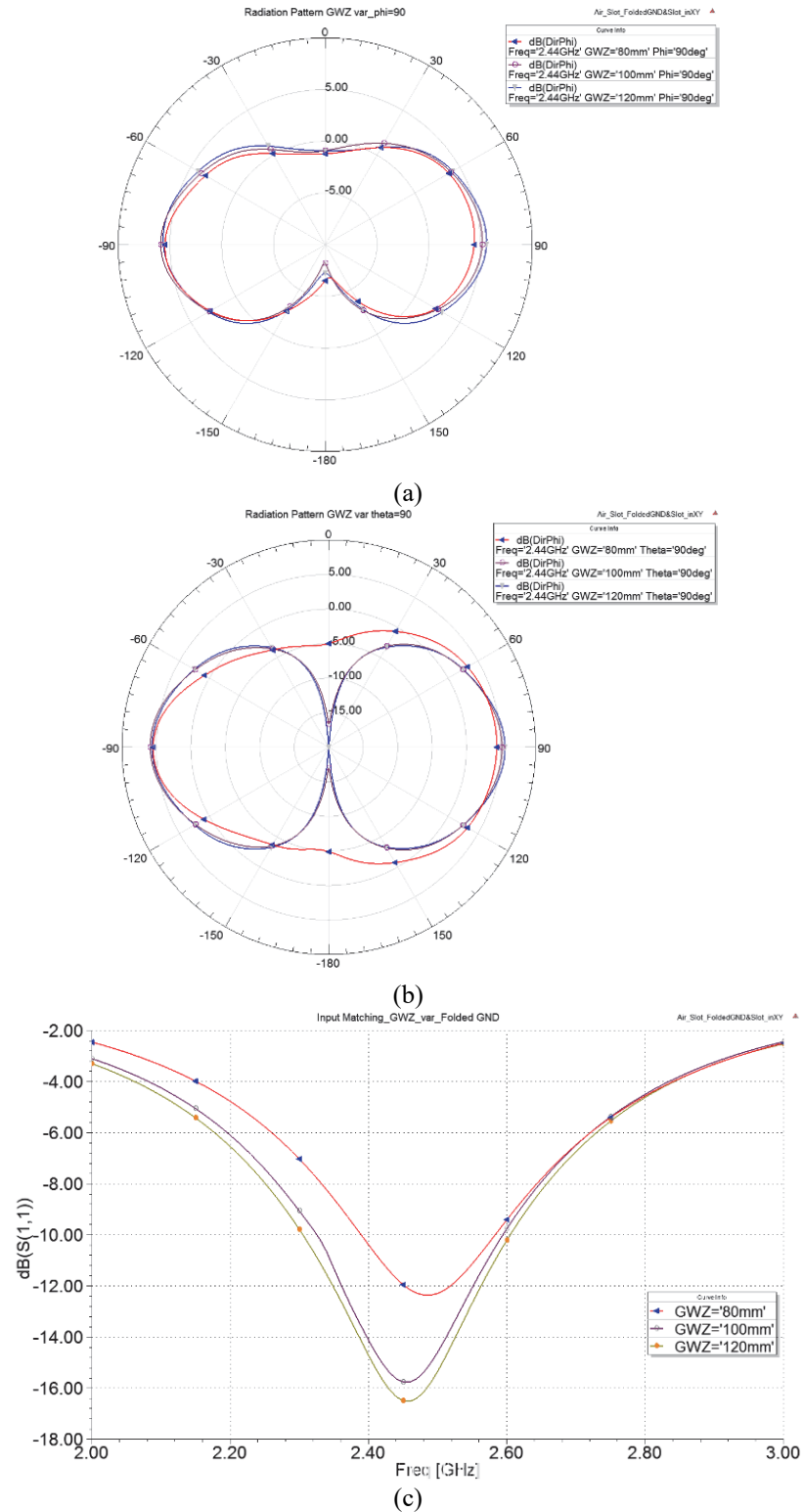


Fig. 3-12 Folding ground plane in slot's axial direction and studying GWZ variation for $GW=120\text{mm}$, a) ϕ polarized directivity at 2.44GHz in $\phi=90^\circ$ plane, b) ϕ polarized directivity at 2.44GHz in $\theta=90^\circ$ plane, and c) Input reflection coefficient

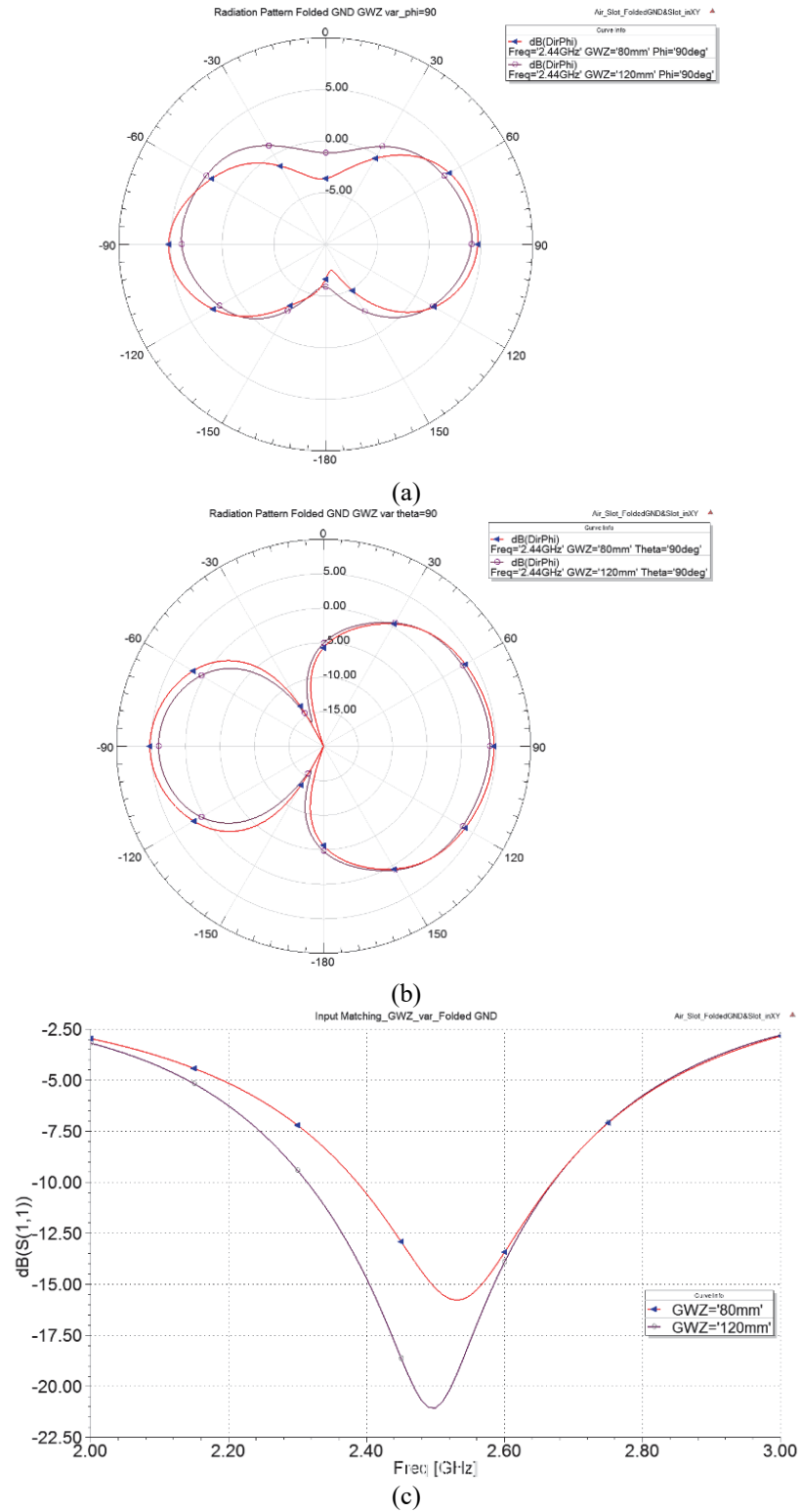


Fig. 3-13 Folding ground plane in slot's axial direction and studying GWZ variation for $GW=80\text{mm}$, a) ϕ polarized directivity at 2.44GHz in $\phi=90^\circ$ plane, b) ϕ polarized directivity at 2.44GHz in $\theta=90^\circ$ plane, and c) Input reflection coefficient

3.2.4 Folded Slot Antenna

In the previous sections, we have only folded the ground plane, but slot antenna was planar which means $GWZ > \text{SlotL}$. Here, we go one step further and even fold the slot antenna as shown in Fig. 3-14

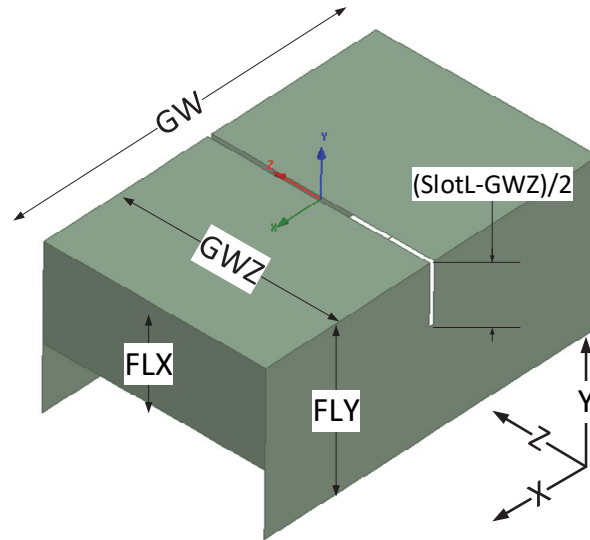


Fig. 3-14 Folded slot antenna

A folded slot antenna can be analyzed as a combination of three groups of radiators:

- The center main radiator toward broadside which has major contribution in the pattern because of maximum field distribution on its length. As folding the ground plane and the slot length, makes the aperture smaller, we expect to see lower directivity and broader beam achieved toward the broadside.
- Two slot radiators folded on the side walls. Electric field intensity over the ending sections of slots is lower comparing to the central section of slot mounted toward Y axis. Even these slot sections do not have tangible contribution in the far field pattern in the XY plane which is perpendicular to their aperture plane, together with folded ground plane, they have a significant role in broadening the radiation pattern in the YZ plane by radiating toward $\theta=0^\circ$ and $\theta=180^\circ$.

- Two folded ground planes normal to the X axis. Even there is no slot radiator on these planes, surface current running on them radiate at $\phi=0^\circ$ and $\phi=180^\circ$ direction along X axis and broaden the pattern in the XY plane.

3.2.4.1 Simulations and modeling of folded slot antenna

Here, the folded slot antenna is simulated and the results verify our hypothesis and expectations. Both Fig. 3-15 (b) and Fig. 3-16 (b) confirm that the directivity at $\phi=0^\circ$ and 180° directions in the azimuth plane (XY) experiences 5dBi increase from -5dBi to 0dBi where GWZ decreases from 80mm to 40mm. Similar to folded ground plane, these side walls direct and suppress the back radiation which will cause both amplitude and beam-width of back radiation to be decreased significantly.

As shown in Fig. 3-15 (c) and Fig. 3-16 (c), antenna resonance frequency shifted up slightly. It means current distribution on folded slot antenna is slightly different than the planar slot and its effective length or aperture is smaller than its physical length. It is obvious that the folded sections are also contributing in the radiation pattern as they are part of the antenna's overall length, however their role is less significant than the straight slot that has no discontinuity or bend along its length.

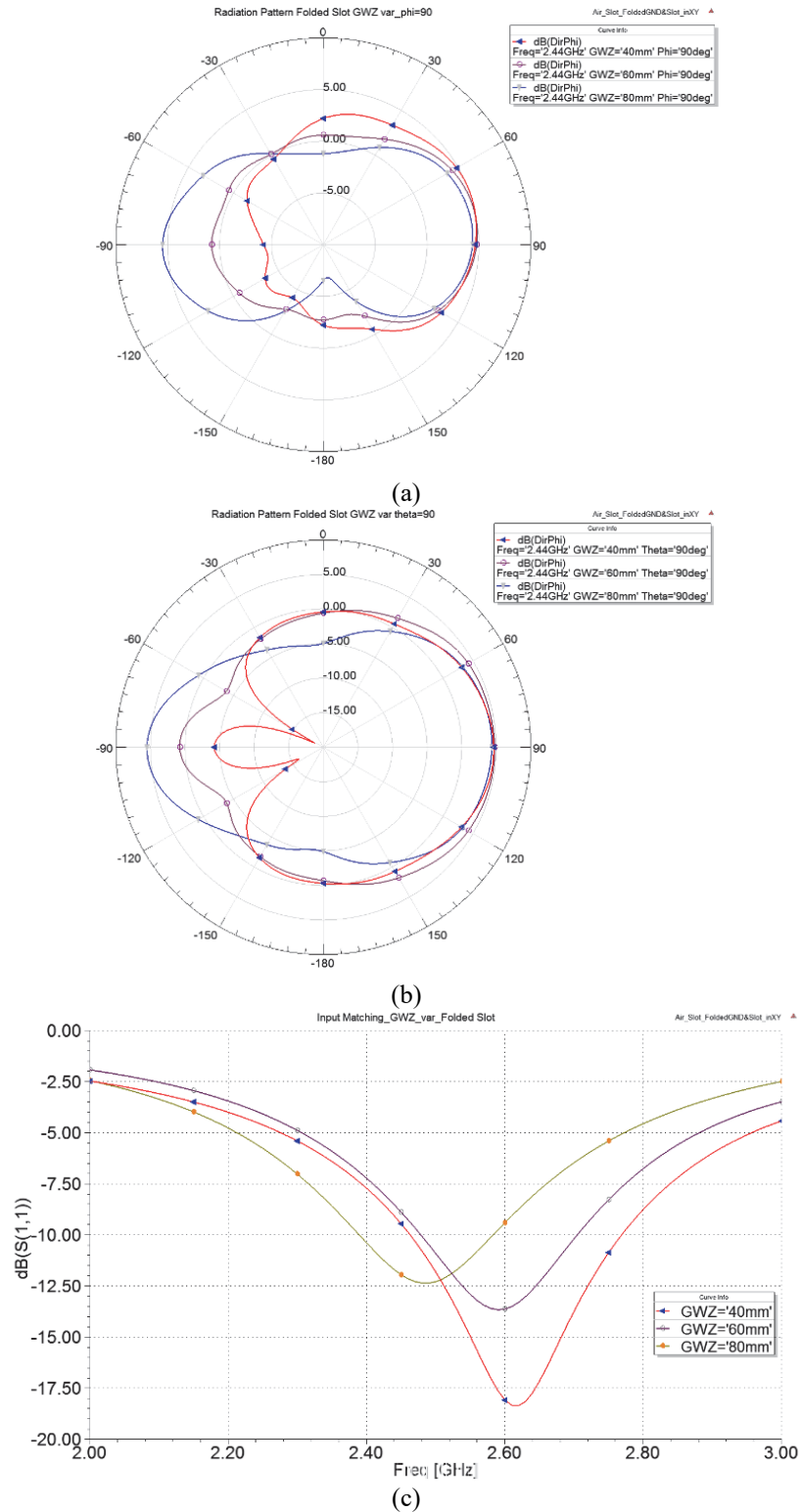


Fig. 3-15 Folding slot in slot's axial directions and studying GWZ variation for $GW=120\text{mm}$, a) ϕ polarized directivity at 2.44GHz in $\phi=90^\circ$ plane, b) ϕ polarized directivity at 2.44GHz in $\theta=90^\circ$ plane, and c) Input reflection coefficient

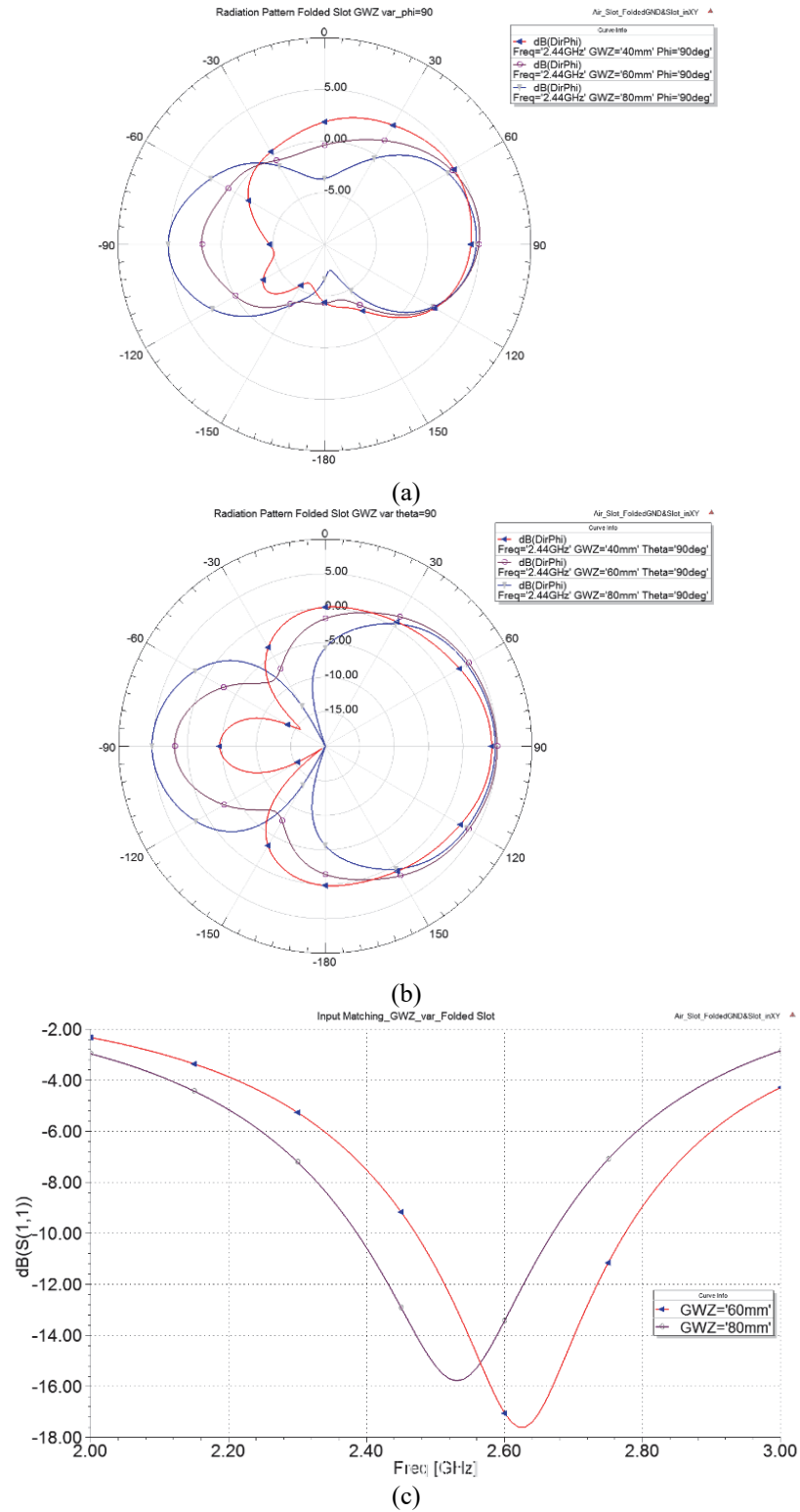


Fig. 3-16 Folding slot in slot's axial directions and studying GWZ variation for $GW=80\text{mm}$, a) ϕ polarized directivity at 2.44GHz in $\phi=90^\circ$ plane, b) ϕ polarized directivity at 2.44GHz in $\theta=90^\circ$ plane, and c) Input reflection coefficient

3.2.4.2 Analytical solution for folded slot antenna

Here we attempt to analytically confirm all the results achieved in the previous section. The following assumptions are made to simplify the analysis.

- 1- Folding the ground plane will not affect nominal magnetic current distribution along the slot antenna
- 2- Contribution of the two folded sections in the far field radiation pattern is ignored and only the contribution of the center slot which is toward the broadside has been taken into account.

Nominal Magnetic current density running in the slot mounted on vertical faces of the cube has a sinusoidal form as given by (3-1) where $l/2$ indicates the whole slot length, parts of which are being folded on top and bottom faces of the cube, hence the effective radiating length is equal to GWZ . Note that primed variables (x', y', z') are used to emphasize source coordinates. Equation (3-1), (3-2) and (3-3) are given for slots located on $x' = GW/2$ and $|z'| = GW/2$ faces of the cube respectively where the latter is the folded and truncated section of the former on top/bottom faces of the cube and SW indicates slot width as shown in Fig. 3-17.

$$\mathbf{M}_1(x', y', z') = \mathbf{a}_z M_0 \sin \left[k \left(\frac{SL}{2} - |z'| \right) \right] \text{ for } |z'| \leq \frac{GWZ}{2}, |y'| < \frac{SW}{2}, x' = \frac{GW}{2} \quad (3-1)$$

$$\mathbf{M}_2(x', y', z') = \mathbf{a}_x M_0 \sin \left[k \left(\frac{SL - GW - GWZ}{2} + x' \right) \right] \text{ for } z' = -\frac{GWZ}{2}, |y'| < \frac{SW}{2}, x' = \frac{GW}{2} \quad (3-2)$$

$$\mathbf{M}_3(x', y', z') = -\mathbf{a}_x M_0 \sin \left[k \left(\frac{SL - GW - GWZ}{2} + x' \right) \right] \text{ for } z' = \frac{GWZ}{2}, |y'| < \frac{SW}{2}, x' = \frac{GW}{2} \quad (3-3)$$

where $k = k_o \sqrt{\epsilon_r}$ is the wavenumber in the substrate and $\mathbf{a}_z M_0 = -2\mathbf{n} \times \mathbf{a}_y E_0$.

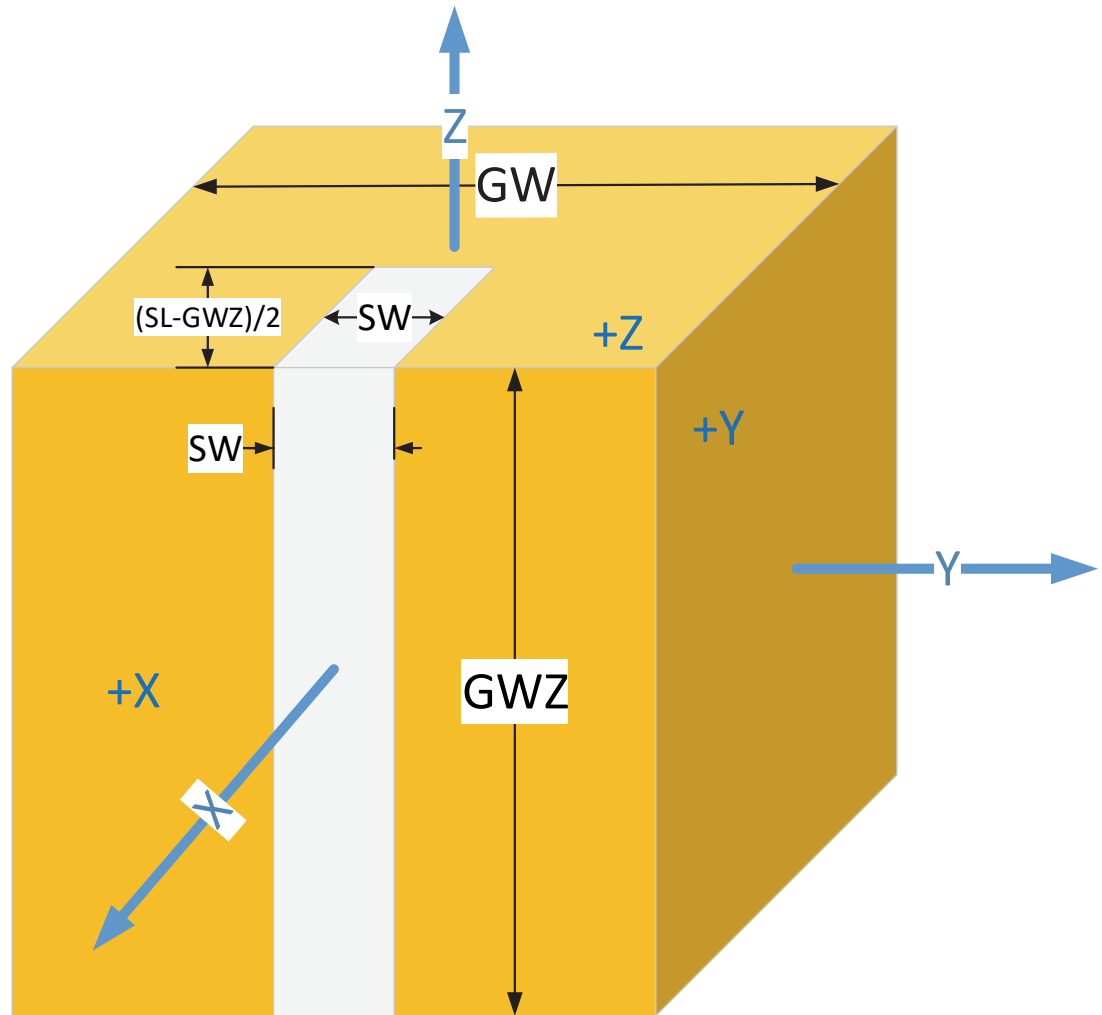


Fig. 3-17 Folded slot antenna on a cubic structure

Substitution of (3-1) in a vector potential integral of (3-4) will yield magnetic field according to (3-7) and (3-8).

$$F_{z1} = \frac{\varepsilon_0}{4\pi} \int_S M_{z1}(x', y', z') \frac{e^{-jk_o R}}{R} ds' \quad (3-4)$$

$$F_{xn} = \frac{\varepsilon_0}{4\pi} \int_S M_{xn}(x', y', z') \frac{e^{-jk_o R}}{R} ds', n=2, 3 \quad (3-5)$$

$$F_{z1} = \frac{\varepsilon_0}{4\pi} \int_{-\frac{GWZ}{2}}^{\frac{GWZ}{2}} \int_{-\frac{SW}{2}}^{\frac{SW}{2}} M_{z1}(x', y', z') \frac{e^{-jk_o R}}{R} dy' dz'$$

$$F_{xn} = \frac{\varepsilon_0}{4\pi} \int_{\frac{GW-SL+GWZ}{2}}^{\frac{GW}{2}} \int_{-\frac{SW}{2}}^{\frac{SW}{2}} M_{xn}(x', y', z') \frac{e^{-jk_o R}}{R} dy' dx', n = 2, 3 \quad (3-6)$$

Where

$$R = r - r' \cos \psi = r - \mathbf{r}' \cdot \widehat{\mathbf{a}}_r = r - y' \sin \theta \cos \phi - y' \sin \theta \sin \phi - z' \cos \theta$$

$$\mathbf{H}_1 = -j\omega \mathbf{F} = -j\omega F_{\theta 1} \mathbf{a}_\theta = j\omega F_{z1} \sin \theta \mathbf{a}_\theta \quad (3-7)$$

$$\mathbf{H}_n = -j\omega (F_{\theta n} \mathbf{a}_\theta + F_{\phi n} \mathbf{a}_\phi) = -j\omega (-F_{xn} \cos \theta \cos \phi \mathbf{a}_\theta + F_{xn} \sin \phi \mathbf{a}_\phi), n = 2, 3$$

$$H_1 = \frac{j k_o}{\eta_o 4\pi} (\sin \theta \mathbf{a}_\theta) \int_{-\frac{GWZ}{2}}^{\frac{GWZ}{2}} \int_{-\frac{SW}{2}}^{\frac{SW}{2}} M_{z1}(x', y', z') \frac{e^{-jk_o R}}{R} dy' dz'$$

$$\mathbf{H}_n = \frac{j k_o}{\eta_o 4\pi} (-\cos \theta \cos \phi \mathbf{a}_\theta + \sin \phi \mathbf{a}_\phi) \int_{\frac{GW-SL+GWZ}{2}}^{\frac{GW}{2}} \int_{-\frac{SW}{2}}^{\frac{SW}{2}} M_{xn}(x', y', z') \frac{e^{-jk_o R}}{R} dy' dx', n = 2, 3 \quad (3-8)$$

where

$$R = r - r' \cos \psi = r - \mathbf{r}' \cdot \widehat{\mathbf{a}}_r = r - x' \sin \theta \cos \phi - y' \sin \theta \sin \phi - z' \cos \theta$$

The far field electric field can be calculated from magnetic field using (3-9).

$$\mathbf{H}_1 = \frac{j}{\eta_0} \frac{k_0 e^{-jk_0 r}}{4\pi r} (\sin\theta \mathbf{a}_\theta) \int_{-\frac{GWZ}{2}}^{\frac{GWZ}{2}} \int_{-\frac{SW}{2}}^{\frac{SW}{2}} M_0 \sin \left[k \left(\frac{SL}{2} - |z'| \right) \right] e^{-jk_0(-x' \sin\theta \cos\phi - y' \sin\theta \sin\phi - z' \cos\theta)} dy' dz'$$

$$\mathbf{H}_n = \frac{j}{\eta_0} \frac{k_0 e^{-jk_0 r}}{4\pi r} \left(-\cos\theta \cos\phi \mathbf{a}_\theta + \sin\phi \mathbf{a}_\phi \right) \int_{\frac{GW-SL+GWZ}{2}}^{\frac{GW}{2}} \int_{-\frac{SW}{2}}^{\frac{SW}{2}} M_0 \sin \left[k \left(\frac{SL - GW - GWZ}{2} + x' \right) \right] e^{-jk_0(-x' \sin\theta \cos\phi - y' \sin\theta \sin\phi - z' \cos\theta)} dy' dx', \quad n = 2, 3$$

$$\mathbf{E}_1 = \eta_0 H_{\theta 1} \mathbf{a}_\phi = j \frac{M_0 e^{-jk_0 r} \sin\left(\frac{k_y SW}{2}\right)}{\pi r \sin\theta} \frac{1}{k_y} \left\{ \cos\left(k_z \frac{GWZ}{2}\right) \cos\left(k \frac{SL - GWZ}{2}\right) - \sin\left(k_z \frac{GWZ}{2}\right) \sin\left(k \frac{SL - GWZ}{2}\right) \cos\theta - \cos\left(k \frac{SL}{2}\right) \right\} \mathbf{a}_\phi \quad (3-9)$$

$$\mathbf{E}_n = \eta_0 (H_{\theta 2} \mathbf{a}_\phi + H_{\phi 2} \mathbf{a}_\theta) = 2jM_0 \frac{e^{-jk_0 r} e^{jk_z \frac{GWZ}{2}} e^{jk_x \frac{GW}{2}} \sin\left(k_y \frac{SW}{2}\right)}{4\pi r (k_0^2 - k_x^2)} \frac{1}{k_y} \left\{ k_0 e^{jk_x \frac{GWZ - SL}{2}} + jk_x \sin\left(k_0 \frac{SL - GWZ}{2}\right) - k_0 \cos\left(k_0 \frac{SL - GWZ}{2}\right) \right\} (-\cos\theta \cos\phi \mathbf{a}_\phi + \sin\phi \mathbf{a}_\theta), \quad n = 2, 3$$

where

$$k_x = k \sin\theta \cos\phi, k_y = k \sin\theta \sin\phi \quad \text{and} \quad k_z = k \cos\theta$$

For a half wavelength long slot antenna, one can simplify (3-9) and derive (3-10).

$$\begin{aligned}
\mathbf{E}_1 &= j \frac{M_0 e^{-jk_0 r}}{2\pi r \sin\theta} \times \frac{\sin\left(k_y \frac{SW}{2}\right)}{k_y} \left\{ \cos\left(k_z \frac{GWZ}{2}\right) \sin\left(k_0 \frac{GWZ}{2}\right) \right. \\
&\quad \left. - \sin\left(k_z \frac{GWZ}{2}\right) \cos\left(k_0 \frac{GWZ}{2}\right) \cos\theta \right\} \mathbf{a}_\phi \\
\mathbf{E}_2 &= 2jM_0 \frac{e^{-jk_0 r} e^{jk_z \frac{GWZ}{2}} e^{jk_x \frac{GW}{2}} \sin\left(\frac{k_y SW}{2}\right)}{4\pi r (k_0^2 - k_x^2) k_y} \left\{ k_0 e^{-j\frac{\pi}{2} \sin\theta \cos\phi} e^{jk_x \frac{GWZ}{2}} + jk_x \cos\left(k_0 \frac{GWZ}{2}\right) \right. \\
&\quad \left. - k_0 \sin\left(k_0 \frac{GWZ}{2}\right) \right\} (-\cos\theta \cos\phi \mathbf{a}_\phi + \sin\phi \mathbf{a}_\theta) \\
\mathbf{E}_3 &= -2jM_0 \frac{e^{-jk_0 r} e^{jk_z \frac{GWZ}{2}} e^{jk_x \frac{GW}{2}} \sin\left(\frac{k_y SW}{2}\right)}{4\pi r (k_0^2 - k_x^2) k_y} \left\{ k_0 e^{-j\frac{\pi}{2} \sin\theta \cos\phi} e^{jk_x \frac{GWZ}{2}} + jk_x \cos\left(k_0 \frac{GWZ}{2}\right) \right. \\
&\quad \left. - k_0 \sin\left(k_0 \frac{GWZ}{2}\right) \right\} (-\cos\theta \cos\phi \mathbf{a}_\phi + \sin\phi \mathbf{a}_\theta)
\end{aligned} \tag{3-10}$$

where

$$k_x = k_0 \sin\theta \cos\phi, k_y = k_0 \sin\theta \sin\phi \quad \text{and} \quad k_z = k_0 \cos\theta$$

where Z and Y are defined in (3-9). In (3-11), the electric field is decomposed into three components where only E_Y is a function of ϕ . Additionally, here we have considered E_Y to be equal to zero in the negative half space. This assumption is made in order to model slots cut on the cube side walls as directive elements meaning their back radiation toward the inner space of the cube is ignored. This will simplify the problem since the analysis can be done using formulas and concepts from circular arrays of directive elements. In later sections, we see that this assumption is true since the folded slot array is designed such that the electric field intensity inside the cube is negligible. Also note that element patterns do not remain the same as the observation angle (ϕ) changes in the azimuth plane. Each slot illuminates the span of angles around the broadside of its corresponding cube face, hence the maximum of element patterns also rotates as the observation angle (ϕ) varies in the azimuth plane.

$$\mathbf{E}_1 = j \frac{M_0 e^{-jk_r}}{\pi r \sin \theta} \times EY_1 \times EZ_1 \mathbf{a}_\phi$$

where

$$EY_1 = \begin{cases} \frac{\sin\left(k_y \frac{SW}{2}\right)}{k_y}, & -90 \leq \phi \leq 90 \\ 0, & 90 < \phi < 270 \end{cases} \quad (3-11)$$

and

$$EZ_1 = \cos\left(k_z \frac{GWZ}{2}\right) \sin\left(k_o \frac{GWZ}{2}\right) - \sin\left(k_z \frac{GWZ}{2}\right) \cos\left(k \frac{GWZ}{2}\right) \cos \theta$$

$$\mathbf{E}_2 = 2jM_0 \frac{e^{-jk_o r}}{4\pi r} EZ_2 EY_2 EX_2 (-\cos \theta \cos \phi \mathbf{a}_\phi + \sin \phi \mathbf{a}_\theta) \text{ (top face)}$$

$$\mathbf{E}_3 = -2jM_0 \frac{e^{-jk_o r}}{4\pi r} EZ_3 EY_3 EX_3 (-\cos \theta \cos \phi \mathbf{a}_\phi + \sin \phi \mathbf{a}_\theta) \text{ (Bottom face)}$$

where

$$EY_2 = EY_3 = \frac{\sin\left(k_y \frac{SW}{2}\right)}{k_y}$$

and

$$EX_2 = EX_3 = \frac{e^{jk_x \frac{GW}{2}}}{(k_o^2 - k_x^2)} \left\{ k_o e^{-j\frac{\pi}{2} \sin \theta \cos \phi} e^{jk_x \frac{GWZ}{2}} + jk_x \cos\left(k_o \frac{GWZ}{2}\right) - k_o \sin\left(k_o \frac{GWZ}{2}\right) \right\} \quad (3-12)$$

$$EZ_2 = \begin{cases} e^{jk_z \frac{GWZ}{2}}, & 0 \leq \theta \leq 90 \\ 0, & 90 < \theta < 180 \end{cases}$$

$$EZ_3 = \begin{cases} 0, & 0 \leq \theta \leq 90 \\ e^{jk_z \frac{GWZ}{2}}, & 90 < \theta < 180 \end{cases}$$

As shown in (3-13) far field of folded slot can be obtained by adding up contribution of all three sections of the slot in the far field radiation pattern. Co and cross polarized directivity of a slot antenna and a folded slot antenna with GWZ=40mm are shown in Fig. 3-18 and Fig. 3-19, respectively. As was expected from analytical calculations, 3dB beam width of antenna increases from 78° to 84° where slot is folded. Similar structure shown in Fig. 3-20 is EM simulated and far field results are shown in Fig. 3-21 and Fig. 3-22 to verify analytical results.

$$\mathbf{EF} = \mathbf{E}_1 + \mathbf{E}_2 + \mathbf{E}_3$$

(3-13)

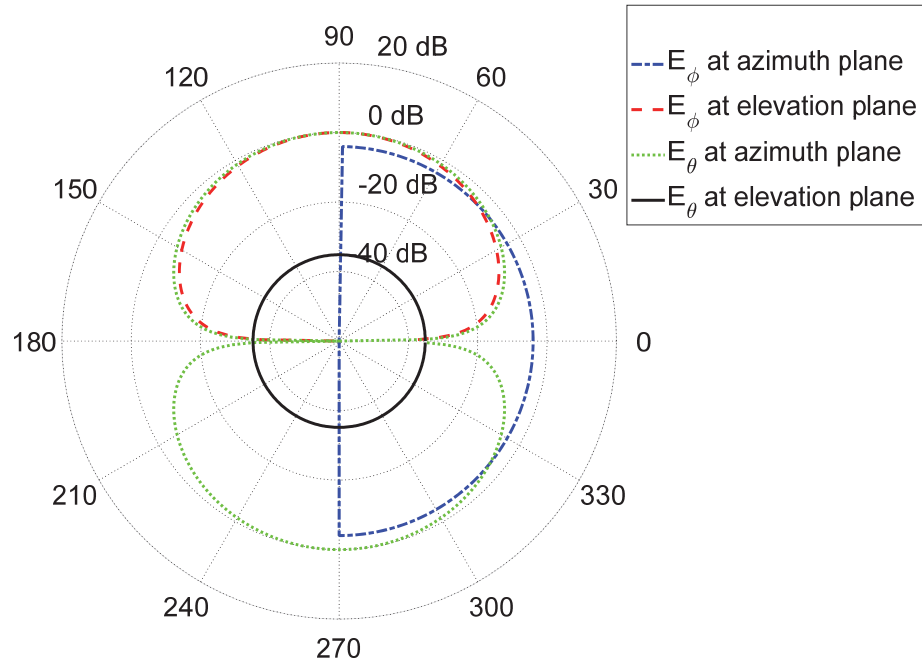


Fig. 3-18 Analytically calculated normalized directivity at 2.45GHz of a folded slot antenna for $SL=61.25\text{mm}$, $GWZ=60\text{mm}$, $SW=1\text{mm}$, $GW=39.5\text{mm}$ and $a=GW/2$, (3dB Beam width for E_ϕ at elevation plane= 78°)

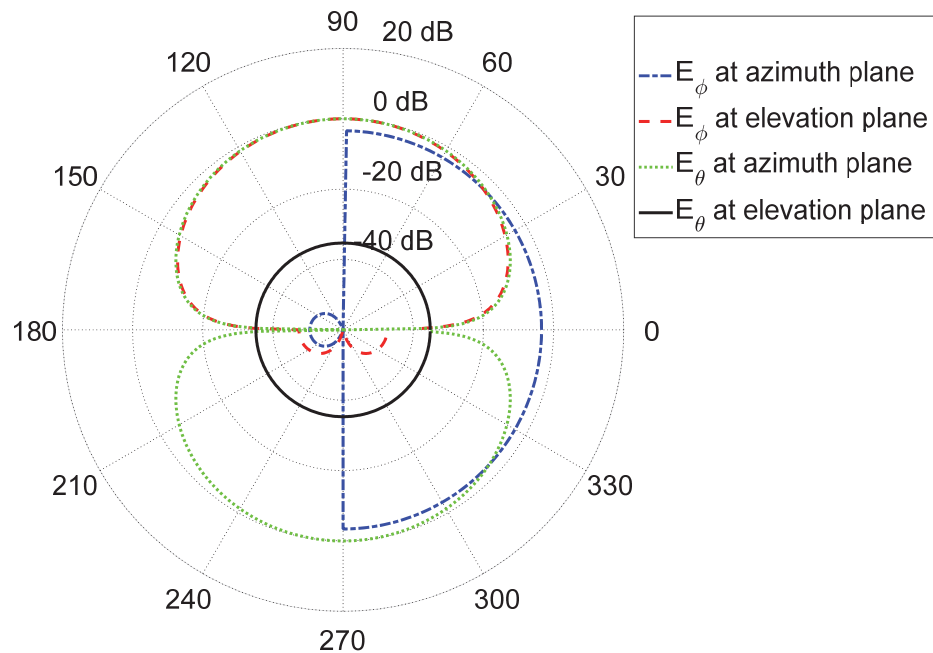


Fig. 3-19 Analytically calculated normalized directivity at 2.45GHz of a folded slot antenna for $SL=61.25\text{mm}$, $GWZ=30\text{mm}$, $SW=1\text{mm}$, $GW=39.5\text{mm}$ and $a=GW/2$, (3dB Beam width for E_ϕ at elevation plane= 84°)

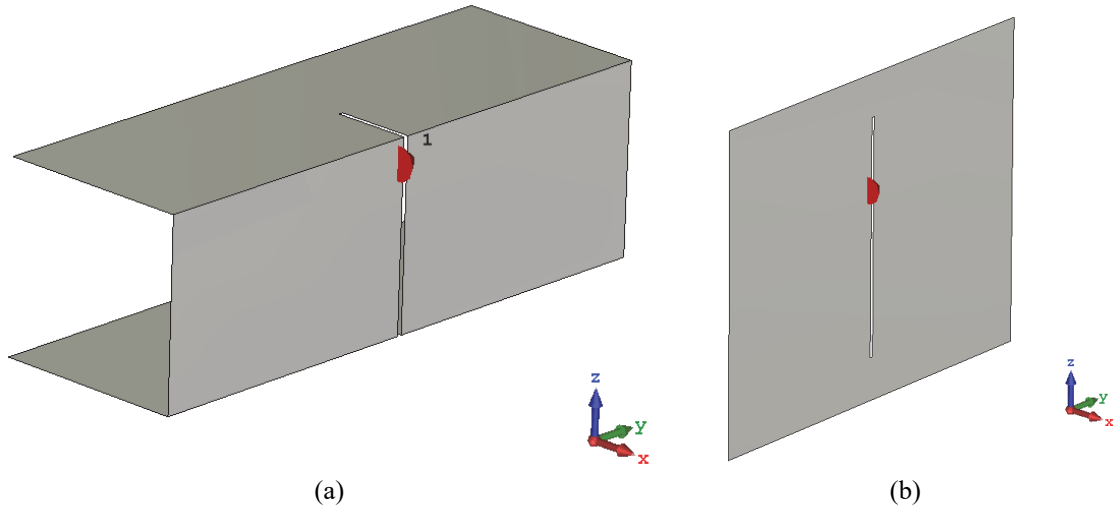


Fig. 3-20 Folded slot antenna on a cubic structure, a) folded slot antenna, ad b) Straight slot antenna

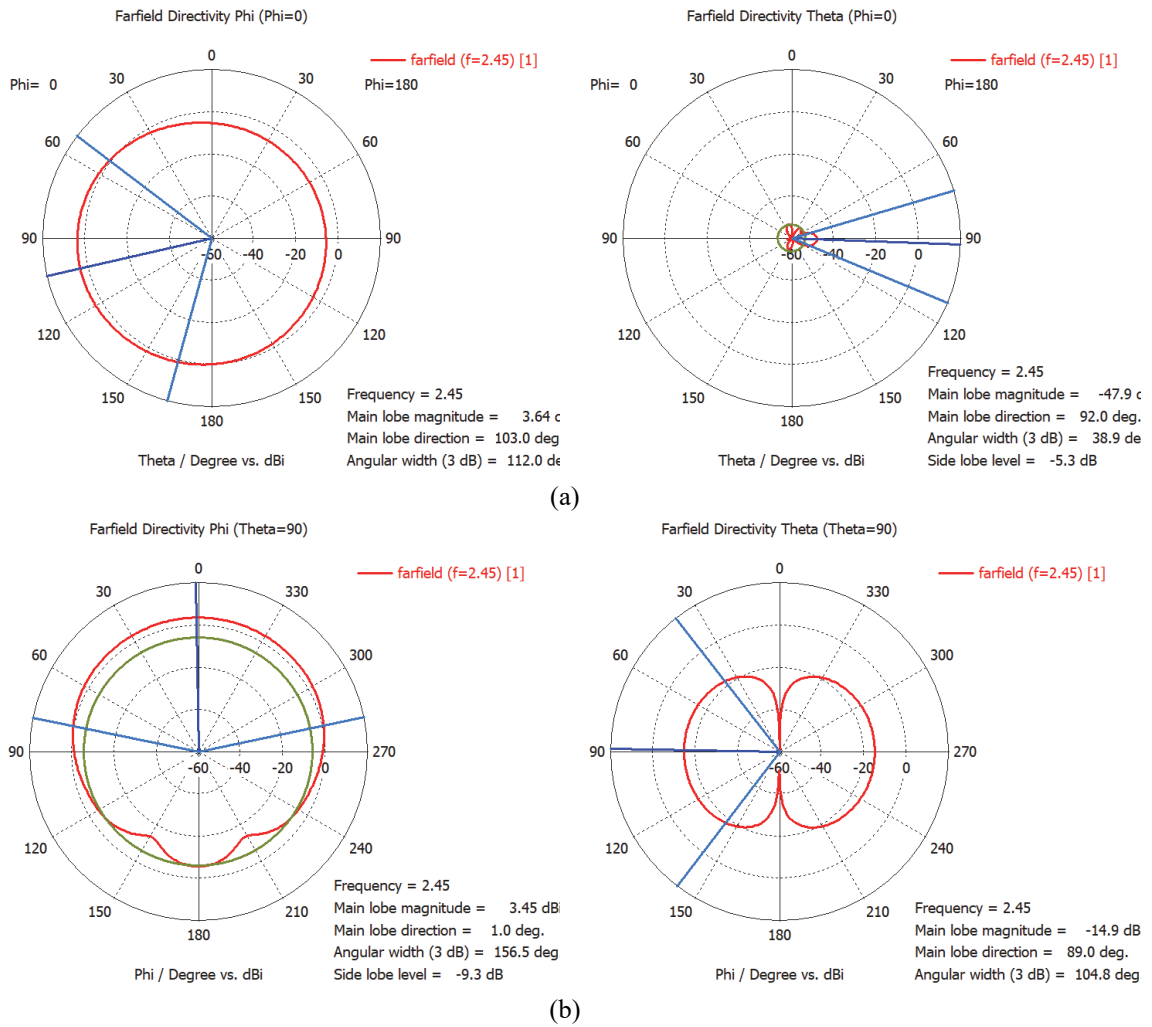


Fig. 3-21 Normalized directivity at 2.45GHz obtained through EM simulation for a folded slot antenna shown in with $SL=73.5mm$, $GWZ=40mm$, $SW=1mm$, $GW=125mm$ and $a=GW/2$, a) elevation plane, and b) Azimuth plane (3dB Beam width for E_{θ} at elevation plane= 112.5°)

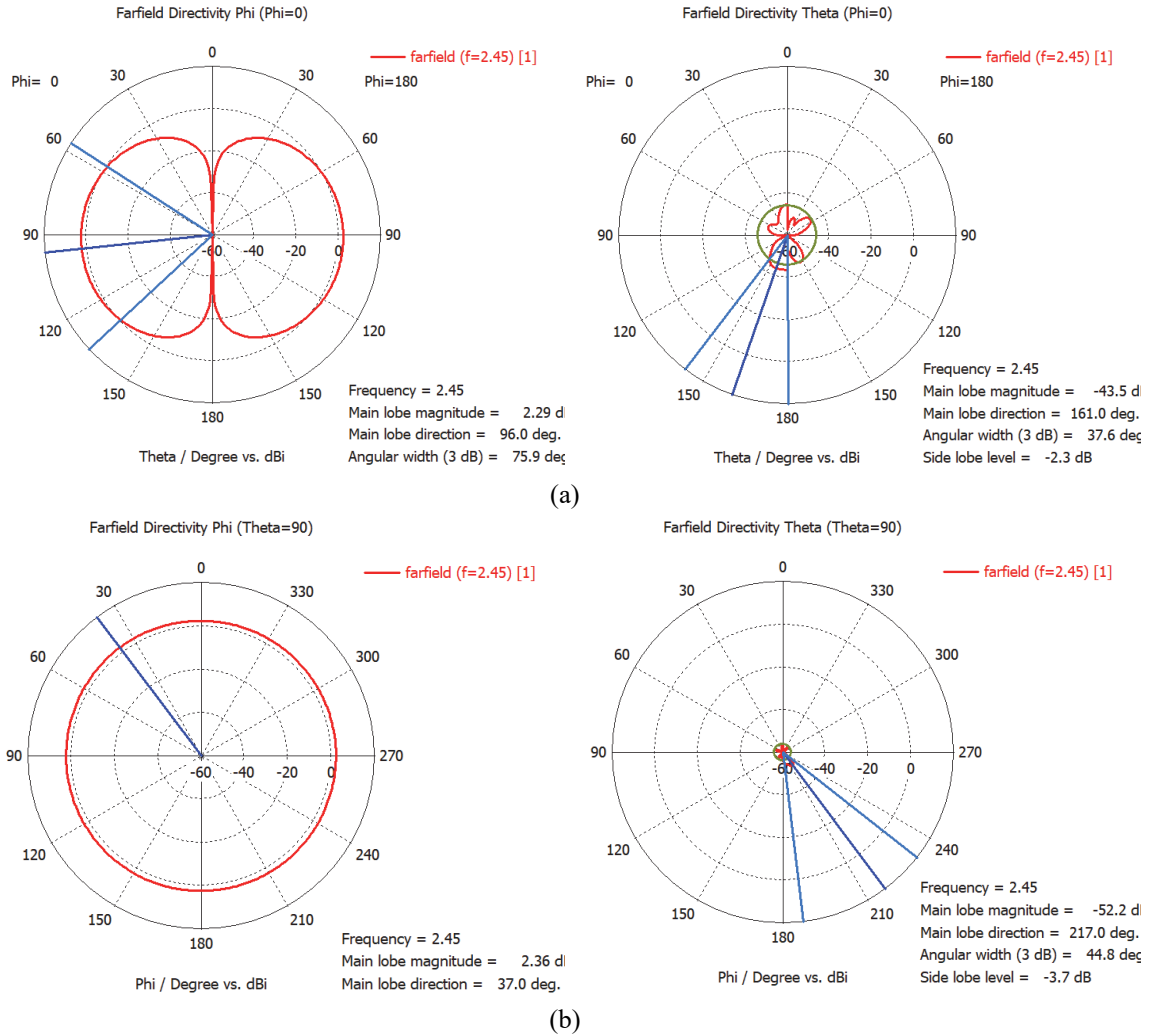


Fig. 3-22 Normalized directivity at 2.45GHz obtained through EM simulation for a folded slot antenna shown in with $SL=73.5\text{mm}$, $GWZ=100\text{mm}$, $SW=1\text{mm}$, $GW=125\text{mm}$ and $a=GW/2$, a) elevation plane, and b) Azimuth plane (3dB Beam width for E_ϕ at elevation plane= 75.5°)

3.3 Cubic slot antenna array

Since we have four slot antennas on the vertical faces of our cubic structure, we can use circular array theory to model our cubic antenna. All the configurations introduced in this research can be analyzed by this theory. In the following subsections, we first start by discussion of circular arrays with isotropic elements. The special case of directive elements is then brought into context and finally we consider a particular case of circular array with slot antenna elements.

3.3.1 Circular array theory

3.3.1.1 Circular array with isotropic elements

Circular arrays in general case have been investigated by many researchers specially Balanis [67]. In the general case, the reference antenna element rotates around an axis and repeated every $\phi_n = \frac{360}{N}$ where N is the number of elements. All antenna elements are supposed to have an omnidirectional pattern in the plane of rotation. Equations to calculate the array factor of such antenna can be found in the literature [67].

Circular arrays with isotropic elements or elements whose radiation pattern will not change by rotation around the axis of the array can be analyzed similar to planar arrays. As element factor $EF(\varphi)$ is common for all elements, one can bring it outside of sigma and divide the far field radiation pattern to element factor and array factor, each can be calculated and analyzed separately.

$$E = \sum_{n=1}^N a_n \frac{e^{-jkR_n}}{|R_n|} EF(\varphi) = AF \times EF(\varphi) \quad (3-14)$$

$$AF = \sum_{n=1}^N a_n \frac{e^{-jkR_n}}{|R_n|} \quad (3-15)$$

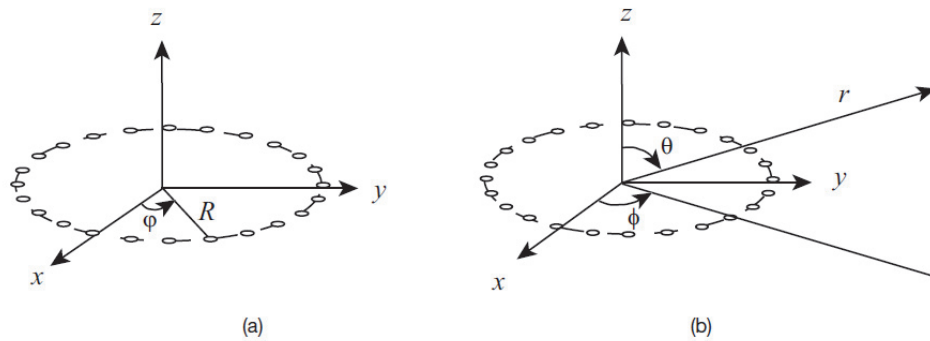


Fig. 3-23 Figure from a book which shows circular array configuration, a) source local coordinate, and b) far field coordinate at observation point (courtesy of [67])

Beam steering of a *uniform* array with element rotation in the azimuth plane of $\theta_0 = 90^\circ$ needs proper variation of progressive phase difference, ϕ_0 . Rotation of elements will not change the beam steering principle. The radiation pattern of a circular array

consisting of four isotropic elements with $2 \times a$ equal to a quarter of wavelength and half wavelength have been shown in Fig. 3-24.

As shown in Fig. 3-24, a uniform circular antenna array with $a = \frac{\lambda}{8}$ does not have any null, but it has directive radiation pattern with noticeable front to back ratio which is steering according to the variation of progressive phase. Having a non-uniform circular array can improve the performance of beam steering as the amplitude of the electric fields radiating from different elements can vary to achieve the desired beam steering characteristic. In multi-feeds cubical array structures, amplitude weight and phase of each antenna element can be adjusted for steering the beam at a desired direction at the expense of a more complicated feeding network.

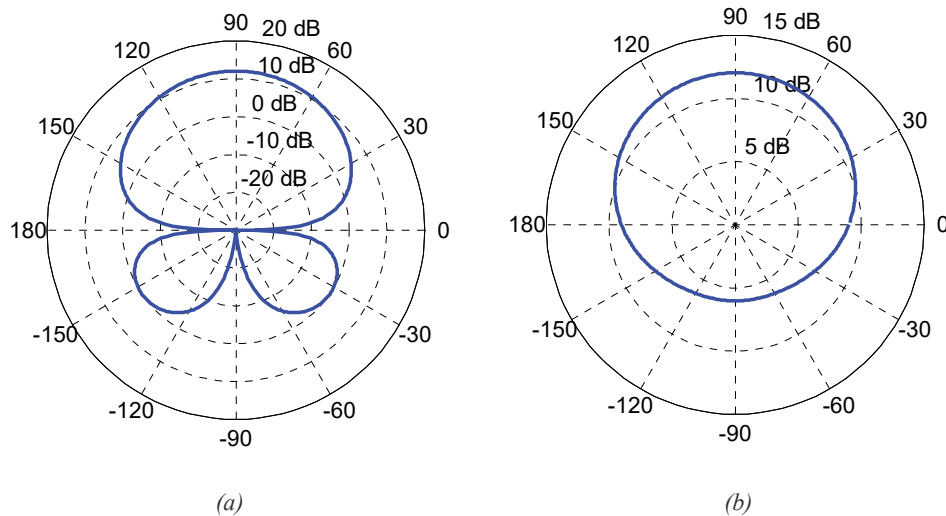


Fig. 3-24 Theoretical Array Factor of a basic 2.445GHz circular uniform array for a) $a = \frac{\lambda}{4}$ and b) $a = \frac{\lambda}{8}$

3.3.1.2 Circular array with directive elements

If antenna elements in a circular array have directive radiation patterns as opposed to omnidirectional, the analysis becomes more complicated. Our cubic slot array with four vertical slot radiators placed on its side walls, falls under this category as the antenna element factor is not omnidirectional and rotates based on the location of element in the array.

Here, phase center of antenna elements is not relocated with respect to the center axis of the circular array. Hence, required progressive phase shift can be extracted from the

conventional circular array factor equation. However, rotation of element factor needs to be considered in the calculation of far field radiation pattern. It means phase of electric fields needs to match the general theory of circular array. Also note that, elements do not have equal contributions in the array factor as their weights are different over an arbitrary span of angles in the space. So, progressive phase shift of the array shown in Fig. 3-25 can be calculated from $\alpha_n = -k a \sin \theta_0 \cos(\phi_0 - \phi_n)$ where a is equal to half of the edge length of the cube or radius of the equivalent circular array.

To consider contribution of element factor and its rotation around its own axis in the directivity of the circular array, total electric field and radiation pattern of the circular array is extracted in the following equations. It is clear that we cannot define distinguished and independent array factor and element factor anymore as they are merged together.

Usually, in circular arrays, antenna elements are not radiating symmetrically in the observation plane and they are self-axis rotated. In this case, element factor and array factor cannot be separated and the array radiation pattern needs to be calculated directly through general equations as (3-16) and (3-17).

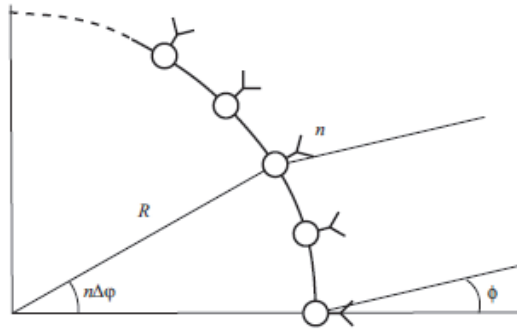


Fig. 3-25 Configuration of circular array with directive antenna elements (Courtesy of [69])

$$E = \sum_{n=1}^N a_n \frac{e^{-jkRn}}{R_n} EF(|\varphi - \varphi_n|) = \frac{e^{-jkr}}{r} \sum_{n=1}^N a_n e^{+jk a \sin \theta \cos(\phi - \phi_n)} EF(|\varphi - \varphi_n|) \quad (3-16)$$

$$\begin{aligned}
E &= \frac{e^{-jkr}}{r} \sum_{n=1}^N I_n e^{j[k a \sin \theta \cos(\phi - \phi_n) + \alpha_n]} \text{EF}(|\varphi - \varphi_n|) \\
&= \frac{e^{-jkr}}{r} \sum_{n=1}^N I_n e^{jka[\sin \theta \cos(\phi - \phi_n) - \sin \theta_0 \cos(\phi_0 - \phi_n)]} \text{EF}(|\varphi - \varphi_n|) \\
&= \frac{e^{-jkr}}{r} \sum_{n=1}^N I_n e^{jka[\cos(\psi) - \cos(\psi_0)]} \text{EF}(|\varphi - \varphi_n|) \\
&= \frac{e^{-jkr}}{r} \sum_{n=1}^N I_n e^{jk\rho_0 \cos(\phi_n - \xi)} \text{EF}(|\varphi - \varphi_n|)
\end{aligned} \tag{3-17}$$

where

$$\xi = \tan^{-1} \left[\frac{\sin \theta \sin \phi - \sin \theta_0 \sin \phi_0}{\sin \theta \cos \phi - \sin \theta_0 \cos \phi_0} \right]$$

$$\rho_0 = a[(\sin \theta \cos \phi - \sin \theta_0 \cos \phi_0)^2 + (\sin \theta \sin \phi - \sin \theta_0 \sin \phi_0)^2]^{1/2}$$

$$d = \left(\frac{2\pi}{N}\right) a \text{ a distance between antenna elements placed on a circular perimeter}$$

3.3.2 Circular array with slot antenna elements

3.3.2.1 Analytical solution

To achieve an omnidirectional radiation pattern from a cubic structure, the following assumption was made.

The four radiating elements placed on vertical faces of the cube can model a circular array with Z being the axis of rotation. Here, the distance between antenna elements and the center of rotation is defined as a which is equal to half of the cube edge length $GW/2$, as can be seen in Fig. 3-26.

Circular arrays in general have been investigated by many researchers [67]–[69]. In the general case, the reference antenna rotates around an axis and is repeated every $\phi_n = \frac{360}{N}$ degrees where N is the number of elements. All antenna elements are assumed isotropic point sources with omnidirectional patterns in the plane of rotation. Equations to calculate the array factor of such circular antennas can be found in the literature [13].

In our proposed cubic structure which is a circular array with slot antennas as radiating elements the situation is more complex because the array elements are not

omnidirectional (isotropic) hence their radiation pattern also rotates as their physical location on the array changes. This situation is depicted in Fig. 3-26 where yellow lightning bolts and double arrows are used to illustrate the angular sector illuminated, by each antenna element. Therefore, the effect of rotation of elements also needs to be considered in the calculation of far field radiation pattern.

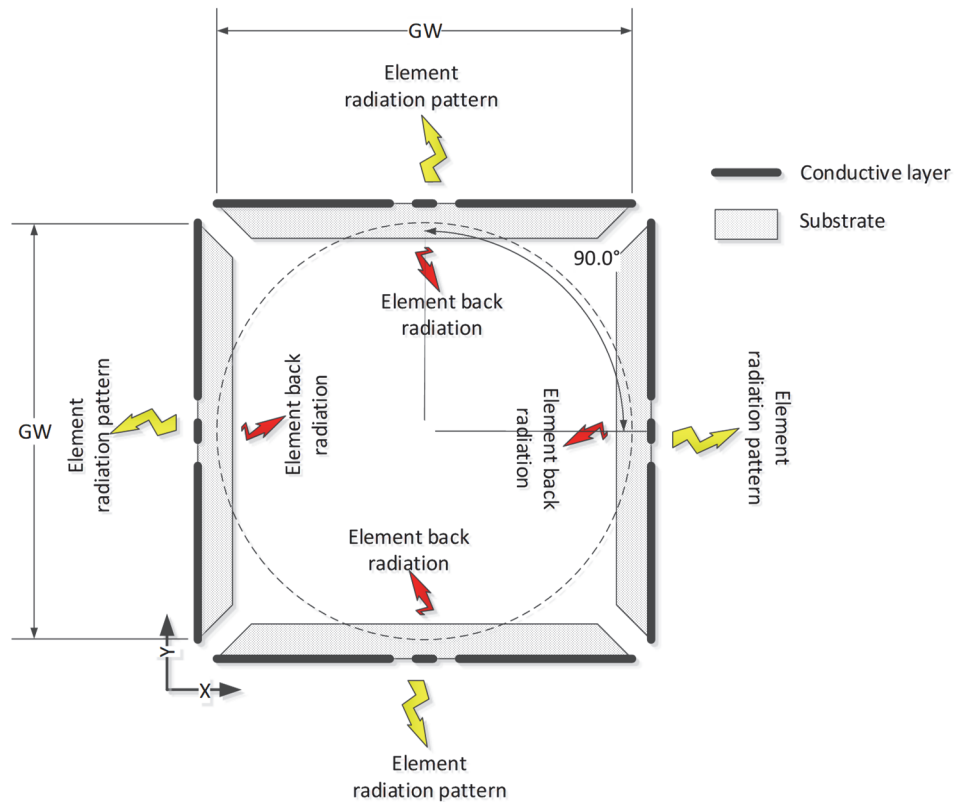


Fig. 3-26 Top view of our proposed array analyzed as a circular array.

In (3-18) electric field of circular array has been modified in such a way that element rotation around its own axis is considered in addition to rotation around center of the cube. In this case, total far field of the antenna cannot be simply calculated by multiplying array factor (AF) and element factor (EF), but electric field of each antenna element is orientation-dependent, as shown by inclusion of $EF(|\varphi - \varphi_n|)$ in equation (3-18) where φ_n designates the location of n^{th} element.

$$E = \sum_{n=1}^N a_n \frac{e^{-jk_0 R_n}}{R_n} \text{EF}(|\varphi - \varphi_n|) = \frac{e^{-jk_0 r}}{r} \sum_{n=1}^N a_n e^{+jk_0 a \sin\theta \cos(\varphi - \varphi_n)} \text{EF}(|\varphi - \varphi_n|) \quad (3-18)$$

in which $a_n = I_n e^{\alpha_n}$, are the element excitations and the distance R_n is approximated by r for the amplitude terms and by factor $r - a \sin\theta \cos(\varphi - \varphi_n)$, for the phase terms according to [Fig. 6.109 b [67]].

In calculation of progressive phase between elements, it is worth to note that phase center of antenna elements is not relocated with reference to the center of circular array, however as mentioned earlier since array elements do not have omnidirectional radiation pattern, and each element pattern only illuminates a specific angular sector of the 4π steradian, the corresponding space diversity needs to be taken into account. It means, based on the related beam-widths, element spacing and rotation angle around the cube, over a particular span of observation angles, we assume only two elements contribute to the final far field array factor. The schematic in Fig. 3-27 exemplifies this two-at-a-time contribution of neighboring elements for the entire range of observation angles in the azimuth plane.

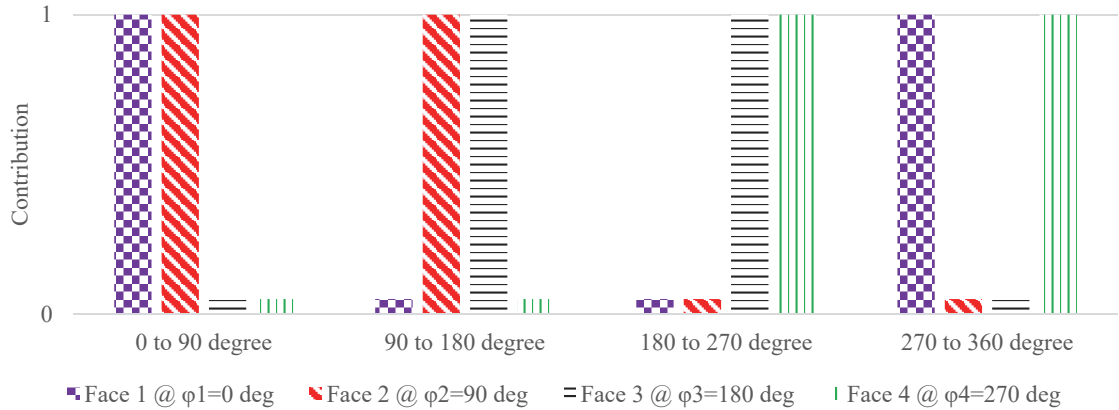


Fig. 3-27 Contribution of neighboring elements in array factor over the entire observation angles in the azimuth plane.

Hence, the progressive phase shift to steer the pattern to θ_0 and ϕ_0 can be calculated from equation (3-19).

$$\alpha_n = -k_0 a \sin\theta_0 \cos(\varphi_0 - \varphi_n) \quad (3-19)$$

In contrast to planar antennas, circular arrays are inherently appropriate in achieving an omnidirectional radiation pattern when all antennas are excited in-phase ($\alpha_n = 0$) with the sum amplitudes and $I_n = I = 1$.

$$E = \frac{Ie^{-jk_0r}}{r} \sum_{n=1}^N e^{j[k_0a \sin\theta \cos(\varphi - \varphi_n)]} EF(|\varphi - \varphi_n|) \quad (3-20)$$

3.3.2.2 Simulation and modeling

Here we model a circular array antenna made of slot antennas where each antenna has a finite ground plane as shown in Fig. 3-28. Results have been compared for different values of the parameter a which is the radius of circular array. For the sake of consistency, we have used the same parameters for ground plane dimensions. Length of ground plane which is parallel to slot's axis is named GWZ and width of ground plane which is perpendicular to slot axis is designated by GW. It is worth to mention that here we modeled the array based on slots cut in PEC plates without any substrate.

In Fig. 3-29, we compared antenna input reflection coefficient in the presence of adjacent antennas. The antenna reflection coefficient degraded by decreasing a which means due to the coupling between antennas and specially antenna and ground planes of adjacent elements, antenna element will be detuned where minimum input reflection coefficient from -35dB for $a=75\text{mm}$ increased to -12dB for $a=50\text{mm}$.

In Fig. 3-30, Fig. 3-31, and Fig. 3-32, antenna radiation pattern for $a=75\text{mm}$, 55mm, and 50mm are compared against each other, respectively. As observed, the maximum directivity is almost equal for three cases, but side lobe level in elevation plane as well as back lobe radiation decreased significantly when a is decreasing from $a=75\text{mm}$ to 50mm. For $a=50\text{mm}$ shown in Fig. 3-32 where all planes are connected together and formed a unified ground plane, the pattern is not much distorted comparing to $a=75\text{mm}$ or $a=55\text{mm}$ shown Fig. 3-30 and Fig. 3-31 due to reduction of ground plane edge effects. For $a=50\text{mm}$, we are not dealing with a finite ground plane anymore, as the antenna ground plane is replaced with a folded ground plane studied in the previous section.

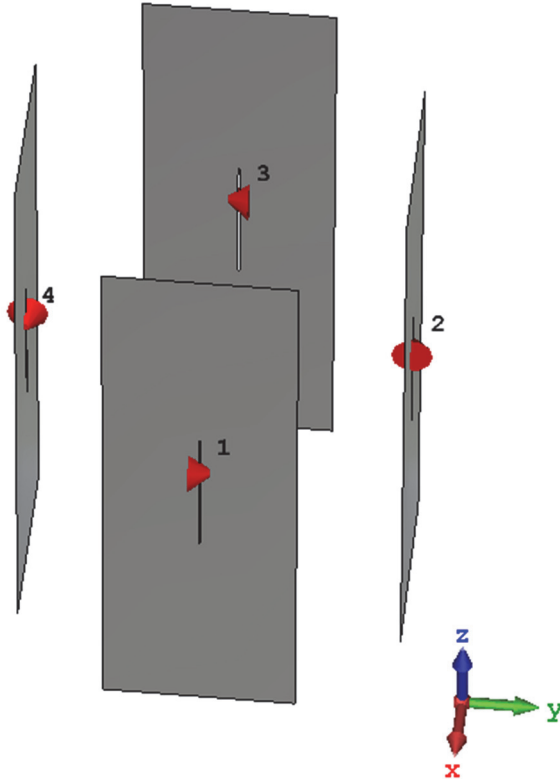


Fig. 3-28 Circular array made of four slot antenna elements

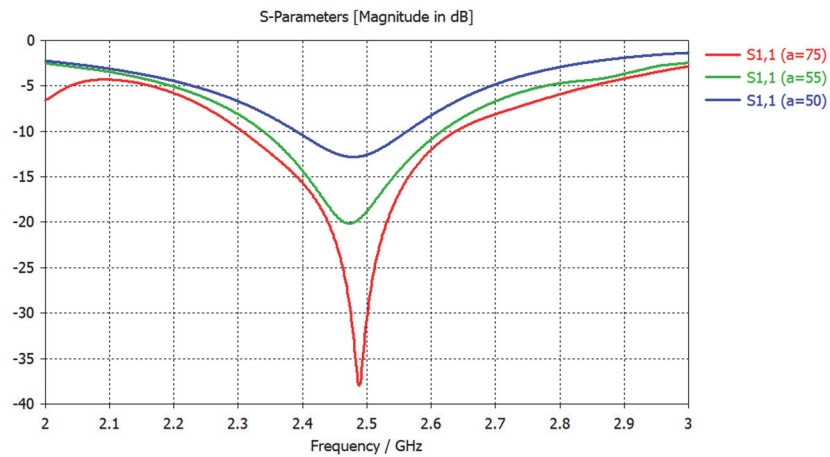


Fig. 3-29 Input reflection coefficient of slot antenna circular array for radius of 50, 55, 75mm

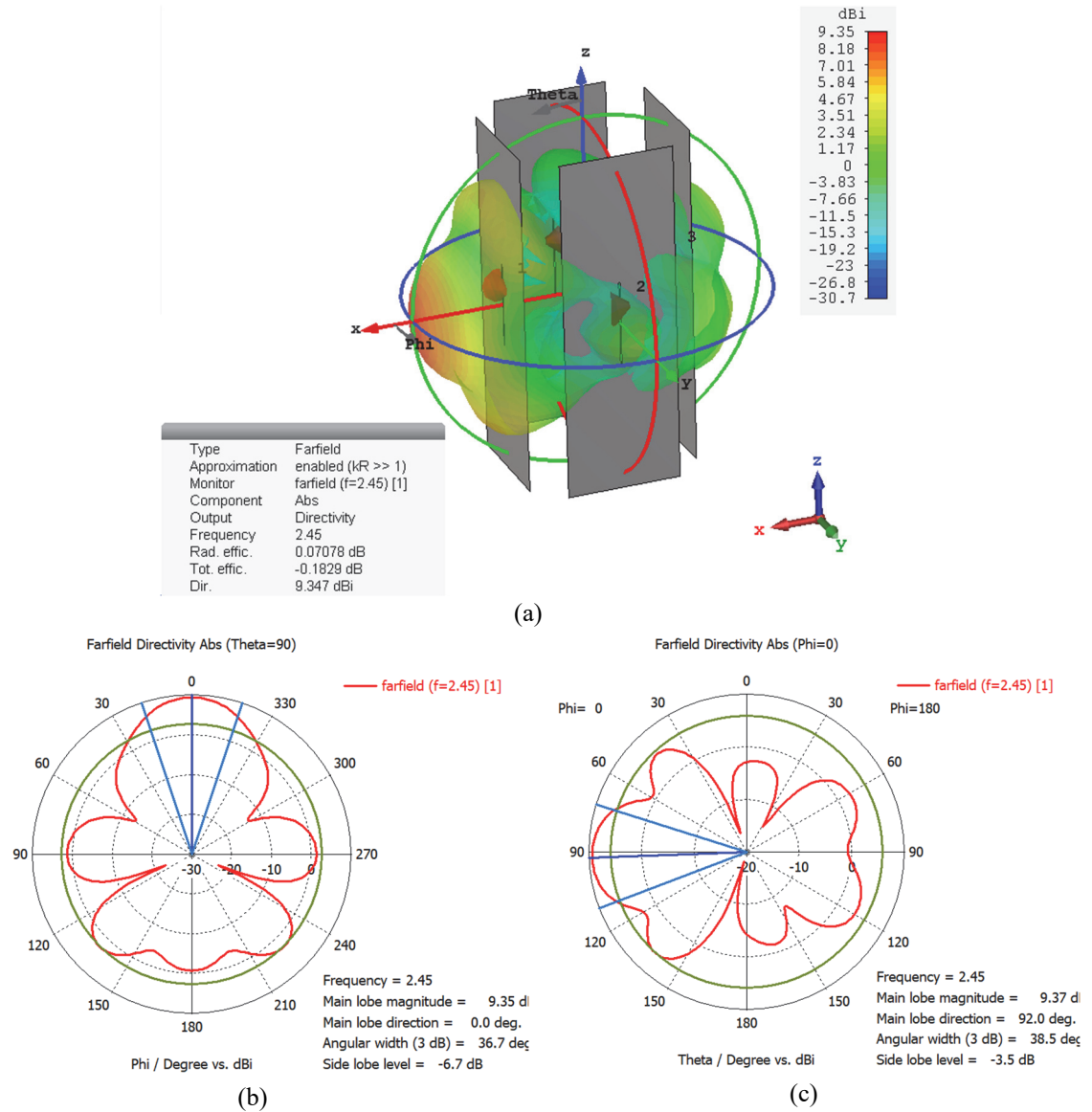


Fig. 3-30 Circular antenna array for $a=75\text{mm}$, a) Total directivity at 2.45GHz in 3-D space, b) Total directivity at 2.45GHz in $\theta=90^\circ$ plane, and c) Total directivity at 2.45GHz in $\phi=0$ plane

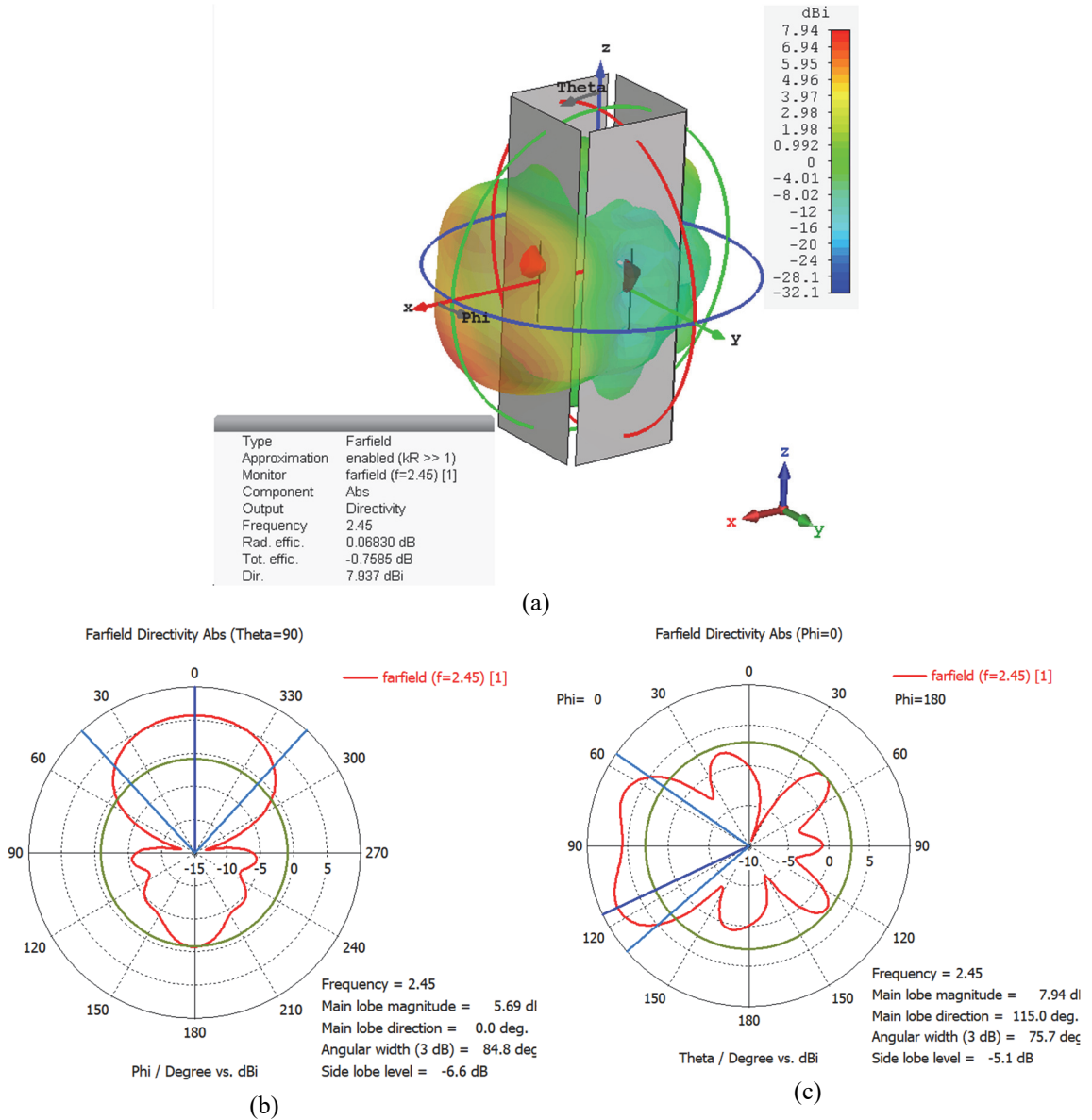


Fig. 3-31 Circular antenna array for $a=55\text{mm}$, a) Total directivity at 2.45GHz in 3-D space, b) Total directivity at 2.45GHz in $\theta=90^\circ$ plane, and c) Total directivity at 2.45GHz in $\phi=0$ plane

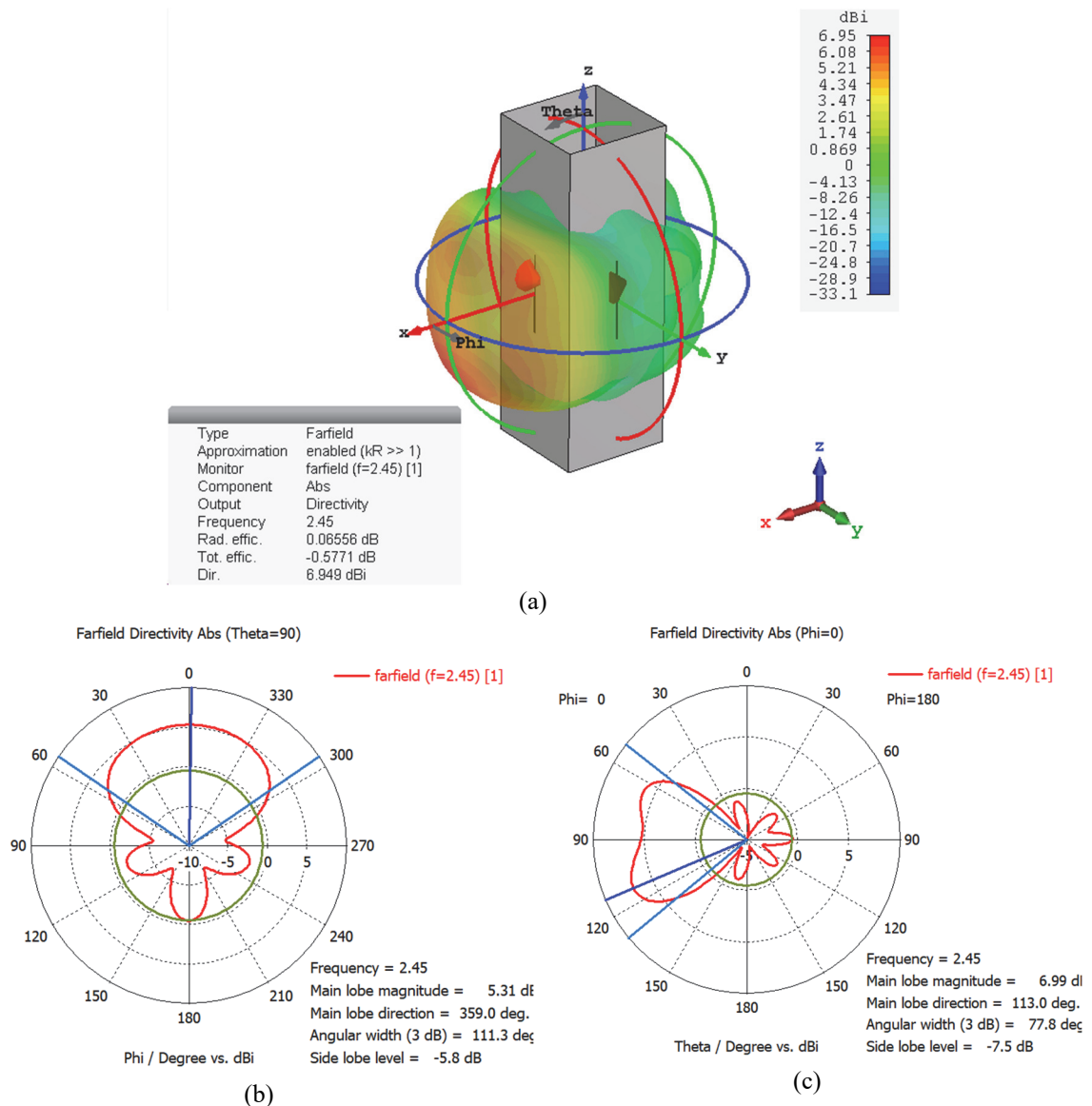


Fig. 3-32 Circular antenna array for $a=50\text{mm}$, a) Total directivity at 2.45GHz in 3-D space, b) Total directivity at 2.45GHz in $\theta=90^\circ$ plane, and c) Total directivity at 2.45GHz in $\phi=0$ plane

3.3.3 Circular array with folded slot antenna element

3.3.3.1 Analytical

Our proposed structure consists of four finite length radiating slots bent on top and bottom faces of a cube as shown in Fig. 3-33.

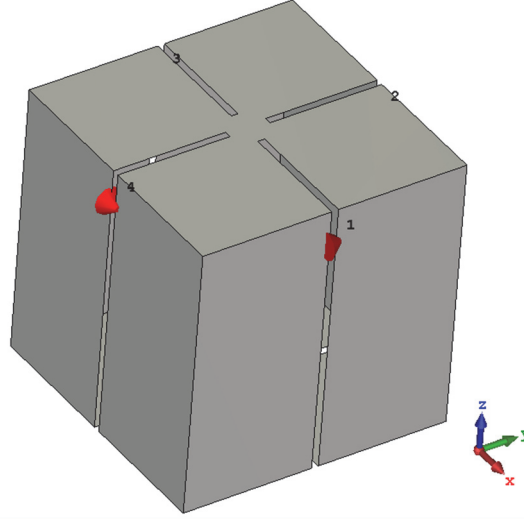


Fig. 3-33 Multi-feed cubic slot circular array excited through lamped ports

Based on the following assumptions, we can substitute element factor in (3-20) with the far field ϕ polarized electric field derived in (3-11) to achieve total radiation pattern of the cubic antenna as shown in (3-21).

Assumption 1: Back radiation of slot has no contribution in the far field radiation pattern as it is enclosed by the cube.

Assumption 2: slot radiation pattern has been derived assuming infinite ground plane. Diffraction effects happening as a result of bending of the cube edges to connect the ground planes, is beyond the focus of this research and have been ignored.

$$\mathbf{E} = \frac{e^{-jkr}}{r} \sum_{n=1}^N e^{+jkasin\theta \cos(\phi - \phi_n)} \mathbf{EF}_n(\varphi) \quad (3-21)$$

Due to the cubic shape of the proposed array, as shown in Fig. 3-33 not all faces are contributing in the radiation pattern evenly at all angles of ϕ . However, this space diversity of directive antenna elements has been considered in the calculating element factor in (3-13). Substituting ϕ in (3-11) with $(\phi - \phi_n)$ where $\phi_n = 0^\circ, 90^\circ, 180^\circ, \text{ and } 270^\circ$ lead to (3-22) where $\mathbf{EF}_1, \dots, \mathbf{EF}_4$ correspond to four folded slot antenna mapped on faces of the cubic structure shown in Fig. 3-33 and are given in (3-22).

$$\begin{cases} \mathbf{EF}_1 = \mathbf{EF}(|\phi - 0^\circ|) \text{ when } 270^\circ \leq \phi \leq 90^\circ \text{ for } \phi_n = 0^\circ \\ \mathbf{EF}_2 = \mathbf{EF}(|\phi - 90^\circ|) \text{ when } 0^\circ \leq \phi \leq 180^\circ \text{ for } \phi_n = 90^\circ \\ \mathbf{EF}_3 = \mathbf{EF}(|\phi - 180^\circ|) \text{ when } 90^\circ \leq \phi \leq 270^\circ \text{ for } \phi_n = 180^\circ \\ \mathbf{EF}_4 = \mathbf{EF}(|\phi - 270^\circ|) \text{ when } 180^\circ \leq \phi \leq 360^\circ \text{ for } \phi_n = 270^\circ \\ \mathbf{EY}_n \text{ is zero elsewhere} \end{cases} \quad (3-22)$$

Considering the space diversity of elements and their contributions only over a specific portion of space, (3-23) describes how element factors are contributing in the array far field \mathbf{Ea} in 3-D space.

$$\begin{cases} \mathbf{Ea} = \{\mathbf{EF}_1 e^{jkasin\theta \cos(\phi-0)} + \mathbf{EF}_2 e^{jkasin\theta \cos(\phi-90)}\} & , 0^\circ \leq \phi \leq 90^\circ \\ \mathbf{Ea} = \{\mathbf{EF}_2 e^{jkasin\theta \cos(\phi-90)} + \mathbf{EF}_3 e^{jkasin\theta \cos(\phi-180)}\} & , 90^\circ \leq \phi \leq 180^\circ \\ \mathbf{Ea} = \{\mathbf{EF}_3 e^{jkasin\theta \cos(\phi-180)} + \mathbf{EF}_4 e^{jkasin\theta \cos(\phi-270)}\} & , 180^\circ \leq \phi \leq 270^\circ \\ \mathbf{Ea} = \{\mathbf{EF}_4 e^{jkasin\theta \cos(\phi-270)} + \mathbf{EF}_1 e^{jkasin\theta \cos(\phi-0)}\} & , 270^\circ \leq \phi \leq 360^\circ \end{cases} \quad (3-23)$$

As will be observed later in chapters 4 and 5 in comparison with the simulated pattern, Fig. 3-34 furnishes a very good approximation of omnidirectional pattern in mode 1 and proves the validity of the analysis discussed.

Although it is worth mentioning that the above formula provides a somewhat ideal solution for the problem at hand since it does not take into account the effect of mutual coupling between the slots. Furthermore, it also treats each slot as an individual element, completely separate from other elements while in some structures reported in chapter 4, the slots on the vertical walls, are connected on the top and bottom faces of the cube which is in contrast to Fig. 3-33. These factors could contribute to small deviation of actual pattern from the theoretical one presented in Fig. 3-34 and Fig. 3-35.

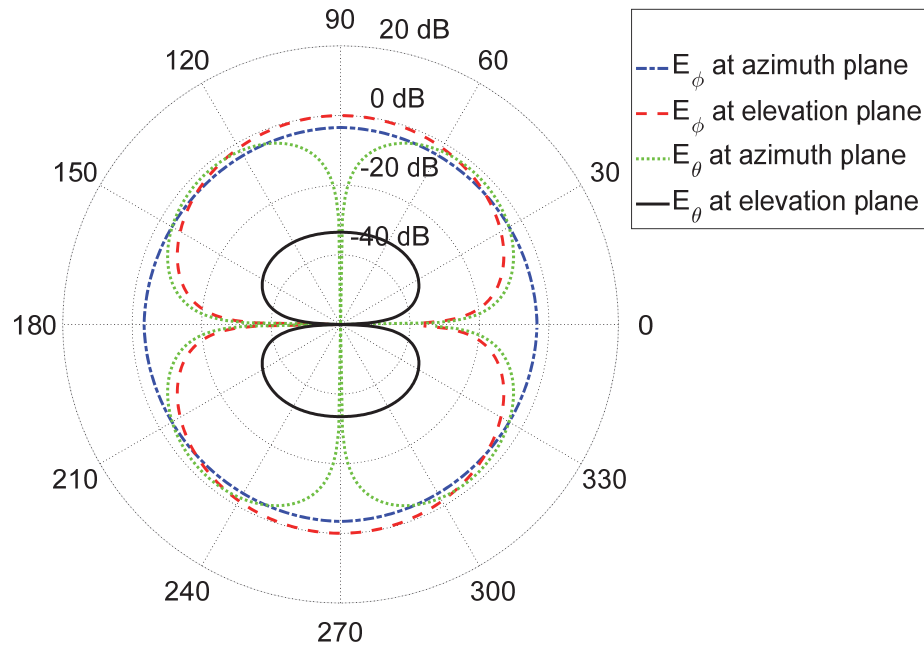


Fig. 3-34 Analytically calculated normalized directivity of a circular folded slot antenna array at 2.45GHz for $SL=73.5\text{mm}$, $GWZ=70\text{mm}$, $SW=1\text{mm}$, $GW=39.5\text{mm}$ and $a=GW/2$, (3dB Beam width for E_ϕ at elevation plane= 84°)

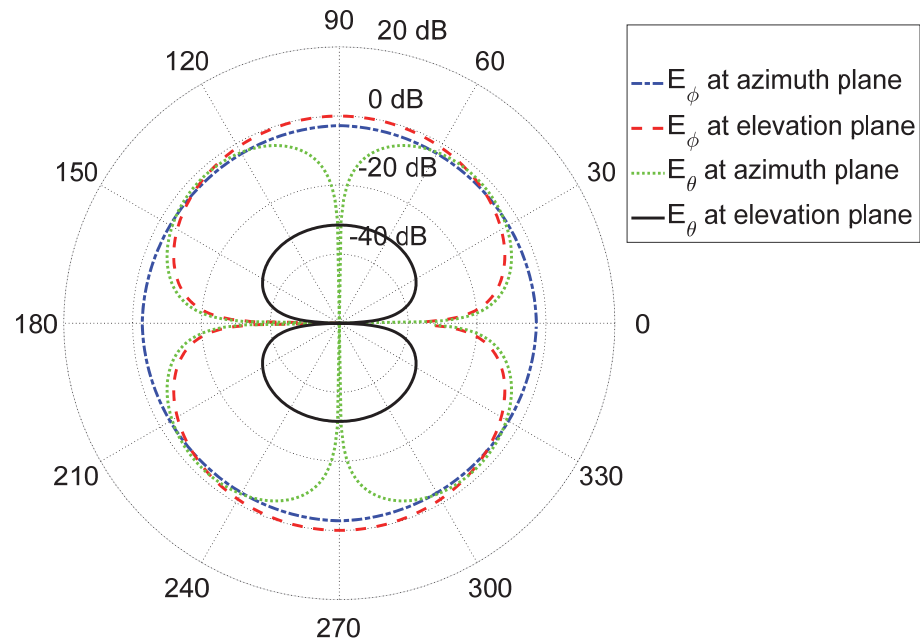


Fig. 3-35 Analytically calculated normalized directivity of a circular folded slot antenna array for $SL=73.5\text{mm}$, $GWZ=40\text{mm}$, $SW=1\text{mm}$, $GW=39.5\text{mm}$ and $a=GW/2$, (3dB Beam width for E_ϕ at elevation plane= 92°)

Structure shown in Fig. 3-33 has been EM simulated and co and cross pol directivity for both folded and straight slot are shown in Fig. 3-36 and Fig. 3-37. Results confirm very

low cross polarization and 3dB beamwidth increase in the elevation plane pattern from 82.5° to 92° after folding slot with $GWZ=40\text{mm}$.

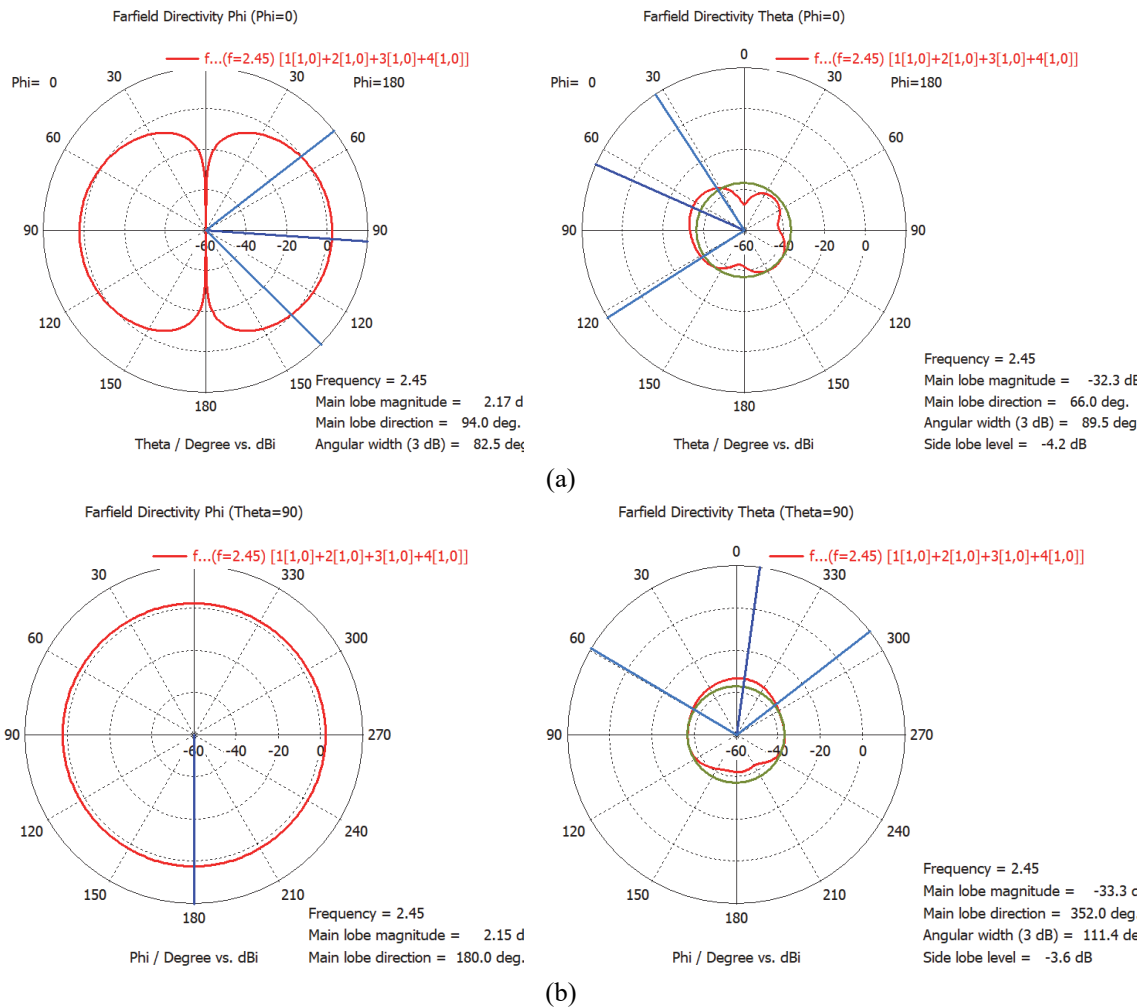


Fig. 3-36 Normalized directivity obtained through EM simulation for a circular folded slot antenna array shown in Fig. 3-33 at 2.45GHz for $SL=73.5\text{mm}$, $GWZ=40\text{mm}$, $SW=1\text{mm}$, $GW=39.5\text{mm}$ and $a=GW/2$, a) Elevation plane when all elements are excited in phase, and b) Azimuth plane when all elements are excited in phase (3dB Beam width for E_ϕ at elevation plane= 82.5°)

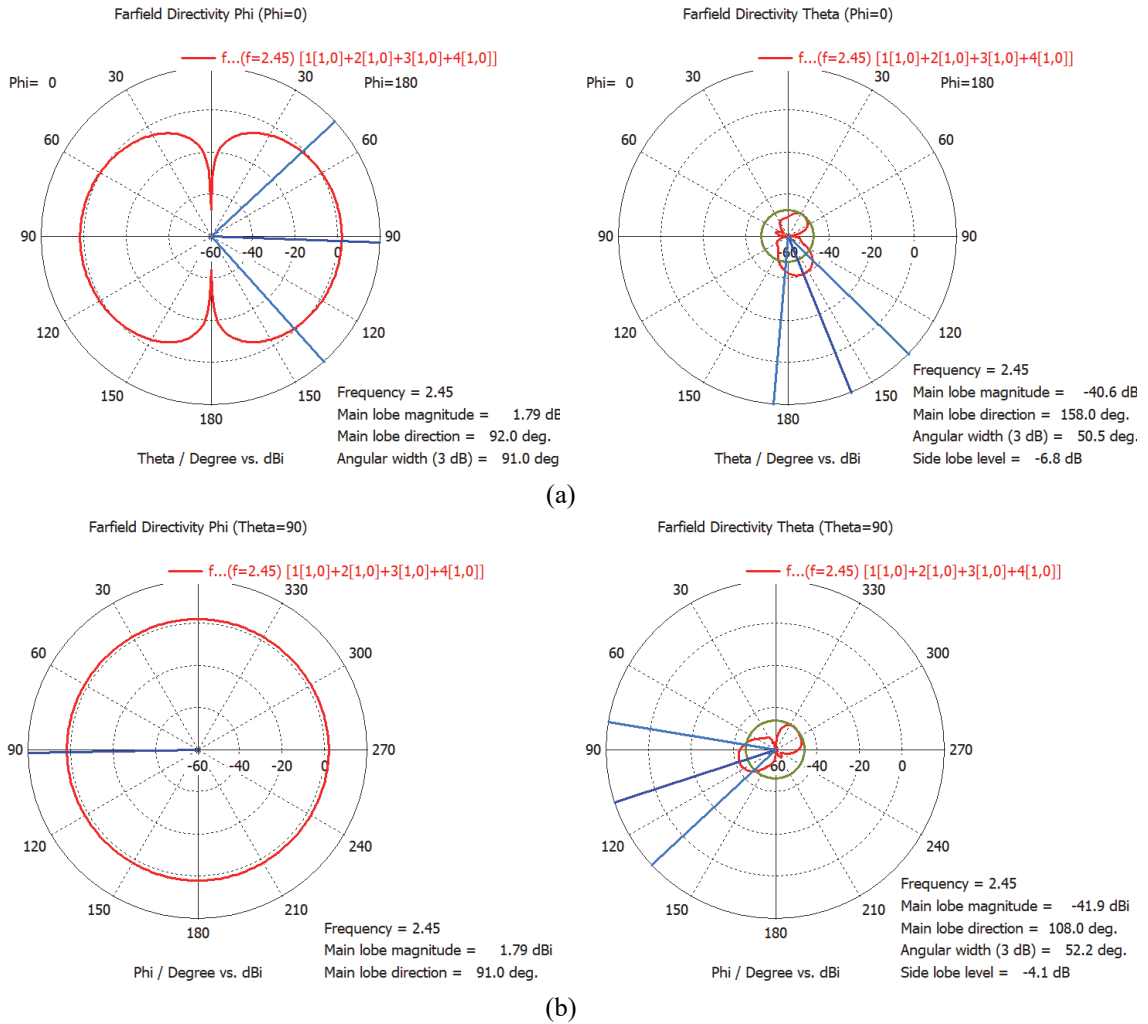


Fig. 3-37 Normalized directivity obtained through EM simulation for a circular folded slot antenna array shown in Fig. 3-33 at 2.45GHz for $SL=73.5\text{mm}$, $GWZ=100\text{mm}$, $SW=1\text{mm}$, $GW=39.5\text{mm}$ and $a=GW/2$, a) Elevation plane when all elements are excited in phase, and b) Azimuth plane when all elements are excited in phase (3dB Beam width for E_ϕ at elevation plane= 91.5°)

To simulate and analyze the structure shown in Fig. 3-33, in section 5.2, we mounted four slot antennas on four faces of a cube excited independently to study and compare coupling and far field radiation pattern against the previous case where four slot antennas on separate planar perfect electric conductors where treated as a circular array.

3.4 Mutual coupling in circular slot array

Mutual coupling between antenna elements affects array performance and deviates antenna array factor from analytical calculations. With the assumption of having antenna elements with isotropic radiation patterns, even though elements are arranged in a planar

or circular array, coupling between elements is only impacted by their distance while it is independent from their relative orientation. However, the above statement is not valid when we are dealing with directive antenna elements with broadside radiation pattern. Arranging these elements in a planar array configuration may decrease the coupling between elements due to weak end fire radiation comparing to circular array configuration with rotated elements facing to the center with low front to back ratio, like slots on opposite faces of the cube. Here, we have used a simple planar slot antenna with finite ground plane as a building block to study the coupling in circular arrays with rotated elements. Radiation pattern of the antenna element used in this study is illustrated in Fig. 3-4 b which confirms 0dB front to back ratio with maximum directivity of 5.2dB at broad side direction and null at the end-fire direction at 2.45GHz. It is worth to mention that coupling depends of antenna loading condition and our study is only legitimate when all elements are terminated in 50Ω . However, it helps us to see the trend.

As shown in Fig. 3-38, four planar slot antennas are replicated and rotated to form a circular array with radius of a . Using EM full wave simulator, the array is simulated for three variations in the radius, namely $a=50\text{mm}$, 55mm , and 75mm where slots' ground planes are connected only for the case of $a=50\text{mm}$. Fig. 3-28 shows the array geometry in CST EM simulator.

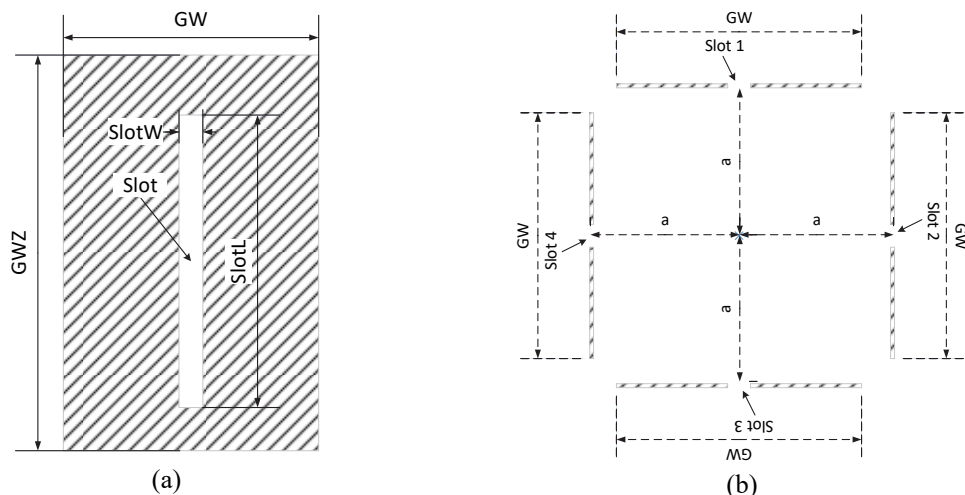


Fig. 3-38 Circular array geometry used for coupling simulation, $GW=100\text{mm}$, $GWZ=300\text{mm}$, $SlotL=73.5\text{mm}$, and $SlotW=1\text{mm}$, a) slot antenna element, and b) circular array

In the array under study where slot 1 is excited, slot 2 and 4 are its side neighbor elements and slot 3 is located in front of it. As slot 1 and 3 are facing each other, we expect

stronger coupling between them comparing to the coupling between slot 1 and its side neighbors, i.e. slot 2 or slot 4. Here, we only illustrated coupling coefficients between slot 1 and 2 and also between slot 1 and 3 which can represent whole coupling matrix thanks to reciprocity between elements and dealing with a symmetric structure.

Magnitude of coupling between slots 1 and 2 (side neighbor slots) and 1 and 3 (slots facing each other) are illustrated in Fig. 3-39 with S_{31} and S_{21} for three variations of a , radius of the array, for a 2.45GHz slot antenna.

- $|S_{21}|$ - $|S_{31}|$: We have observed that coupling between slots facing each other (here slots 1 and 3) is stronger than side neighbors (here slot 1 and 2) where array radius is large enough (here $a=75\text{mm}$), but almost equal for small array radiuses where slots happens to be in the vicinity of each other or even their ground plans are in touch. However, the difference between magnitude of S_{21} and S_{31} reduces by decreasing a and it is negligible for $a=55\text{mm}$ and $a=50\text{mm}$ due to the effect of neighbor ground planes in the vicinity of slot. It is worth to mention that ground planes of slots are connected to each other where $a=50\text{mm}$.
- $|S_{21}|$ and $|S_{31}|$: reducing the radius of array increases the coupling to both element 2 and 3 unless antenna ground planes touch each other where $a=50\text{mm}$. In this case, both coupling magnitudes drop down due to the extra boundary condition forced on the cube which suppresses some electric fields.
- It is worth to mentioned that variations of S_{11} with radius of circular array shown in Fig. 3-29 is partially responsible for coupling variation as well because poor input matching affects power delivered to the array as well as the amount of power being coupled to other elements. Fig. 3-29 confirms that S_{11} gets worse for small radiuses. Lower S_{11} is rooted in the mutual coupling between antenna elements as well as the ground planes.

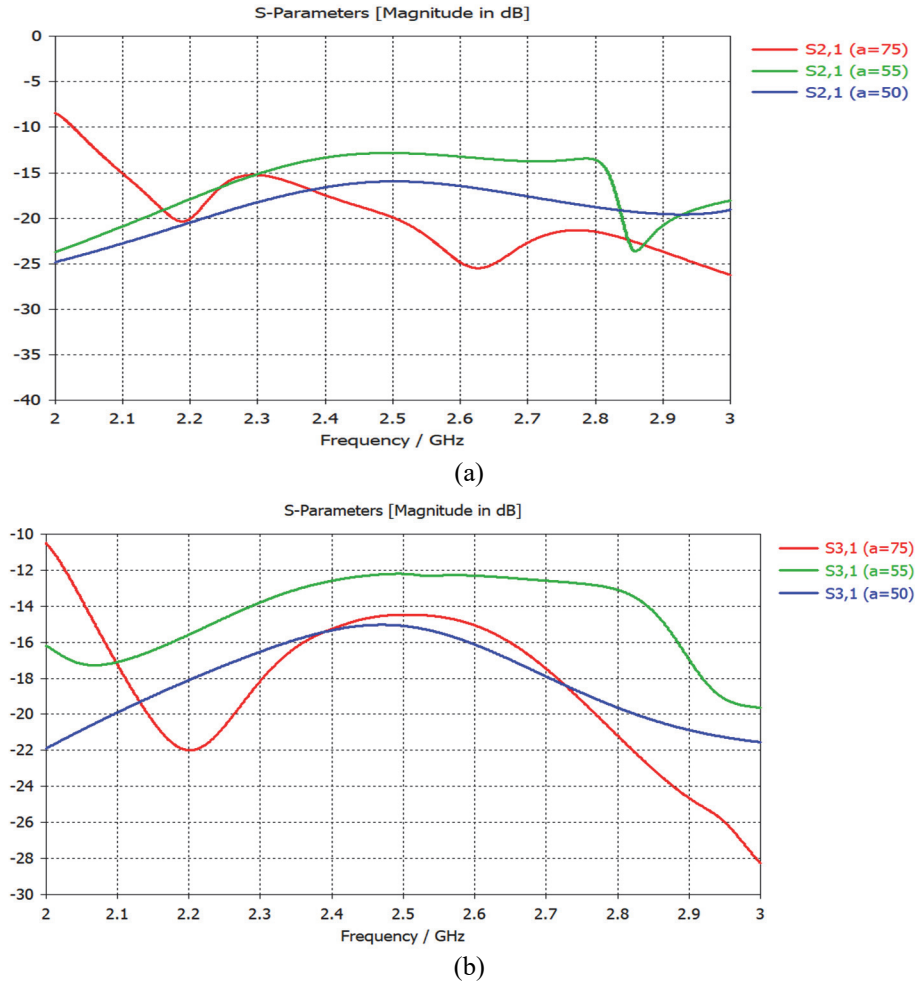


Fig. 3-39 Magnitude of coupling between, a) slot 1 and 2 (neighbors), and b) slot 1 and 3 (facing each other)

Phase of coupling between slots 1 and 2 (side neighbors) and 1 and 3 (elements facing each other) are illustrated in Fig. 3-40 for three variations of a , radius of the array, for a 2.45GHz slot antenna. Here we observe around 130° phase variation in both couplings (slots facing each other (S_{31}) and side neighbors (S_{21})) when radius of array is decreased from $a=75$ mm to $a=50$ mm. Assuming $\lambda_0=123$ mm at 2.45GHz, radius variations can be translated to 40 mm= $\lambda_0/3.1=117^\circ$ between slot 1 and 3 and 28 mm= $\lambda_0/4.4=82^\circ$ between slot 1 and 2. Even these phase variations specially for slots facing each other are close to the phase calculated based on TEM propagation, we can not have a theoretical calculation based on TEM propagation, as these antenna elements are not in the far field region. However, it can be used as a very rough estimation.

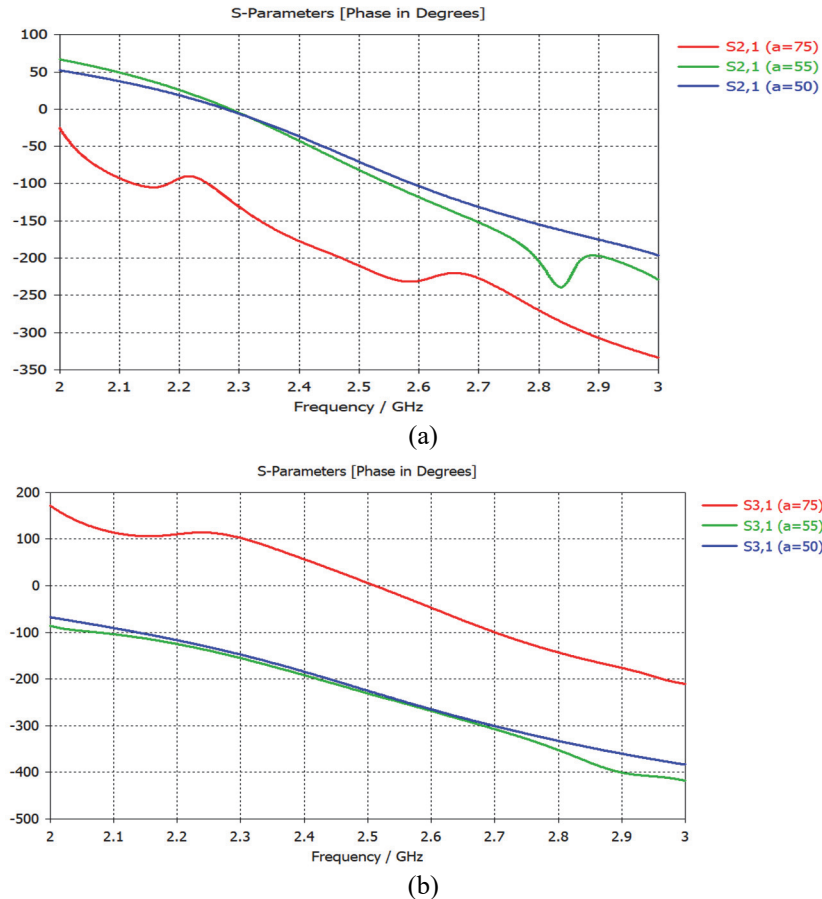


Fig. 3-40 Phase of coupling between, a) slot 1 and 2 (neighbors), and b) slot 1 and 3 (facing each other)

We have not observed noticeable phase difference between $a=50\text{mm}$ and $a=55\text{mm}$ cases, even though ground planes are connected in the former.

3.5 Single feed cubic slot antenna

Regularly, in array structures we will end up with as many RF ports as the number of elements, each one exciting one single antenna element. All antenna elements can be excited through an external feed network which is an important part of the design. Eliminating feed network and designing the array such that all antenna elements share a single feed can simplify the design and fabrication and as a result lowers the cost. For instance, in traveling wave antennas where all elements are cascaded and excited through a signal travelling all the way down the array, one RF feed can excite the array and power is delivered to the next element through its neighbor elements in the array [67]. Reflect arrays and transmit arrays are two non-planar examples of single feed array.

To simplify the fabrication, having a single feed structure was a major feature preserved in almost all of our designs.

3.5.1 Planar folded single feed slot antenna

In planar structures, especially slot antennas, a variety of techniques have been employed for in-phase excitation of antenna sections where each section is around half a wavelength long. Some researchers folded a multi wavelength planar antenna like dipole or slot to get in-phase electric field on all half wavelength sections of the antenna and realize a high gain single feed array. We have extended the planar folding technique to three-dimensional space and developed a single feed cubic structure with omni-directional radiation pattern where all radiators on four cube side walls, are excited in phase. It means a multi wavelength slot antenna array is folded and wrapped around a cube to get in-phase radiation from individual slots mapped on one of the side walls of the cube. Three different configurations are proposed to meet the requirements in each design.

Fig. 3-41 shows a planar slot antenna with four vertical branches all excited in-phase at the desired operating frequency. To better understand this configuration, in Fig. 3-42 we have plotted magnetic current and electric field in slots with blue and red arrows. At the resonance frequency of the structure, zero electric field locations shown with black dots happened to be located between two branches with an equal distance from each branch. This structure offers a high gain radiation pattern as it is technically a planar array with high gain broadside radiation.

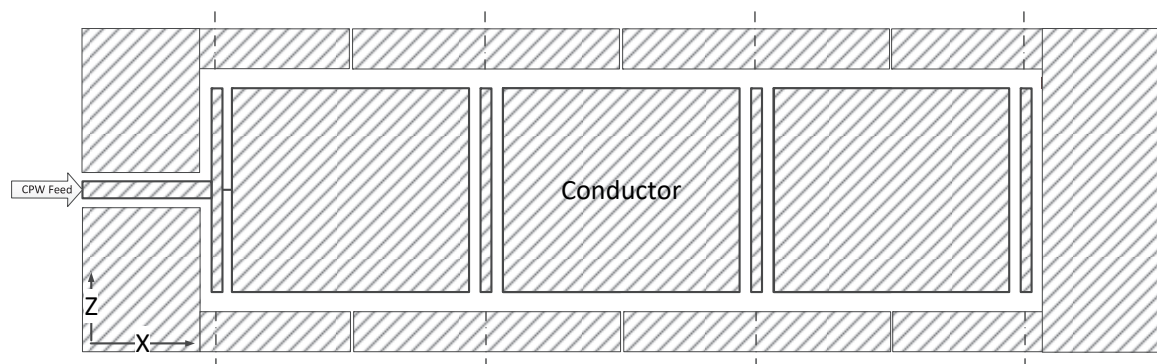


Fig. 3-41 folded slot antenna, structure 1 CPW feed

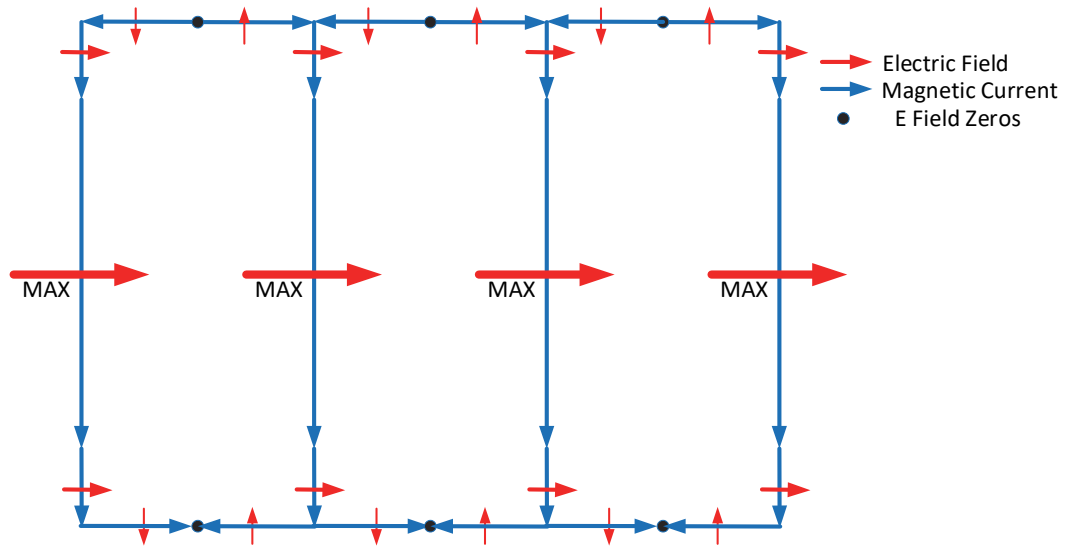


Fig. 3-42 CPW fed planar annular slot antenna

Annular ring slot antenna shown in Fig. 3-43 is the 2nd single feed architecture extended to three-dimensional space in our set of proposed structures. In Fig. 3-44 blue and red arrows respectively represent magnetic field and electric field on a ring slot antenna with perimeter of $2 \times \lambda$ where it is excited at the center of one side. Considering maximum electric field at the feeding point, zeros happened to be located at corners, resulting in out of phase electric field in each pair of parallel slots which verifies a destructive radiation pattern at broadside. However, wrapping the planar annular slot around a 3-D structure like a cube, we could achieve an omnidirectional radiation pattern through four in-phase vertical slots on four faces of the cube. This configuration is shown in the next section.

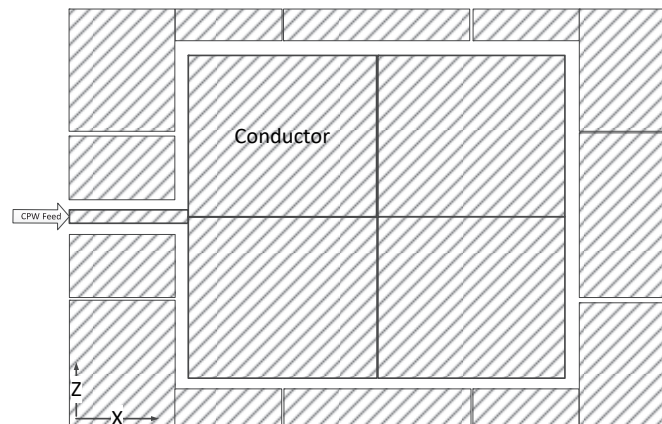


Fig. 3-43 CPW fed planar annular slot antenna

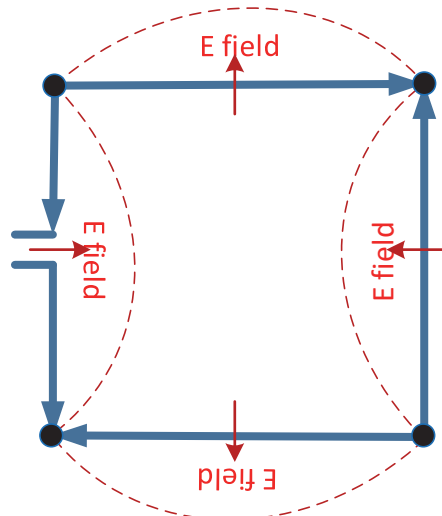


Fig. 3-44 CPW fed planar annular slot antenna

Fig. 3-45 illustrates a multi wavelength slot which is meandered and folded at appropriate distances to guarantee constructive radiation from vertical sections. Magnetic currents and electric fields shown with blue and red arrows respectively in Fig. 3-46, verify in-phase electric fields and co directional magnetic fields on vertical sections of the slot which leads to constructive radiation. However, zeros happen to be located at the center of horizontal slots with a destructive radiation pattern. The antenna is excited through a microstrip line beneath the slot with an offset from the location of maximum electric field. As will be elaborated in the next section, this structure is wrapped around a cube to generate in-phase electric field on vertical walls and out- of-phase electric field on the top and bottom faces and as a result an omnidirectional radiation pattern in the azimuth plane.

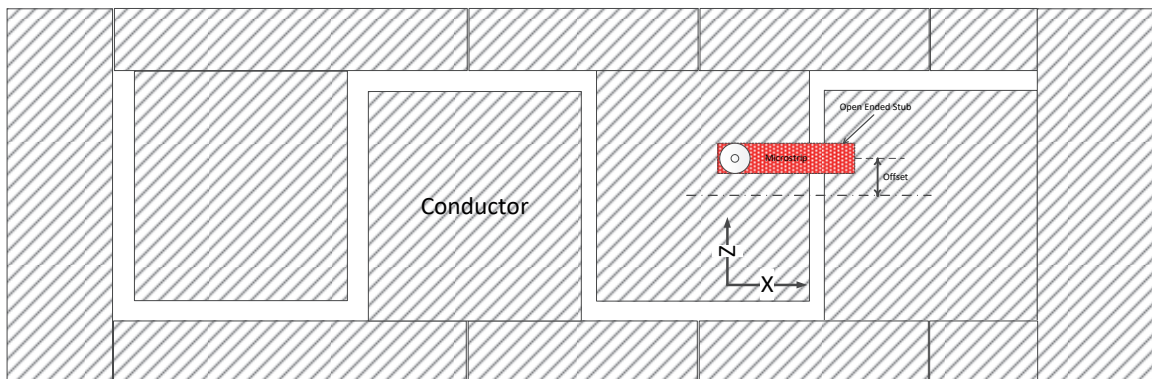


Fig. 3-45 Microstrip fed planar folded slot antenna

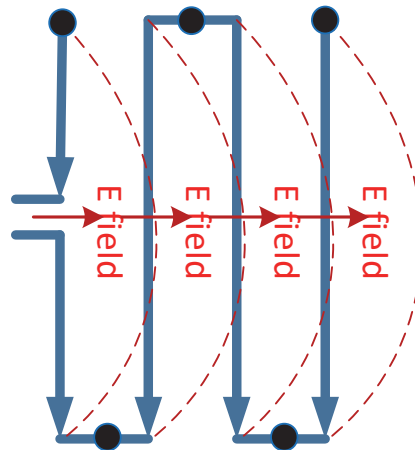


Fig. 3-46 Magnetic current and electric field on Microstrip fed planar folded slot antenna

3.5.2 3-D folded single feed slot antenna

We extended all planar single feed configurations already explained in the section 3.5.1 to three-dimensional space to create 3-D cubic compatible single feed configurations. Different configurations employed in our cubic design are reported at following.

Fig. 3-47 shows our 3-D folded antenna array designed based on planar folded slot antenna array illustrated in Fig. 3-41. In Fig. 3-47 (a) which shows the single mode 3-D structure on FR4, the planar structure is wrapped around a cube to achieve an omnidirectional radiation pattern in the azimuth plane from in-phase radiators located on vertical faces of the cube. Fig. 3-47 (b) shows a similar structure but on Rogers substrate with permittivity of 3 designed for a reconfigurable antenna where top face of the cube is reserved for a patch antenna. Nominal magnetic current and electric field of first structure shown in Fig. 3-47 (a) are illustrated in Fig. 3-48 which verifies how in-phase and out-of-phase electric fields on vertical faces and top/bottom faces are achieved, respectively. Second structure shown in Fig. 3-47 (b) has similar magnetic current distribution discussed in section 5.3.

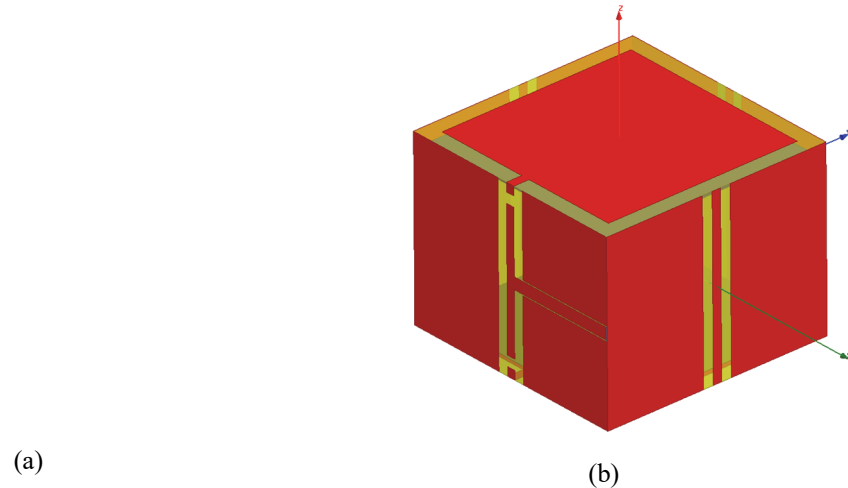


Fig. 3-47 3-D folded slot antenna array structure, a) singlemode structure on FR4 substrates, and b) Reconfigurable structures on Rogers

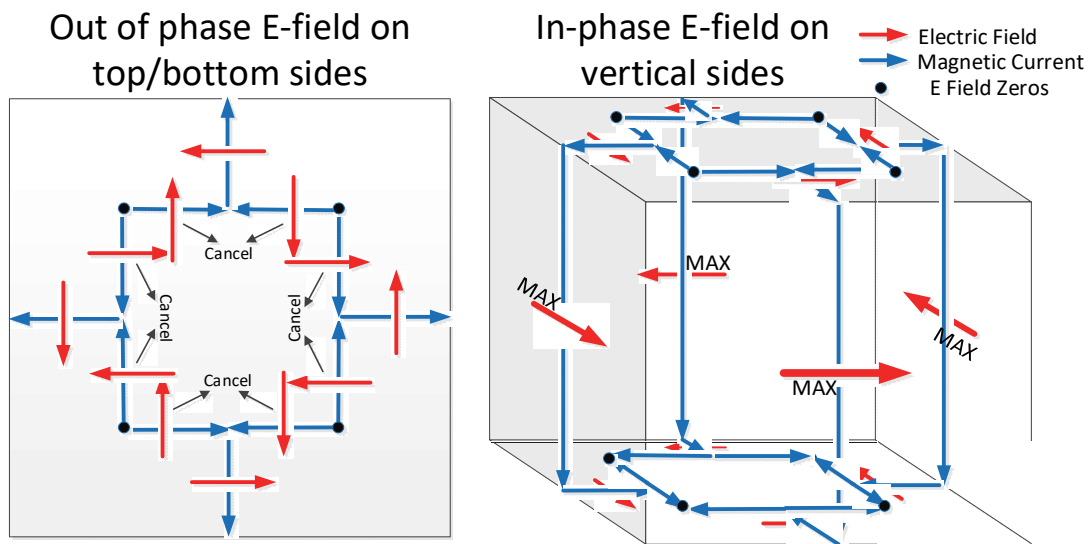


Fig. 3-48 Nominal magnetic current and electric field on 3-D folded slot antenna array

Extending planar annular ring slot antenna shown in Fig. 3-43 to three-dimensional space, a single feed 3-D annular ring slots antenna on cubic structure achieved as shown in Fig. 3-49 (b). As shown in Fig. 3-49 (a), it has co directed magnetic currents and in-phase electric fields on its vertical faces to offer omnidirectional radiation pattern in the azimuth plane.

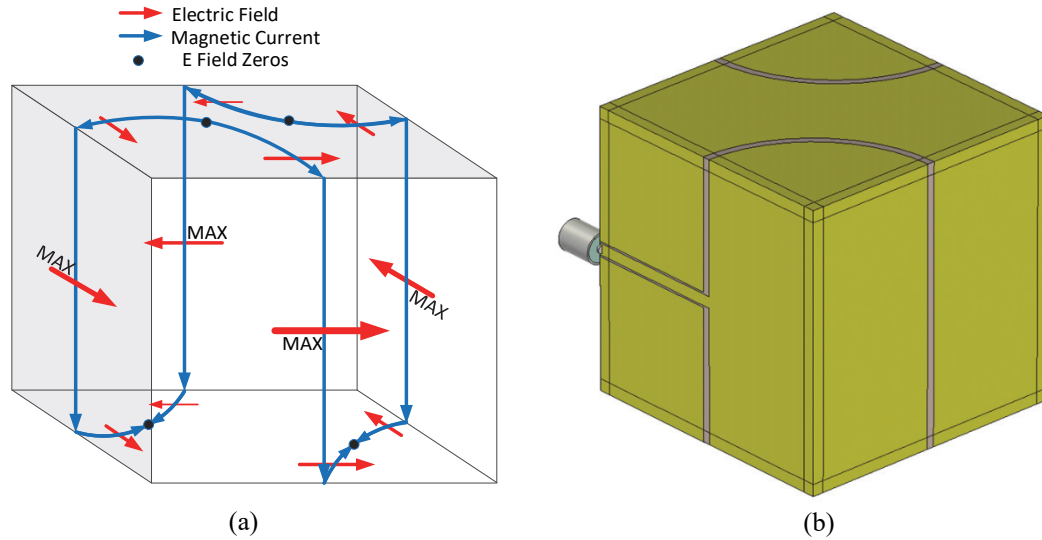


Fig. 3-49 3-D annular ring slot antenna with single feed, a) nominal magnetic currents and electric fields, and b) cubic structure

A 3-D folded microstrip fed slot antenna shown in Fig. 3-50 (b) is designed by extending the planar structure shown in Fig. 3-45 to three-dimensional space and wrapping it around a cube. Fig. 3-49 (a) illustrates co directed magnetic currents and in-phase electric fields on vertical faces of the cubic structure to obtain omnidirectional radiation pattern in the azimuth plane through a single microstrip feed line.

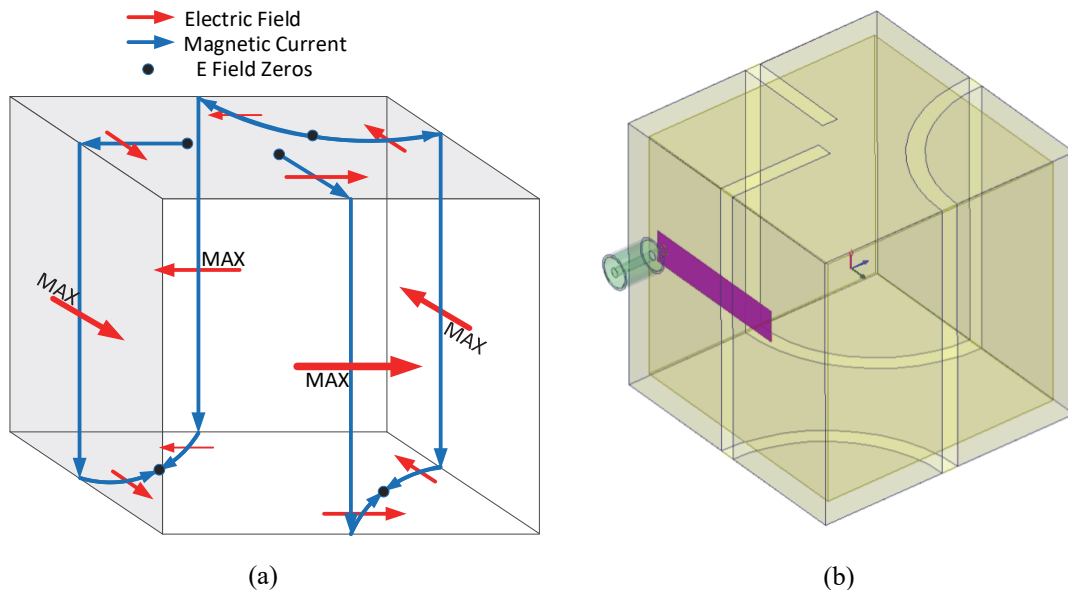


Fig. 3-50 3-D folded microstrip fed slot antenna, a) nominal magnetic currents and electric fields, and b) cubic structure

3.6 Conclusion

In this chapter, first a planar slot has been analyzed and effects of ground plane on slot performance have been studied. After analyzing a slot with infinite ground plane, we illustrated how truncating or folding a ground plane could affect radiation pattern and input matching of the slot antenna. We have concluded that folding a slot antenna broadens its beamwidth and suppresses slot's back radiation. As folded slot antenna is the building block in our cubic structures, an analytical solution for a folded slot antenna has also been presented.

Starting with the theory of general circular arrays with isotropic elements, the theory for a circular array with directive elements has then been studied. Based on these concepts and the assumption of approximating the cubic array with a circular array, we derived theoretical formulations to analytically calculate the radiation pattern of our cubic antenna structure. A circular array with slot antenna elements is then modeled and simulations were conducted to study the effects of variation in array radius and connection between antenna ground planes, on slot radiation pattern, input matching and coupling between slot antennas.

At the end, through extending planar configuration of single slot to three-dimensional space, three folded slot cubic architectures have been developed. They offer single feed excitation to achieve omnidirectional radiation pattern in the azimuth plane. More details on these structures is presented in chapter 4.

Chapter 4

4 Cubic architectures with omnidirectional radiation pattern

4.1 Introduction

After proper investigation of 3-D antenna architectures, extensive literature survey in the field and design, analysis and evaluation of innovative 3-D configurations, we proposed 3-D folded microstrip slot as a novel fundamental architecture in designing 3-D conformal antenna packages in order to offer effective 3-D solution to wireless sensor network applications as well as other telecommunication protocols. 3-D folded slot can be employed in design and fabrication of a variety of 3-D cubical, cylindrical, or spherical antennas with simple omnidirectional radiation pattern as well as advanced reconfigurable radiation patterns with MIMO capabilities. We have designed both omnidirectional and reconfigurable 3-D cubic antennas for application in wireless sensor networks where the former is reported here and the latter is covered in the next chapter.

Omnidirectional radiation pattern is a common required pattern especially for mobile devices or WSN nodes which are preferred to be insensitive to their orientation toward the main hub or base station. Furthermore, a horizontally polarized omnidirectional antenna can lower the interference with frequently-used vertically polarized devices in the ISM band which leads to enhancement of the network performance. Therefore, smart antennas with reconfigurable radiation patterns can noticeably improve the performance however they can increase the system overall complexity. Hence the challenge is to try to integrate these new additional levels of functionality into our antenna package, such that to arrive at an efficient solution in terms of volume, size, pricing and maintenance resources.

Extending the benefits of microstrip slot antenna [5] to three dimensions, we proposed cubic structures with slot elements introduced as 3D folded slot antennas. In addition to being simple and wideband, slot array is advantageous as it can be bent and wrapped around the cube to offer a conformal antenna solution. To achieve omnidirectional radiation pattern with horizontal polarization, we managed to generate a uniform flow of ϕ directed current on the unified conductive body of the cube to accomplish constructive radiation in the azimuth plane from various parts of the conformal folded slot mapped on a cubic antenna-package. This will require in-phase excitation of antenna elements, here cube faces, which is proved to be a challenging task in single-fed antenna structures. The single-fed design is selected in view of the WSN requirements to keep the structure simple for low cost fabrication purposes.

We have proposed three structures in this chapter, microstrip-fed 3-D folded cubic slot antennas, CPW-fed 3-D folded annular ring slot antennas, and 3-D folded slot antenna array which are discussed in sections 4.2 and 4.3, and 4.4, respectively.

Our proposed structures offer promising solutions for variety of applications due to their simple low-cost 3-D printable structure, conductive outer surface, and horizontally-polarized omnidirectional radiation pattern in the azimuth plane. All the prototypes proposed in this chapter are designed and simulated to function at 2.44 GHz ISM band. In addition to manual PCB fabrication, we also explored the feasibility of economical 3-D printing fabrication for our devices presented in sections 4.2 and 4.3. Fully-functional architectures of microstrip-fed slot and CPW-fed annular ring slot cubic antenna-packages

were successfully printed by the aid of Objet EDEN 3-D printer while conductive layers were patterned using copper tape. The fabrication of the CPW-fed annular ring slot cubic antenna is proved to be more straightforward owing to the single-layer feeding structure. The CPW-fed antenna can be patterned on the surface of a cube while the microstrip-fed antenna needs a microstrip line to be pattern inside the cube as well.

The conformal folded slot design also allows for accommodation of potential electronic circuits inside the cube therefore offering compact solutions for wireless applications. All the structures were measured and proved to be successful. The results from these two sections have been published or submitted for publication.

In section 4.4, we extended the planar slot antenna structure to three dimensions and propose a single CPW-fed conformal 3-D folded slot antenna array which provides a cost-effective, durable and symmetric package solution for WSN applications. The modified version of this structure has the potential for future reconfigurable designs which has been studied and reported in chapter 5.

4.2 Microstrip Fed 3-D Folded Cubic Slot Antenna

In this section, we have reported our first proposed 3-D cubic antenna with main application in wireless sensor network which has been published in AWPL[1]. Employing microstrip fed 3-D folded slot antenna topology, we could achieve an omnidirectional pattern with horizontal polarization. The structure which is compatible with 3-D printing has been fabricated from Ro3003 substrate and Objet VeroGray material. The interior of the cubic structure can be used to place electronic circuits of transceiver and sensor. The measurement results verify the simulation and a maximum gain of 1.95dBi at azimuth plane and bandwidth of 14% at center frequency of 2.495GHz have been achieved. The cubic antenna has an edge length of 33mm and covers ISM 2.45GHz frequency band which has vast application in wireless sensor networks and telecommunication devices.

A 3D cube antenna with application in wireless sensor network is presented in this paper. Employing microstrip-fed 3D folded slot antenna topology, a horizontally polarized omnidirectional radiation pattern in azimuth plane was obtained. The structure which is

compatible with 3D printing was fabricated from RO3003 substrate and Objet VeroGray material. The interior of the cubic structure can be used to place electronic circuits of transceiver and sensor. Measurement results verify simulation and a maximum gain of 1.95dBi in the azimuth plane and bandwidth of 14% at the center frequency of 2.495GHz were achieved. The cubic antenna has an edge length of 33mm and covers the ISM 2.45GHz frequency band which has vast application in wireless sensor networks and telecommunication devices.

4.2.1 Analysis and design

The objective is to design and implement a cubic 3-D printable antenna with horizontally polarized omnidirectional radiation pattern while reserving the interior space for integration or installation of sensor, transceiver, and other electronic circuits. It can be met at best by employing a circular array with four antenna elements, all excited uniformly to achieve an omnidirectional radiation pattern. Here, four vertical faces of the cube which are parallel to z-axis have been assumed as four uniform and in-phase radiators in the circular array as shown at Fig. 4-2 (a).

4.2.1.1 3-D Folded Slot Antenna

Multi wavelength planar antennas can be folded in such a way that parallel half wavelength sections radiate constructively to improve the gain of the antennae [70]. Also, their single port excitation eliminates the embedded power divider/combiner needed to feed the half wavelength antenna elements in an array. Fig. 4-19 (a) shows how a microstrip slot antenna with length of two wavelength can be folded at locations with zero electric field (black points) to obtain in-phase magnetic current and electric field on each section, shown with blue and red arrows, respectively. As shown in Fig. 4-1(b), we propose modifying and extending the folded slot antenna concept to 3-Ds and wrapping a cube with a multi wavelength microstrip slot antenna in order to have four in-phase vertical slot antenna elements on vertical faces of the cube to offer a three-dimensional packaging solution as well as an omnidirectional radiation pattern. The locations with zero electric field, magnetic current flow, and electric field vectors were shown with black points, blue arrows, and red arrows, respectively. Fixing the zero-electric field at center of arc slots on top and bottom faces of the cube leads to same direction magnetic current on vertical faces and

consequently maximum in-phase E_ϕ at center of vertical faces. It is worth pointing out that distance between the locations with zero electric field is around half a guided wavelength in slot line as expected. In contrast to folding a planar antenna that leads to higher directivity because of constructive radiation at a specific direction, folding the antenna in 3-Ds can produce omnidirectional radiation pattern as a result of in-phase symmetric and constructive radiation in azimuth plane.

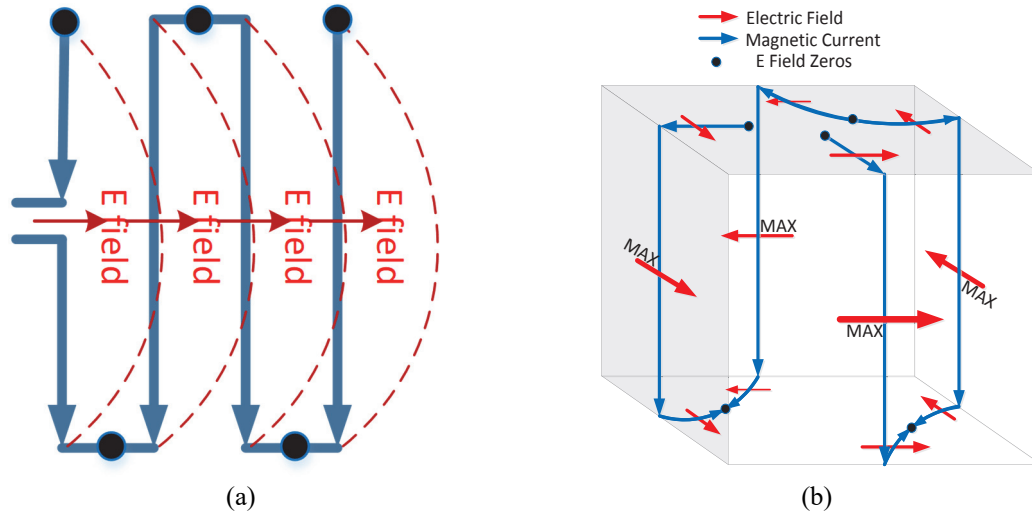


Fig. 4-1 Folded Slot Antenna (a) Planar 2D, (b) 3-D Cubic.

4.2.1.2 Geometry and Excitation

As illustrated in Fig. 4-2 (a), a cube has been made from a dielectric substrate with thickness of h and a slot antenna was cut out in the metallic layer covered the cube faces. The slot line has been considered as four half-wavelength sections, centered at vertical faces of the cube, connected together through slot arcs on top and bottom faces, and truncated on top face at both ends. The part of slot which is between its last fold at top edge of the cube and its end on top face is named as "Slot Extension on Top" or $TSlotEx$ which is equal to half of the length of arcs or $\frac{l\pi}{8}$ where l is the cube edge length. Ansys HFSS was utilized to determine the total length of the slot.

The multi-wavelength slot antenna is excited through an open ended microstrip transition which is placed beneath the slot with an offset from the center of vertical face of the cube where the first maximum electric field happens. As shown in Fig. 4-2, the microstrip line is shifted upward from the center to avoid high impedance transition to slot

for appropriate matching to 50Ω . Offset from center and length of microstrip open ended stub are tuning parameters for impedance matching [5]. Using HFSS, proper impedance matching at 2.45GHz could be achieved with a 6.5 mm open ended microstrip stub for slot width of 2 mm. Radiation pattern of the antenna can be deteriorated if a parameter variation changes the electric field distribution over the slot and relocates maximum locations.

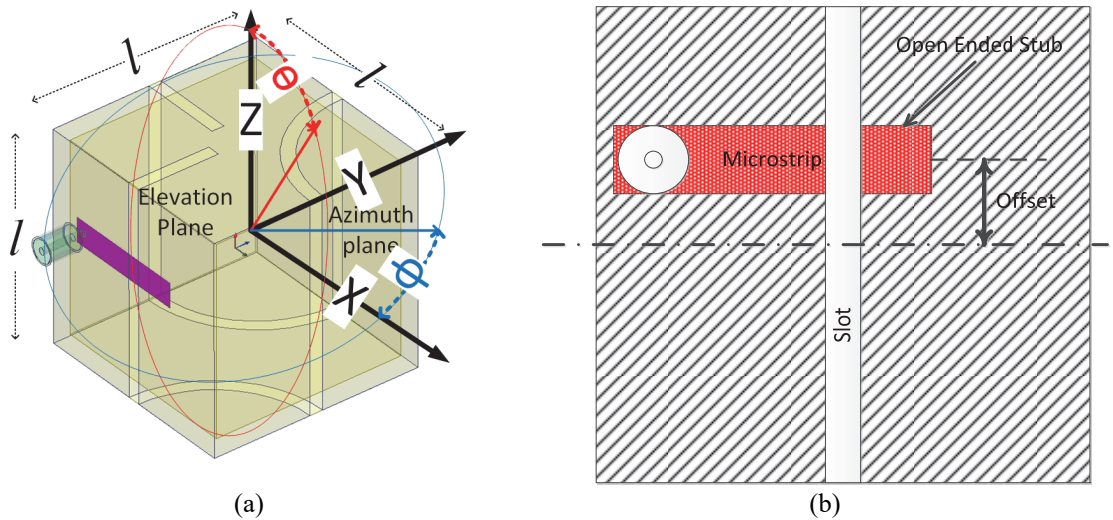


Fig. 4-2 (a) Geometry of antenna, and (b) Microstrip feeding.

4.2.2 Simulation and Parametric Study

4.2.2.1 Simulation

Here, we used VeroGray (also known as RGD850) to prototype our cube by Objet EDEN 350V 3-D printer. Its dielectric constant of 2.97 and loss tangent of 0.02 at 2.45GHz were measured by Agilent SPDR, Split Post Dielectric Resonator. At the same time, we used Rogers RO3003 with dielectric constant of 3 (very close to VeroGray) as reference for both simulation and extra prototype. Dimensions of the antenna calculated analytically were optimized through simulation by the aid of HFSS and shown in Table 4-1 Coupling between slot antennas on faces of the cube as well as the effect of folding the slot at edges of the cube are key factors to be considered in optimization.

Table 4-1. Dimensions of our proposed microstrip fed 3-D folded cubic slot antenna

Dimension	value	Unit
Edge length of cube	33	mm
Slot Width	2	mm
Total slot Length	235.5	mm
Feed offset from top	14.5	mm
Feed Width	3.8	mm
Dielectric Thickness	1.55	mm
Relative Permittivity	3	-
Tangent loss of VeroGray	0.02	-
Length of OC Stub	6.5	mm
Radius of the arcs	16.5	mm

4.2.2.2 Parametric Study

Contrary to the most of planar antennas, variations of the 3-D geometry in 3-D cubic antennas significantly influence the input impedance and radiation pattern. In this section, we investigate several important parameters that affect the performance of the antenna.

a. Width of Slot

Width of slot has direct relation with its impedance and reverse relation with its effective permittivity. Here, as shown in Fig. 4-3 (a), the impedance of 50Ω could be achieved from a microstrip transition to slot width of 2mm. Antennas with wide slots have higher cross polarization in favor of greater bandwidth, however in this structure it results in wiping off more ground plane and amplifying the coupling between antenna sections that deteriorate the radiation pattern and increase the ripples in the azimuth plane as shown in Fig. 4-3 (b). Therefore, obtaining a right value for the slot width is a challenging task since both bandwidth and pattern requirements have to be considered in the optimization process.

b. Extended Length of Slot on Top Face

In the proposed configuration, "Slot Extension on Top" or "TSlotEx" parameter, plays a significant role in tuning for an omnidirectional radiation pattern in addition to shifting the resonant frequency of the antenna. Changing the TSlotEx would shift the

locations of the maximum electric field in the slot resulted in deforming the radiation pattern and increasing the ripple in the azimuth plane as shown in Fig. 4-3 (c).

c. Potential Circuit inside Cube

Fig. 4-4 (a) shows the electric field intensity in presence of electronic circuits modeled by placing a PEC box in the interior space of the cube. It can be seen that the value of electric field is low enough so it will guarantee that no significant interaction with the circuit board inside would happen and hence as shown in Fig. 4-4 (b) the effects on the device performance and antenna radiation pattern are negligible enough so can be neglected.

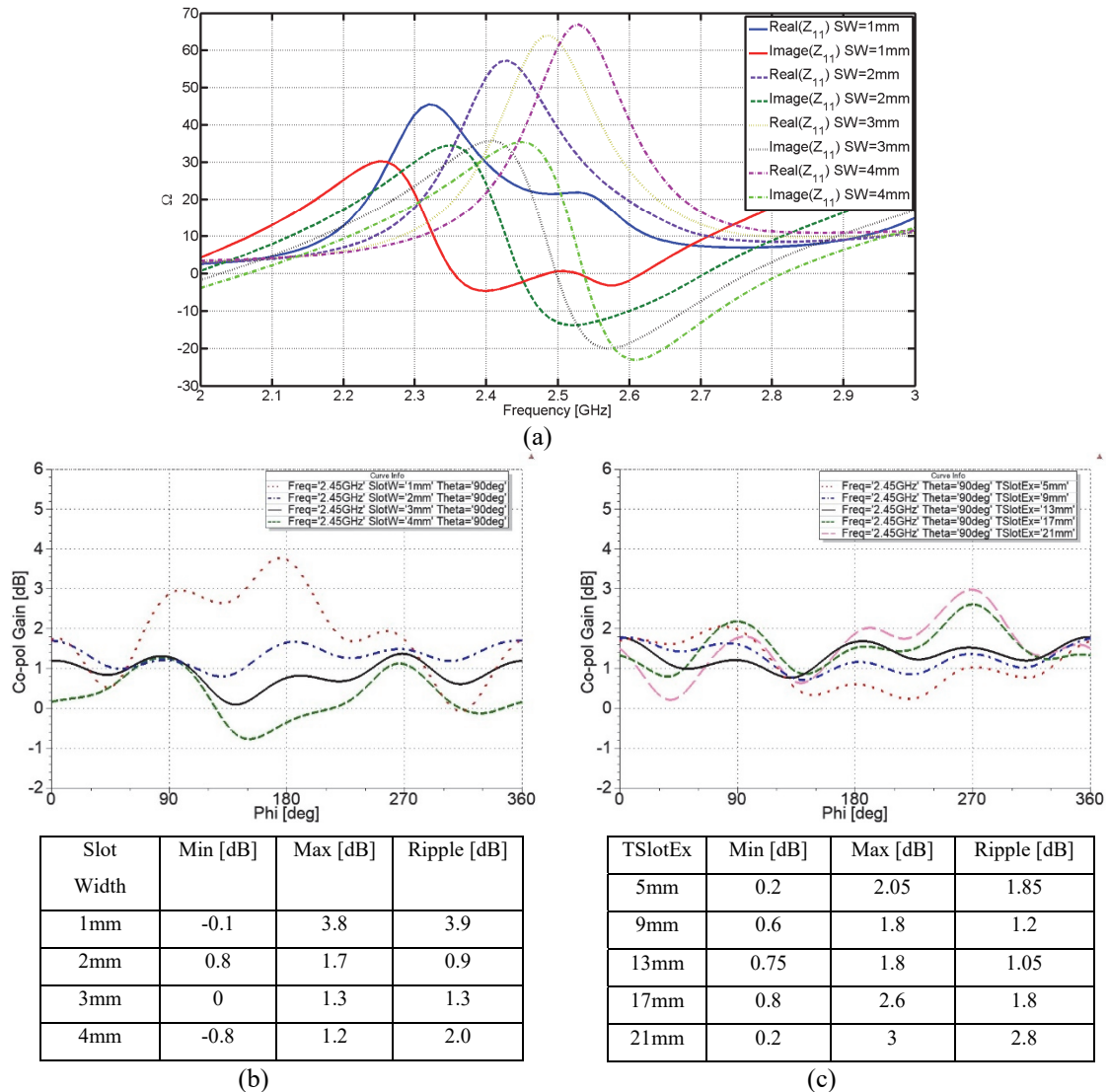


Fig. 4-3 , Parameter study (a) Input reflection coefficient Vs. Width of slot, (b) Radiation Pattern vs. Width of slot, and (c) Radiation Pattern Vs. Extended length of slot on top face of cube

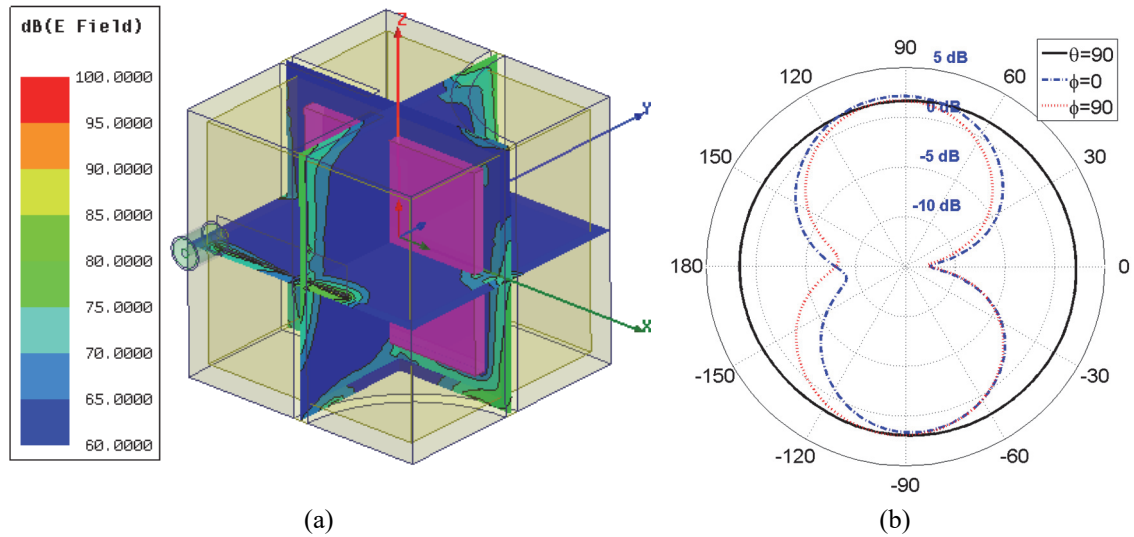


Fig. 4-4 Effect of potential electronic circuit modeled by a PEC box in pink on antenna performance (a) Intensity of Electric field in logarithmic scale, and (b) Far field radiation pattern.

4.2.3 Fabrication and Measurement

Two prototypes at operating frequency of 2.45GHz were fabricated, one using Rogers RO3003 substrate and the other one using 3-D printed VeroGray. In RO3003 implementation shown in Fig. 4-5 (a), the antenna was assembled manually from fabricated PCBs, while in VeroGray implementation shown in Fig. 4-5 (b), the cube was printed by Objet EDEN350v 3-D printer and manually patterned with copper tapes.

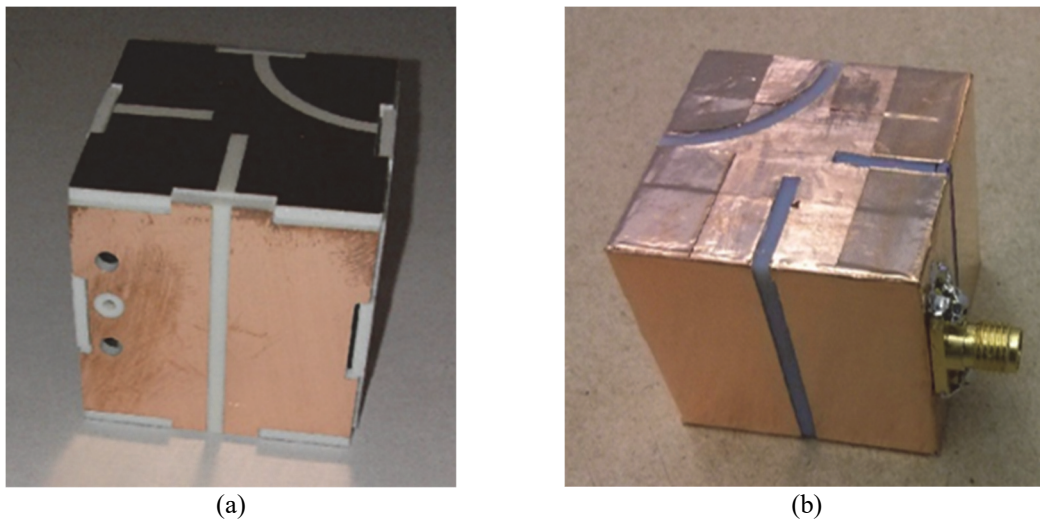


Fig. 4-5 (a) PCB fabrication, and (b) 3-D printing.

Input reflection coefficient of both fabricated prototypes were measured and compared with simulation results in Fig. 4-6. Bandwidth of 7% at the center frequency of 2.43GHz for RO3003 prototype and 14% at the center frequency of 2.495GHz for VeroGray prototype show a frequency shift of -26MHz for the former and +40MHz for the latter compared with simulation results. In addition, the manual implementation and patterning by copper tape causes fabrication error that is partially responsible for frequency shift of both prototypes.

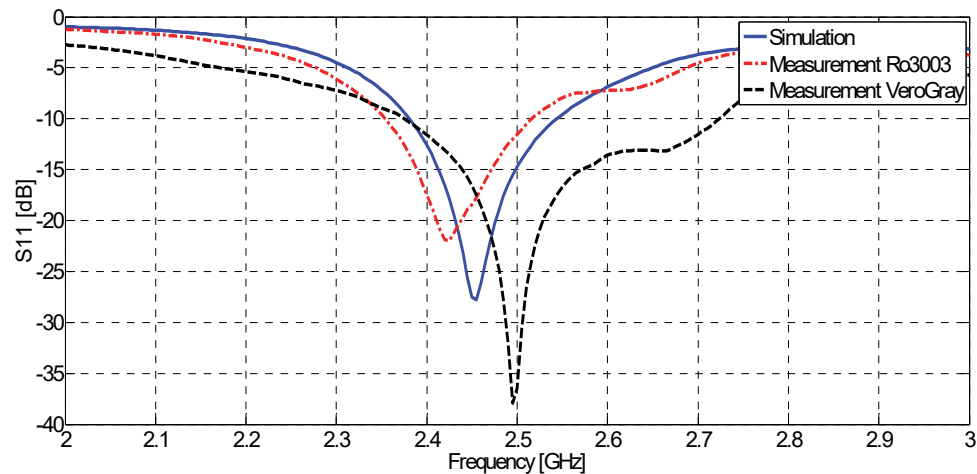


Fig. 4-6 Input reflection coefficient

Radiation pattern measurement is a challenge for 3-D antennas, because mounting the structure in anechoic chamber needs a custom-designed antenna holder together with external RF connectors placed on the surface of the cube. Although the attempt has been made to keep the interaction minimum, still antenna pattern is disturbed to some extent and its performance degraded. Elevation and azimuth plane radiation pattern measurement were conducted separately in a far field antenna chamber to lower the interaction with measurement setup. Applying proper calibration, the gain and radiation patterns of antenna made by VeroGray was measured as illustrated in Fig. 4-7 versus simulation results. Here azimuth plane is defined as XY and elevation plane as XZ referenced to Fig. 4-2 (a). As expected from analysis and after proper tuning, an omnidirectional radiation pattern with maximum gain of 1.95dBi in the azimuth plane was achieved through measurement which is in good agreement with simulation results with maximum gain of 2.2dBi. The gain measured using a standard horn to calibrate the anechoic chamber. The SMA connector mounted on the cube for measurement purpose disturbs the far field radiation to some

extent, but it can be omitted when transmitter is placed inside the cube in practical applications. Interaction between measurement equipment, SMA connector, measurement cable and the antenna as well as manual fabrication by hand and difference in material properties resulted in minor mismatch between simulation and measurement results.

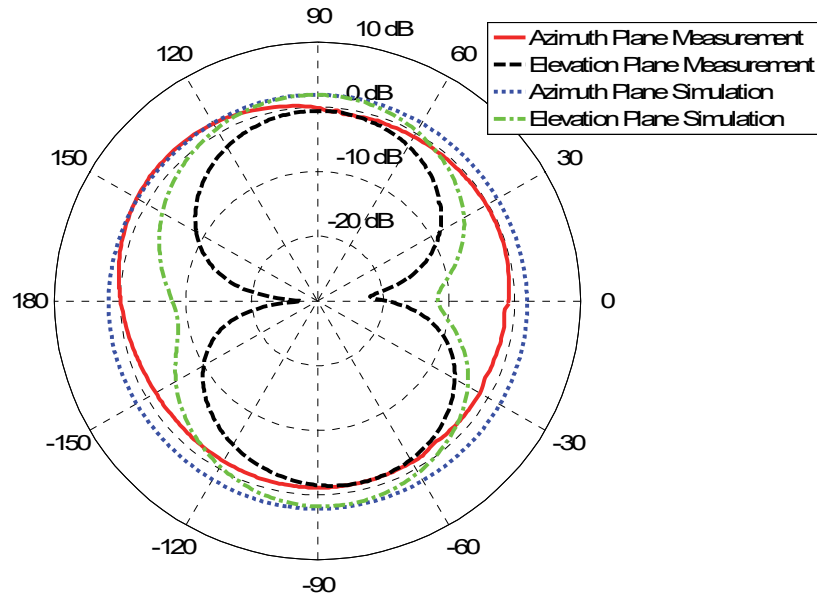


Fig. 4-7 Gain of proposed microstrip fed 3-D folded cubic slot antenna at 2.44GHz through far field Measurement Vs. Simulation results.

4.3 3-D Folded Annular Slot Antenna-Package

In this section, a novel 3-D conformal annular slot antenna is proposed and patterned in single layer over a 3-D printed cubic package with conductive surface in order to achieve a horizontally polarized omnidirectional radiation pattern in the azimuth plane. Bottom metal layer which was printed inside the cube in our former design has been eliminated in our new design where a CPW feedline is employed as opposed to microstrip line to feed the slot antenna. To verify the concept, a cubic antenna-package at 2.4GHz has been designed and fabricated for wireless sensor network (WSN) applications application. The cube is printed by Objet 3-D printer from Verogray material with thickness of 1.55mm and covered with copper tape with slots being cut out of its surface at appropriate locations. The measurements are in good agreement with simulations. A maximum measured gain of 2.53 dBi at the azimuth plane and a bandwidth of 11% are achieved.

4.3.1 Design Considerations

Application of higher modes annular ring slot antenna in mobile communications has been studied in [71]. We extended the annular ring slot antenna to 3-Ds and proposed a 3-D antenna-package with a wideband horizontally-polarized omnidirectional radiation pattern in the azimuth plane.

4.3.1.1 *Field Distribution over 3-D Folded Slot Antenna*

Considering that electric field is perpendicular to the slot antenna's axis, a planar annular ring slot antenna with multi wavelength circumference is excited at higher modes where the electric field radiated by different sections of slot is out of phase and cancel out at broadside [71]. In Fig. 4-8, field distribution on a planar folded annular slot is compared to our proposed 3-D folded annular slot antenna where red and blue arrows represent notional tangential electric field and magnetic current, respectively. Tangential Electric field and notional magnetic current reverse their phase and direction around zero electric field locations shown with black points and they have a maximum between two adjacent zero locations. In the planar structure shown in Fig. 4-8 (a), slot antenna is bent at locations with zero electric field resulted in out of phase electric field and magnetic current in four sections of planar slot radiated destructively in the far field broadside direction.

In the same manner in our proposed structure described in Fig. 4-8 (b) having zeros centered at four arcs located on top and bottom faces of cubic structure resulted in destructive radiation from these faces.

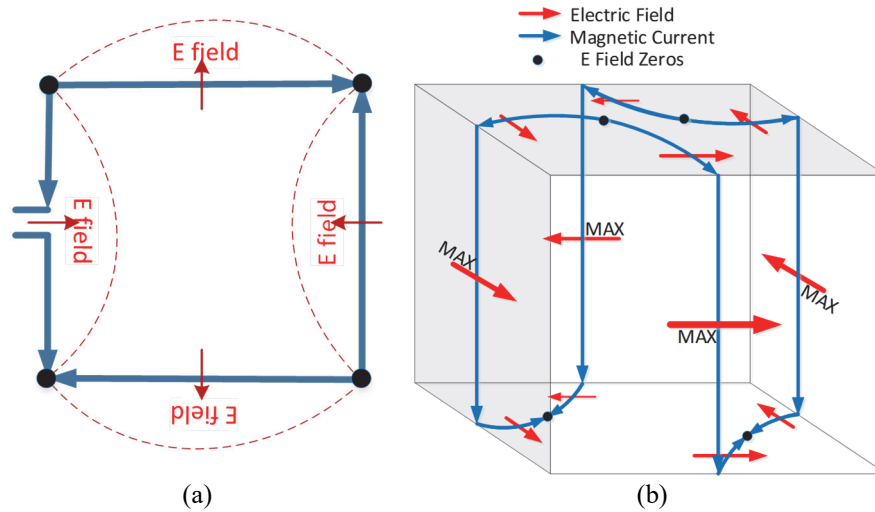


Fig. 4-8 Notional tangential electric field and magnetic current distribution of a) planar annular slot antenna, b) proposed 3-D folded annular ring slot antenna

On the other hand, having maximum electric field centered on vertical faces of cube explains how our proposed 3-D folding helps the antenna to create in-phase magnetic currents and electric fields on four vertical sections of slot antenna in 3-D space. Hence, the multi wavelength annular slot antenna wrapped around a 3-D structure such as a cube, offers horizontally-polarized omnidirectional radiation pattern in the azimuth plane resulted from co-directed magnetic currents in vertical slots.

4.3.1.2 Geometry and Excitation

As shown in Fig. 4-9 (a), a multi wavelength annular ring slot antenna is wrapped around a cube and folded at edges in such a way that electric wave forms in slot has four maximums at center of vertical slots (parallel to Z axis) and four zeros on top and bottom quarter arc slots on the cube. Thus, electric field is constructively added up in-phase in the azimuth plane while radiation from slots carved on top and bottom faces of the cube cancel out each other. It will stimulate a ϕ -directed current flowing on the unified conductive body of the antenna leading to the desired radiation pattern.

As shown in Fig. 4-9 (a), the antenna consists of four in-phase excited vertical slot antennas connected as a 3-D folded ring through slot arcs on top and bottom faces of the cube. A cubic substrate thickness of h is supporting the slots. In Fig. 4-9 (a), l is the length of the cube edge and the antenna is fed at one of its maximum electric field locations which happens to be at the center of one of the vertical faces of the cube. The antenna operating

frequency is related to the total electric length of the slot which depends on the cube size and the width of slots. By using EM simulation tools such as Ansys HFSS, the nulls and maximums of the electric field on the slot antenna are tuned out to be at the center of slot arcs and center of vertical faces, respectively. The length of annular slot wrapped around the cube is around twice the guided wavelength in microstrip slot which can be interpreted as half wavelength distance between nulls as expected. It should be emphasized that the distribution of electric field especially the position of electric field maxima over the slot antenna is very important in achieving the best performance.

The 3-D slot antenna is excited through an in-layer 50Ω coplanar waveguide being cut out of the same conductor layer as the slot antennas on the cube. The slots on the surface of the cube not only act as radiators but act as transmission lines to feed adjacent slots as well. Single port excitation through a CPW line on the same layer as the antenna simplifies its fabrication process considerably. The transition from antenna to CPW line is illustrated in Fig. 4-9 (b).

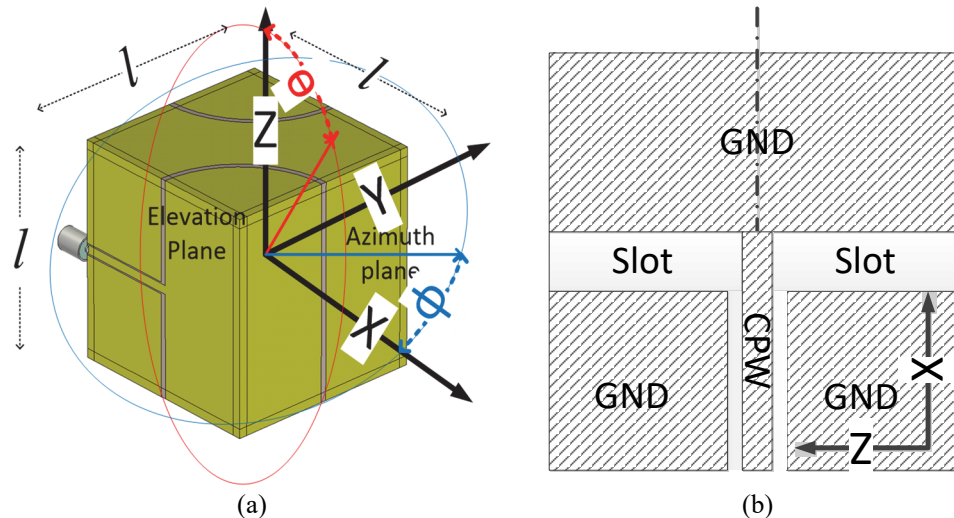


Fig. 4-9 a) Antenna geometry, b) CPW feeding configuration

4.3.2 Simulations and Critical Parameters

4.3.2.1 Antenna Simulations

We prototyped a cubic antenna-package operating at 2.4 GHz for WSN application. To confirm the compatibility of the structure with 3-D printing, our cubic prototype was printed from Verogray RGD850 by the aid of Objet EDEN 350V 3-D printer. Verogray

was characterized by Agilent SPDR (Split Post Dielectric Resonator) kit and the relative permittivity of 2.97 and the loss tangent of 0.02 at 3 GHz were achieved. Table 4-2 shows dimensions of the antenna after final optimization and tuning by the aid of HFSS. Coupling between different sections of the antenna located on the faces of the cube and folding the slot over cube edges make the final design parameters slightly deviate from simplified model based on length of slot antenna. The reflection coefficient and radiation patterns of the antenna are shown in Fig. 4-10 and Fig. 4-11 respectively.

Table 4-2. Dimension of proposed antenna for 2.4GHz

Dimensions	Value	Unit
Cube Edge Length	36.73	mm
Slot Width	1	mm
Slot Length	263	mm

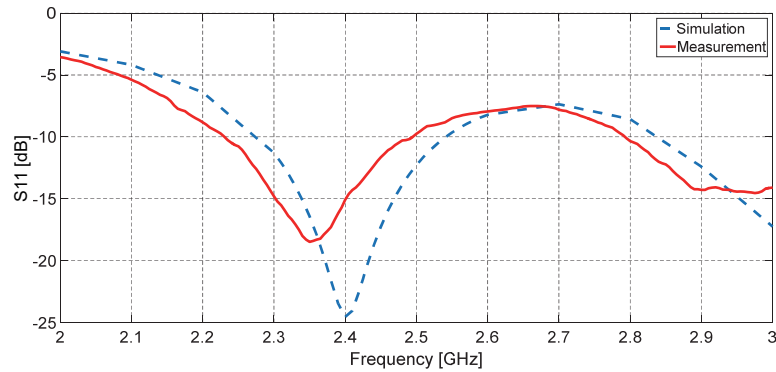


Fig. 4-10 Input reflection coefficient acquired through measurement vs. simulation results

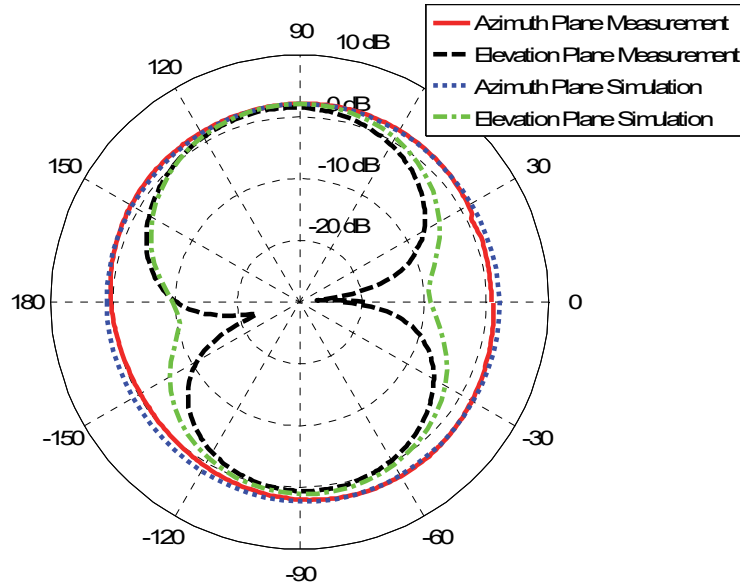


Fig. 4-11 Antenna gain patterns acquired through measurement at 2.44GHz vs. simulation results

The bandwidth of 11% at 2.4 GHz is obtained. The antenna offers an omnidirectional radiation pattern with the simulated maximum gain of 2.6 dBi and radiation efficiency of 85%. Here, azimuth plane is defined as XY and elevation plane as XZ as shown in Fig. 4-9 (b).

4.3.2.2 Effect of the Slot Width

As already discussed in Fig. 4-8, in order to acquire an omnidirectional radiation pattern in the azimuth plane with acceptable ratio of co to cross polarizations; maximum and zero electric field density need to be fixed at desired locations on the cube faces. Considering the fact that most of the printable materials with relatively low dielectric loss have dielectric constant around 3, the only variable parameters that actually play significant roles in the proper design of the antenna-package are the length and width of slot. The slot length discussed in the previous section, here we will elaborate on the effect of its width.

Width of slot is a key parameter especially in fine tuning and optimization of the proposed antenna. As shown in Fig. 4-12, changing the width of slots can shift the resonant frequency of the antenna and affect the input matching because both slot impedance and its electric length are functions of slot width.

Variation of slot width influences radiation patterns. The ideal slot antennas operate base on the assumption of infinite conductor. Here, we have a limited conducting surface

on the cube. The wider the slot width, the more current will be deviated from its normal path. In another word, widening the slot wipes off the conductive surface, so it reduces the conductive ground which perturbs the surface current distribution. The perturbation of currents not only results in deterioration of omnidirectional pattern but also increases the interaction between different sections of the antenna, leading to increase in the cross-polarization level. As shown in Fig. 4-12 and Fig. 4-13, slight decrease in width of slot from 1.25 mm to 0.75 mm shifts down the resonant frequency of the antenna and increases its cross polarization, respectively.

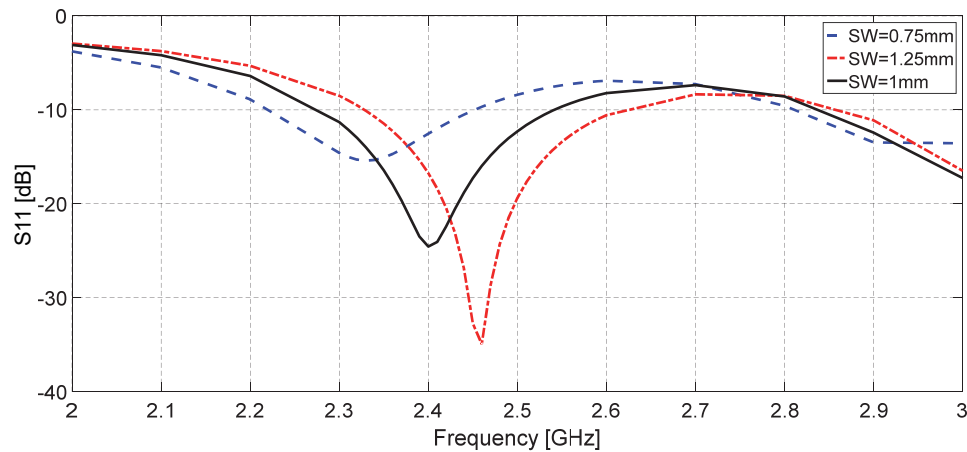


Fig. 4-12 Input reflection coefficient of antenna versus width of slot

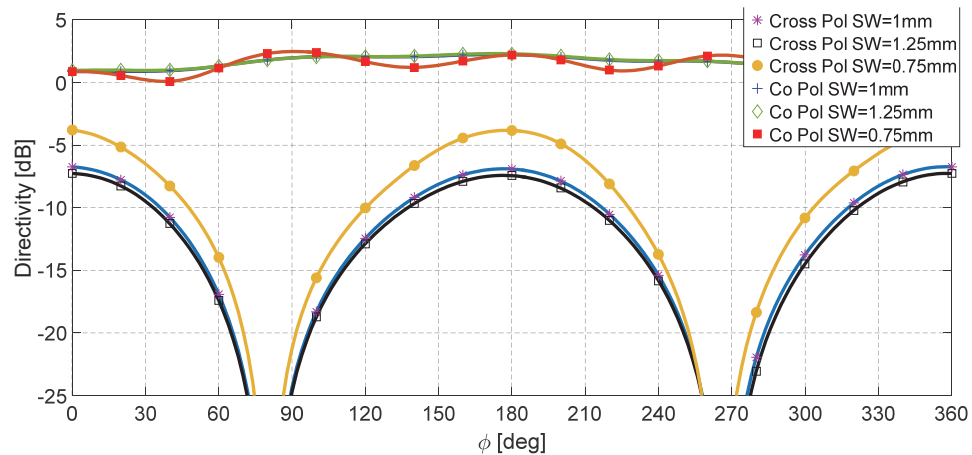


Fig. 4-13 Co and cross polarization directivity for different slot widths at 2.44GHz

This is not a linear effect since we can see a tangible jump in co to cross polarization level for slot width (SW) decreased from 1 mm to 0.75 mm while it is almost the same for

SW=1 mm and SW=1.25 mm. To meet the requirement of input impedance matching and desired radiation pattern with low cross polarization at the same time, we chose SW=1mm.

4.3.2.3 Effect of Circuit inside the Cube

Reserving the internal volume of cubes for placement of electric circuits is one of the main objectives of the proposed design which qualifies its application as an antenna-package. Here, we have investigated the effect of an electric circuit modeled by a PEC plate placed inside the cube. The intensity of the electric field inside the cube in presence of the PEC plate is shown in Fig. 4-14 which verifies negligible interaction with circuit board and no significant effect on the antenna performance and radiation pattern. It is worth to mention that assuming the cube as a resonator, its size has been chosen such a way no to resonate any mode at our operating frequency to guarantee negligible electric field inside the cube.

4.3.3 Fabrication and Measurement

The antenna shown in Fig. 4-15 is fabricated by the aid of Objet EDEN350v 3-D printer from Verogray material to confirm its 3-D printing compatibility. We then manually patterned the cube with copper tapes.

Fig. 4-10 illustrates input reflection coefficient of the fabricated prototype versus simulation results where the resonant frequency of 2350 MHz shows 50 MHz (about 2%) shift with respect to that of the simulation. The manual implementation of the antenna specially patterning the copper tape is mostly responsible for the frequency shift. However, 10 dB input reflection coefficient bandwidth of 11% obtained for the fabricated prototype is in very good agreement with the simulation.

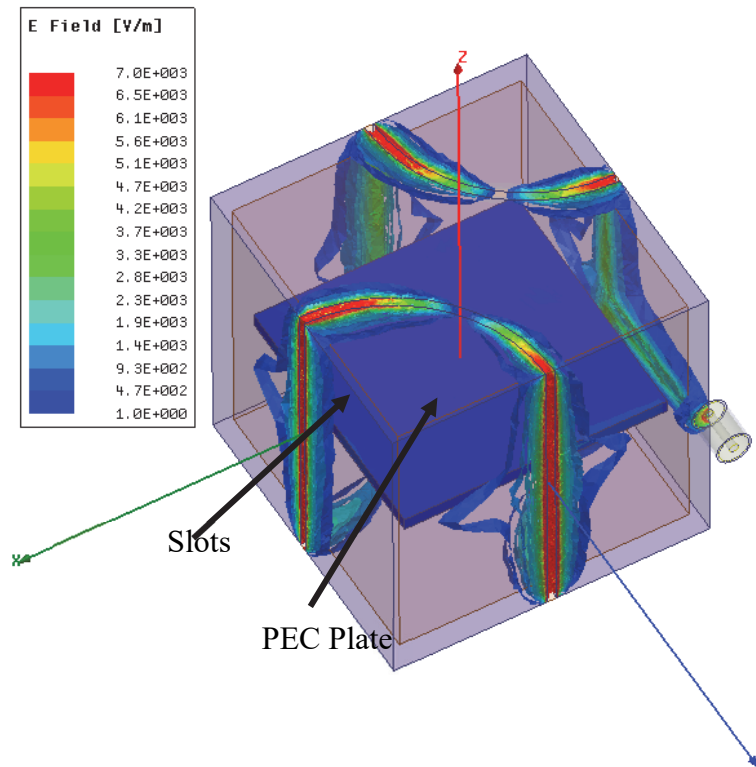


Fig. 4-14 Intensity of E-field at 2.44GHz in presence of circuits modeled by a PEC plate

Measuring the radiation patterns of the 3-D cubic antennas is a very challenging task due to lack of compatible standard antenna holder with low interaction with antenna body in measurement set-up. As shown in Fig. 4-16, we have mounted the antenna on a light holder in a far field antenna chamber and measured the radiation patterns in the elevation and azimuth planes separately in order to lower the interaction between antenna and measurement equipment and cables. The chamber itself was equipped with fiber optic interfaces, stable low-noise amplifiers, advanced measurement algorithms with averaging techniques, and robust mechanical infrastructures to handle on-the-fly measurement to reduce the noise and vibration.

Fig. 4-11 illustrates an omnidirectional radiation pattern with maximum gain of 2.53 dBi in the azimuth plane acquired through measurement and gain calibration using standard horn in the far field antenna chamber which is in good agreement with the simulation results. The SMA connector mounted on the cube for measurement purposes, coaxial cables and measurement setup are major factors in disturbing the radiation pattern and its deviation from a pure omnidirectional pattern in the azimuth plane. However, they can be eliminated in industrial application when a transmitter is installed inside the

structure. The manual fabrication and using nonstandard materials are other factors in minor mismatch between measurement and simulation results which can be resolved in industrial production.



Fig. 4-15 Fabricated antenna

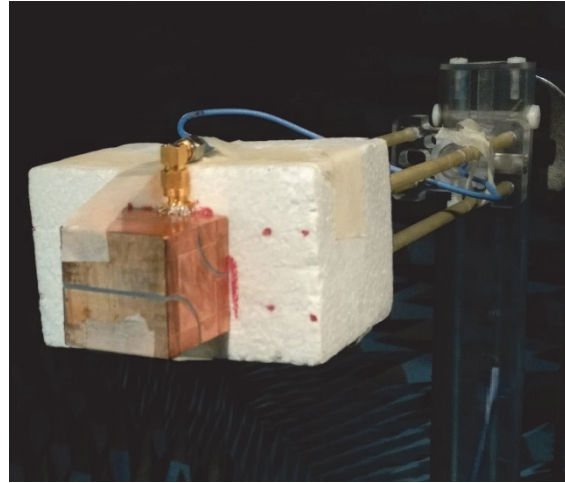


Fig. 4-16 Measurement set-up

4.4 3-D Folded Cubic Slot Antenna Array

In this section, a 3-D folded slot antenna array mapped on a hollow cubic structure with conductive outer surface is reported. Proposed antenna is capable of generating wideband ϕ -polarized omnidirectional radiation pattern in the azimuth plane through constructive radiation of the cube walls. The architecture is 3-D printable and the interior cube space is saved for accommodation of extra electronic devices, thereby introducing a low cost compact solution for wireless sensor network (WSN) applications. To verify the application of the proposed architecture in WSN, a cubic prototype with an edge length of 33.84mm operating at 2.45GHz has been fabricated using FR4 PCB and gain of 1.32dB in the azimuth plane and 10dB input return loss bandwidth of 12% have been achieved.

4.4.1 Design consideration

In order to produce a horizontally polarized omnidirectional radiation pattern, in-phase phi-polarized electric fields, (as shown with red arrows), should be set up in the azimuth plane of the cubic antenna of Fig. 4-17. The magnetic current distribution arising from such E field, designated by blue arrows, is analogous to the magnetic current flow of

rectangular slots placed on all four side walls (vertical faces) of the cube with the length of the slots being parallel to the z-axis. Such current configuration will create maximum E field in the center of the slots, so as desired, maximum gain is obtained in the azimuth. To ensure minimum radiation in unwanted directions, i.e. top and bottom of the cube, the E field should have nulls on these faces. As evident from Fig. 4-17, the continuation of currents to the top and bottom surfaces of the cube will cause out-of-phase E fields which conclusively result in cancellation of radiation along these directions.

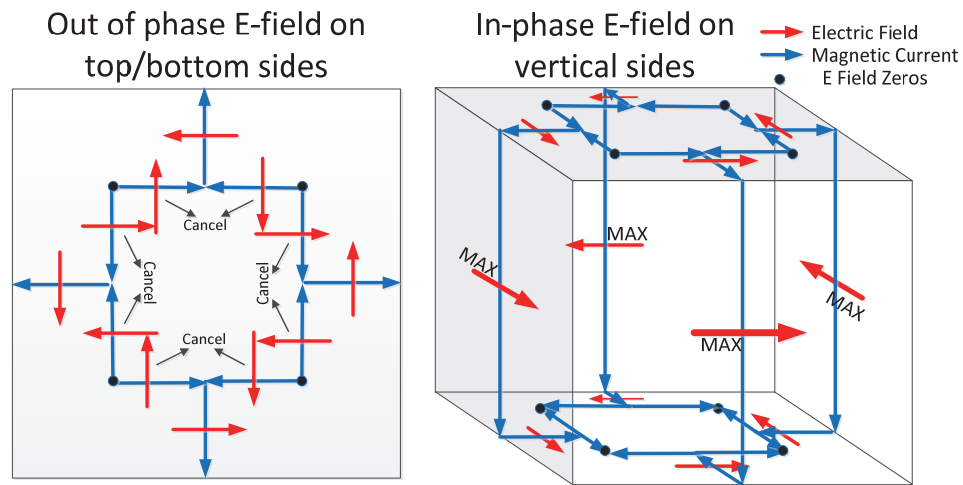


Fig. 4-17 Designing antenna based on nominal magnetic current and electric field distribution.

To realize the above vision, a rectangular folded slot antenna array as shown in Fig. 4-18, has been wrapped around the conductive surface of a cube. The cube structure is made of FR4 substrate. To ensure in-phase radiation from vertical slots on side walls of the cube, the length of the slots, along with the cube edge lengths have been tuned and optimized. The dimensions of the square ring slot cut on top and bottom faces have also been tuned to guarantee minimum power radiation at these directions. Table 4-3 shows dimension of antenna structure operating at 2.45GHz.

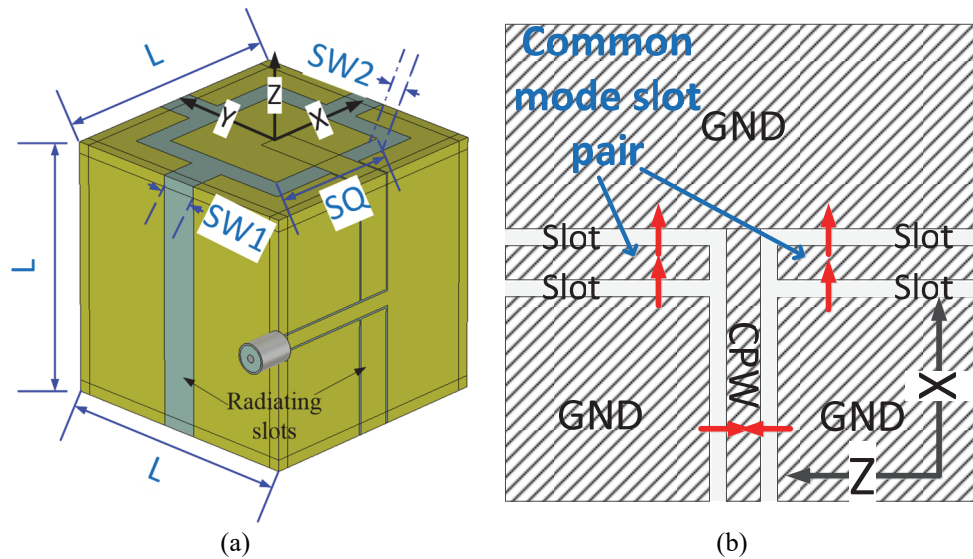


Fig. 4-18 3-D antenna geometry and its feeding architecture. a) Proposed 3-D folded slot antenna array, b) Differential and common electric field on CPW line and radiator slots.

Table 4-3. Dimension of Antenna Structure reported in Fig. 4-18 (a)

Parameter	Dimension	Description
SW1	5mm	Width of Side Slots
SW2	3mm	Width of Top Square Slot
SQ	18×18mm ²	Top conductive square
L	33.84mm	Dimension of cube
h	60mil	Substrate Thickness
ϵ_r	4.3	Permittivity of FR4

4.4.2 Feeding structure

Carrying the signals only in one conductive layer and having adjustable dimensions to serve high frequency applications on different technologies, make coplanar waveguide (CPW) transmission lines favorable. Particularly a CPW line will simplify the feeding in conformal antenna configurations such as the proposed cube, where the number of metal layers are limited to the outer surface of the object. Here, as depicted in Fig. 4-18 (a) a CPW line is employed at -Y face of the cube, to excite the antenna. It is worth mentioning that since a slot antenna exhibits a very high impedance at the center, the feeding becomes slightly challenging. Based on Babinet principle, the impedance of a half wavelength slot antenna in infinite PEC plane which is dual of a dipole (with 70Ω at the center feeding

point) would be around 500Ω at the center [72]. According to [72], folding the slot to an array is a practical solution to lower its impedance at the feeding point down to $\frac{Z_{Slot}}{n^2}$ in which n , is the number of slots. Since such solution has been adopted for the present case of the cubic antenna, with $n = 4$ slots, this equation yields the input impedance of 31.25 Ohms which is only a ball park number. However, for the present case of cubic slot antenna, the exact value of input impedance also depends on the width of the slot, thickness and dielectric constant of the substrate, finite ground plane and using lossy conductive layers.

In order to achieve a perfect omnidirectional radiation pattern in azimuth plane, equal contribution of all radiating slots in radiation pattern is required. To lower the contribution of directly excited slot on -Y face of the cube in radiation pattern and lowering its radiation resistance, it has been replaced with two narrow slots in common mode as shown in Fig. 4-18. This helped to accomplish an omnidirectional radiation pattern. Electric fields are shown by red arrows in Fig. 4-18 (b) to illustrate how two narrow vertical radiating slots along Z are excited at common mode through a horizontal CPW line along X. These narrow slots have been achieved by adding a conductor in the middle of originally wide slot where its width was tuned and optimized to achieve an omnidirectional radiation pattern in the azimuth plane.

4.4.3 Current Distribution

Current distributions for the radiating and non-radiating walls are shown in Fig. 4-19-a and Fig. 4-19 (b), respectively. The flow of current for all four radiating (side) walls is identical, in the sense that it is transverse to the slot length (directed across the width of the slot) on each face, as illustrated by horizontal arrows in Fig. 4-19 (a) This will eventually forms a Φ -directed current flowing around the cube on the side walls, resulting in a Φ -polarized omnidirectional far-field pattern in the azimuth (XY) plane. It is clear from Fig. 4-19 (b) that the top (bottom) faces are non-radiating due to destructive (out-of-phase) summation of currents flowing on their surface. This will lead to the perfect omnidirectional pattern in the azimuth as desired.

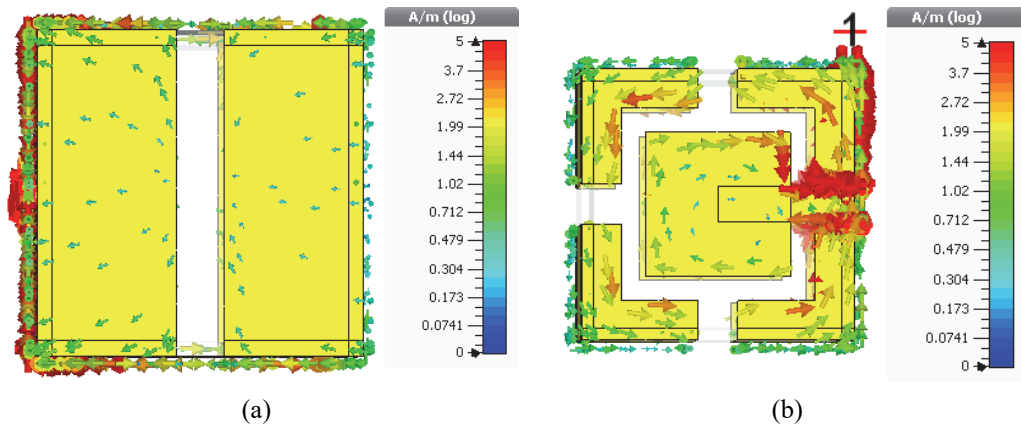


Fig. 4-19 Current distribution of 3-D structure, a) Vertical sides, and b) Top/Bottom side

4.4.4 Antenna Fabrication

As shown in Fig. 4-20, an open cube T shaped planar PCB board from FR4 has been fabricated using lithography technology and folded and stuck using copper tapes to form a cube. Dimensions of the structure are listed in Fig. 4-18. Even we have prototyped using planar PCB fabrications, proposed structure is fully compatible with 3-D printing.

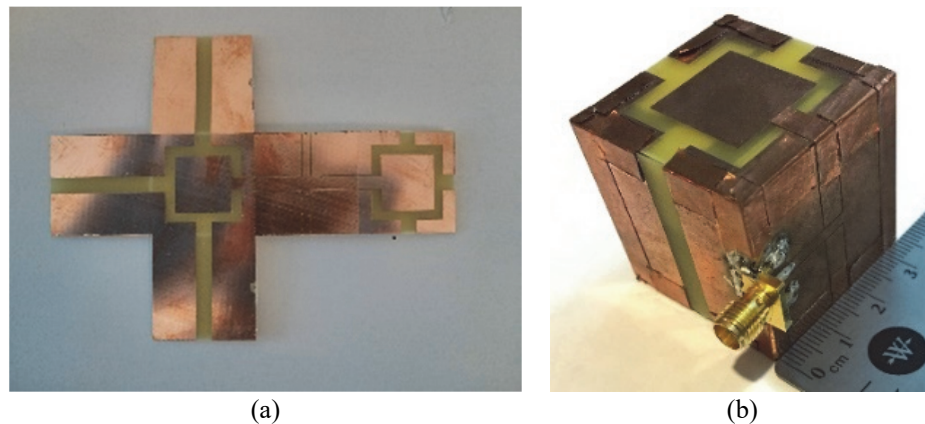


Fig. 4-20 Prototype manufacturing, a) Flattened open cube view, and b) 3-D fabricated cube

4.4.5 Measurement and Simulation Results

This antenna is resonating at 2.45GHz and its 300MHz frequency bandwidth covers the ISM frequency at best. The input reflection loss of the antenna has been measured and is in good agreement with the simulation results as shown in Fig. 4-22. The radiation pattern of the antenna has been measured in a far field antenna chamber using the setup shown in Fig. 4-21 and its gain calculated using a standard horn to calibrate the anechoic chamber. The measurement result is shown in Fig. 4-23 versus the simulated results for

both elevation and azimuth planes which have been measured separately. The simulated and measured results exhibit good agreement. The slight difference observed between plots in Fig. 4-23 can be contributed mainly to the manual manufacturing and a rather imperfect measurement setup like having SMA connectors and coax cable connected to the antenna.

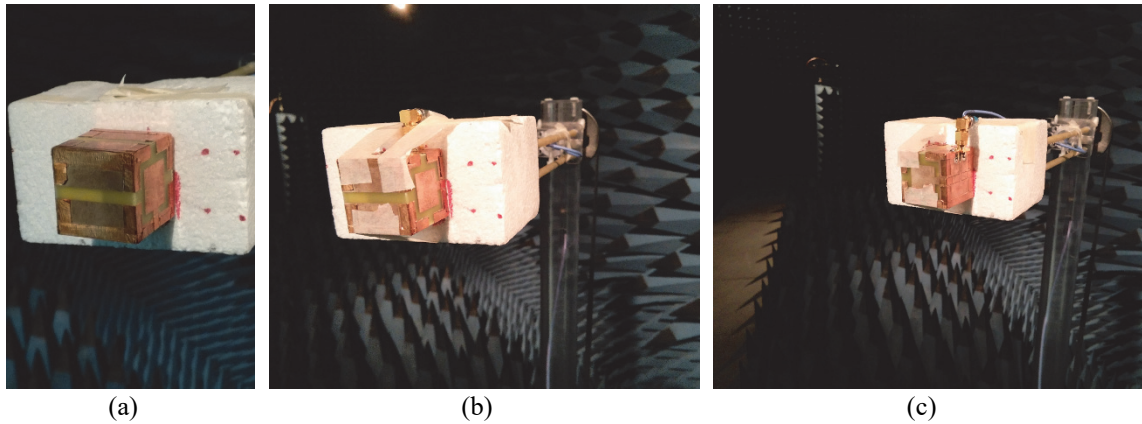


Fig. 4-21 Radiation Pattern Measurement Setup at three orthogonal planes in Far field Antenna Measurement Chamber, a) XZ, b) XY, and c) YZ

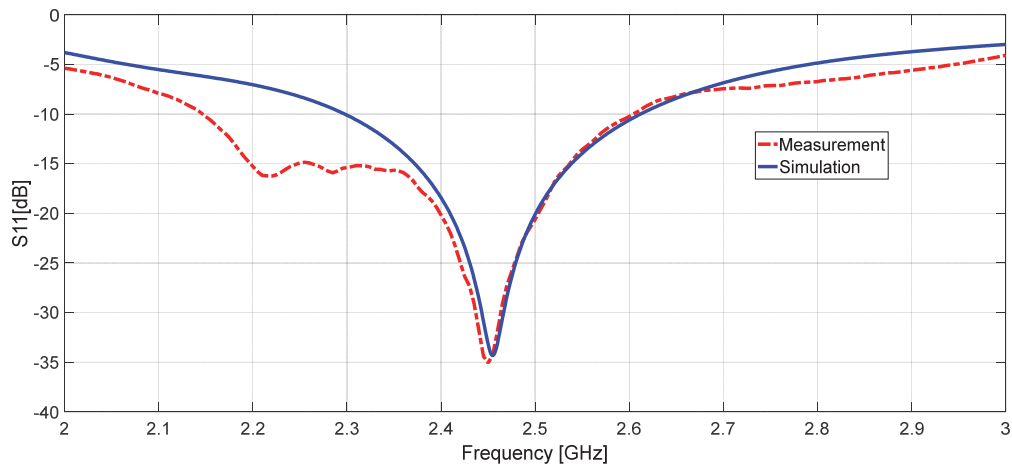


Fig. 4-22 Input reflection coefficient of the proposed antenna

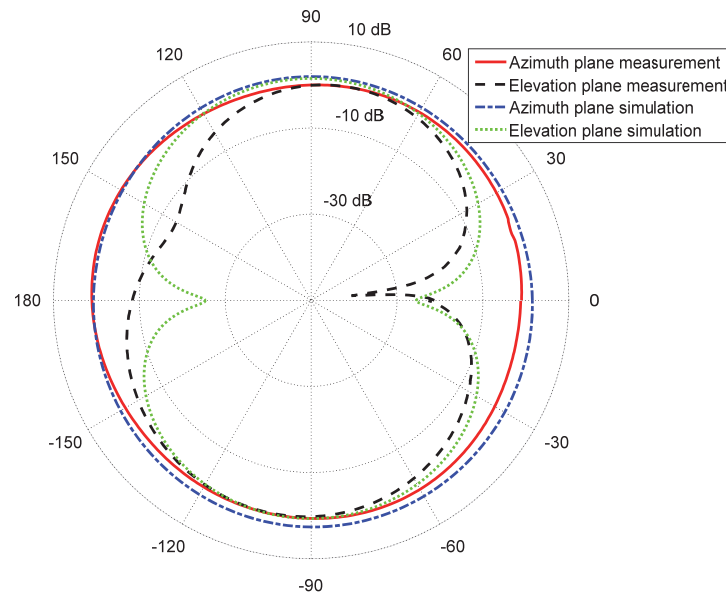


Fig. 4-23 Antenna gain in Elevation and Azimuth cuts at 2.45GHz

4.5 Conclusion

First structure: As a summary, in this section, a cubic slot antenna operating at 2.45GHz with maximum gain of 1.95dBi, and bandwidth of 14% was designed and fabricated. The measurement results have been illustrated and showed to have good agreement with the simulations, verifying the capability of the proposed antenna to cover the ISM bandwidth used by ZigBee monitoring wireless networks. The structure is 3-D printable and can enclose sensors, transmitter and processor circuits inside and offer all in one packaged solution for WSN.

Second structure: To achieve an omnidirectional radiation pattern in the azimuth plane with horizontal polarization, we proposed a novel wideband 3-D annular slot antenna configuration. To verify the application of the antenna in wireless sensor networks, a cubic prototype operating at 2.4 GHz has been designed. Maximum gain of 2.53 dBi, and bandwidth of 11% were achieved through measurement. The 3-D printable antenna-package structure can offer all in one packaged solution for WSN by enclosing sensors, transmitter and processor circuits inside.

Third structure: Here a novel 3-D printable antenna structure with horizontally-polarized omnidirectional pattern for WSN applications is presented. The measurement

results were in a good agreement with the simulation results and the antenna is matched at 2.45GHz on 12% bandwidth where maximum gain of 1.32dBi has been achieved. The CPW feeding in our prototype can be substituted with differential feeding through a potential transceiver installed inside the cube in industrial WSN applications.

5 Cubic architectures with reconfigurable radiation pattern

5.1 Introduction

Research on planar arrays of antennas and their reconfigurability has been started long time ago to improve the quality of signal, miniaturize the antenna and alleviate the cost. 3-D antennas are more efficient and compatible with the 3-D geometries of wireless devices like cellphones or sensory nodes in wireless sensor networks, however due to lack of 3-D designs and fabrication procedures, commonly planar antennas with limited functionality are dominant in the market. Recent advancement in 3-D printing technology engrossed researchers in designing three-dimensional objects which can be more efficiently patterned with 3-D smart antenna designs which can form the beam in a desired direction to improve the SNR. In this chapter, we report a single feed reconfigurable folded slot antenna and a multi feed conformal slot antenna which are capable of switching between omnidirectional and directional beams according to the requirements of the system in which they are employed.

Wireless sensor network is an under-development technology responsible for monitoring a variety of parameters for applications such as military, health, and environment related tasks like agriculture and weather forecasting. The networks can be installed in rural areas with strong direct link or urban areas with dominant multipath propagation due to presence of obstacles. As the environmental conditions may vary over

time, employing an antenna with fixed radiation pattern is not always the best solution for high quality and reliable telecommunication links in such an unpredictable circumstance. However, designing reconfigurable antennas with remarkable capability to switch between omnidirectional and directional radiation patterns in order to cover all 4π steradian space around antenna and the competence to adapt their pattern to the condition of the medium can have a direct impact on improving the network quality. In the environment where the communication link has been established between two devices being installed almost at the same altitude, distribution of angle of arrivals is concentrated around horizon and most of the signal is received from endfire, omnidirectional antennas can deliver the best all-around performance whereas in the environment where nodes are communicating vertically for instance with a drone, BTS or satellite, most of the signal is received from the broadside and a directional pattern in the elevation is a more ideal solution.

Space diversity is one of the most practical methods in improving channel signal quality in such an environment. Nowadays almost all wireless devices are employing MIMO and beam forming to take advantage of space diversity, but it is mostly restricted to two dimensional planar structures with limited features in broadside direction. In section 5.2, we have reported a new multi feed cubic conformal slot antenna array which can be used both as a beam steering antenna in the endfire direction as well as a 3-D cubic MIMO architecture. The proposed architecture offers remarkable advantages through using conformal microstrip slot antennas in 3-D to widen the beamwidth. Furthermore, since this is a multiport structure, by changing excitation at the input ports, we can switch between omnidirectional/directional beams in the azimuth plane and obtain various beamwidths through individual or simultaneous excitation of different antenna elements.

In section 5.3, we have targeted applications where an antenna is required to cover all 4π steradian space. Compared to section 5.2, which aimed only the communication in the azimuth plane, this constitutes as a more thorough design where the antenna is expected to be capable of switching between omnidirectional endfire for terrestrial communication and directional broadside for satellite/drone communication. This antenna with reconfigurable azimuth omnidirectional/elevation broadside radiation can markedly improve the performance of wireless sensor networks and will translate to better

adaptability so the sensor will be well-suited for all WSN network layouts. In a specific application as a package for a sensory node in wireless sensor network, all nodes can communicate to each other through an adhoc network by the help of *omnidirectional* radiation patterns in the azimuth plane as well as their hub which can be a drone, satellite or tower, through a beam elevated and pointed toward *broadside* direction. By extending the 2D folded slot antenna array configuration to 3-D and adding reconfigurability to the structure, a novel 3-D cubic antenna architecture is designed and fabricated. A planar slot antenna array composed of four vertical slot elements is folded and wrapped around the cube such that each individual slot is mapped on one of the side walls of the cube. Constructive in-phase radiation from these walls will produce an omnidirectional radiation pattern in the azimuth plane. The proposed structure is also engineered to generate broadside radiation pattern with moderately high gain toward the top or bottom faces of the cube by exciting patch antennas embedded in those corresponding faces. This flexible control of beams in the principal planes along with the simple feed mechanism introduced through a CPW line, makes the proposed design a perfect candidate for low cost mass production available through 3-D printing technologies. In addition to the above-mentioned benefits, the conductive outer surface of the proposed antenna-package also offers EMI protection for potential electronic circuits installed inside.

5.2 Cubic conformal slot antenna array

In this chapter, we have analyzed conformal 3-D slots wrapped around a multi-feed cubic structure and investigated the coupling between slots placed on the cube faces. Additionally, we have compared different methods in modeling the antenna to acquire the radiation pattern. 3-D antenna packages found major applications in wireless sensor networks and WiFi router. We have prototyped the antenna designed at 2.4GHz and verified our investigation through comparing measurement results against simulation.

5.2.1 Antenna Geometry and Prototype Design Consideration

Here a multi feed 3-D slot antenna array has been designed and bent around a cube which can be used as a package of a sensory node in wireless sensor networks or body of a transceiver in mobile repeater applications. The proposed antenna offers a reconfigurable radiation pattern which can switch between an omnidirectional and directional radiation patterns in accordance with altering excitation at the input ports. Also, as we have access to all four feeds, one can use it as a MIMO cube.

Here, we refer to the Z -axis and XY plane as vertical axis and azimuth plane, respectively. Hence, cube faces normal to the $+Z$ and $-Z$ axes considered as the antenna top and bottom faces respectively and faces normal to the $+X$, $-X$, $+Y$, and $-Y$ as the antenna side walls or vertical faces. In this work, four slot antennas have been designed and wrapped around a cube made of a PCB or 3-D printed material to verify different fabrication methods. Each slot antenna is placed at the center of one of the vertical faces of the cube and continued and folded to the top and bottom faces where all slots have been truncated. Slot antennas have been excited through microstrip lines beneath the slots on the top face of the cube to facilitate the feeding network implementation. Geometry of antenna is shown in Fig. 5-1. In this architecture, all slots are excited independently through feeding network.

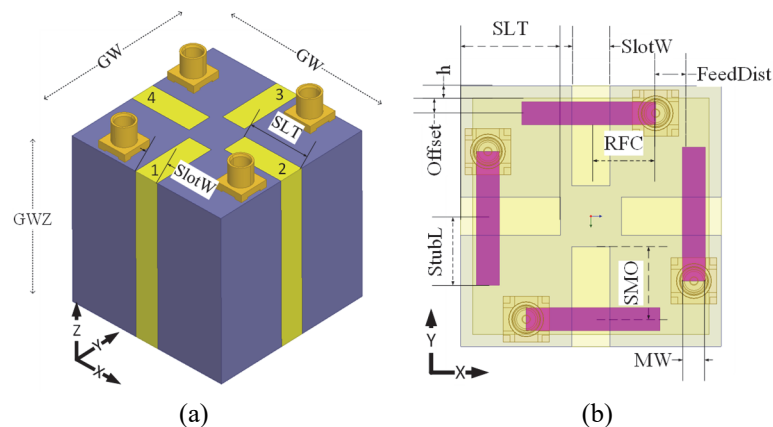


Fig. 5-1 a) Antenna Geometry, b) Current distribution when one antenna is excited

All the microstrip lines feeding the antennas needed to be placed at the bottom layer of the top face of the cube, on the same layer as other components of the feeding network are placed. This section of slot antenna is far from its center and lowers the impedance of

the transition from slot to microstrip line more than required which highlights the need for a wide high impedance slot for proper 50Ω matching to microstrip line. Here, we have used high impedance slots of 5mm width to match them on the top face of the cube.

All four open-ended microstrip lines responsible for slot feedings, are exited through four low profile RF connectors, here AMC connectors. However, they can be excited through potential circuits installed inside the cube for future applications in WSN networks. Design parameters assigned to antenna dimensions shown in Fig. 5-1 are listed in Table 5-1.

Table 5-1. Definition of Design Parameters in Antenna Structure

Parameter	Description
SlotW	Width of vertical slot pair
SlotL	Total length of slot
GW	Dimensions of cube's base (X and Y directions)
GWZ	Height of cube (Z direction)
SLT	Length of slot folded on top/bottom faces of cube $SLT = (SL - GWZ)/2$
Offset	Microstrip feed offset from bottom layer of edge substrate
SMO	Microstrip feed offset from end of slot ($SMO = SLT - Offset$)
StubL	Length of open circuit microstrip line passing slot antenna
FeedDist	Distance between RF connector and bottom layer of vertical face after subtracting the width of neighbor microstrip line to guarantee enough coupling
RFC	RF connector position respect to the center of slot $(RFC = GW/2 - FeedDist - MW - h)$
MW	Microstrip width
ϵ_r	Relative permittivity of substrate
h	Thickness of substrate

5.2.2 Design considerations

In our proposed structure, four slots are folded on a cube to form a circular array antenna with four elements with a directional or omnidirectional radiation pattern in the azimuth plane. Here, we elaborate on analysis and design of a cubic antenna based on circular array theory and conformal antenna concept. Analytical solution for the structure

reported in this section can be found in section 3.3.2 where four folded slot antennas are mapped on a cubic structure with conductive outer layer. Similar to the case studied in section 3.3.2, here each antenna is contributing in the far field pattern only in half of angular space in the azimuth plane. Contribution of antenna elements is shown in Fig. 3-27. The same justification can be repeated where slot antennas are backed by a substrate with thickness of h , referred as *microstrip slot antennas* in this document. Having substrate will affect antenna resonant frequency, coupling and efficiency depending on thickness and permittivity of the material. Therefore, antenna width and length need to be tuned to yield proper resonance frequency. Here, we have connected all four conductors to form a cube with four slot antennas mounted on its vertical faces. Length of slot is chosen accordingly to maintain the desired resonance frequency for slot antenna elements. Feed offset and length of open circuit stub are chosen for proper matching. To serve all applications in wireless sensor networks and majority of telecommunication systems at 2.44GHz ISM frequency band, we have prototyped one antenna based on the proposed structure operating at 2.44GHz. The dimensions of such antenna are shown in Table 5-2.

Table 5-2. Dimension of proposed antenna for 2.44GHz

Dimensions	Value	Unit
GW	34	mm
GWZ	34	mm
SlotW	5	mm
SlotL	60	mm
SLT	13	mm
Offset	2	mm
StubL	9	mm
FeedDist	4	mm
MW	3	mm
ϵ_r	4.3	
h	1.55	mm

As the structure is symmetric, all four slot antennas have the same input reflection coefficient where full wave simulation result is illustrated in Fig. 5-2. The coupling between slot antennas located next to each other on vertical faces of the cube, i.e. side

neighbors is different from slots placed on opposite walls, facing each other and both are plotted at Fig. 5-3 and Fig. 5-4.

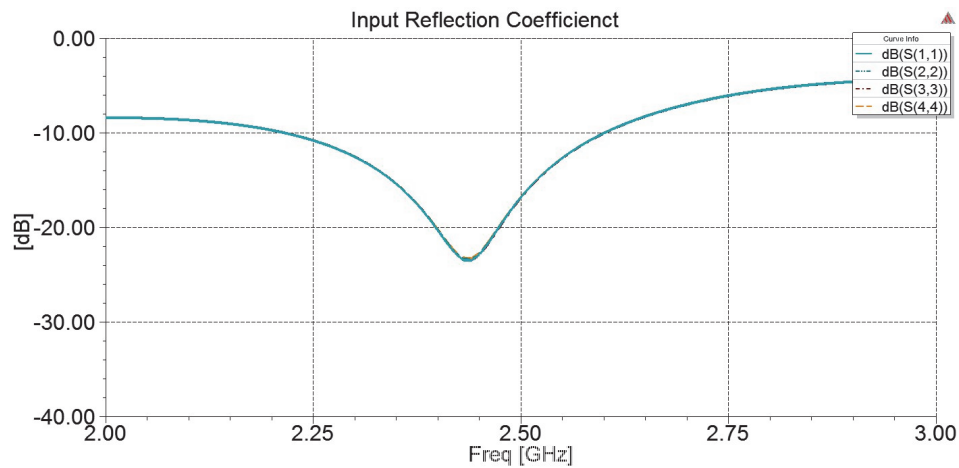


Fig. 5-2 Input reflection coefficient of a single folded slot obtained from full wave simulation

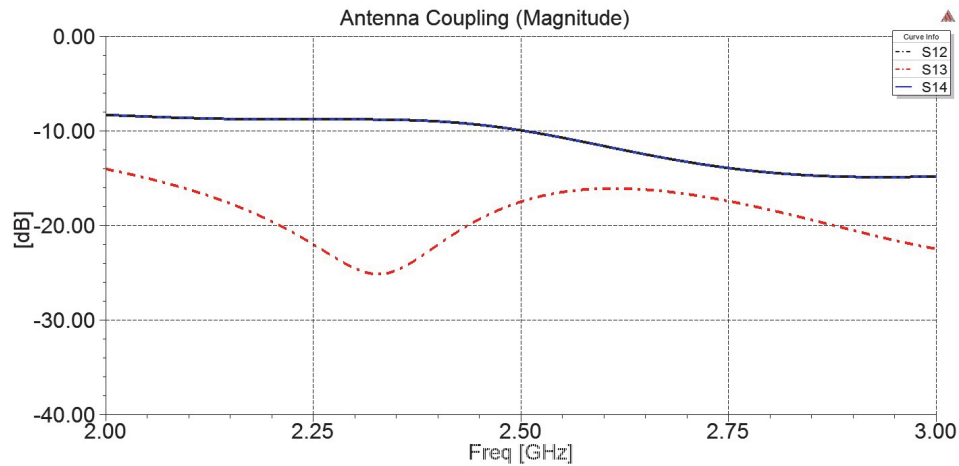


Fig. 5-3 Magnitude of coupling between slot antennas on cube faces obtained from full wave simulation

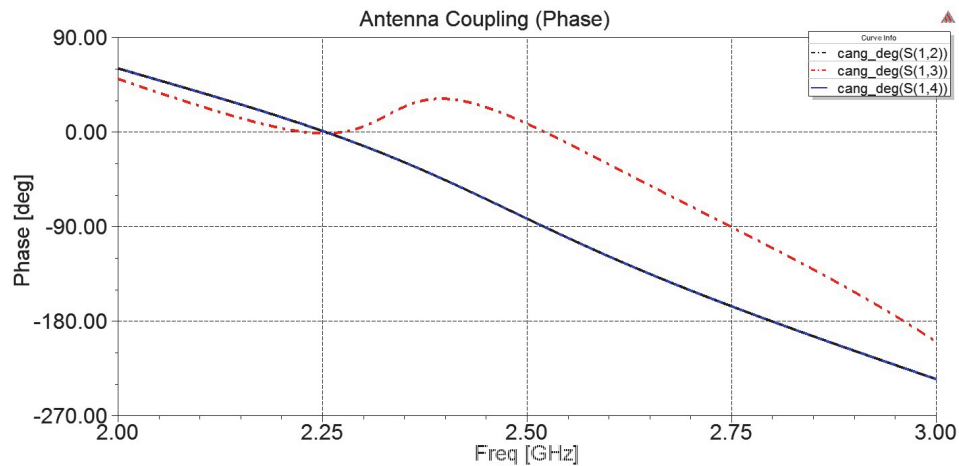


Fig. 5-4 Phase of coupling between slot antennas on cube faces obtained from full wave simulation

5.2.2.1 Slot excitations for reconfigurable radiation pattern

The architecture can be excited such that the beam can be steered in toward different directions in the azimuth plane and adjust the beam width. The simplest way to steer the beam and point the main lobe at directions normal to vertical faces of the cube is to excite the corresponding desired face/faces. In case one slot is excited, a narrow radiation pattern illustrated in Fig. 5-5 will be achieved which can be steered within 90° resolution. Fig. 5-6 shows the case for which two slots are excited at the same time; therefore, bandwidth increases from narrow to medium and we can steer the pattern within 90° resolution. As shown in Fig. 5-7, exciting three slots simultaneously will increase the beam width even more and still the pattern is steerable in the azimuth plane.

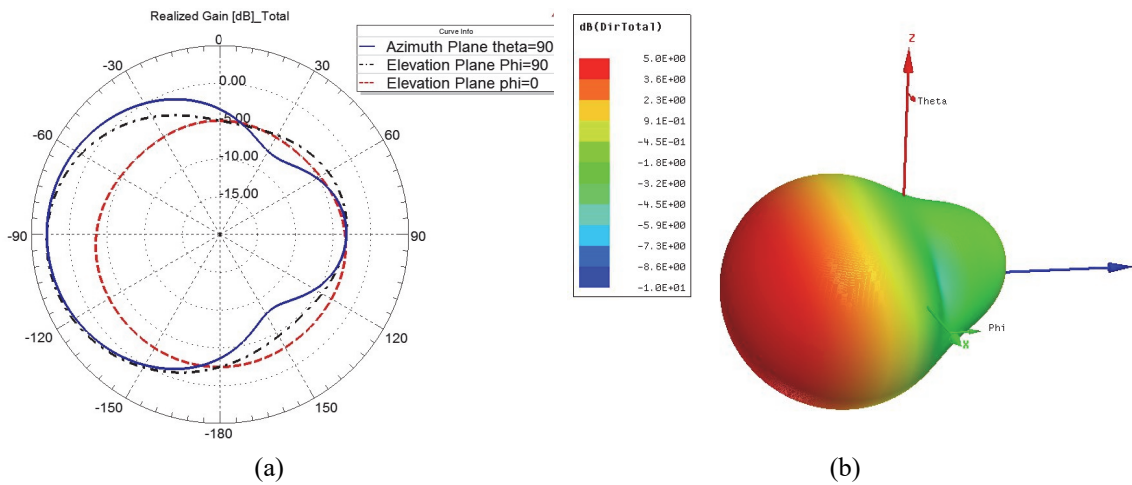


Fig. 5-5 Total realized gain of antenna at 2.44GHz in case only slot 1 is excited, a) Realized Gain, b) Directivity

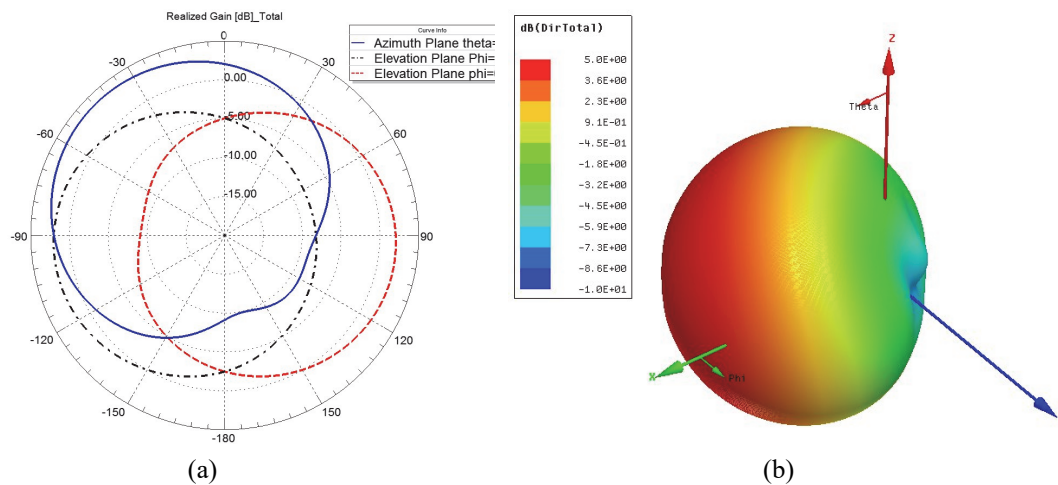


Fig. 5-6 Total realized gain of antenna at 2.44GHz in case two slots are excited slot1 and slot 2, a) Realized Gain, b) Directivity

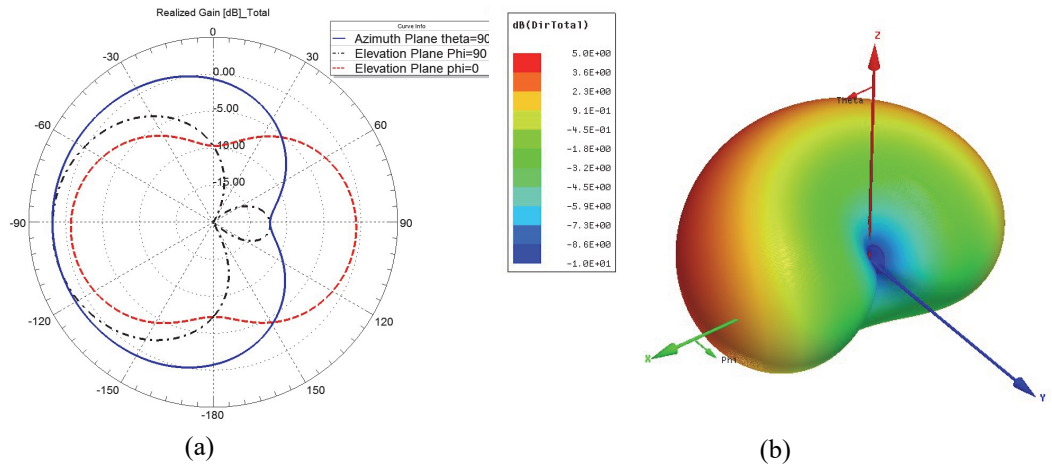


Fig. 5-7 Total realized gain of antenna at 2.44GHz in case three slots are excited slot4, slot1 and slot 2, a) Realized Gain, b) Directivity

To obtain a horizontally polarized omnidirectional radiation pattern from the cube antenna, all slots need to be excited in-phase as shown in Fig. 5-8. In antennas with omnidirectional radiation, pattern flatness is an important parameter and often times it is difficult to design a perfectly omnidirectional antenna and keeping pattern flatness at the same time. It proves to be even more challenging parameter in cubic antennas with multi elements arranged as a circular array. Pattern flatness of the radiation pattern of the proposed antenna in the azimuth plane shown in Fig. 5-9 verifies low ripples on the pattern due to φ directed current distribution on the body of the cube. This is an advantage of the cubic slot antenna over cubic antennas with other types of elements like dipoles.

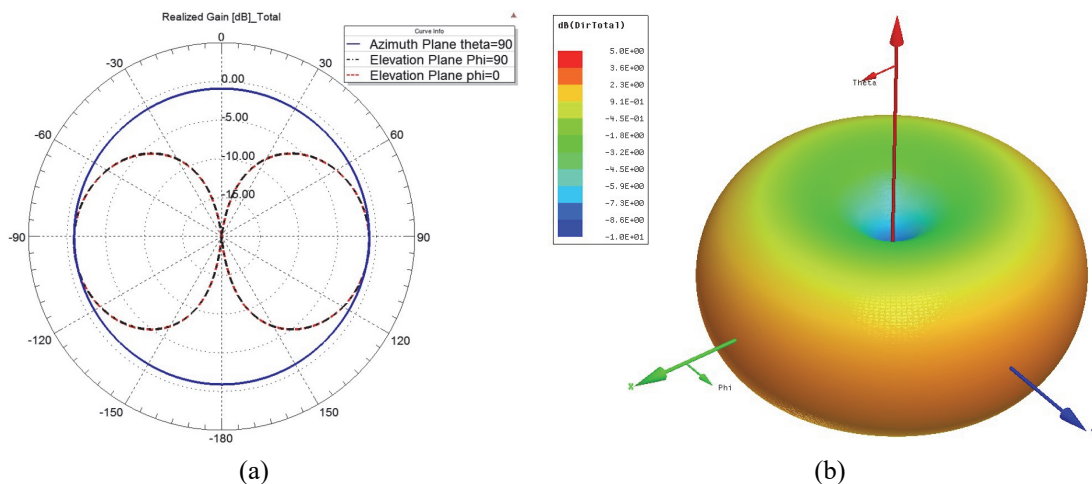


Fig. 5-8 Total realized gain of antenna at 2.44GHz in case all slots are excited for an omnidirectional radiation pattern, a) Realized Gain, b) Directivity

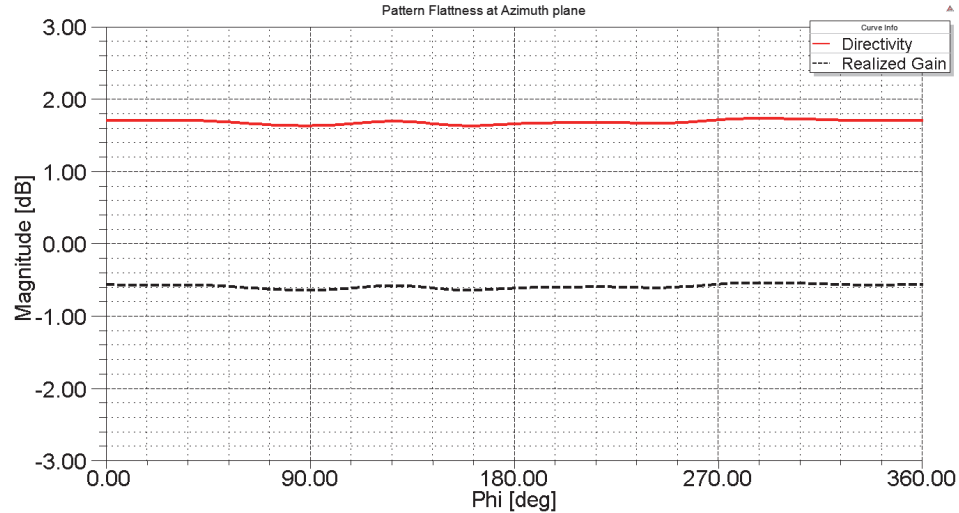


Fig. 5-9 Pattern Flatness at Azimuth plane

5.2.2.2 MIMO application

The multi feed antenna is a good candidate for MIMO applications with pronounced diversity gain and correlation coefficient. The 2×2 MIMO characteristics of the proposed antenna have been calculated in HFSS when each time just two ports of the antenna have been excited. Correlation coefficient and diversity gain of 2×2 MIMO have been illustrated in Fig. 5-10 and Fig. 5-11, respectively.

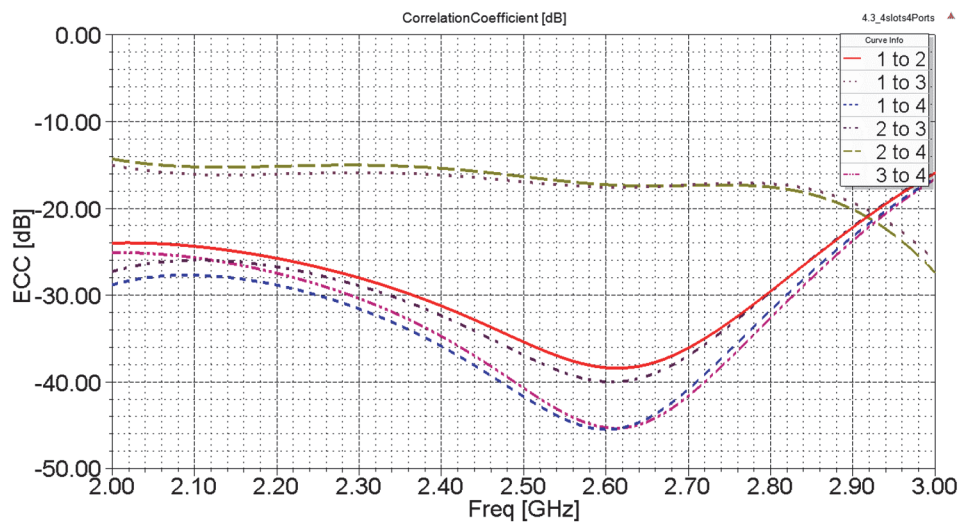


Fig. 5-10 Correlation Coefficient in dB scale for two ports excitation obtained from full wave simulation

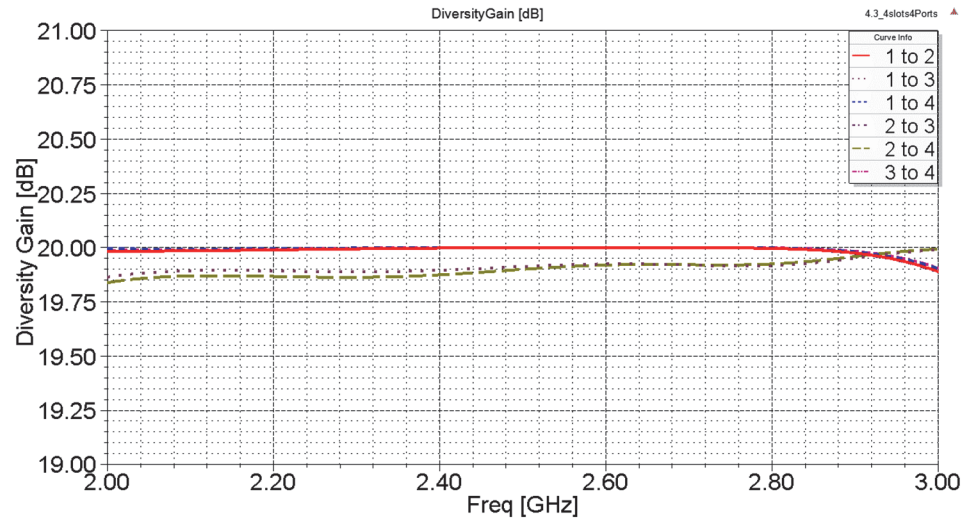


Fig. 5-11 Diversity Gain in dB scale for two ports excitation obtained from full wave simulation

5.2.3 Parameter study and coupling

Here, we have studied five major geometrical parameters of the cube antenna which have the most effects on input matching, coupling and directivity; List of parameters for which this parameter study is carried out is as follows. SlotW (width of slot), GW (size of cube), SlotL (total length of slot antenna), and StubL (length of open circuit stub).

5.2.3.1 Width of slot

Impedance and radiation resistance of slot antennas depend on the width of the slot where wider the slot, higher the impedance Fig. 5-12 shows input matching for three values of SlotW. Guaranteed matching at 2.44GHz could be obtained when SlotW=5mm.

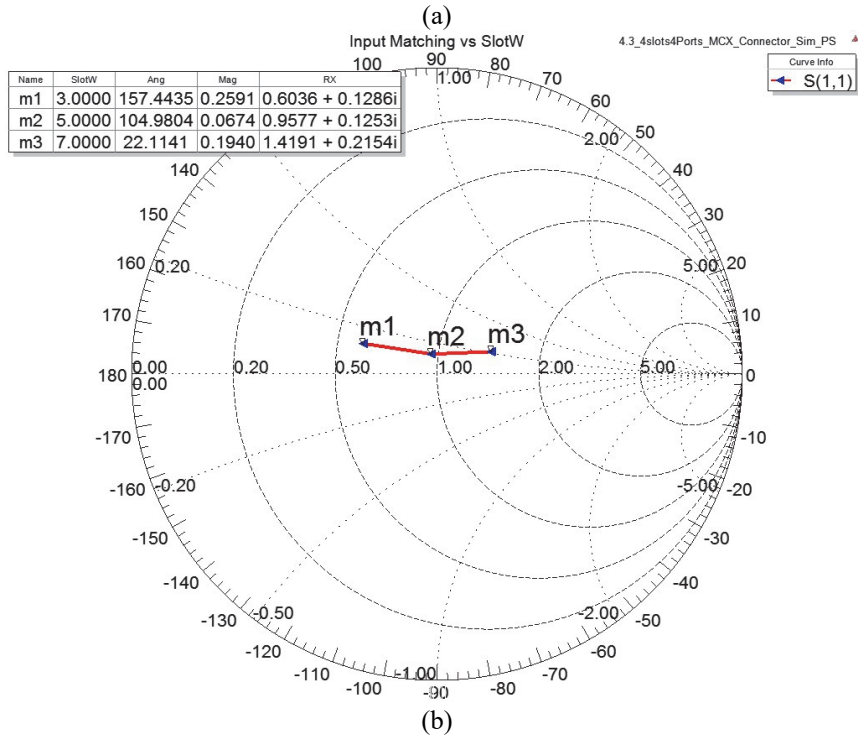
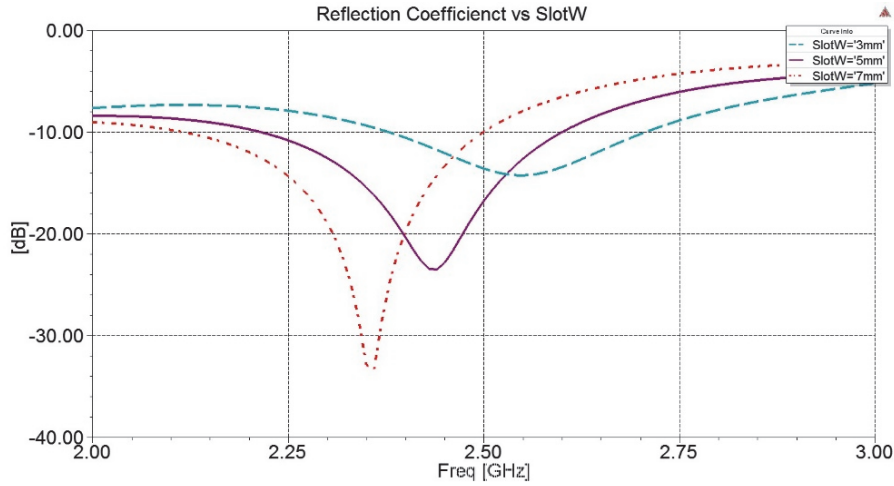


Fig. 5-12 Input matching vs width of slot

Also, it is obvious from Fig. 5-12 how changes in SlotW can detune the resonance frequency of the antenna. Since slot width dimension also affects coupling between antenna elements, the coupling has been plotted versus slot's width for the proposed structure and is shown in Fig. 5-13. As can be seen in Fig. 5-13 widening the slot increases both magnitude and phase of coupling coefficient between elements placed on opposite walls while we observe almost intangible effect on coupling coefficient between side neighbours.

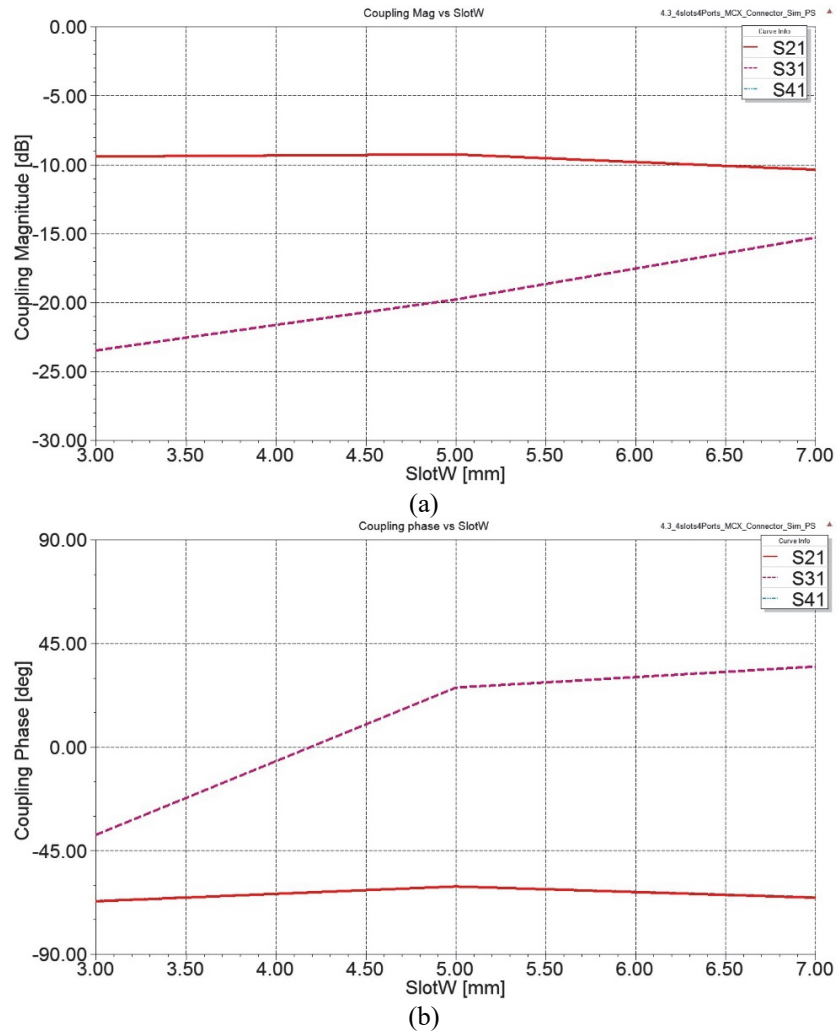


Fig. 5-13 Coupling versus width of slot, a) Magnitude, and b) Phase

In our proposed structure, slot antenna is used as array element where increasing the slot width leads to bigger aperture in the azimuth plane and as a result narrower beam in the same plane. However, it does not effect the beam width in the elevation plane as illustrated in Fig. 5-14.

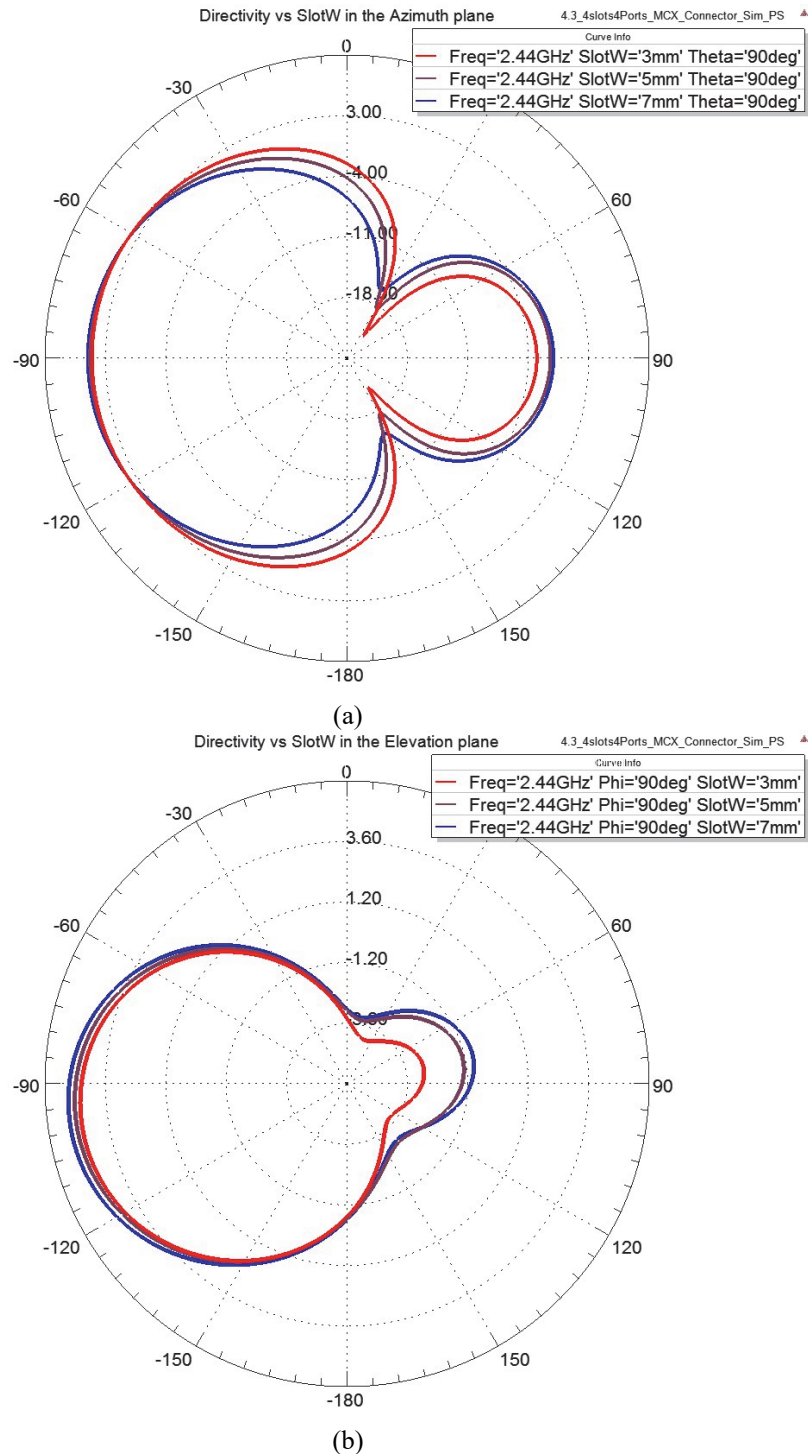


Fig. 5-14 Co pol directivity vs width of slot, a) Azimuth plane, and b) Elevation plane

5.2.3.2 Size of cube

Here, a parameter study has been done for input matching, coupling, and directivity versus GW, which represents cube size in our structure. As shown in Fig. 5-15, variation in cube size will not drastically affect the input matching for a fixed slot length. However,

it will change the bending location on the slot and feeding offset from the end of the slot which contribute to minor changes observed in plots of Fig. 5-15. Fig. 5-16 shows enlarging the cube will increase the coupling phase as was expected due to longer distance between antenna elements.

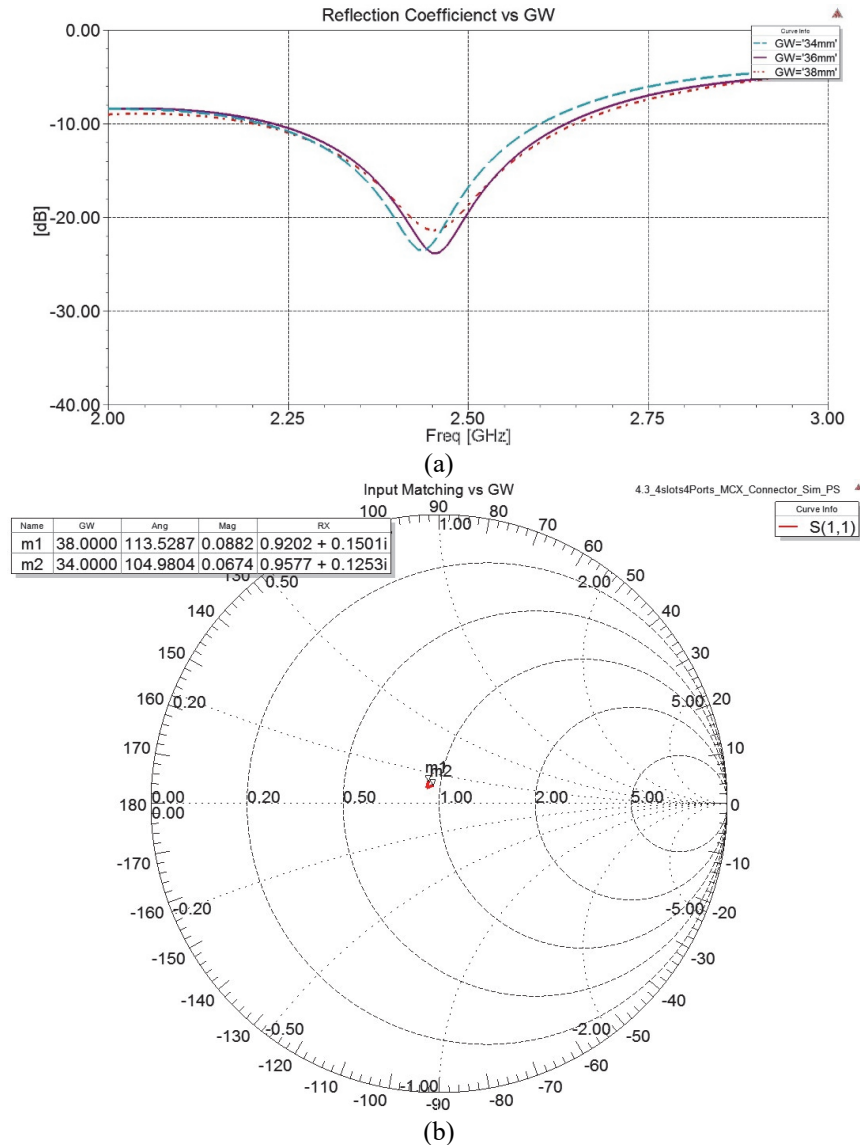


Fig. 5-15 Input matching versus cube size (GW)

We did not observe tangible changes in coupling magnitude between slots facing each other on opposite walls however the coupling between side neighbors increased around 4dB. This is mainly due to the enlargement of cube faces which creates longer distance between neighbor slots as well as more isolation between truncated ends of the slots on the top and bottom faces, and also their corresponding microstrip feedlines.

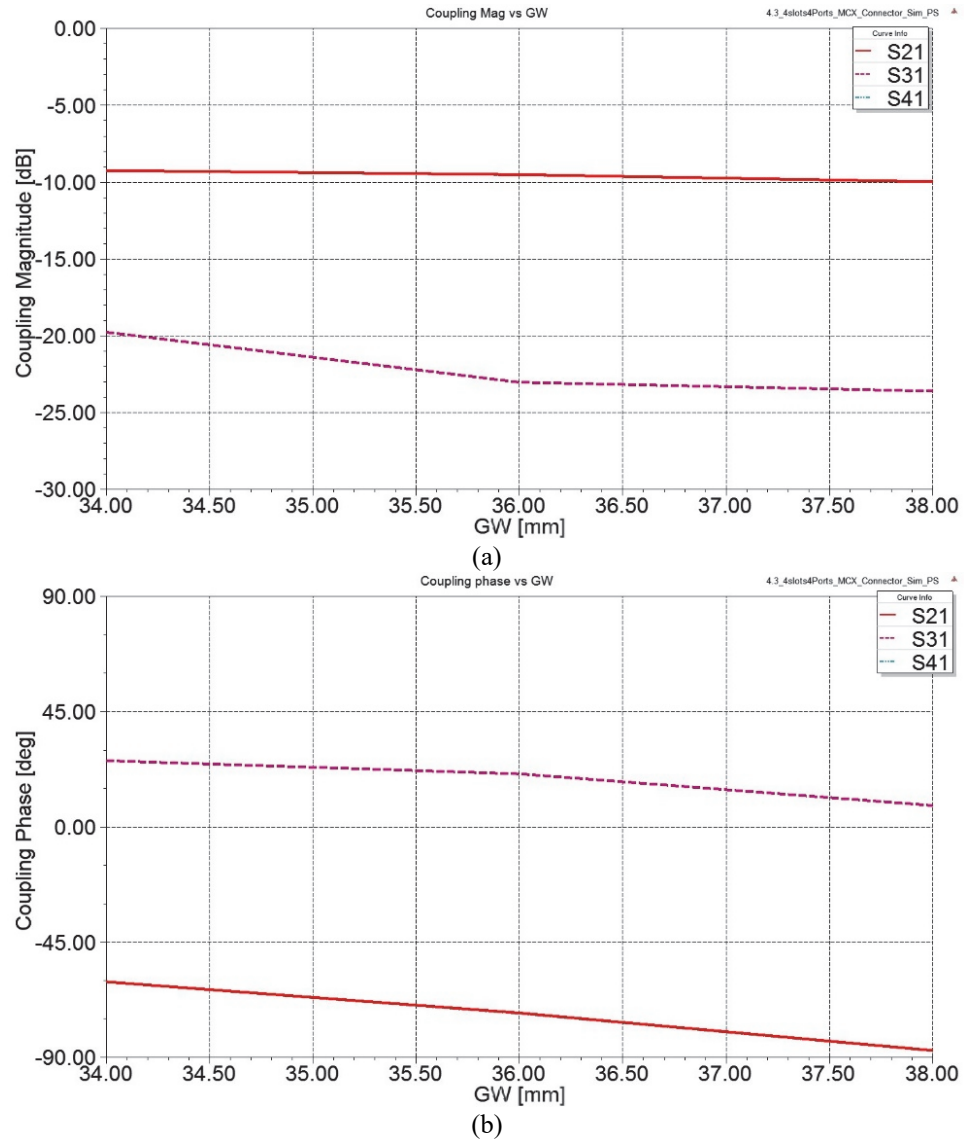


Fig. 5-16 Coupling versus cube size (GW) at 2.44GHz, a) Magnitude, and b) Phase

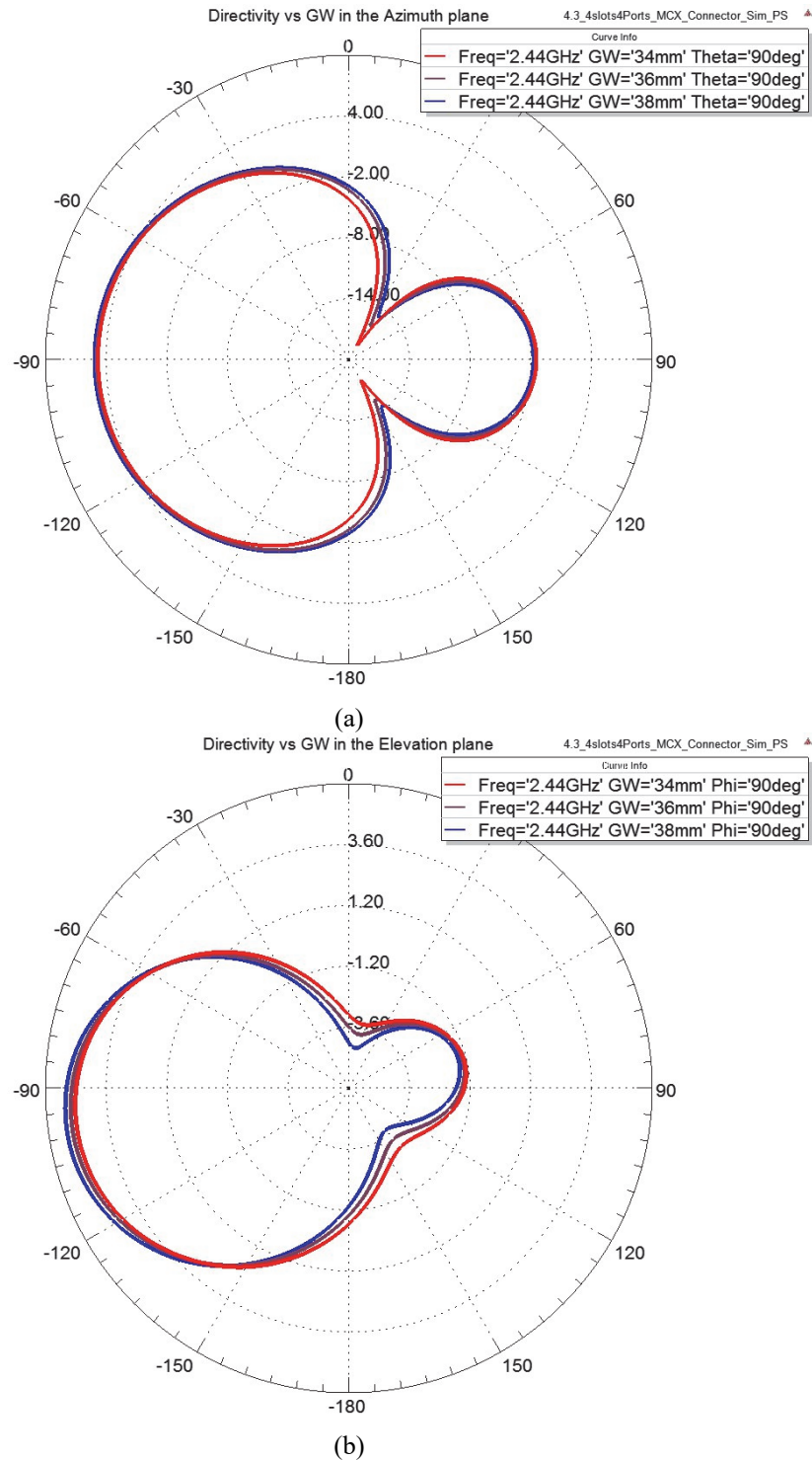


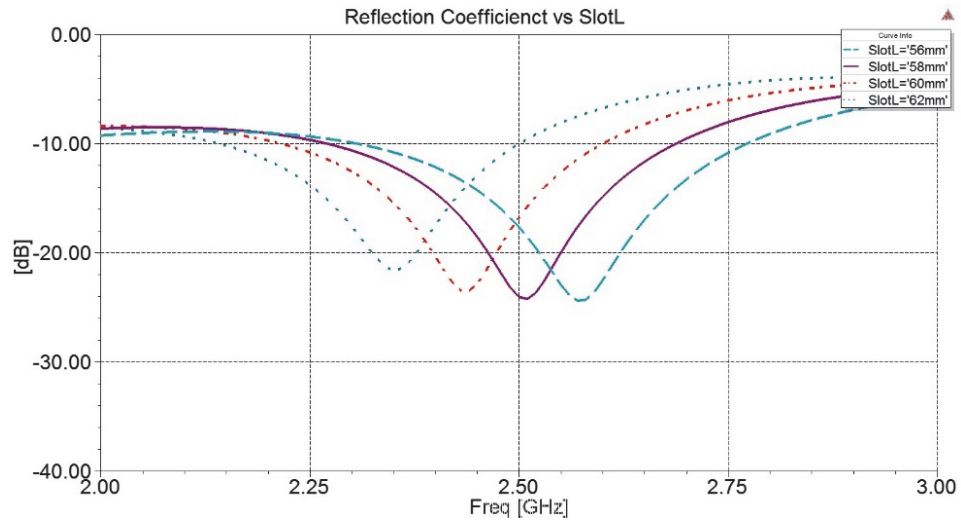
Fig. 5-17 Co pol directivity vs size of cube (GW) at 2.44GHz, a) Azimuth plane, and b) Elevation plane

5.2.3.3 Total length of slot antenna

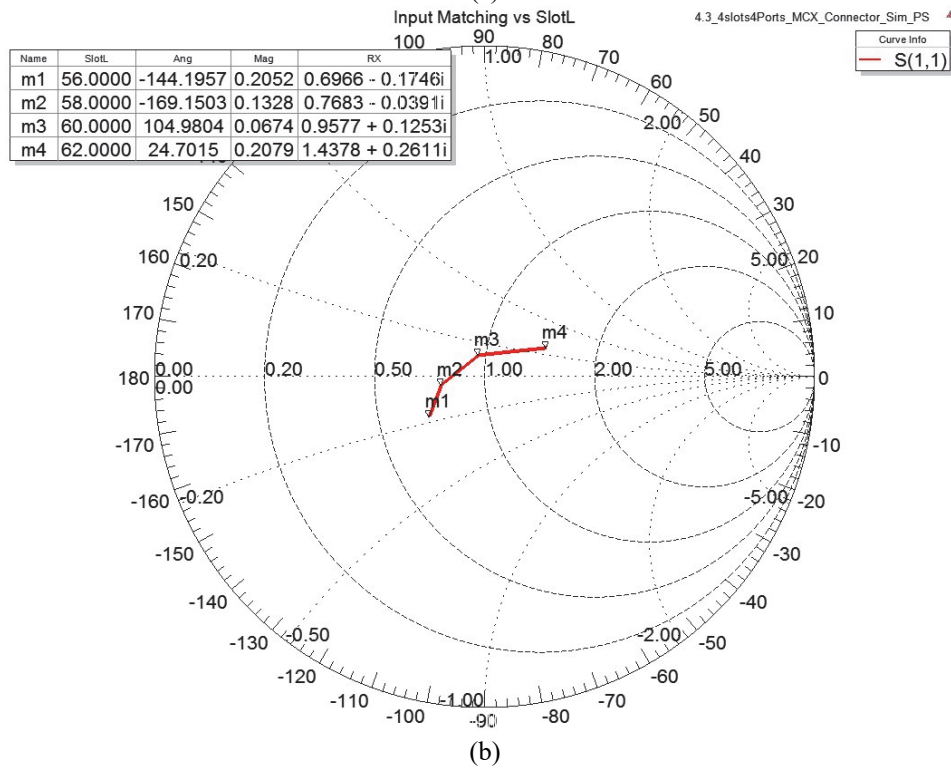
SlotL is another design parameter that its variations are studied in this section. SlotL represents the total length of each slot antenna in our structure and it describes a small

section on the top face of the cube which continues down over the entire length of the vertical wall and then bends on the bottom face of the cube. So essentially it can be decomposed into three parts, one major section of cube edge length long and two small sections truncated on the top and bottom faces. It is clear that SlotL determines is directly affecting the resonance frequency and the input matching of the cube and as verified in Fig. 5-18 the larger the total length of the slot, the higher the resonance frequency.

Fig. 5-19 (a) confirms that the length of the slot does not affect coupling between antennas facing each other on opposite walls, but it noticeably increases the coupling between neighbour antennas due to lack of isolation between parts of the antenna and its side neighbor bended on the top or bottom faces of the cube. Assuming an electric field profile on the slot which is zero at both ends and maximum at the center, the longer the slot, the larger the phase at the location of microstrip feeding because of the increase in distance between microstrip feed and end of the slot. As a result, in both cases the coupling phase increases when slot is getting longer which is verified in Fig. 5-19 (b) with the assumption of negative phases for waves traveling between the slots. Increasing the length of slots lead to decrease in the beamwidth in the azimuth plane partially due to more out-of-phase coupling to neighbour antennas which moderately cancels out side radiations and makes the beam more focused as verified in Fig. 5-20 (a). However, detuning the antenna from its desired resonance frequency can be responsible for variation of directivity in the elevation plane as well which both are intangible, shown in Fig. 5-20 (b). It is worth to mention that it is responsible for a small part of directivity variation in the azimuth plane as well.



(a)



(b)

Fig. 5-18 Input matching vs total length of slot antenna, a) S_{11} , and b) smith chart

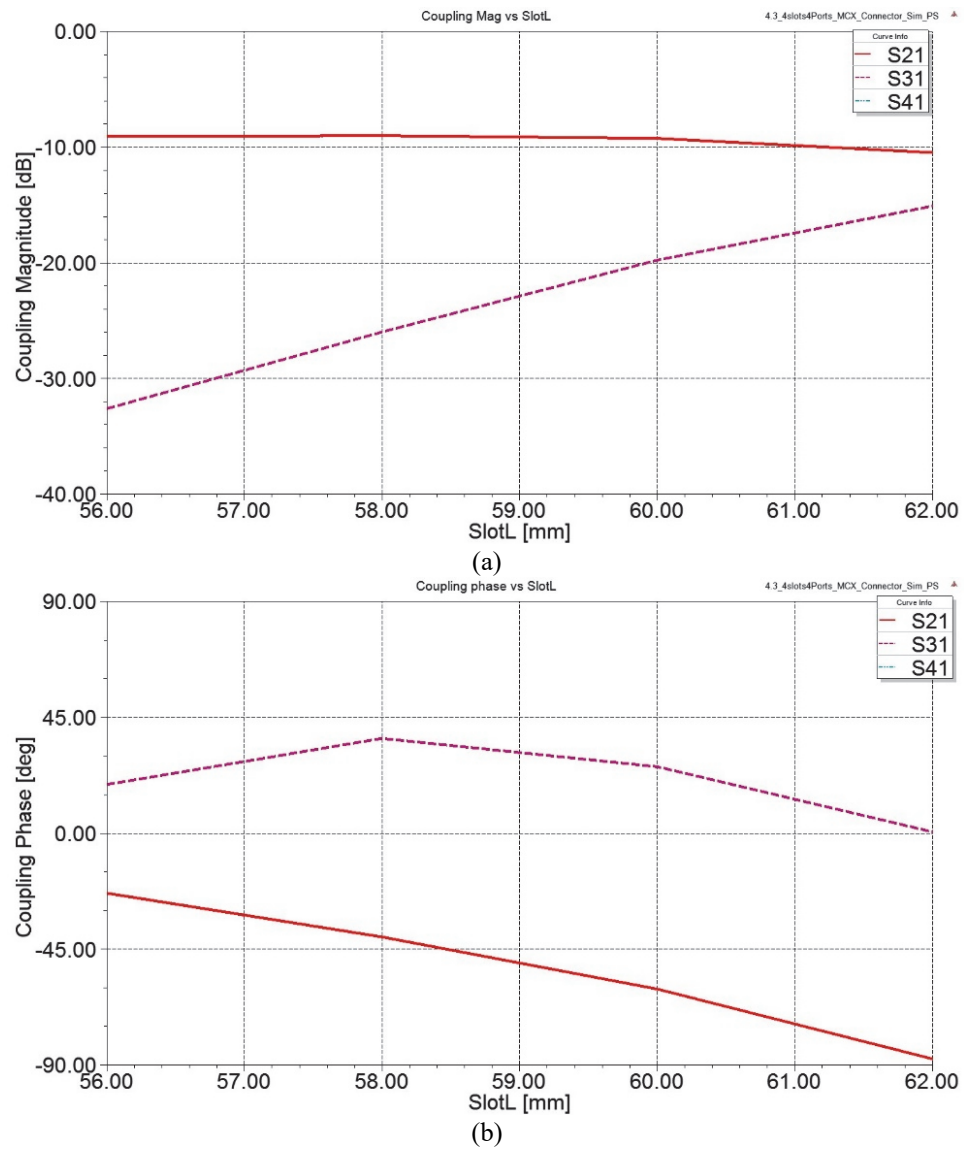
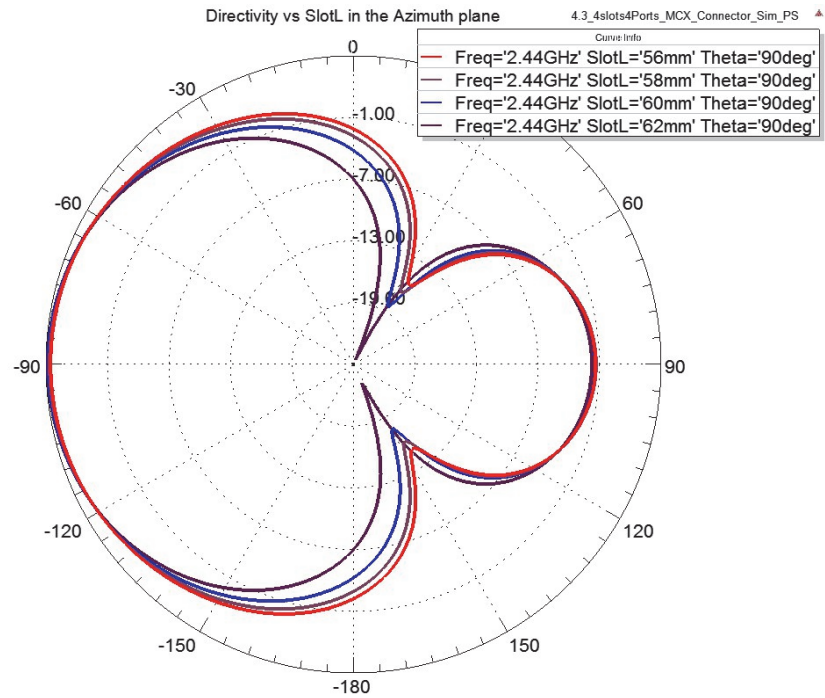
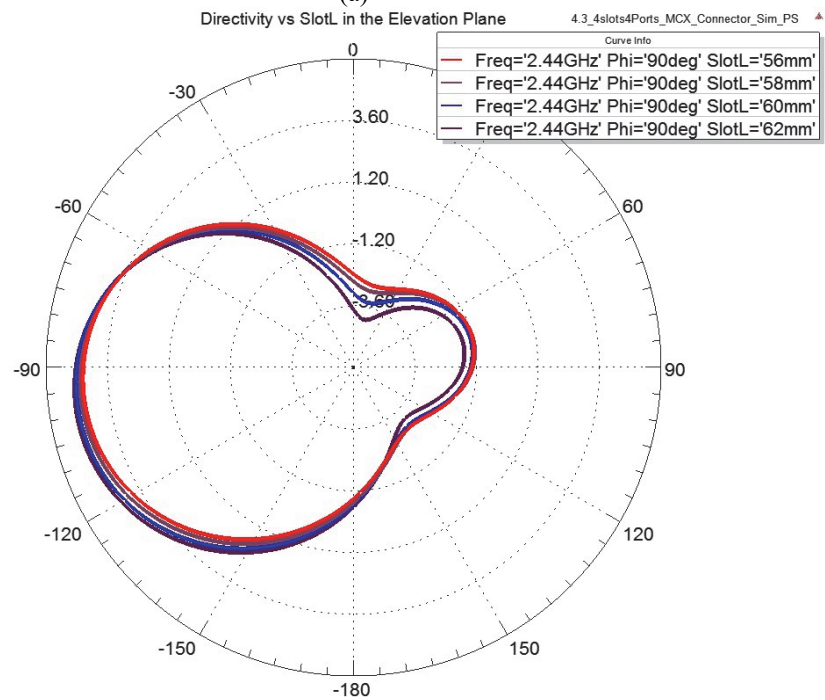


Fig. 5-19 Coupling between antennas vs total length of slot antenna at 2.44GHz, a) Magnitude, and b) phase



(a)



(b)

Fig. 5-20 Co pol directivity vs total length of slot antenna (SlotL) at 2.44GHz, a) Azimuth plane, and b) Elevation plane

5.2.3.4 Length of open circuit stub

Length of open circuit stub is directly related to the antenna matching where the longer the stub, the lower the minimum S11, and the higher the impedance at 2.44GHz, both verified in Fig. 5-21 (a) and (b).

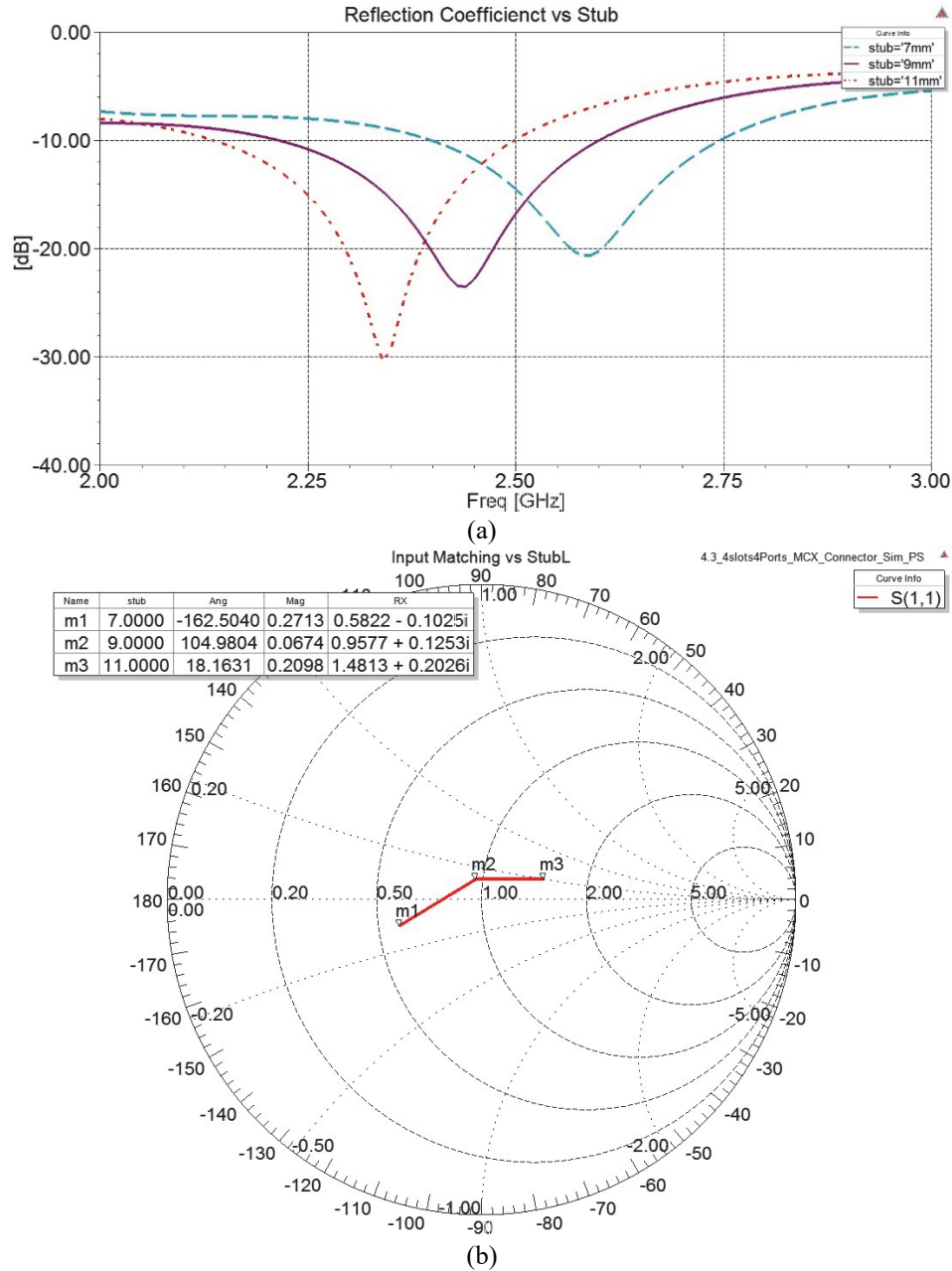


Fig. 5-21 Input matching versus length of open circuit stub

Longer stubs resulted in stronger coupling between neighbour stubs on top face of the cube where it does not affect the coupling between face to face slots. However, we see more phase shift in coupling between face to face slots for long stubs due to the longer distance

between end of stub and slot-stub intersection while it won't follow the same trend for neighbor slots. It is rooted in a different type of coupling to neighbor slots which is between microstrip lines on top. Effect of slot length on magnitude and phase of coupling are confirmed in Fig. 5-22. Based on the same hypothesis in previous section, the shorter the stub, the lower the coupling and wider the beam in the azimuth plane and as expected less directivity in the elevation plane, both illustrated in Fig. 5-23.

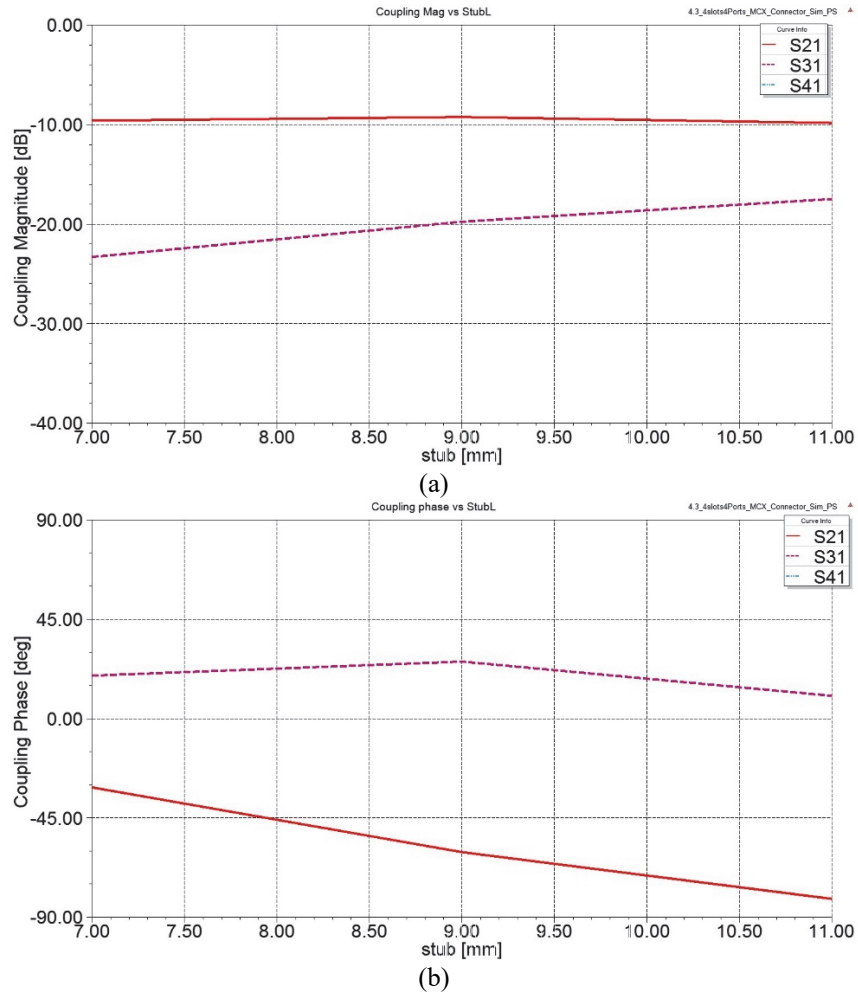
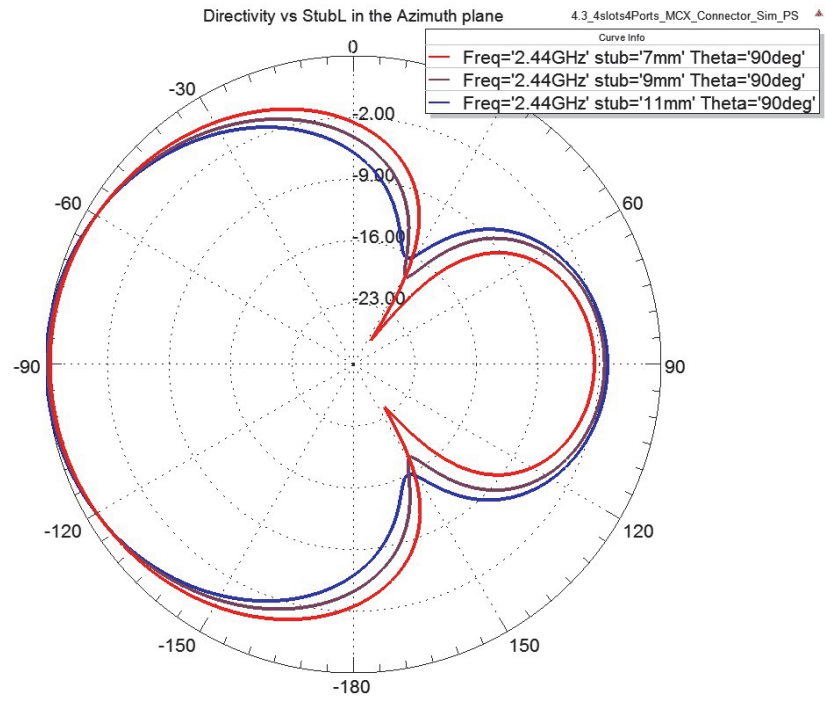
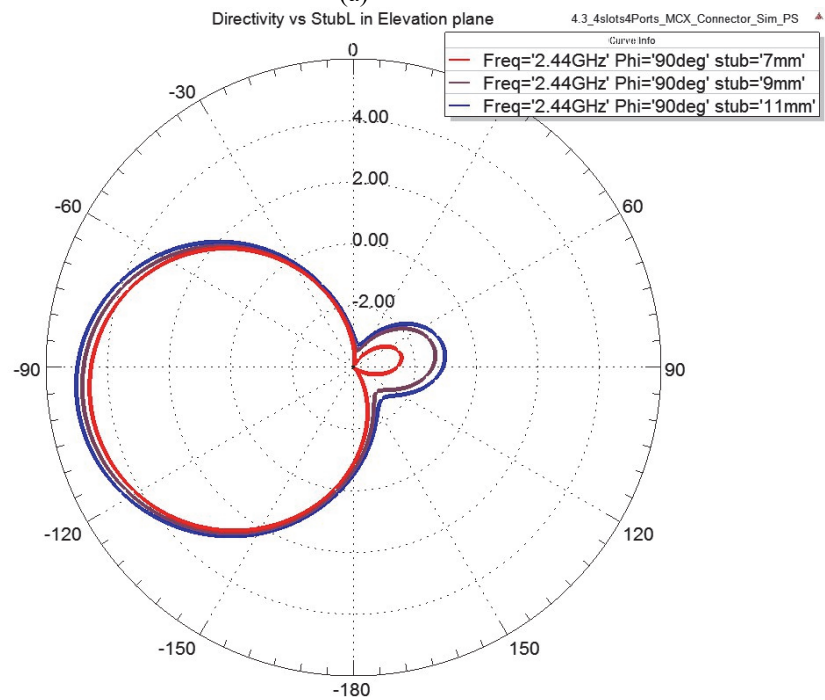


Fig. 5-22 Coupling between antennas vs length of stub at 2.44GHz, a) Magnitude, and b) phase



(a)



(b)

Fig. 5-23 Co pol directivity vs total length of stub (StubL) at 2.44GHz, a) Azimuth plane, and b) Elevation plane

5.3 Reconfigurable Cubic Slot Antenna

In this section, a cubical 3-D folded slot antenna array with reconfigurable radiation patterns is reported which is capable of switching between omnidirectional radiation pattern in the azimuth plane and broadside radiation pattern to the either bottom or top faces of cube. As the internal space of the cube is reserved, it can find its main application in wireless sensor networks where electronic circuits can be installed in the cube to have a small smart package. The architecture is fully 3-D printable to facilitate its fabrication as an industrial product. To verify the design, a cubic prototype at 2.4 GHz with edge length of $39.5 \times 39.25 \times 30 \text{mm}^3$ has been fabricated with Rogers AD300 laminate and gain of 2.85 dBi and 4.2dBi and input matching bandwidth of 21% and 2.7% have been achieved for omnidirectional and broadside radiation patterns, respectively.

In the following sections after a review on antenna geometry, design considerations are elaborated and then the antenna fabrication and comparing measurement and simulation results will be discussed. Finally, discussion of parameter study and structure analysis will be presented.

5.3.1 Antenna Geometry

Here, we propose a cubic antenna with reconfigurable radiation pattern which can switch between directional and omnidirectional radiation patterns. The antenna consists of a set of slots wrapped around a cubic structure performing as radiators or transmission lines based on the antenna mode. Changing status of switches embedded in the antenna body will excite slots at different modes, generating desired radiation pattern.

Here, we refer to Z-axis and XY plane as vertical axis and azimuth plane, respectively. Hence, cube faces normal to +Z and -Z axes considered as the antenna top and bottom faces respectively and faces normal to +X, -X, +Y, and -Y as the antenna side walls or vertical faces. As shown in Fig. 5-24, this antenna is excited in -Y face of the cube through a CPW line for measurement purposes. However, in industrial applications, a different feeding network may be implemented to simplify the interface between antenna body and a potential transceiver installed inside cubic structure for a specific application.

Our proposed reconfigurable antenna works based on switching modes which means antenna can switch between different radiation patterns following the state of RF switches embedded in the antenna body as shown in Fig. 5-25.

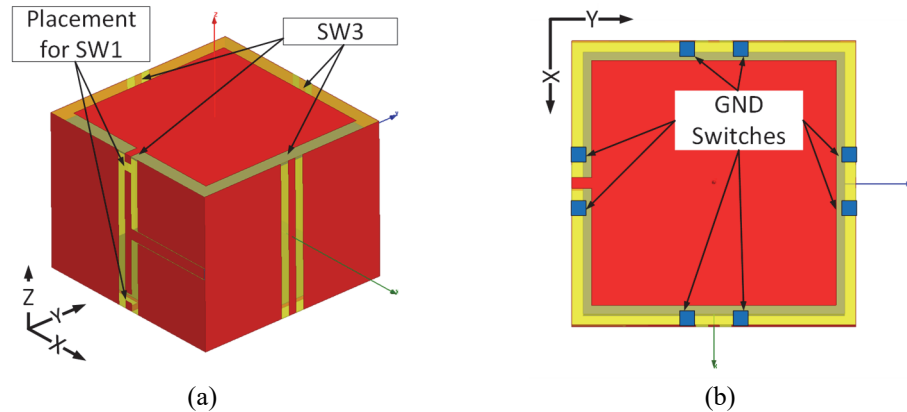


Fig. 5-24 Antenna structure including switches, a) Perspective view, and b) Top view

Designing the antenna such a way to meet the requirements of input reflection loss and antenna radiation pattern at the same time in different switching modes is quite challenging as any part of the circuit is contributing in the radiation pattern in both modes.

In order to assist better understanding of the cube geometry, major sections of the antenna illustrated in Fig. 5-25 are listed and discussed in detail at following.

CPW feed line: The proposed antenna is fed through a single CPW feed line placed on -Y face of the cube.

Slot pairs: There are two parallel vertical slots on all four faces of the cube parallel to Z. Each vertical face can perform as a radiator or transmission line by exciting its slot pair in common or differential mode, respectively. All slot pairs are connected to two square slot rings on top and bottom faces of the cube.

Ring slots surrounding square patches: There are ring slots enclosing square patches on top and bottom faces of the cube. Ring slots are always connected to slot pairs while square patches may be connected to the center signal line of the slot pairs only in second radiating mode.

Ground planes: Both top and bottom faces of the cube have conductive bottom layers performing as ground plane in broadside radiation modes when it is connected to the body of antenna through specific RF switches.

Three different types of switches have been used in our proposed structure as following:

Signal switches: There are two RF switches placed on -Y face of the cube shown as SW1 which can connect/disconnect the center signal line of the slot pairs to the top and bottom patches.

Slot short circuit switches: There are 2 RF switches placed on -Y vertical face of the cube shown as SW2 which can connect/ disconnect the edges of slot pairs.

Ground plane switches: There are 16 (two sets of 8) GND switches shown as SW3 which connect/disconnect patch ground plane of top/bottom faces to the body (side walls) of the cube.

Design parameters assigned to antenna dimensions shown in Fig. 5-25 listed in Table 5-3.

Table 5-3. Definition of Design Parameters in Antenna Structure.

Parameter	Description
SlotW	Total width of vertical slot pair including the center conductor (=CPWW+2×CPWG)
CPWG	Gap width in vertical CPW (Antenna CPW)
CPWW	Line width in vertical CPW (Antenna CPW)
FeedCPWG	Gap width in horizontal CPW (Feed CPW)
FeedCPWW	Line width in horizontal CPW (Feed CPW)
SlotWZ	Width of top square slot
PatchW	Top conductive square
GNDW	Width of patch ground plane
GW	Dimensions of cube's base (X and Y directions)
GWZ	Height of cube (Z direction)
Cube	Dimension of cube
SCZ	Distance between SW1 and center of cube face
ϵ_r	Relative permittivity of substrate
H	Thickness of substrate

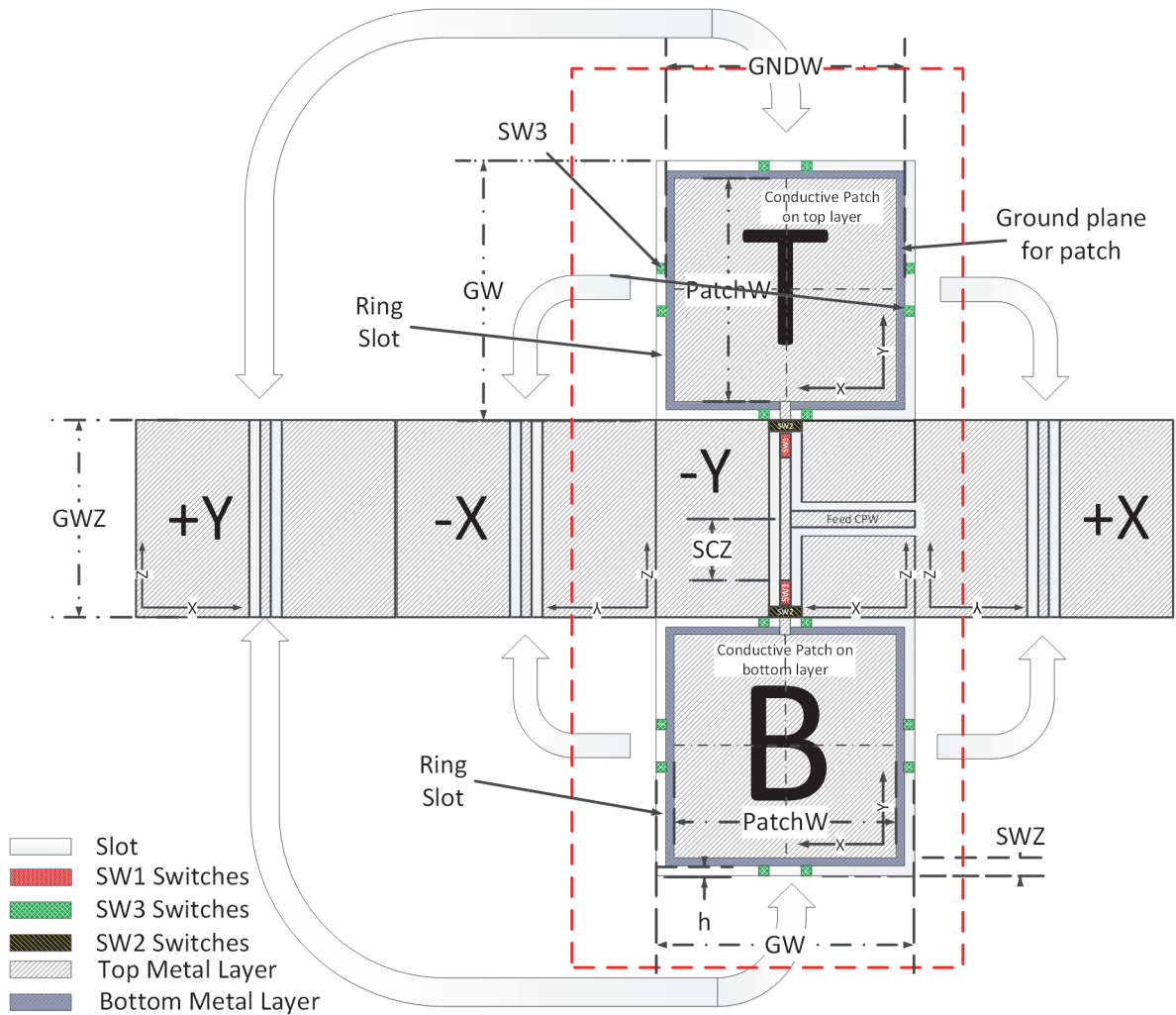


Fig. 5-25 T-shaped flattened view of cubic antenna in slot array mode. Top and bottom faces are designated with T and B respectively. Arrows are for the purpose of illustrating how different faces are folded against the edges to make the final cube antenna. Also, the middle part of the figure is enclosed by a dashed red rectangle to highlight the top and bottom faces connection to the $-Y$ face of the cube where the CPW feeding is accommodated.

5.3.2 Design Considerations

Here, we have used a folded slot antenna array and wrapped it around a cube in order to achieve reconfigurable radiation patterns while maintaining a satisfactory input matching as well. By changing the state of switches, our proposed antenna can switch between the following modes to generate different radiation patterns. Each mode has been designed based on a planar structure then folded on a cube. Below a brief summary of antenna characteristics in each mode is given. A thorough analytical study on antenna performance and feeding can be found in subsections A and B respectively.

Mode 1: Omnidirectional radiation pattern in the azimuth plane:

In this mode, all vertical slot pairs on side walls of the cube parallel to Z axis (normal to -X, +X, -Y, and +Y) are excited in common CPW mode and in-phase so their radiations add constructively in the azimuth plane. This will generate an omnidirectional radiation pattern in the azimuth as desired. Common mode excitation is discussed in the next subsection.

Mode 2: Directional radiation pattern toward top and bottom: As opposed to the omnidirectional pattern in the azimuth, in this mode the antenna can generate interchangeable directional patterns toward either top or bottom (+Z/-Z) planes. For this to happen, the square patch antennas on top and bottom faces of the cube are excited alternatively. This way the radiated beam can be focused toward the desired direction (excited patch) and be completely deviated from the opposite side due to its patch being disconnected from the feedline. To focus the radiation toward one direction and eliminate it in the opposite direction, ground plane switches are connected and disconnected alternatively as well. These aspects are elaborated more in the following.

5.3.2.1 Analytical

a. Mode 1

Mode 1 which is the omnidirectional mode of the reconfigurable antenna has been reviewed in section 3.3.2.1 where we derived (3-20).

In order to produce a horizontally polarized omnidirectional radiation pattern, in-phase phi-polarized electric fields, as shown with red arrows, should be set up in the azimuth plane of the cubic antenna of Fig. 5-26. The magnetic current distribution arising from such electric field, designated by blue arrows, is analogous to the magnetic current flow of rectangular slots placed on all four side walls (vertical faces) of the cube with the length of the slots being parallel to the X-axis. Such current configuration will create maximum electric field in the center of the slots, so as desired, maximum gain is obtained in the azimuth plane. To ensure minimum radiation in unwanted directions, i.e. top and bottom of the cube, the electric field should have nulls on these faces. As evident from Fig. 5-26 (b), the continuation of currents to the top and bottom surfaces of the cube will cause out-of-phase electric fields which conclusively result in cancellation of radiation along

these directions. As shown in Fig. 5-26, such a slot magnetic current/electric field configuration was achieved through wrapping a planar folded slot array around a cube.

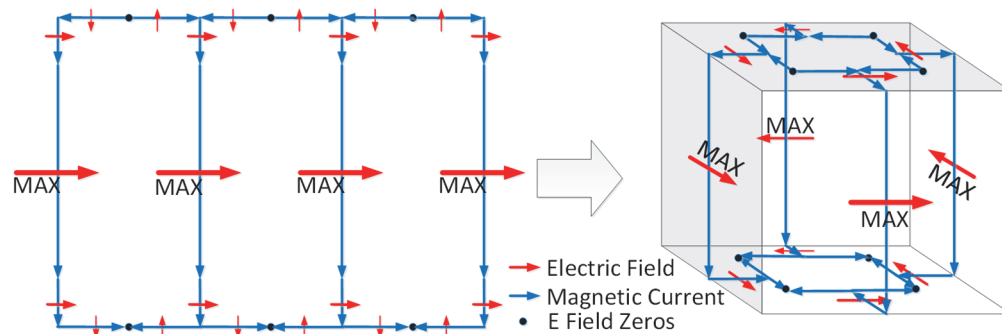


Fig. 5-26 Designing antenna based on nominal magnetic current and electric field distribution.

To realize the above vision, a planar slot antenna array is folded in inward direction following the arrows shown in Fig. 5-25 to wrap a cube. In the following, first the analysis of the planar slot array is presented.

A full-wave simulation of the planar model of folded slot array reveals that when dimensions of slots and the CPW feed line are chosen appropriately, in-phase radiation of antenna elements is possible. Fig. 5-27 shows the in-phase electric field distribution on all vertical slots which leads to constructive radiation and a broadside directive radiation pattern. The standing wave formed on half wavelength slots has a maximum electric field aligned to the CPW line at the center and zero electric field at horizontal top and bottom slots connecting the ends of vertical slots. Fig. 5-27 is essentially the planar (flattened) view of our original 3-D structure already introduced in Fig. 5-24, and it serves to better verify our design methodology using the current distributions.

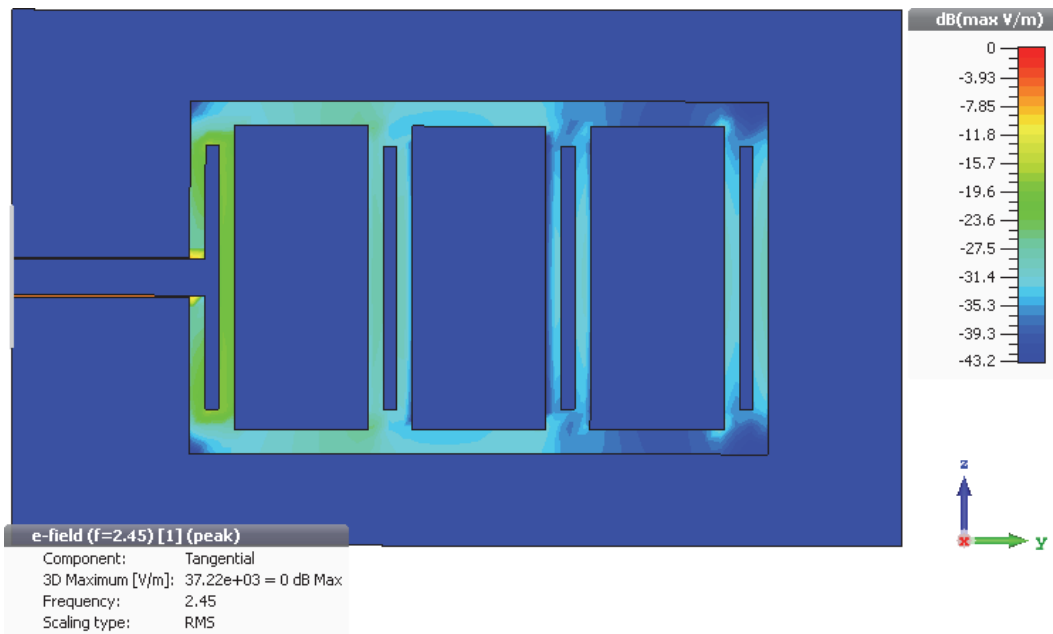


Fig. 5-27 Electric field intensity over 2D folded slots

In the next step, in order to create the 3-D folded slot array, the flatten model of Fig. 5-25 should be wrapped around a cubical structure to provide the omnidirectional pattern in the azimuth. However, given the fact that radiation has to be cancelled on top and bottom faces of the cube, and considering our final goal of reconfigurability, we have chosen two directive radiators on the top and bottom faces of the cube which are kept in non-radiating mode in mode 1 and thus have no contribution in the radiation pattern. In fact, they produce directional patterns for the 2nd mode as will be discussed in the following subsection.

The completed 3-D antenna package is depicted in Fig. 5-24. To ensure in-phase radiation from vertical slots on side walls of the cube, the length of the slots, along with the cube edge lengths have to be tuned and optimized. Having common mode slot pairs instead of single slots helps to balance the radiation pattern in all four slots especially the slot on -Y face which is directly excited through a CPW line. Apart from balancing the radiation of all the faces, the added conductor provides the opportunity to make the cube antenna reconfigurable as will be explained in connection with feeding modes in the next section.

b. Mode 2

To achieve a directive radiation pattern toward top/ bottom, we have modeled these faces as two square patch antennas with very small ground planes extended less than quarter wave length from the edge of the patch and surrounded by vertical conductive walls.

The alternate switching scheme for this mode was briefly explained in the beginning of section III and is elaborated in the next subsection in relation with excitation and feeding of the antenna. It can be seen in Fig. 5-25 that the ground plane of the active patch on top surface is connected to the body of the cube by having the switches on the ON state. This will extend the ground boundary condition to all four surrounding walls which will help to significantly remedy the diffraction effect of finite ground plane and as a result to produce a directional beam pointed toward one direction; top direction in the case of top patch excitation and bottom direction in the case of bottom patch activation. Fig. 5-28 along with Table 5-4, serve to show steps taken to achieve a directive patch-like radiation from a cubic structure. Different models from a simple conventional patch to a more sophisticated configuration of patch and switches on the cubic configuration, are explored in Table 5-4 and their radiation characteristics are compared in Fig. 5-28.

For conventional patches, it is obvious from Fig. 5-28 that both the front to back ratio and gain are increased from model 1 to model 3. The substantial increase in the density of surface currents on the outer boundary of truncated ground plane in model 1 is responsible for low gain and rather poor front to back ratio as already proved with experimental [73] and numerical studies [74] and [75], whereas in model 2 and model 3, the extension of substrate beyond the ground plane helps to attenuate undesired surface currents to a high degree which will result in higher gain and better front to back ratio.

As we move on to building our cubic structure, model 3 is evolved to model 4 where cube surrounding walls are now covered with conductive surface (See Table 5-4). The appearance of metallic walls helps to boost front to back ratio owing to cancellation of spurious radiations in the back-lobe regions however gain drops due to increase in the level of cross polarized component as can be seen in Fig. 5-28.

Lastly our cubic antenna in mode 2, designated as baseline along with model 6 (for the case of bottom patch being excited) are compared with models 1 to 3. It is seen how the values of front to back ratio in conventional patches of first three models in Fig. 5-28, are noticeably below those of baseline and model 6 which proves that the effect of diffraction from the edges of a finite ground plane is more pronounced in the back lobe region as already stated in [67]. However, such dramatic effects have been neutralized to a very good degree in our proposed antenna due to the presence of vertical cube walls and the fact that the bottom patch is disconnected and inactive in this mode. This proves how the alternate switching scheme for top and bottom patches serves to produce another key feature in our cubic antenna; the bottom patch could be perceived as a parasitic element which is not radiating by itself but its presence helps reduce the diffraction effects and hence lower the intensity of back lobe radiation. The positive effect of parasitic elements on improving pattern is also observed in similar studies on reconfigurable antennas as discussed in [76].

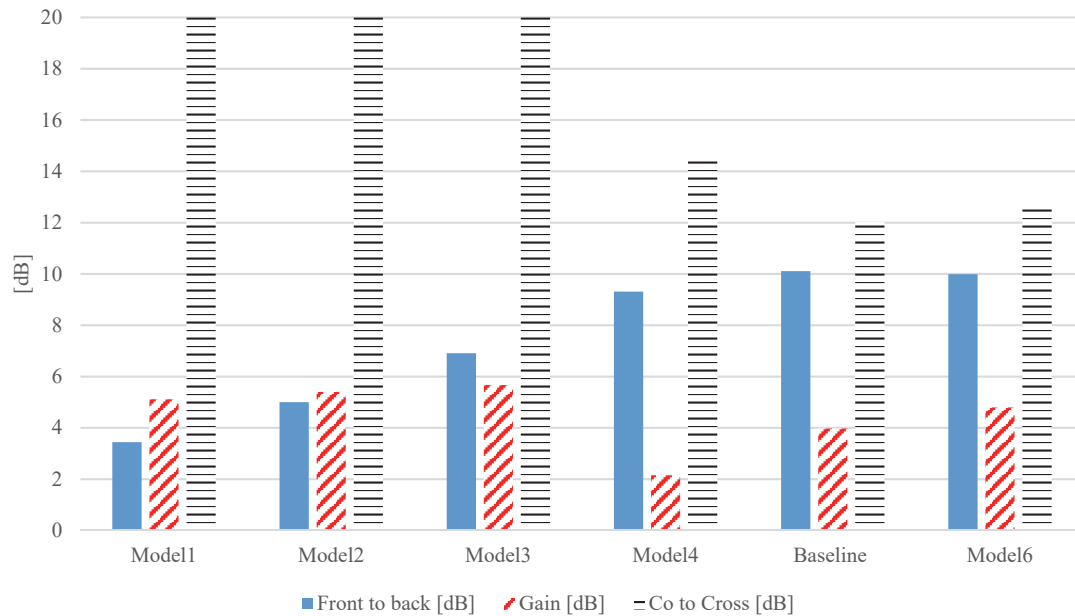
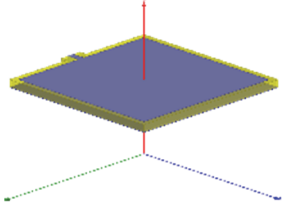
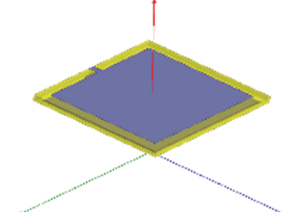
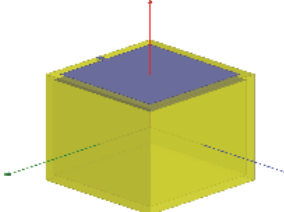
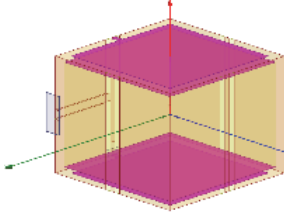
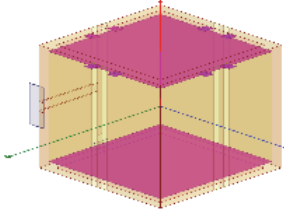
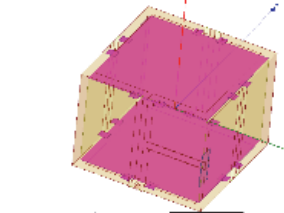


Fig. 5-28 Different deviation from baseline cubic antenna

Table 5-4. description for Different deviation from baseline cubic antenna Fig. 5-28

	Description	Structure picture
Model1	Top patch with finite ground plane and substrate	
Model2	Top patch with finite ground plane and extended substrate	
Model3	Top patch with finite ground plane on a cubic substrate	
Model4	Cubic antenna in Mode 2 without ground plane switches	
Baseline	Cubic antenna in Mode 2	
Model6	Cubic antenna in Mode 2 with identical ground plane switches for the patch on the opposite side	

In our proposed model deactivation of parasitic (bottom) patch is done through a switch which can disconnect it from the surrounding vertical walls (extended ground plane in this mode) to guarantee that the patch performs as a director (as opposed to reflector when it is connected to the ground plane), which eventually helps the top patch antenna to radiate a more directional beam by suppressing undesired back lobes. The distance between active patch (radiator in this mode) and the parasitic patch is determined by the cube height which has a significant effect on antenna performance as elaborated in parametric studies of section 05.3.2.4.

In order to verify that the inner volume of the cube can be reserved for placement of electronic circuits, we need to ensure that the internal electric field is negligible within proper distance from cube walls. This has been verified using full wave simulations and the results are illustrated in Fig. 5-29 for three z-constant planes where all guarantee very low electric field at the center of the cube. Fig. 5-30 shows normalized electric field inside the cube at different x and y locations varying versus altitude in z direction. It confirms that within a 12mm×12mm×12mm cubic area at the center of the cube, electric field intensity is attenuated to -25dB lower than its maximum.

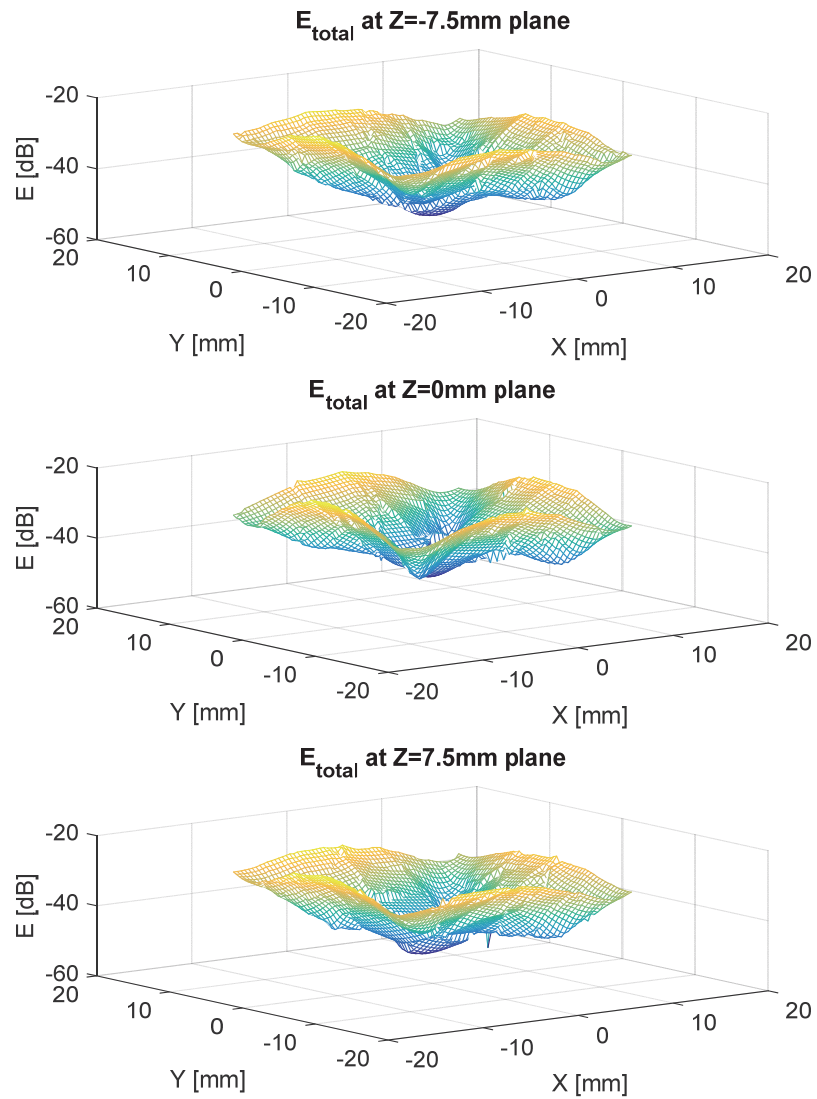


Fig. 5-29 Total normalized electric field at 2.44GHz at different Z planes inside cube

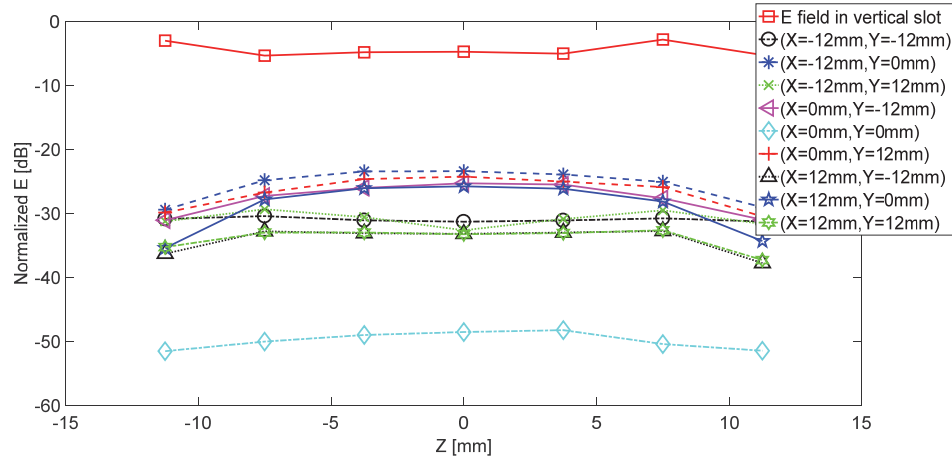


Fig. 5-30 Total normalized electric field at 2.44GHz at different XY locations inside cube

5.3.2.2 Excitation and Feeding structure

In order to simplify the fabrication and offer high performance at potential high frequency applications, the antenna is excited through a CPW line placed on $-Y$ face of the cube. The vertical slot pair placed on this face switches between common mode (radiating slot mode) and differential mode (CPW transmission line mode), to respectively achieve omnidirectional azimuth pattern in mode 1 and directional pattern towards top/bottom faces in mode 2, needless to say the feeding line should be matched at both cases. In the following, first our choice of the CPW line for feeding purposes is justified.

Designing the feeding structure of slot antennas is challenging and sometimes needs complicated microstrip structures. Coplanar waveguide is one of the most common transmission lines in various systems as it only needs one conductive layer and its characteristic impedance is not closely dependent to substrate thickness while its line width and gap can be adjusted accordingly to achieve a desired impedance at any scale. Additionally, it has better overall performance especially at high frequency applications provided that the gap size is optimized. Another reason for the CPW line being the favorable feeding choice, is the simplicity and adaptability it provides especially for conformal structures. However, since a slot antenna exhibits a very high impedance at the center, the feeding becomes slightly challenging.

Based on Babinet principle, the impedance of a half wavelength slot antenna would be around 500Ω at center [72]. Folding the slot to an array is one of the most promising

solutions to lower its impedance at the feeding point down to $\frac{Z_{Slot}}{n^2}$ where n is the number of slots [38].

According to Fig. 5-26, electric field maxima happen at the center of each slot. The antenna is fed at one of these maxima locations on -Y face of the cube through the CPW line. The slot on this face is called the feeding slot. Similar to planar folded slot arrays, proposed 3-D folded slot array antenna offers lower impedance at the feeding point comparing to a half wavelength slot which facilitates its matching. Electric fields shown by red arrows in Fig. 5-31 (a) illustrate how vertical slot pair is excited at even mode (common mode) through a horizontal CPW line in differential or transmission mode. The differential mode of the horizontal CPW line leads to negligible radiation as opposed to considerable radiation from common or radiating mode vertical slot pair because of in-phase electric fields generated across its gaps. The width of conductor and gaps have been optimized and tuned for an omnidirectional radiation pattern in the azimuth plane. Transition from the feeding CPW line transverse to the radiating slot needs proper design, tuning and optimization as well.

As opposed to common mode excitation in mode 1, the vertical slot pair in -Y face of the cube is now excited in differential mode similar to a high impedance CPW. The electric field directions along the slots are illustrated in Fig. 5-31 (b). In this configuration half of the differential mode vertical slot pair performs like a transmission line between input 50Ω CPW and active top/bottom antenna while the rest of slot pairs shown as *SCZ* performs as an open circuit stub to match 50Ω input CPW feed line to high impedance differentially-excited slot pair on -Y face. As the patch is fed through a high impedance line, an inset feeding for patch is not required. Patch ground plane is connected to the body of the cube using SW3 switches sharing one control voltage.

For the arrangement shown in Fig. 5-25, the top antenna is getting excited while the bottom patch is disconnected from the feedline. Hence radiation is focused on top and is cancelled toward the bottom. Our proposed configuration can alternatively excite the two patches placed at both ends of the slot pair by the aid of changing the state of switches.

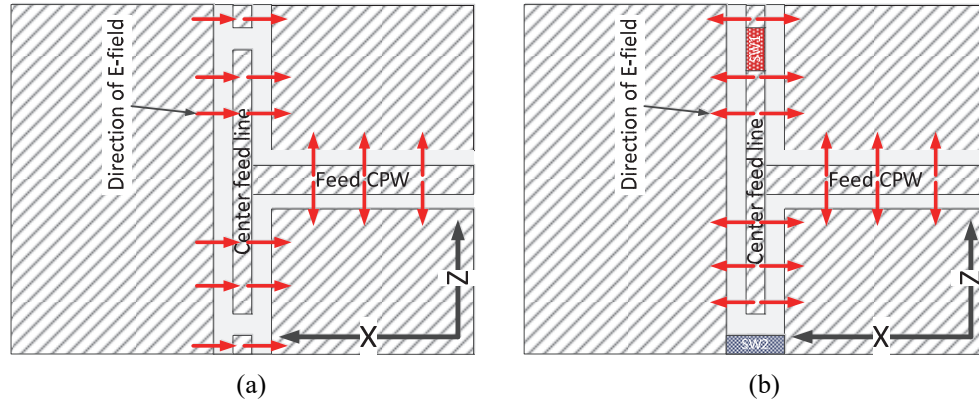


Fig. 5-31 Antenna excitation modes using CPW transmission line, (a) common mode slot pair, and (b) differential mode slot pair.

5.3.2.3 Reconfigurable antenna performance

Our proposed structure is 3-D printable and can easily be mass produced at low costs using 3-D printers. However, here we have fabricated the antenna from six PCBs where each one serves as one face of the cube as shown in Fig. 5-32. Because most of 3-D printer materials have relative permittivity of around 3, we have designed our prototype considering a relative permittivity of 3 for substrate and used AD300 in our prototyping. The cubical design was converted to an open planar design which could be routed and etched by PCB fabricators using lithography or milling machines and assembled and attached to each other to form a cube as shown in Fig. 5-33. We have used copper tape in the edges of the cube to connect the joints. Dimensions of structure made of AD300 are shown in Table 5-2.

Here, we present simulation results for both reconfigurable modes and compare them against measurement results in the following subsection.

Table 5-5. Dimensions of Antenna Structure

Parameter	Dimension	Description
SlotW	5mm	Slot width
CPWG	1.75mm	Gap width
CPWW	1.5mm	Edge to edge distance between slot pairs
FeedCPWG	0.2mm	Gap in feeding CPW
FeedCPWW	2mm	Center line width in feeding CPW line
SlotWZ	2.75mm	Width of slot on top/bottom faces of cube
PatchW	34mm×34mm	Width of patch of top/bottom faces
GNDW	36.5mm	Width of patch ground plane
GW	39.5mm	Length and width of cube
GWZ	30mm	Height of cube
Cube volume	39.5×39.5×30 mm ³	
SCZ	13.5mm	Length of open circuit stub
ϵ_r	2.97	Relative permittivity of substrate
H	1.55mm	Thickness of substrate

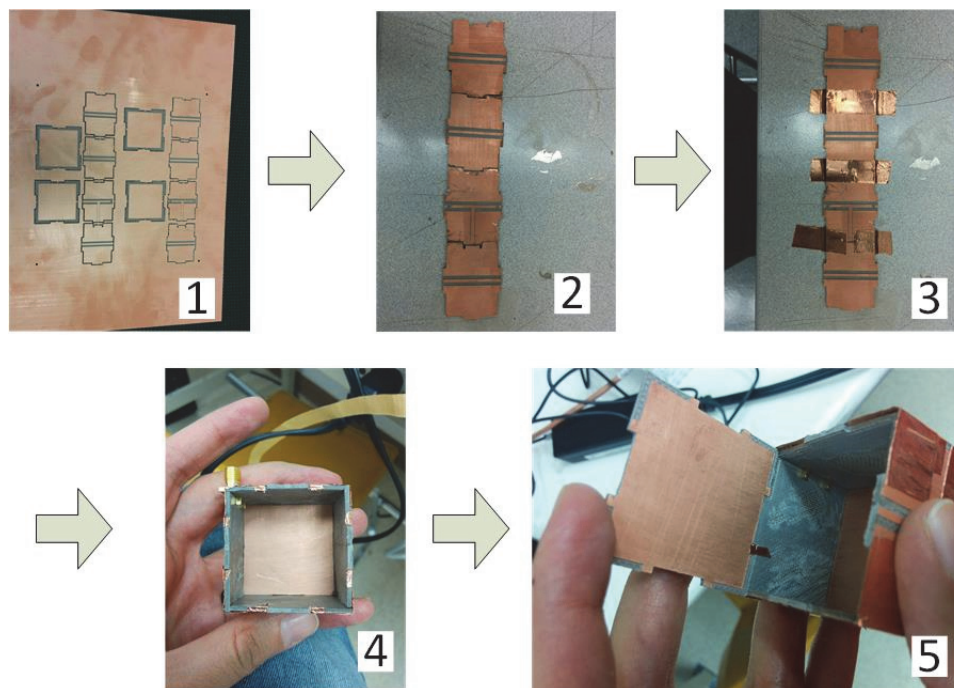


Fig. 5-32 Fabrication process

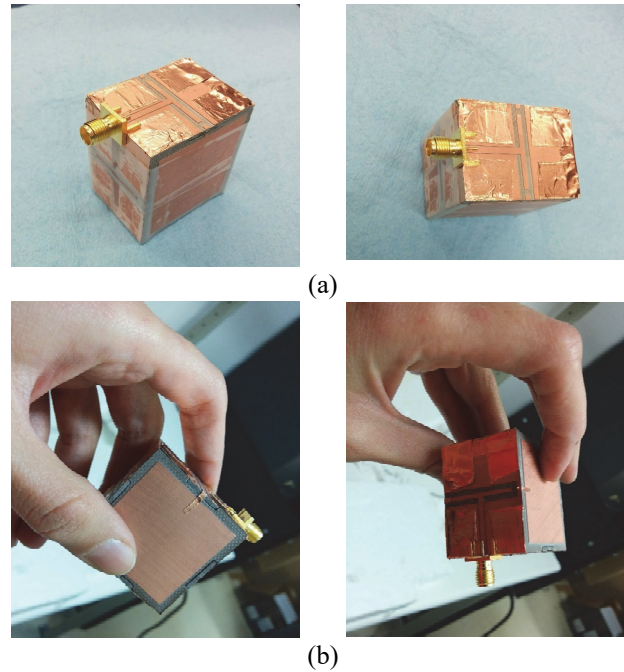


Fig. 5-33 Fabricated antenna (a) mode 1, (b) mode 2

a. Input matching

In Fig. 5-34, input matching of antenna in mode 1 and mode 2 obtained from simulation is compared to the measurement results. As can be seen in both cases the results meet the requirements and antenna offers appropriate matching in 2.4GHz ISM band and 504MHz and 65MHz bandwidth in mode 1 and mode 2, respectively. Slight discrepancy between simulation and measurement roots in manual fabrication of antenna and presence of a high profile SMA connector on cube body.

b. Radiation pattern

Antenna realized gain plots at 2.44GHz are illustrated in Fig. 5-35 (a) and (b) for mode 1 and 2, respectively, which show good agreement between simulation and measurement. However, due to noticeable size of SMA connector on antenna body and some undesired interaction with measurement setup, (e.g. blockage effect caused by cables and metallic parts of the mast) the measured antenna radiation pattern is slightly deviated from the simulation results.

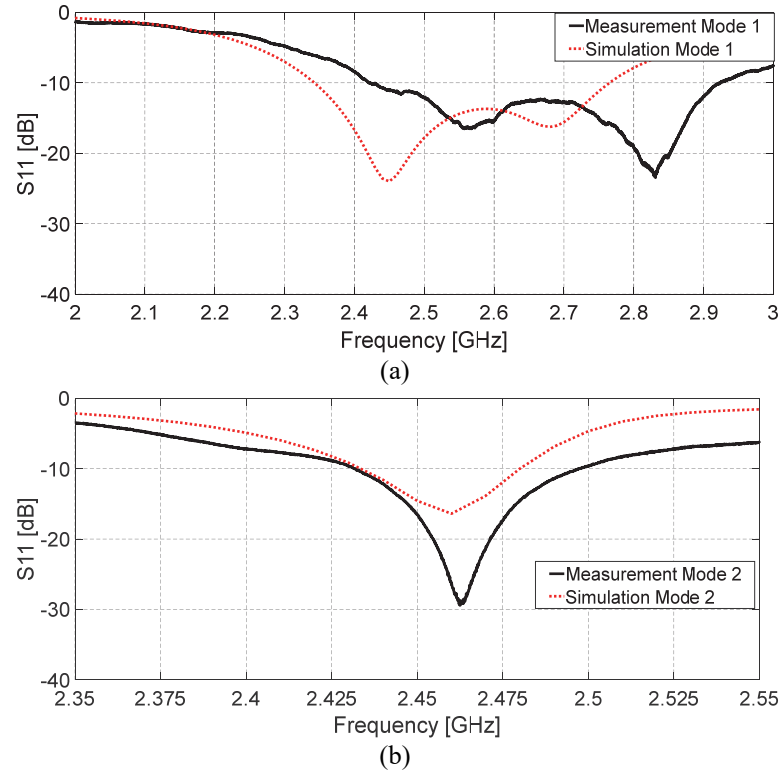


Fig. 5-34 Input reflection coefficient, (a) mode1, (b) mode 2

Using a standard horn to calibrate the anechoic chamber, maximum measured realized gain of 2.85dBi and 4.2dBi was achieved for mode 1 and mode 2, respectively. This agrees well with our design goal of having a low gain omnidirectional pattern in the azimuth plane in mode 1 and a more directive broadside beam in mode2.

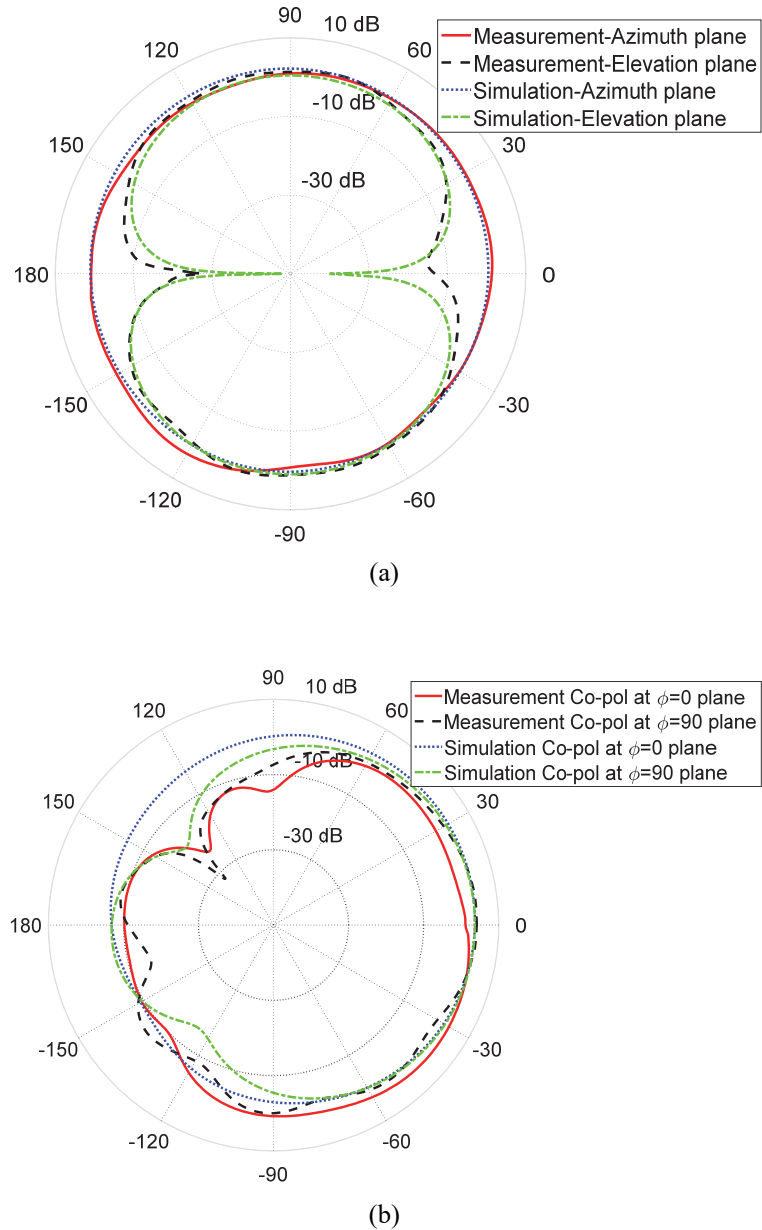


Fig. 5-35. Realized gain from Simulation vs measurement at 2.44GHz, a) mode 1, and b) mode2

c. Current Distribution

Mode 1

In the proposed structure, current distribution is altered depending on the functioning mode of the reconfigurable cube. For omnidirectional mode in the azimuth plane, current distribution on excited face of the cube can be found in Fig. 5-36 and dominant horizontal current flow toward left proves a constructive radiation and horizontal (φ polarized) electric field from excited face of the cube. Also, illustrated in Fig. 5-36,

radiation from differential current flow of horizontal CPW feed line is canceled out and does not contribute in the far field radiation pattern. The current distribution over the surface of the cube is shown in Fig. 5-37. It is clear that the current flowing transverse to the slot and rounding over the cube in φ direction generates φ polarized far-field radiation pattern.

The magnetic current over the slots illustrated in Fig. 5-38 confirms that the maximum and minimum magnetic current locations are set at the center of the slots and the corner of the top square, respectively. These results are in good agreement with theory of slot radiation and also validate the analytical approach taken in the first stage of the design as previously illustrated in Fig. 5-26.

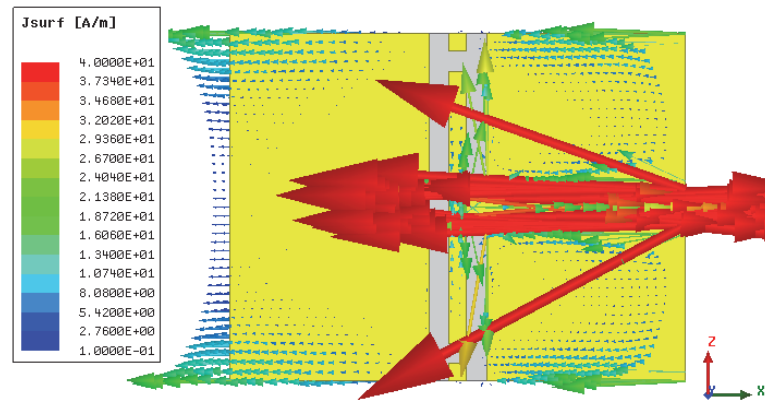


Fig. 5-36. Current distribution on the excited face of the cube

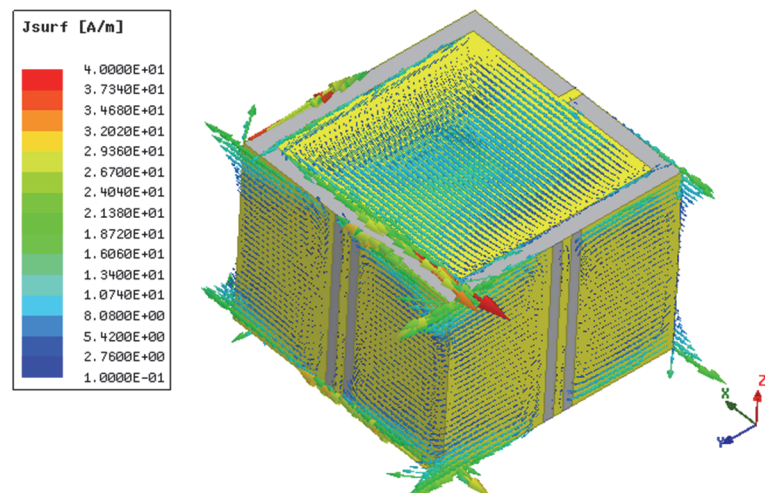


Fig. 5-37. Surface current distribution over conductive parts of the cube at 2.44GHz

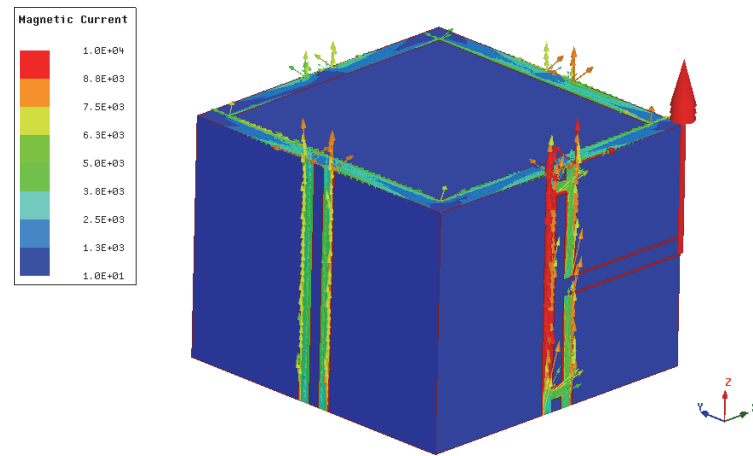


Fig. 5-38. Magnetic current distribution over slots at 2.44GHz

Mode 2

Switching to directional mode, square patches would be the main contributor in the radiation pattern while the density of current is very low on the cube side walls comparing to top/bottom faces as shown in Fig. 5-39 and Fig. 5-40.

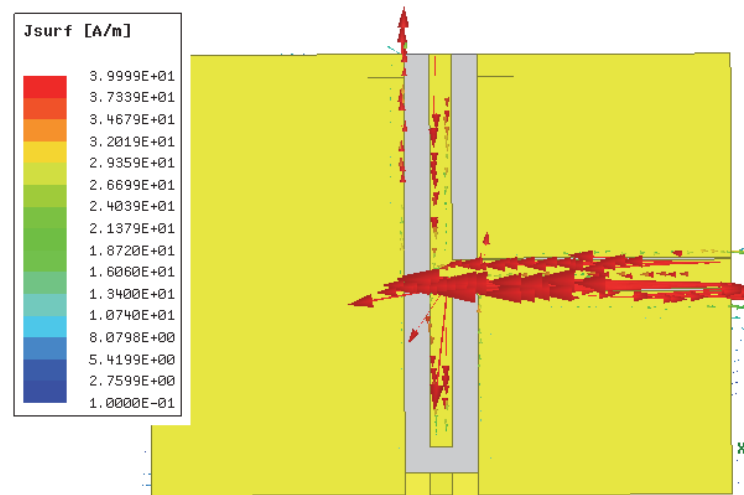


Fig. 5-39. Current distribution on -Y face in patch mode at 2.44GHz

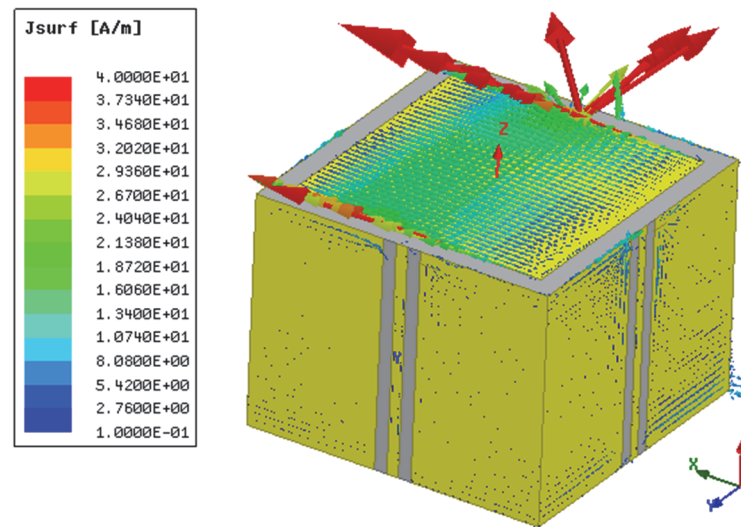


Fig. 5-40. Current distribution on cube antenna in patch at 2.44GHz

5.3.2.4 Parameter Study

In this section, we study the variation of some key geometrical parameters. It is worth to mention that such a complex structure cannot be only designed by optimizing the key parameters and the objective of this section is to and illustrate how strongly they would affect antenna performance. In order to gain some insights into the basics of input matching for our cubic structure, using the analytical equations in [9], we have plotted characteristic impedance and guided wavelength of a single slot as shown in Fig. 5-40. It is obvious that for a wider slot due to increase of its characteristic impedance, a more aggressive change in antenna matching will be expected. This graph will be used in later subsections to explain some antenna radiation characteristics as the slot width changes. Slots used in our antenna structure can be categorized into two groups; slots on top/bottom faces of the cube which have strong influence on antenna pattern in mode 2 with no tangible effect on mode 1 and slots on vertical side walls which hardly affect mode 2 but have noticeable effect on the pattern in mode 1.

In the following subsections, using full wave simulations in HFSS, we have studied geometrical variations in both antenna modes.

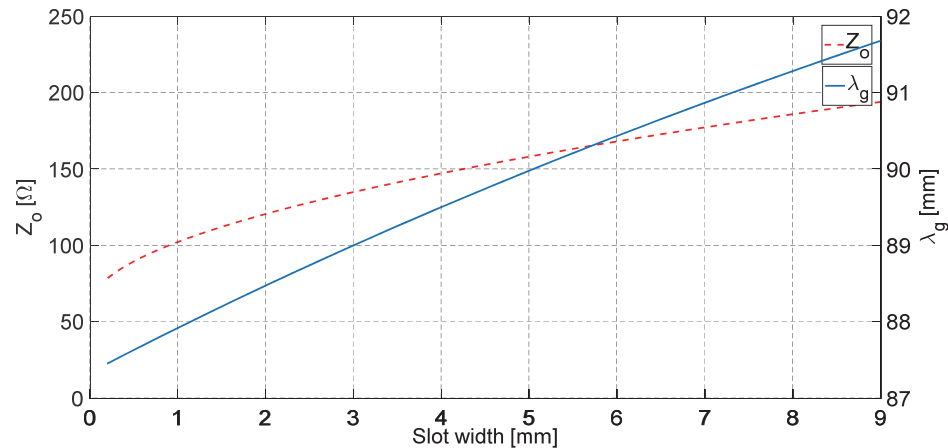


Fig. 5-41 Characteristic impedance and guided wavelength in a microstrip slot vs. slot width for relative permittivity of 3 and substrate thickness of 1.55mm

a. Mode 1

Width of slot on side faces

Here, variation of width of the slot(s) on side walls of the cube has been studied. For the purpose of keeping the same resonance frequency, cube size has not been changed as it determines the resonance in mode 1. Fig. 5-42 represents change of omnidirectional pattern and input matching as the slot width on side walls vary within a 20% range. It can be seen from Fig. 5-42(a) that the original slot width of 5mm yields an omnidirectional pattern. Fig. 5-42(b) verifies the antenna in mode 1 resonates at 2.44GHz and its 10dB input matching bandwidth is wide enough to cover the entire 2.4GHz ISM band. Deviation of slot width from the optimal value of 5 mm, deteriorates the omnidirectional pattern since it disturbs the current distribution on the cube and moves the peaks and nulls of electric field from their ideal locations (as previously shown in Fig. 5-37). It also negatively impacts the input impedance as is clear from Fig. 5-42(b). Since in mode 1, vertical slots placed on side walls are excited in common mode, their behavior can be explained using the equivalent single slot model. According to Fig. 5-41, a slight change of slot width can drastically alter the characteristic impedance which will translate to change of input matching condition.

Another important fact to notice from Fig. 5-42(a) is that although variation of slot width disturbed the optimal impedance match condition at the desired frequency of 2.44 GHz, the bandwidth is still wide enough to cover almost the entire 2.4GHz ISM band when

the slot width changes within 10% of the optimal value. This confirms that when the bandwidth is concerned, the proposed design has the advantage of not being too sensitive to the width of the slots which is beneficial from the point of view of fabrication tolerances.

Variation of width of the slot(s) on top/bottom faces of the cube has been studied while maintaining the same resonant frequency by keeping cube size constant which determines the resonance in mode 1. We have observed that the design is not sensitive to the width of slot on top and bottom faces of cube and it has minor effect on omnidirectional radiation pattern in the azimuth plane in mode 1.

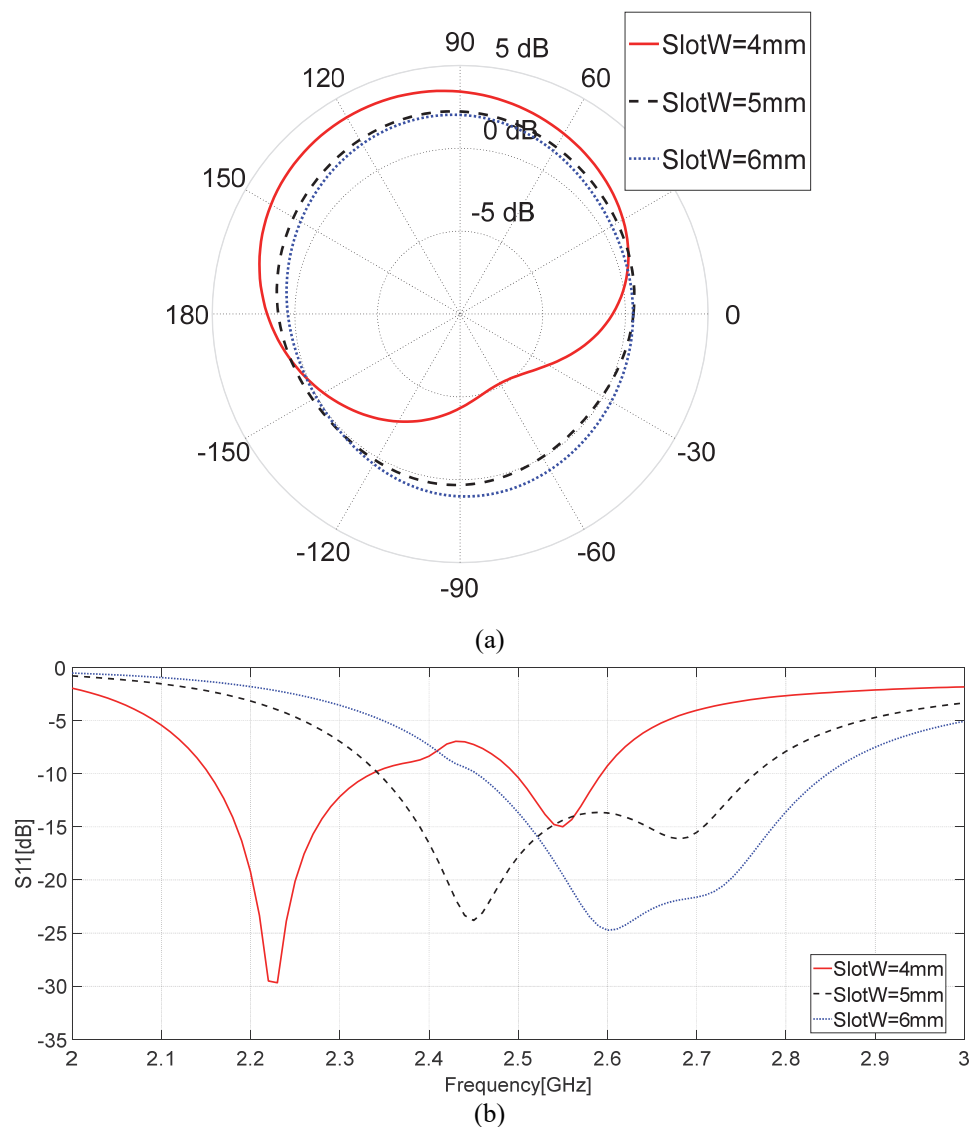


Fig. 5-42 Model parameter study for width of slot, (a) Co pol directivity at 2.44GHz in the azimuth plane $\theta = 90$, and (b) S_{11}

Cube size

In mode 1 cube size determines the slot length and as a result the antenna resonant frequency. Our proposed structure has the same length in X and Y directions, indicated by the GW parameter, while its height along Z, designated by GWZ is smaller. The parameter GW is swept within a 50% range and its effect on directivity, and input matching has been investigated in Fig. 5-43 (a) and (b), respectively. As can be seen from Fig. 5-43 it changes the resonance condition and as a result affects the omnidirectional pattern.

The parameter GWZ is swept within almost 30% of its optimal value and its effect on input matching is illustrated in Fig. 5-44 where it is observed how resonance frequency changes as the cube height varies. It can be seen that for lower values of GWZ the value of front to back ratio is small (close to 0dB) which indicates a purely omnidirectional pattern.

As the cube height increases, since it disturbs the in-phase radiation condition for the slots on vertical walls, the level of front to back ratio enhances due to more deviation from the omnidirectional radiation. Fig. 5-45 also shows for higher values of the cube height, we achieve more directivity and narrower beam area. This higher directivity can be attributed to two main reasons. First, the higher values of GWZ , translates to an increase of the length of vertical slots and eventually the aperture size. Second, the undesirable increase in the level of front to back ratio for large values of the cube height and deviation from the omnidirectional pattern which means having more radiation in one direction.

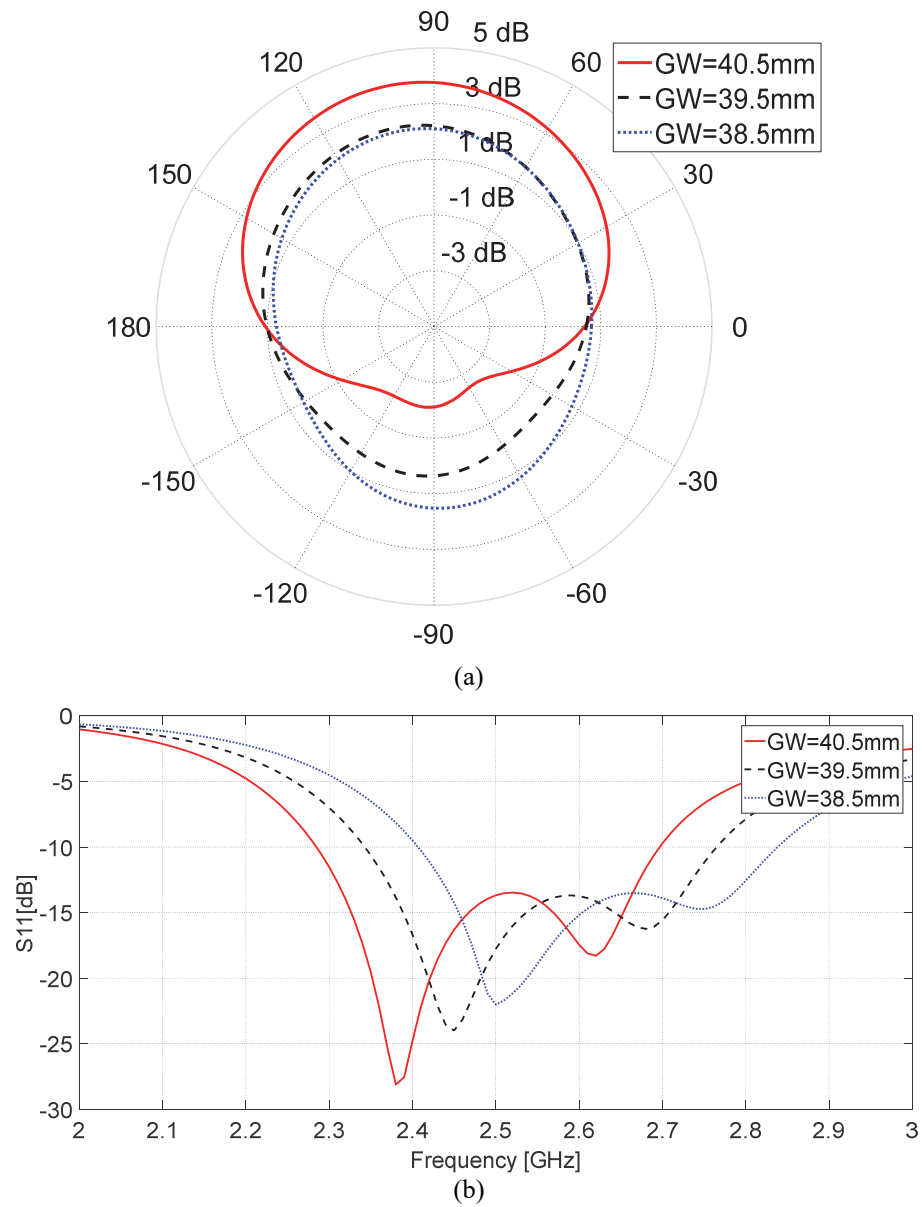


Fig. 5-43 Mode 1 Parameter study on cube size (GW), (a) Co-pol directivity at 2.44GHz in the azimuth plane $\theta=90$, and (b) S_{11}

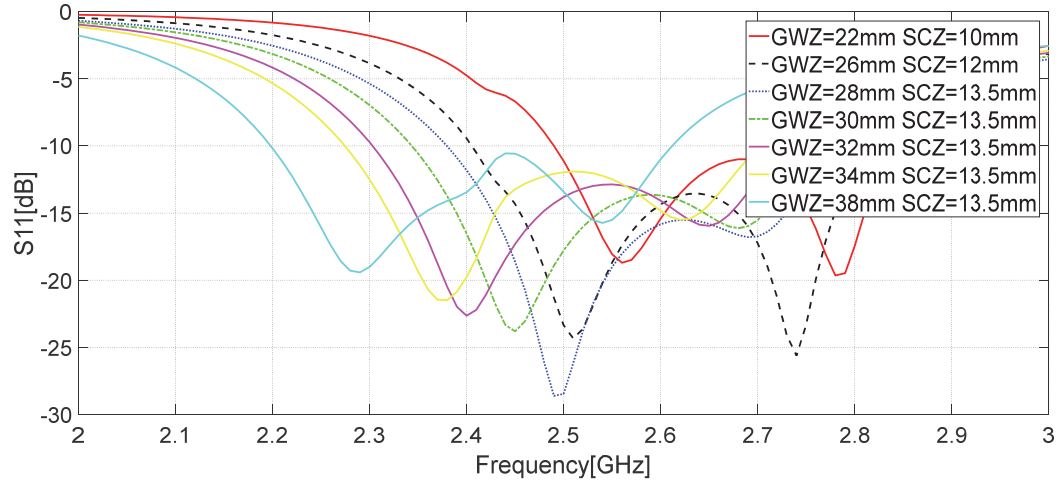


Fig. 5-44 Input reflection coefficient variation versus cube height in mode 1

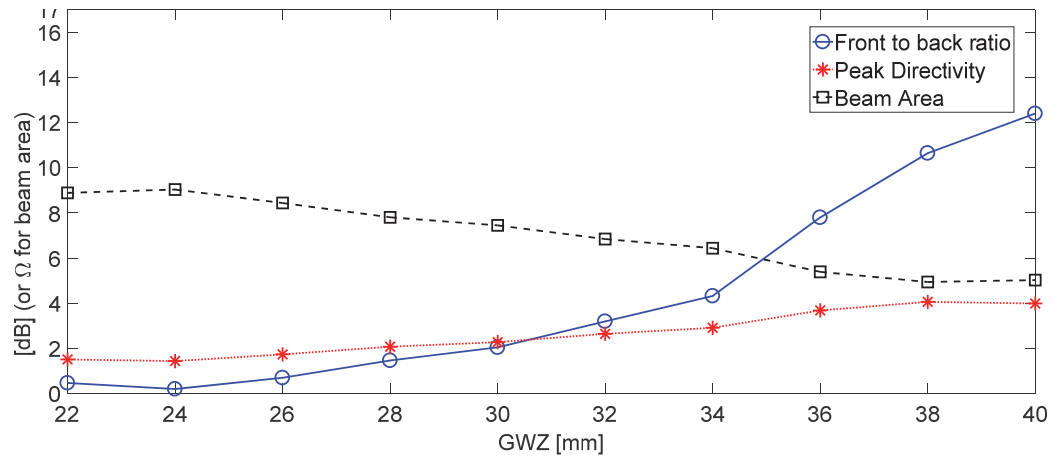


Fig. 5-45 Antenna parameter variation at 2.44GHz versus cube height in mode 1

b. Mode 2

Variation of width of slot on top/bottom faces of cube while keeping the patch size constant

In Fig. 5-46(a) and (b), width of slots on top/bottom face of the cube is changing from 1.75mm to 3.75mm synchronized with cube dimensions in X and Y in order to keep the dimensions of square patch on top/bottom face unchanged.

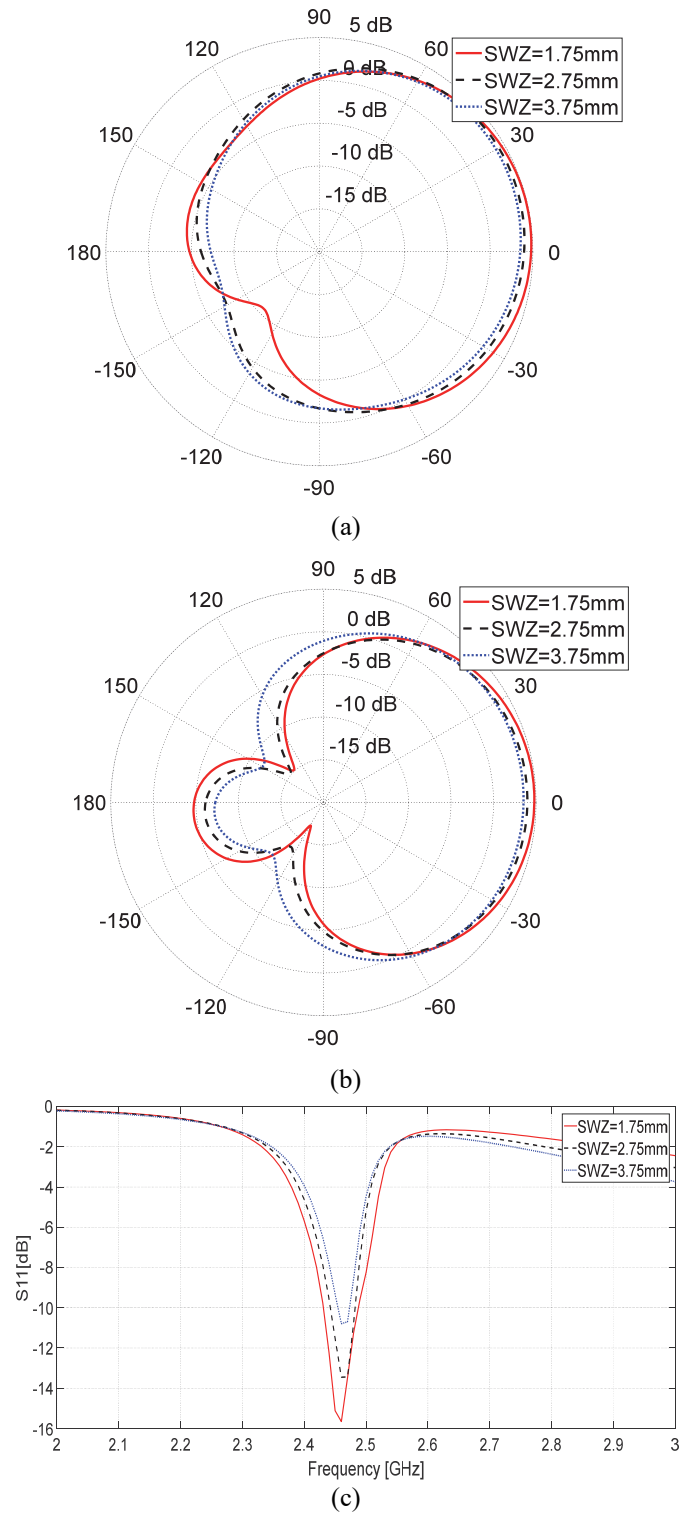


Fig. 5-46 Mode 2: SlotWZ parameter study, (a) Co-pol directivity at 2.44GHz in $\phi=0$ plane, (b) Co-pol directivity at 2.44GHz in $\phi=90$ plane, (c) S_{11}

Here, dimensions of patch are fixed while its edge distance to the conductive wall of cube (SlotWZ) which encloses the patch as a cavity, is changing.

As can be seen in Fig. 5-46, both patterns and input matching remain fairly intact. This was expected since the variation of SlotWZ in terms of wavelength in dielectric is between $0.024\lambda_r$ to $0.052\lambda_r$ which does not affect the attenuation of surface waves in substrate to a high degree and as a result cannot change the matching or radiation characteristics of the antenna.

Variation of cube height and coupling to the patch on the opposite side

As shown in Fig. 5-47, in mode 2 cube size does not directly affect the resonant frequency of the antenna as long as the feeding and matching circuit for the patch antenna will not change. However, the distance between active or excited patch on one face and the patch that is not excited on the opposite face, together with the height of cube walls can affect the radiation properties of the antenna. As mentioned earlier in section III-A.2, this distance determines the coupling between parasitic and active elements therefore its variation should significantly influence the antenna performance as can be seen Fig. 5-48.

By increasing the cube height, the amount of surface currents flow on the conductive walls of the cube increases which will result in some spurious radiation at undesired angles. This widens the beam area and leads to lower values of directivity and co to cross ratio as shown in Fig. 5-47.

We also notice that the front to back ratio is maximum for our chosen cube height of 30 mm, and it drops as GWZ accepts smaller or larger values. This is mainly because, there is an optimal distance for which all radiators contributing in the far field, including both active and parasitic elements, have out of phase radiations in the back-lobe region, which will result in back lobe suppression and maximum front to back ratio.

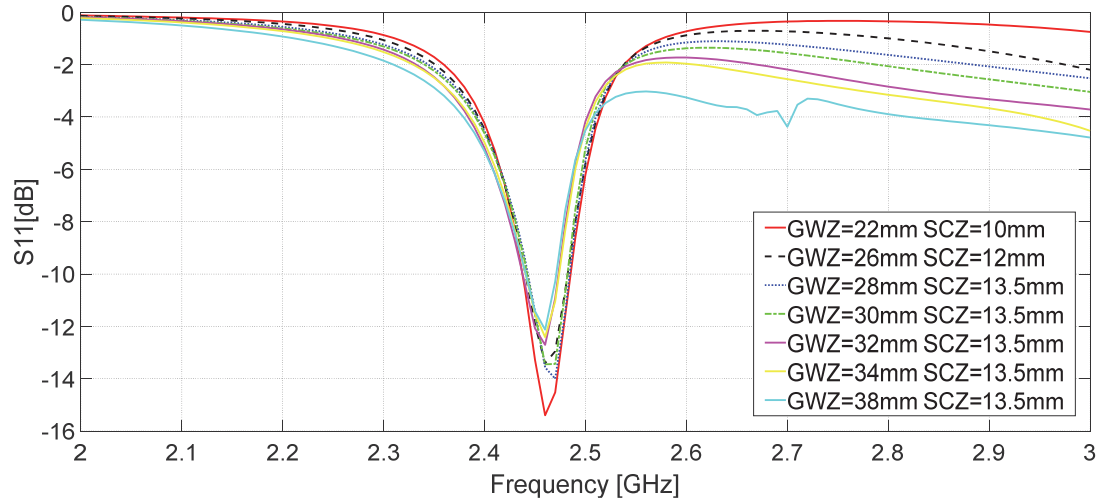


Fig. 5-47 Input reflection coefficient variation versus cube height in mode 2

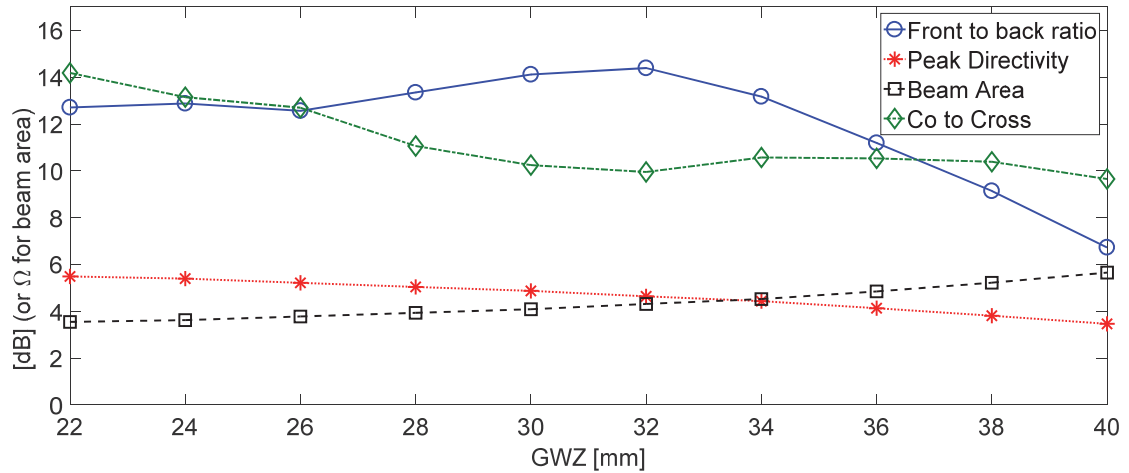


Fig. 5-48 Antenna parameter variation at 2.44GHz versus cube height in mode 2

Stub length

Stub length, SCZ (introduced in Fig. 5-25) is a key parameter and the most important dimension in both mode 1 and mode 2 that needed to be tuned for the best input matching. In the following the stub length has been swept around the original optimal value and variation of S_{11} parameter is displayed in Fig. 5-49. Length of SCZ in mode 1 affects the common mode slot pair excitation and in mode 2 changes the impedance of open circuit CPW stub. Proper matching at both modes achieved by choosing $SCZ=13.5\text{mm}$.

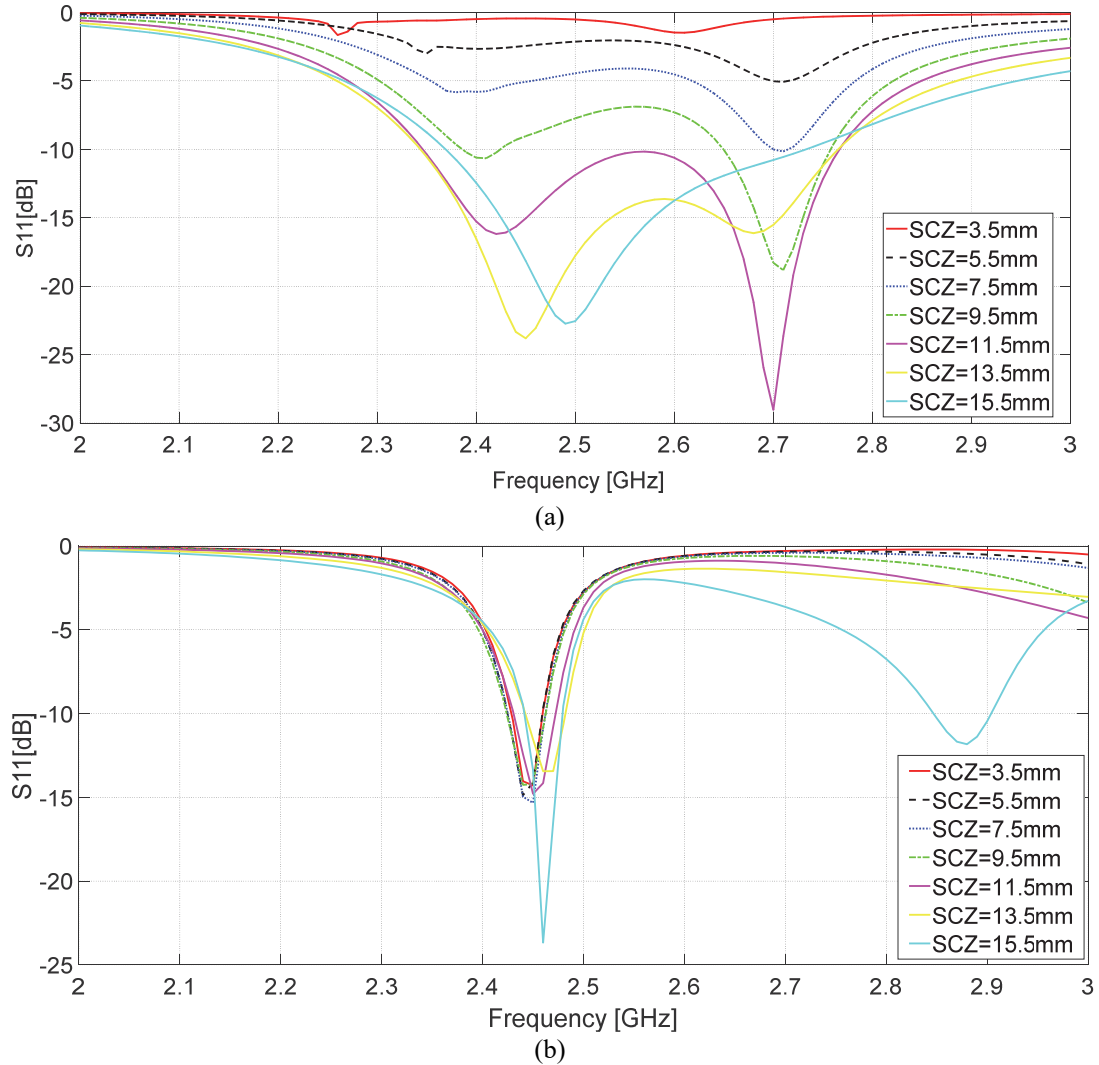


Fig. 5-49 Input reflection coefficient variation versus stub length SCZ, (a) mode 1, (b) mode 2

5.4 Conclusion

1st structure: Using 3-D folded conformal antenna, a novel multiport cubic slot architecture has been reported to serve applications required MIMO or beam forming. Employing the proposed architecture, we have designed a cubic antenna package operating at 2.4GHz with bandwidth of 15% and gain of 4dB to -1dB depending on the reconfigurable mode it has been used in.

2nd structure: Here a novel reconfigurable 3-D antenna structure for WSN applications has been presented. The antenna package is capable of generating both

omnidirectional (mode 1) and patch-like (mode 2) radiation patterns. The former has been accomplished through 3-D folded slot array mapped on the cube side walls, whereas the latter has been achieved through excitation of patch antennas embedded on the top and bottom faces of the cube. The measurement results were in a good agreement with simulation results and the antenna was matched at 2.44GHz with maximum gain of 2.85dBi and 4.2dBi in mode 1 and mode 2, respectively. The proposed structure proves to be a good candidate for WSN applications.

Chapter 6

6 Conclusion and future research

6.1 Conclusion

Wireless sensor network is one of the key technologies in the recent decade which serves a vast majority of applications such as military, health, and environmental-related tasks like agriculture and weather forecasting. Such a network relies on low cost sensory nodes capable of working in harsh operational conditions while offering high performance and reliable communication links. Essentially a conductive hermetic package which encloses a wireless device can offer the most reliable solution. The conductive hermetic body can guarantee the device immunity against EMI and electron bombardment in space

applications as well as moisture absorption and contamination in environmental monitoring. Additionally, such a structure will isolate the circuit from external environment which makes it a perfect solution for antenna packaging technologies.

Following the main objective of my PhD program, I have investigated the possibility of using 3-D cubic antennas in wireless sensor networks and designed and implemented novel architectures to meet the requirements of the wireless communication between sensory nodes and main hub. All proposed architectures were 3-D printable to facilitate the manufacturing and lower the costs. Various analyses and measurements have been done on the antennas to improve and highlight their applications in wireless communication.

In this thesis, we proposed 3D folded slot antenna as a novel conformal solution to be integrated with conductive packages. 3D folded slot is an extension of planar folded slot antennas to three-dimensional space which can be wrapped around a conductive 3D structure, here a cube. Single feed excitation of the 3D folded slot can lower the cost, simplify the fabrication and enhance the reliability. It was the main objective in most of our designs which could be handled using novel architectures and conquering challenges in the design. However, a multi-feed structure is designed as well for specific applications. Not only the single excitation, but also a novel feeding structure has been developed to add reconfigurability to a single feed structure to switch among different radiation patterns in order to improve network performance using space diversity. Higher performance in WSN will enhance battery life as well which is one of the most critical features.

In chapter 4, we have elaborated on the design, fabrication and measurement of three single feed cubic antenna-package configurations. All the proposed structures offer horizontally polarized omnidirectional radiation pattern in the azimuth plane but they do not possess the reconfigurability feature and have been fabricated through standard PCB manufacturing as well as 3-D printing. The material presented in this chapter are either published [2], [77] or submitted for publication.

- “*Microstrip Fed 3-D Cubic Folded Slot Antenna*” presented in section 4.2 was the first implemented structure which offers an omnidirectional radiation pattern in the azimuth plane. It is a single feed structure which used a microstrip line printed

inside the cube to excite the 3D folded slot printed on outer conductive layer of the cube.

- “*CPW Fed 3-D Cubic Folded Annular Slot Antenna*” presented in section 4.3 in which we used a CPW line printed in the same layer as antenna is printed to eliminate the internal layer printing and simplify the fabrication, especially for 3D printing. Similar to the previous design, it offers a horizontally polarized omnidirectional radiation pattern in the azimuth plane.
- “*3D cubic folded slot antenna array*” was our third cubic structure with horizontally polarized omnidirectional radiation pattern presented in section 4.4 which used CPW line to limit the design to one metal layer similar to the second structure. However, this structure was the basic building block from which we created our reconfigurable design presented in the next chapter. It offers a horizontally polarized omnidirectional radiation pattern in the azimuth plane similar to previous ones.

In chapter 5, we elaborated on design, fabrication and measurement of a cubic structure with reconfigurable radiation pattern as well as analysis and design of a multi-feed cubic antenna for especial applications. These reconfigurable architectures offer interesting features for smart antennas.

- “*Reconfigurable 3D cubic antenna*” presented in section 5.3 is a cubic structure designed after applying major modifications to the “3D cubic slot antenna array”, a single radiation pattern structure reported in section Proposed antenna-package provided three different radiation patterns to support both broadside and endfire communications. It is designed, fabricated and measured to cover all 3-D space around antenna by switching among two broadside radiation patterns toward top and bottom and one omnidirectional radiation pattern illuminating the azimuth plane.
- “*Cubic conformal slot antenna array*” presented in section 5.2 is a multiport cubic structure with beamforming and MIMO communication capability in the azimuth plane. It offers a wide beamwidth in the elevation plane due to conformal slot configuration which improves the antenna performance in terms of

covering more regions. This structure can perform beamforming for full 3-D space coverage through switching excitations between four input ports, turning ON and OFF some elements or applying phase shift and amplitude tapering. This antenna package is an ideal candidate for MIMO communication applications.

	#1	#2	#3	#4	#5
Cube size[mm³]	33×33×33	36.7×36.7×36.7	33.84×33.84×33.84	39.5×39.5×30	34×34×34
Slot width [mm]	2	1	5/3	5/2.75	5
Permittivity	2.97	2.97	4.3	3	4.3
Thickness [mm]	1.55	1.55	1.55	1.55	1.55
Omnidirectional/Directional	Y/N	Y/N	Y/N	Y/Y	Y/Y
Gain [dBi]	1.95	2.53	1.32	2.85/4.2	-1/4
10dB Bandwidth	14%	11%	12%	21%/2.7%	15%

1. Microstrip-Fed 3D Folded Slot Antenna on a Cubic Structure [11]
2. Three-dimensional folded annular slot antenna-package [12]
3. 3D folded slot antenna array (to be published)
4. Pattern Reconfigurable Cubic Slot Antenna (to be published)
5. Cubic conformal slot antenna array (to be published)

6.2 Future research

We suggest further research in the following areas based on findings in this document.

With regards to modeling and analysis, a method to analyze and simulate a 3-D cubic slot antenna was introduced in this document. This method modeled the structure as a circular antenna array made of folded slot antenna elements with simplifying assumptions. However, one can develop a more advanced analytical theory and solution while considering all factors like diffraction from the edges, connectivity between ground planes,

and coupling among antenna elements. Additionally, numerical solutions are suggested for proposed cubic structures to facilitate the design and to speed up the simulation.

With regards to fabrication, cubic antenna architectures reported in this document have been implemented using conventional PCB fabrication methods. However, only two structures have been implemented using basic 3D printing technology. Fabrication of all structures using advanced multi-material 3D printers is suggested to better evaluate the performance of the proposed structure as a promising candidate for low cost wireless sensor networks.

Characterizing Objet 3-D printer materials, two structures were manufactured using Objet 3D printers where copper tape used as conductor. However, more materials and fabrication methods could be investigated to better fulfill the requirements of microwave frequency circuits.

In all cubic structures, the internal volume is reserved for placement of telecommunication circuits. It would be interesting to use the proposed antenna-packages to design and manufacture a unified sensory node with including electronic circuit, sensors and switches with the application in wireless sensor network or other WiFi or Bluetooth devices.

References

- [1] S. Shamsinejad, F. De Flaviis, and P. Mousavi, "Microstrip-Fed 3-D Folded Slot Antenna on Cubic Structure," *IEEE Antennas Wirel. Propag. Lett.*, vol. 15, pp. 1081–1084, 2016.
- [2] S. Shamsinejad, F. M. Monavar, F. De Flaviis, G. Moradi, and P. Mousavi, "Three-dimensional-folded annular slot antenna-package," *Microw. Opt. Technol. Lett.*, vol. 59, no. 8, pp. 1871–1876, Aug. 2017.
- [3] C.-Y. Chong and S. P. Kumar, "Sensor networks: evolution, opportunities, and challenges," *Proc. IEEE*, vol. 91, no. 8, pp. 1247–1256, 2003.
- [4] E. MacDonald *et al.*, "3D Printing for the Rapid Prototyping of Structural Electronics," *IEEE Access*, vol. 2, pp. 234–242, Dec. 2014.
- [5] Y. Yoshimura, "A microstripline slot antenna (short papers)," *Microw. Theory Tech. IEEE Trans. On*, vol. 20, no. 11, pp. 760–762, 1972.
- [6] J. A. Paulsen, M. Renn, K. Christenson, and R. Plourde, "Printing conformal electronics on 3D structures with Aerosol Jet technology," in *Future of Instrumentation International Workshop (FIIW), 2012*, 2012, pp. 1–4.
- [7] D.-I. N. Heininger, T. P. Mansikkamäki, M. Kivikoski, and I. Y.-H. Lee, "Advanced antennas for mobile phones," in *Proceedings of International Symposium on Antennas and Propagation, Korea, 2005*.
- [8] M. Ahmadloo and P. Mousavi, "Application of novel integrated dielectric and conductive ink 3D printing technique for fabrication of conical spiral antennas," in *2013 IEEE Antennas and Propagation Society International Symposium (APSURSI)*, 2013, pp. 780–781.
- [9] M. Ahmadloo and P. Mousavi, "A novel integrated dielectric-and-conductive ink 3D printing technique for fabrication of microwave devices," in *Microwave Symposium Digest (IMS), 2013 IEEE MTT-S International*, 2013, pp. 1–3.
- [10] A. Rida, L. Yang, R. Vyas, and M. M. Tentzeris, "Conductive Inkjet-Printed Antennas on Flexible Low-Cost Paper-Based Substrates for RFID and WSN Applications," *IEEE Antennas Propag. Mag.*, vol. 51, no. 3, pp. 13–23, Jun. 2009.
- [11] G. Orecchini *et al.*, "Inkjet printed organic transistors for sustainable electronics," in *Electronic Components and Technology Conference (ECTC), 2010 Proceedings 60th*, 2010, pp. 985–989.
- [12] V. Rodriguez, "A Brief History of Horns-From Early History to Latest Developments," *Compliance*, vol. 10, pp. 2–4, 2010.
- [13] A. Enayati, S. Brebels, W. De Raedt, and G. A. E. Vandenbosch, "3D-Antenna-in-Package Solution for Microwave Wireless Sensor Network Nodes," *IEEE Trans. Antennas Propag.*, vol. 59, no. 10, pp. 3617–3623, Oct. 2011.
- [14] I. T. Nassar and T. M. Weller, "Development of Novel 3-D Cube Antennas for Compact Wireless Sensor Nodes," *IEEE Trans. Antennas Propag.*, vol. 60, no. 2, pp. 1059–1065, Feb. 2012.
- [15] I. T. Nassar, T. M. Weller, and J. L. Frolik, "A Compact 3-D Harmonic Repeater for Passive Wireless Sensing," *IEEE Trans. Microw. Theory Tech.*, vol. 60, no. 10, pp. 3309–3316, Oct. 2012.

-
- [16] X. Chen, K. Church, and H. Yang, "High speed non-contact printing for solar cell front side metallization," in *2010 35th IEEE Photovoltaic Specialists Conference (PVSC)*, 2010, pp. 001343–001347.
- [17] J. Czyżewski, P. Burzyński, K. Gawęł, and J. Meisner, "Rapid prototyping of electrically conductive components using 3D printing technology," *J. Mater. Process. Technol.*, vol. 209, no. 12–13, pp. 5281–5285, Jul. 2009.
- [18] I. T. Nassar and T. M. Weller, "An electrically-small, 3-D cube antenna fabricated with additive manufacturing," in *2013 IEEE Topical Conference on Wireless Sensors and Sensor Networks (WiSNet)*, 2013, pp. 58–60.
- [19] I. T. Nassar, H. Tsang, K. Church, and T. M. Weller, "A high efficiency, electrically-small, 3-D machined-substrate antenna fabricated with fused deposition modeling and 3-D printing," in *2014 IEEE Radio and Wireless Symposium (RWS)*, 2014, pp. 67–69.
- [20] C. M. Kruesi, R. J. Vyas, and M. M. Tentzeris, "Design and Development of a Novel 3-D Cubic Antenna for Wireless Sensor Networks (WSNs) and RFID Applications," *IEEE Trans. Antennas Propag.*, vol. 57, no. 10, pp. 3293–3299, Oct. 2009.
- [21] C. Kruesi and M. M. Tentzeris, "'Magic-Cube' antenna configurations for ultra compact RFID and wireless sensor nodes," in *IEEE Antennas and Propagation Society International Symposium, 2008. AP-S 2008*, 2008, pp. 1–4.
- [22] G. Monti, L. Catarinucci, C. Vasanelli, and L. Tarricone, "3D patch antenna using a cardboard substrate for RFID reader applications," in *Microwave Conference (EuMC), 2012 42nd European*, 2012, pp. 884–887.
- [23] M. F. Farooqui and A. Shamim, "An inkjet printed near isotropic 3-D antenna with embedded electronics for wireless sensor applications," in *Antennas and Propagation Society International Symposium (APSURSI), 2014 IEEE*, 2014, pp. 326–327.
- [24] S. Nikolaou, P. Vryonides, D. E. Anagnostou, and M. Al-Tarifi, "Development of an ultra compact dual band antenna on a one cubic centimeter (1 cm³) surface," in *IEEE Antennas and Propagation Society International Symposium, 2009. APSURSI '09*, 2009, pp. 1–4.
- [25] Q. Rao and G. Wen, "Ultra -small cubic folded strip antenna for handset devices," in *IEEE Antennas and Propagation Society International Symposium, 2008. AP-S 2008*, 2008, pp. 1–4.
- [26] D. L. H. Tong, P. Minard, A. Louzir, and J.-F. Pintos, "Compact multiselector antenna system using folded Vivaldi radiators," in *2011 IEEE International Symposium on Antennas and Propagation (APSURSI)*, 2011, pp. 1364–1367.
- [27] J. J. Adams and J. T. Bernhard, "A Modal Approach to Tuning and Bandwidth Enhancement of an Electrically Small Antenna," *IEEE Trans. Antennas Propag.*, vol. 59, no. 4, pp. 1085–1092, Apr. 2011.
- [28] J. J. Adams, S. C. Slimmer, T. F. Malkowski, E. B. Duoss, J. A. Lewis, and J. T. Bernhard, "Comparison of Spherical Antennas Fabricated via Conformal Printing: Helix, Meanderline, and Hybrid Designs," *IEEE Antennas Wirel. Propag. Lett.*, vol. 10, pp. 1425–1428, 2011.
- [29] S. R. Best, "The radiation properties of electrically small folded spherical helix antennas," *IEEE Trans. Antennas Propag.*, vol. 52, no. 4, pp. 953–960, Apr. 2004.
- [30] S. Yun, K. Kim, and S. Nam, "Outer-Wall Loop Antenna for Ultrawideband Capsule Endoscope System," *IEEE Antennas Wirel. Propag. Lett.*, vol. 9, pp. 1135–1138, 2010.

- [31] S. B. Cohn, "Slot Line on a Dielectric Substrate," *IEEE Trans. Microw. Theory Tech.*, vol. 17, no. 10, pp. 768–778, Oct. 1969.
- [32] S. B. Cohn, "Slot line-an alternative transmission medium for integrated circuits," in *Microwave Symposium, 1968 G-MTT International*, 1968, pp. 104–109.
- [33] E. A. Mariani, C. P. Heinzman, J. P. Agrios, and S. B. Cohn, "Slot Line Characteristics," *IEEE Trans. Microw. Theory Tech.*, vol. 17, no. 12, pp. 1091–1096, Dec. 1969.
- [34] H. G. Akhavan and D. Mirshekar-Syahkal, "Approximate model for microstrip fed slot antennas," *Electron. Lett.*, vol. 30, no. 23, pp. 1902–1903, 1994.
- [35] A. Van de Capelle, D. Amandt, and J. Hermans, "Analysis model for the microstrip slot antenna," in *Microwave Conference, 1978. 8th European*, 1978, pp. 312–316.
- [36] H.-C. Liu, T.-S. Horng, and N. G. Alexopoulos, "Radiation of printed antennas with a coplanar waveguide feed," *Antennas Propag. IEEE Trans. On*, vol. 43, no. 10, pp. 1143–1148, 1995.
- [37] L. Zhu and K. Wu, "Complete circuit model of microstrip-fed slot radiator: Theory and experiments," *Microw. Guid. Wave Lett. IEEE*, vol. 9, no. 8, pp. 305–307, 1999.
- [38] H.-S. Tsai and R. A. York, "FDTD analysis of CPW-fed folded-slot and multiple-slot antennas on thin substrates," *Antennas Propag. IEEE Trans. On*, vol. 44, no. 2, pp. 217–226, 1996.
- [39] H. S. Tsai and R. A. York, "Quasi-optical amplifier array using direct integration of MMICs and 50 /spl Omega/ multi-slot antennas," in *Microwave Symposium Digest, 1995., IEEE MTT-S International*, 1995, pp. 593–596 vol.2.
- [40] T. M. Weller, L. P. Katehi, and G. M. Rebeiz, "Single and double folded-slot antennas on semi-infinite substrates," *Antennas Propag. IEEE Trans. On*, vol. 43, no. 12, pp. 1423–1428, 1995.
- [41] S. Lim and H. Ling, "Design of electrically small, pattern reconfigurable Yagi antenna," *Electron. Lett.*, vol. 43, no. 24, pp. 1326–1327, Nov. 2007.
- [42] S. Muhamud-Kayat, M. T. Ali, M. K. M. Salleh, and M. H. M. Rusli, "Reconfigurable gap-coupled back-to-back truncated rhombus-like slotted patch antenna with steerable beams," in *2014 21st International Conference on Telecommunications (ICT)*, 2014, pp. 338–342.
- [43] V.-A. Nguyen, M.-H. Jeong, M.-T. Dao, and S.-O. Park, "Four-port beam reconfigurable antenna array for pattern diversity system," *IET Microw. Antennas Propag.*, vol. 6, no. 10, pp. 1179–1186, Jul. 2012.
- [44] D. Patron, D. Piazza, and K. R. Dandekar, "Wideband planar antenna with reconfigurable omnidirectional and directional radiation patterns," *Electron. Lett.*, vol. 49, no. 8, pp. 516–518, Apr. 2013.
- [45] J. T. Bernhard, "Reconfigurable Antennas," *Synth. Lect. Antennas*, vol. 2, no. 1, pp. 1–66, Jan. 2007.
- [46] J. Sarrazin, Y. Mahe, S. Avrillon, and S. Toutain, "Pattern Reconfigurable Cubic Antenna," *IEEE Trans. Antennas Propag.*, vol. 57, no. 2, pp. 310–317, 2009.
- [47] Yue Li, Zhijun Zhang, Wenhua Chen, and Zhenghe Feng, "Polarization Reconfigurable Slot Antenna With a Novel Compact CPW-to-Slotline Transition for WLAN Application," *IEEE Antennas Wirel. Propag. Lett.*, vol. 9, pp. 252–255, 2010.

- [48] P.-Y. Qin, Y. J. Guo, A. R. Weily, and C.-H. Liang, "A Pattern Reconfigurable U-Slot Antenna and Its Applications in MIMO Systems," *IEEE Trans. Antennas Propag.*, vol. 60, no. 2, pp. 516–528, Feb. 2012.
- [49] M.-I. Lai, T.-Y. Wu, J.-C. Hsieh, C.-H. Wang, and S.-K. Jeng, "Design of reconfigurable antennas based on an L-shaped slot and PIN diodes for compact wireless devices," *IET Microw. Antennas Propag.*, vol. 3, no. 1, pp. 47–54, Feb. 2009.
- [50] M. M. Fakharian, P. Rezaei, and A. A. Orouji, "Reconfigurable Multiband Extended U-Slot Antenna with Switchable Polarization for Wireless Applications," *IEEE Antennas Propag. Mag.*, vol. 57, no. 2, pp. 194–202, Apr. 2015.
- [51] M. F. Jamlos *et al.*, "A Beam Steering Radial Line Slot Array (RLSA) Antenna with Reconfigurable Operating Frequency," *J. Electromagn. Waves Appl.*, vol. 24, no. 8–9, pp. 1079–1088, Jan. 2010.
- [52] M. W. Young, S. Yong, and J. T. Bernhard, "A Miniaturized Frequency Reconfigurable Antenna With Single Bias, Dual Varactor Tuning," *IEEE Trans. Antennas Propag.*, vol. 63, no. 3, pp. 946–951, Mar. 2015.
- [53] C.-Y. Chiu and R. D. Murch, "Experimental results for a MIMO cube," in *IEEE Antennas and Propagation Society International Symposium 2006*, 2006, pp. 2533–2536.
- [54] C. Y. Chiu and R. D. Murch, "Design of a 24-port MIMO cube," in *2007 IEEE Antennas and Propagation Society International Symposium*, 2007, pp. 2397–2400.
- [55] A. Nemeth, L. Sziics, and L. Nagy, "MIMO Cube Formed of Slot Dipoles," in *Mobile and Wireless Communications Summit, 2007. 16th IST*, 2007, pp. 1–5.
- [56] G. Shaker, S. Safavi-Naeini, N. Sangary, and M. M. Tentzeris, "Inkjet Printing of Ultrawideband (UWB) Antennas on Paper-Based Substrates," *IEEE Antennas Wirel. Propag. Lett.*, vol. 10, pp. 111–114, 2011.
- [57] J. J. Adams *et al.*, "Conformal Printing of Electrically Small Antennas on Three-Dimensional Surfaces," *Adv. Mater.*, vol. 23, no. 11, pp. 1335–1340, Mar. 2011.
- [58] "NovaCentrix & nScript awarded \$1M to develop all-in-one system for 3D printing electronics," *3ders.org*. [Online]. Available: <http://www.3ders.org/articles/20141024-novacentrix--nscript-awarded-to-develop-all-in-one-system-for-3d-printing-electronics.html>. [Accessed: 10-Jul-2015].
- [59] LPKF, "3-Dimensional Circuitry Laser-Direct Structuring Technology (LPKF-LDS) for Moulded Interconnect Devices," http://www.lpkf.com/_mediafiles/1797-lpkf-lds-process.pdf. [Online]. Available: http://www.lpkf.com/_mediafiles/1797-lpkf-lds-process.pdf. [Accessed: 17-Oct-2014].
- [60] "Cost-Effective Entry into Laser Direct Structuring (LDS) LPKF Fusion3D 1100." [Online]. Available: http://www.lpkf.com/_mediafiles/2249-fusion3d-1100-english.pdf. [Accessed: 14-Nov-2014].
- [61] "LPKF-LDS Process (Laser Direct Structuring) - LPKF Laser & Electronics AG." [Online]. Available: <http://www.lpkf.com/applications/mid/lpkf-lds-process/>. [Accessed: 10-Jul-2015].
- [62] Y. Xiong and Z. Qu, "Antenna 3D Pad printing solution evaluation," in *2011 IEEE International Symposium on Antennas and Propagation (APSURSI)*, 2011, pp. 2773–2776.

- [63] P. Kiddell, "A Basic Overview of The Pad Printing Process," *Engineered Printing Solution*. [Online]. Available: <http://www.epsvt.com/support/generalIssue.cfm?issID=15>. [Accessed: 10-Jul-2015].
- [64] E. M. Amin and N. C. Karmakar, "Development of a low cost printable humidity sensor for chipless RFID technology," in *RFID-Technologies and Applications (RFID-TA), 2012 IEEE International Conference on*, 2012, pp. 165–170.
- [65] M. D. Balachandran, S. Shrestha, M. Agarwal, Y. Lvov, and K. Varahramyan, "SnO₂capacitive sensor integrated with microstrip patch antenna for passive wireless detection of ethylene gas," *Electron. Lett.*, vol. 44, no. 7, pp. 464–466, Mar. 2008.
- [66] S. Shrestha, M. Balachandran, M. Agarwal, V. V. Phoha, and K. Varahramyan, "A Chipless RFID Sensor System for Cyber Centric Monitoring Applications," *IEEE Trans. Microw. Theory Tech.*, vol. 57, no. 5, pp. 1303–1309, May 2009.
- [67] C. A. Balanis, *Antenna theory: analysis and design, 3rd edition*. Wiley India Pvt. Limited, 2009.
- [68] L. V. John and L. Volakis, "Antenna engineering handbook," *McGraw-Hill Tor.*, 2007.
- [69] L. Josefsson and P. Persson, *Conformal Array Antenna Theory and Design*. John Wiley & Sons, 2006.
- [70] W. L. Stutzman and W. A. Davis, *Antenna theory*. Wiley Online Library, 1998.
- [71] J. C. Batchelor and R. J. Langley, "Microstrip annular ring slot antennas for mobile applications," *Electron. Lett.*, vol. 32, no. 18, pp. 1635–1636, 1996.
- [72] H. G. Booker, "Slot aeriels and their relation to complementary wire aeriels (Babinet's principle)," *J. Inst. Electr. Eng. - Part IIIA Radiolocation*, vol. 93, no. 4, pp. 620–626, 1946.
- [73] M. Sanad, "Microstrip antennas on very small ground planes for portable communication systems," in *Proceedings of IEEE Antennas and Propagation Society International Symposium and URSI National Radio Science Meeting*, 1994, vol. 2, pp. 810–813 vol.2.
- [74] F. Sabath, M. Bucker, and S. Oing, "Influence of finite ground planes on the transmission line current distribution," *IEEE Trans. Magn.*, vol. 32, no. 3, pp. 1501–1504, 1996.
- [75] S. Maci, L. Borselli, and A. Cucurachi, "Diffraction from a truncated grounded dielectric slab: A comparative full-wave/physical-optics analysis," *IEEE Trans. Antennas Propag.*, vol. 48, no. 1, pp. 48–57, 2000.
- [76] M. Jusoh, T. Sabapathy, M. F. Jamlos, and M. R. Kamarudin, "Reconfigurable four-parasitic-elements patch antenna for high-gain beam switching application," *IEEE Antennas Wirel. Propag. Lett.*, vol. 13, pp. 79–82, 2014.
- [77] S. Shamsinejad, F. De Flaviis, and P. Mousavi, "Microstrip-Fed 3D Folded Slot Antenna on a Cubic Structure," *IEEE Antennas Wirel. Propag. Lett.*, vol. Accepted.
- [78] "Blended Reality - Sprout: Immersive Computing & 3D Printer | HP® Official Site." [Online]. Available: http://www8.hp.com/us/en/ads/blended-reality/overview.html?jumpid=reg_r1002_usen_c-001_title_r0001. [Accessed: 11-Jul-2015].
- [79] "HP Designjet 3D and Color 3D Printer - Overview and Specifications." [Online]. Available: http://h20564.www2.hp.com/hpsc/doc/public/display?docId=emr_na-

- c02153305&DocLang=en&docLocale=en_US&jumpid=reg_r1002_usen_c-001_title_r0004. [Accessed: 11-Jul-2015].
- [80] “Rapid Prototyping, Advance Digital Manufacturing, 3D Printing, 3-D CAD | www.3dsystems.com.” [Online]. Available: <http://www.3dsystems.com/>. [Accessed: 11-Jul-2015].
- [81] “Ultimaker,” *Ultimaker.com*. [Online]. Available: <https://ultimaker.com/>. [Accessed: 11-Jul-2015].
- [82] “projet-1000-1500-us.pdf.” [Online]. Available: <http://www.3dsystems.com/files/projet-1000-1500-us.pdf>. [Accessed: 11-Jul-2015].
- [83] “V-Flash for US - 24034-S02-02-A_USMSDS_V-Flash_FTI-GN_English.pdf.” [Online]. Available: http://www.3dsystems.com/products/datafiles/v-flash/msds/24034-S02-02-A_USMSDS_V-Flash_FTI-GN_English.pdf. [Accessed: 11-Jul-2015].
- [84] “Micro Dispense Pump 3D Direct Printing Systems - 3Dn Machine Series Side by Side Technical Specifications - nScrypt.” [Online]. Available: <http://www.nscrypt.com/micro-dispensing-systems-equipment/direct-print-3dn-machines/direct-print-3dn-machine-technical-specifications.php>. [Accessed: 12-Jul-2015].
- [85] Optomec Marketing, “Printed Antennas 3D Printing Additive Manufacturing,” *Optomec Additive Manufacturing*. [Online]. Available: <http://www.optomec.com/additive-manufacturing/printed-electronics/aerosol-jet-core-applications/printed-antennas/>. [Accessed: 11-Jul-2015].
- [86] “Nordson EFD.” [Online]. Available: <http://www.nordsonefd.com/searchengines/google/en/GeneralDispensing/?gclid=Cj0KEQjwoIitBRDTgeiZq93F2LQBEiQAMfXL0T2SM4f5IP58f9tVbUaLmHEQqnXhqqKnjmy6bt37dbUaAmgY8P8HAQ>. [Accessed: 12-Jul-2015].
- [87] “Design Series 3D Printers for Product Design | Stratasys.” [Online]. Available: <http://www.stratasys.com/3d-printers/design-series>. [Accessed: 11-Jul-2015].
- [88] “PolyJet Materials | Stratasys.” [Online]. Available: <http://www.stratasys.com/materials/polyjet>. [Accessed: 11-Jul-2015].
- [89] “3D printers | 3D models | Rapid Prototyping | voxeljet.” [Online]. Available: <http://www.voxeljet.de/en/>. [Accessed: 11-Jul-2015].
- [90] “Products - Asiga.” [Online]. Available: <https://www.asiga.com/products/printers/>. [Accessed: 11-Jul-2015].
- [91] “Production 3D Printers,” *www.3dsystems.com*. [Online]. Available: <http://www.3dsystems.com/3d-printers/production/overview>. [Accessed: 11-Jul-2015].
- [92] admin, “sPro™ 140,” *www.3dsystems.com*, 11-Oct-2012. [Online]. Available: <http://www.3dsystems.com/3d-printers/production/spro-140>. [Accessed: 11-Jul-2015].
- [93] “sPro™ 230 | www.3dsystems.com.” [Online]. Available: <http://www.3dsystems.com/3d-printers/production/spro-230>. [Accessed: 11-Jul-2015].

Appendix I: 3-D printing

Recently, 3-D printing grows dramatically and its application can be found almost everywhere. In contrast with traditional manufacturing methods which usually are too industrial for huge mass production, 3-D printing is a direct writing method which is faster and cheaper in prototyping, even advanced industrial 3-D printer released in the market as serious competitors for mass production methods. Here, we have reviewed and categorized different methods as following:

I-1. FDM (Fused Deposition Modeling)

FDM is an Extrusion based additive manufacturing technology usually in low cost and home use 3-D printers where a ABS or PLA filament is melting passing through a heated nozzle and cooling down to form the desired object. Such a printers have been produced by companies like Ultimaker, HP, and 3-Systems [78]–[81].

I-2. FTI (Film Transfer Imaging)

FTI is an additive technology in 3-D printing which deposited Photo Polymer Films to fabricate the 3-D object layer by layer. These types of printers are supplied through resin cartridges and have both home and industrial application. ProJet 1000 and ProJet 1500 released by 3-D Systems operate based on this technology [82], [83].

I-3. Inkjet3-DPrinting

Planar Inkjet printing of conductive layout has been introduced and found its application in the market. Recently, the method has been extended to conformal 3-D printing which can print 3-D layouts on 3-D packages and bodies. Nscript is one of major companies in the field which released a 3-D inkjet printing [84].

I-4. Micro dispensing for conformal printing of conductive layout

To pattern the antenna body printed from a dielectric substrate with conductive layout made of silver or copper nanoparticle inks, Micro-dispensing method released by Optomec [85] and Nordson [86] can be used.

I-5. Poly Jetting_ Photo polymer based

Jetting photo polymer to create 3-D object layer by layer is a high precision method which is used in most of Objet printer recently owned by Stratasys [87]. These devices can print multi material objects using up to 4 polymer resin cartridges where one of them is used as support material [88].

I-6. Selective Heat Sintering (SHS)

This method which used for TermoPlastic Powder Fusion was one employed in the first generation of industrial 3-D printers. Printer covers its bed with powder and then patterns it by the aid of fusion. Then the bed moves down and the second layer of powder is deposited on the first layer for fusion. Voxeljet is one of the companies that produces industrial SHS printers [89].

I-7. Stereo Lithography Apparatus (SLA) PhotoPolymerBased

Stereo Lithography fabrication has been introduced as a novel method in microfabrication that uses two beams instead of one in fabrication. Recently, the same technology has been released in the photo polymer based 3-D printing market especially for home use desktop 3-D printers. Each layer of photo polymer resin is patterned by the light and the structure which is up/down created from top to bottom and pulled up from the resins. The precision of the method is very high in comparison with other competitors. Asiga is one of the major companies in the field that released Freeform printers in the market based on this technology [90]. 3-DSystems iPro printer family, and ProJet 6000HD, 7000HD, and ProX 800, and ProX 950 are SLA printers as well [91].

I-8. Selective Laser Melting (SLM) and Selective Laser Sintering (SLS)

SLM and SLS are additive printing technologies with industrial applications in printing Metal and plastics, respectively. To build a 3-D object, the printer melts the metal powder layer by layer using a high precision laser. 3-DSystems sPro 140 and sPro 230 printers are SLM printers and sPro 60 is a SLS printer with great application in production industry [92], [93].

I-9. Robotic dispensing on 3-D objects

Dispenser robots can dispense conductive inks or other materials on 3-D conformal surfaces to pattern the conductive layout and manufacture 3-D antenna and electronics. Nordson EFD is one of major producers of dispensing robots [86].